

Imperial College London

National Heart & Lung Institute

**Myocardial slices as an *in vitro* platform to study  
cardiac disease**

**Ifigeneia Bardi**

B.Sc., MRes

November 2020

A thesis submitted for the degree of Doctor of Philosophy

For those who stood beside me,  
above all my family and partner.

# Declarations

I certify that this thesis and research are products of my own work. Work and involvement of other people is fully acknowledged.

## Copyright declaration

The copyright of this thesis rests with the author and is made available under a Creative Commons Attribution Non-Commercial No Derivatives licence. Researchers are free to copy, distribute or transmit the thesis on the condition that they attribute it, that they do not use it for commercial purposes and that they do not alter, transform, or build upon it. For any reuse or redistribution, researchers must make clear to others the licence terms of this work.

# Abstract

*In vitro* models are the pillars of fundamental research and drug discovery, offering reductionist methods to better understand cellular responses in isolation. Often these methods are oversimplified, which makes their relevance to human biology and clinical translation ambiguous.

Living myocardial slices (LMSs) are viable thin (200-400 $\mu$ m) cardiac tissue slices, with preserved native multicellularity, architecture, mechanical and electrophysiological responses. Recent development in their culture, by us and others, paved the way for long-term preservation of adult mammalian heart tissue *in vitro*, without significant changes in its function and structure. This model has been extensively used in healthy tissue; however, to date, there are no established pathological models to study disease progression *in vitro*.

Here we hypothesised that LMSs can be used as an *in vitro* disease model to study temporal and spatial changes in cardiac function/structure in response to local cardiac damage.

Before inducing cardiac damage, we further improved and characterised the cultured LMS model by designing robust tissue holders, optimising the oxygenation of the media, and establishing the best slice thickness (300 $\mu$ ) for oxygen diffusion and tissue stability in culture. We found that the LMSs were adequately oxygenated in the inner layers and responded to mechanical stimuli with an increase in their contraction and hyperpolarisation of the mitochondrial membrane.

We then developed a cryoinjury model, by applying a cooled probe on the LMSs. We found that injury created a distinct necrotic area, surrounded by a border zone (BZ). The injury resulted in preserved force but electrical instability, with the presence of spontaneous contractions. Microscopic analysis of the BZ showed the presence of high numbers of



spontaneous  $\text{Ca}^{2+}$  sparks, which could be affected by inhibiting the activation of  $\text{Ca}^{2+}$ /calmodulin-dependent protein kinase II (CamKII). The inhibitory effect was more pronounced in endocardial LMSs, showing transmural differences of CamKII under pathological conditions. Structural analysis of the BZ also showed an acute increase of the sarcomere length and loss of t-tubule density upon culture, that could also account for the arrhythmogenicity of the injured LMSs. One application of therapeutic interventions on the model, by using extracellular vesicles (EVs), did not show any functional or molecular improvements.

This thesis demonstrates the significance of using diseased LMSs to study the way that local injury affects tissue stability, function, and structure. Further work is required to better understand the link between spontaneous  $\text{Ca}^{2+}$  and contraction events, as well as finding successful therapeutic interventions.

# Publications

- Dries, E., **Bardi, I.**, Meijling, B. et al (manuscript in revision) Inhibition of CaMKII reduces transmural heterogeneity of arrhythmogenic Ca<sup>2+</sup> events in cryoinjured rat cardiac tissue slices
- Kapnisi, M., Mansfield, C., Marijon, C., Guex, A.G., et al. (2018) Auxetic Cardiac Patches with Tunable Mechanical and Conductive Properties toward Treating Myocardial Infarction. *Advanced Functional Materials*. 28 (21).
- Perbellini, F., Liu, A.K.L., Watson, S.A., **Bardi, I.**, et al. (2017a) Free-of-Acrylamide SDS-based Tissue Clearing (FASTClear) for three dimensional visualization of myocardial tissue. *Scientific Reports*. 7 (5188).
- Perbellini, F., Watson, S.A., **Bardi, I.** & Terracciano, C.M. (2018) Heterocellularity and Cellular Cross-Talk in the Cardiovascular System. *Frontiers in Cardiovascular Medicine*. 5, 143.
- Perbellini, F., Watson, S.A., Scigliano, M., Alayoubi, S., et al. (2017b) Investigation of cardiac fibroblasts using myocardial slices. *Cardiovascular Research*. 114 (1), 77–89.
- Watson, S.A., Duff, J., **Bardi, I.**, Zabielska, M., et al. (2019) Biomimetic electromechanical stimulation to maintain adult myocardial slices *in vitro*. *Nature Communications*. 10 (1).
- Watson, S.A., Scigliano, M., **Bardi, I.**, Ascione, R., et al. (2017) Preparation of viable adult ventricular myocardial slices from large and small mammals. *Nature Publishing Group*. 12, 2623–2639.

# Presentations/Awards

## Poster Presentations

- Cardiac load and mitochondrial adaptation in living myocardial slices - Experimental Models in Physiology – Exeter - June 2018
- The use of living myocardial slices as a novel disease model to study cardiac arrhythmogenicity *in vitro* - International Society for Heart Research - May 2019

## Oral presentations

The use of living myocardial slices as a novel disease model to study cardiac arrhythmogenicity *in vitro* - National Heart & Lung Institute, Postgraduate Review Day – Hammersmith Hospital, London; July 2019

## Funding & Awards

- Clinical Medicine Research (National Heart and Lung Institute) - PhD funding - 2016
- Establishment and evaluation of *in vitro* models of heart disease with human cardiac slices for regenerative studies - British Heart Foundation Centre of Regenerative Medicine Application for Pilot Project Support - 2018

# Acknowledgments

First and foremost, I would like to deeply thank Prof Cesare Terracciano who welcomed me in his wonderful lab, for his continuous support, supervision, and many opportunities that he has provided for me during the 4 years of my PhD. I would also like to thank Prof Carolyn Carr, for her invaluable guidance on metabolic research and great mentoring moments that I still hold with me. My PhD would not be the same without my daily supervisor Dr Filippo Perbellini, who taught me all about slices and helped me during my first steps in the lab. I would also like to express my sincere gratitude to Eef Dries for her undivided support, friendship and great collaboration in the lab.

This PhD would not have been possible without the contributions of many people. I would like to thank Colleen Lopez for her help on the metabolic studies, Bram Meijling for his work on the cryoinjury characterisation, Samuel Watson for his great work and collaboration on myocardial slices, Stephen Rothery (FILM, Imperial College London) for his continuous assistance on image acquisition and analysis, George Sioutas for helping on data processing, Waseem Hasan for his help on oxygen measurements and David Pitcher for his assistance on the 3D printing. Finally, a big thanks to the electrophysiology lab for their suggestions, ideas and for making the lab such a great place to be.

I am, also, really grateful for those outside the lab who supported me through my PhD. First and foremost, my parents and my brother who supported me from the first day I came to the UK until today. George Sioutas has been the pillar of my strength, tirelessly listening and encouraging me to go on. Finally, big thanks to Ilona Sunyovszki, Raquel Nunez, Sam Kit Anan and Eef Dries for being such amazing friends and inspiration to me both for my scientific

career and my personal life. There have been so many other people who made me who I am today, and I will always be grateful for having them in my life.

# Table of contents

Declarations .....	3
Abstract.....	4
Publications .....	6
Presentations/Awards.....	7
Acknowledgments.....	8
Table of contents.....	10
Table of Figures .....	22
List of acronyms .....	25
Chapter 1 Introduction .....	29
<b>1.1 Cardiovascular models</b> .....	<b>30</b>
1.1.1 <i>In vivo</i> models .....	<b>30</b>
1.1.2 <i>In vitro</i> models .....	<b>32</b>
<b>1.1.2.1 Ex vivo heart tissue</b> .....	<b>32</b>
<b>1.1.2.2 Primary isolated cells</b> .....	<b>33</b>
<b>1.1.2.3 Cell lines</b> .....	<b>34</b>
<b>1.1.2.4 Induced pluripotent stem cell - cardiomyocytes</b> .....	<b>34</b>
<b>1.1.2.5 3D <i>in vitro</i> models</b> .....	<b>38</b>
<b>1.2 Living myocardial slices</b> .....	<b>42</b>
1.2.1 Development of the model.....	<b>42</b>
1.2.2 LMS culture .....	<b>45</b>
<b>1.3 Applications of LMS</b> .....	<b>48</b>
1.3.1 Extracellular vesicles .....	<b>48</b>
1.3.2 <i>In vitro</i> model of local injury .....	<b>49</b>
<b>1.3.2.1 Local injury and CamKII activation</b> .....	<b>50</b>

<b>1.4</b>	<b>Recapitulate the <i>in vivo</i> environment in <i>in vitro</i> models</b> .....	<b>52</b>
1.4.1	Electrical stimulation .....	<b>52</b>
1.4.2	Mechanical load .....	<b>53</b>
1.4.2.1	<b>Mechanical stretch – acute responses</b> .....	<b>55</b>
1.4.2.2	<b>Mechanical load – chronic adaptations in pathology</b> .....	<b>57</b>
1.4.3	Metabolism .....	<b>58</b>
1.4.3.1	<b>Metabolism in the healthy heart</b> .....	<b>58</b>
1.4.3.2	<b>Metabolism in heart failure</b> .....	<b>62</b>
1.4.3.3	<b>Mitochondria in response to mechanical load</b> .....	<b>62</b>
1.4.3.4	<b>Metabolism in LMS</b> .....	<b>63</b>
1.4.4	Oxygenation.....	<b>65</b>
1.4.4.1	<b>Cellular responses under ischemia</b> .....	<b>65</b>
1.4.4.2	<b>O<sub>2</sub> dependent molecular changes</b> .....	<b>66</b>
1.4.4.3	<b>Hyperoxygenation</b> .....	<b>66</b>
1.4.4.4	<b>Media Oxygenation <i>in vitro</i></b> .....	<b>67</b>
<b>1.5</b>	<b>Hypothesis</b> .....	<b>70</b>
Chapter 2		
	General methods .....	72
<b>2.1</b>	<b>Source of cardiovascular tissue</b> .....	<b>73</b>
2.1.1	Rat tissue.....	<b>73</b>
2.1.2	Human tissue.....	<b>73</b>
<b>2.2</b>	<b>Living myocardial slice preparation</b> .....	<b>74</b>

2.2.1	Preparation of the slicing solution .....	74
2.2.2	Solution preparation for heart excision.....	76
2.2.3	Preparation of 4% agarose .....	76
2.2.4	Preparation of the specimen holder.....	76
2.2.5	Preparation of the tissue dissection area .....	76
2.2.6	Calibration of the vibrating microtome.....	77
2.2.7	Preparation of the storing bath.....	77
<b>2.2.7.1</b>	<b>Collection of rat hearts</b> .....	79
<b>2.2.7.2</b>	<b>Collection of human hearts</b> .....	80
2.2.8	Preparation of tissue for slicing .....	<b>80</b>
<b>2.2.8.1</b>	<b>Preparation of the rat ventricular block</b> .....	81
<b>2.2.8.2</b>	<b>Preparation of the human ventricular block</b> .....	83
2.2.9	Mounting of the tissue on the specimen holder .....	<b>83</b>
2.2.10	Slicing of the left ventricular tissue .....	<b>85</b>
<b>2.3</b>	<b>Fibre alignment</b> .....	85
<b>2.4</b>	<b>Attachment of tissue holders</b> .....	85
<b>2.5</b>	<b>LMS size measurements</b> .....	88
<b>2.6</b>	<b>LMS culturing system</b> .....	88
2.6.1	Culture Medium .....	<b>88</b>
2.6.2	Culture chambers design.....	<b>89</b>
2.6.3	Placing LMS in culture .....	<b>89</b>



<b>2.7</b>	<b>Assessment of conduction velocity</b> .....	<b>92</b>
2.7.1	Recording of Multielectrode array (MEA) signals .....	<b>92</b>
2.7.2	Analysis of CV.....	<b>93</b>
<b>2.8</b>	<b>LMS force measurements</b> .....	<b>95</b>
2.8.1	Recording LMS contraction traces .....	<b>95</b>
2.8.2	Analysis of contraction traces .....	<b>96</b>
<b>2.9</b>	<b>LMS viability assessment</b> .....	<b>98</b>
2.9.1	Whole LMS viability .....	<b>98</b>
2.9.2	Local changes in LMS viability .....	<b>98</b>
2.9.3	TUNEL assay DNA fragmentation analysis.....	<b>100</b>
<b>2.10</b>	<b>Fixation of LMS</b> .....	<b>101</b>
<b>2.11</b>	<b>Immunofluorescence staining</b> .....	<b>101</b>
<b>2.12</b>	<b>Confocal microscopy</b> .....	<b>103</b>
2.12.1	Imaging procedure .....	<b>103</b>
2.12.2	Confocal image analysis .....	<b>104</b>
2.12.2.1	Analysis of sarcomere length .....	<b>104</b>
2.12.2.2	Collagen quantification .....	<b>106</b>
<b>2.13</b>	<b>LMS Ca<sup>+2</sup> handling</b> .....	<b>108</b>
2.13.1	Optical mapping.....	<b>108</b>
2.13.2	Ca <sup>2+</sup> event analysis.....	<b>109</b>
	<b>Mitochondrial membrane potential</b> .....	<b>110</b>

2.13.3	Assessment of the mitochondrial membrane potential .....	110
2.13.4	Widefield imaging .....	110
2.13.5	Analysis of the $m\Delta\Psi$ .....	113
<b>2.14</b>	<b>Laser diffraction</b> .....	113
<b>2.15</b>	<b>3D printing</b> .....	116
<b>2.16</b>	<b>Lipid supplementation on culture media</b> .....	116
2.16.1	Preparation of palmitate for LMS culture .....	116
<b>2.17</b>	<b>Statistics</b> .....	117
Chapter 3		
	LMS characterisation .....	118
<b>3.1</b>	<b>Introduction</b> .....	119
<b>3.2</b>	<b>Methods</b> .....	121
3.2.1	Slicing solution preparation .....	121
3.2.2	LMS culture .....	122
3.2.3	Contractility .....	122
3.2.4	LMS viability.....	122
3.2.5	Media glucose quantification.....	122
3.2.6	Radiolabelled palmitate/glucose detection .....	123
3.2.6.1	<b>Palmitate consumption</b> .....	123
3.2.6.2	<b>Calculation of palmitate radioactivity</b> .....	125
3.2.6.3	<b>Glucose consumption</b> .....	125
3.2.6.4	<b>Calculation of glucose radioactivity</b> .....	126

Hypoxia measurements.....	128
3.2.7 Media oxygenation.....	128
3.2.8 Sarcomere length measurements.....	128
3.2.9 Mitochondrial membrane potential.....	128
<b>3.3 Results</b> .....	129
3.3.1 Slicing solution .....	129
<b>3.3.2 LMS thickness</b> .....	131
3.3.3 LMS tissue holders .....	131
3.3.4 Tissue culture - Media lipid supplementation.....	135
3.3.5 Tissue culture – LMS O <sub>2</sub> levels .....	136
3.3.6 Tissue culture- Mechanical stimulation.....	139
3.3.7 Metabolic response to different preloads.....	141
<b>3.4 Discussion</b> .....	146
3.4.1 Tissue slicing .....	146
3.4.2 Tissue thickness .....	147
3.4.3 Oxygenation.....	149
3.4.4 Fatty acid media supplementation .....	149
3.4.5 Electro-Mechanical stimulation.....	150
<b>3.5 Limitations and Future work</b> .....	154
<b>3.6 Conclusions</b> .....	156

## Chapter 4

Cryoinjury on LMS - <i>a model to study local cell responses to myocardial injury</i> .....	157
<b>4.1 Introduction</b> .....	158
<b>4.2 Methods</b> .....	160
4.2.1 LMS slice preparation.....	160
4.2.2 Application of cryoinjury.....	160
<b>4.2.3 Conduction velocity (MEA)</b> .....	162
4.2.4 Viability .....	162
4.2.5 Arrhythmogenicity assessment .....	162
<b>4.2.5.1 Arrhythmia provocation protocol for LMS</b> .....	162
4.2.6 Arrhythmia analysis – Spontaneous contractions .....	163
<b>4.2.7 Acute assessment cryoinjury – multiple injuries</b> .....	165
4.2.8 LMS culture .....	167
<b>4.2.9 LMS Ca<sup>+2</sup> handling</b> .....	167
4.2.10 Sarcomere length .....	167
4.2.11 High throughput image analysis of sarcomere length.....	167
<b>4.2.11.1 Preparation of acutely injured LMS and image acquisition</b> .....	167
<b>4.2.11.2 High throughput image analysis</b> .....	168
<b>4.2.12 Collagen I detection</b> .....	170
4.2.13 Connexin 43 quantification.....	170
4.2.14 Transverse and axial tubular network analysis .....	170
<b>4.3 Results</b> .....	171

4.3.1	Cryoinjury characterisation.....	<b>171</b>
4.3.1.1	<b>Conduction velocity</b> .....	171
4.3.1.2	<b>LMS viability - local changes in LMS</b> .....	173
4.3.2	Acute effects of cryoinjury .....	<b>178</b>
4.3.2.1	<b>Contraction</b> .....	178
4.3.2.2	<b>Sarcomere length</b> .....	181
4.3.3	Chronic effects of cryoinjury .....	<b>185</b>
4.3.3.1	<b>Maximum isometric contraction</b> .....	185
4.3.3.2	<b>Contraction kinetics</b> .....	185
4.3.3.3	<b>Increased LMS arrhythmogenicity</b> .....	188
4.3.4	Cytoplasmic Calcium cycling.....	<b>190</b>
4.3.4.1	<b>Calcium transients and spontaneous calcium events</b> .....	190
4.3.4.2	<b>Spontaneous Ca<sup>2+</sup> waves in the LMS</b> .....	192
4.3.4.3	<b>Spontaneous calcium waves – speed and propagation distance</b> .....	194
4.3.5	Structural analysis.....	<b>196</b>
4.3.5.1	<b>T-tubule density</b> .....	196
4.3.5.2	<b>Connexin 43</b> .....	196
4.3.5.3	<b>Collagen deposition</b> .....	200
4.3.5.4	<b>Sarcomere length after 24h remodelling</b> .....	200
4.3.6	Cryoinjury on human LMS.....	<b>203</b>
4.3.6.1	<b>Contraction of human cryoinjured LMS</b> .....	203

4.3.6.2	<b>Arrhythmogenicity on human cryoinjured LMS</b> .....	205
<b>4.4</b>	<b>Discussion</b> .....	207
4.4.1	Injury size.....	207
4.4.2	Arrhythmogenicity .....	209
4.4.2.1	<b>Proarrhythmic triggering</b> .....	209
4.4.2.2	<b>Connexins</b> .....	210
4.4.2.3	<b>Fibrosis</b> .....	211
4.4.2.4	<b>SL heterogeneity</b> .....	211
4.4.3	Contractility .....	212
4.4.3.1	<b>Sympathetic stimulation</b> .....	212
4.4.3.2	<b>Frank-Starling law</b> .....	213
4.4.3.3	<b>Calcium regulation</b> .....	214
	<b>Conclusions</b> .....	216
<b>4.5</b>	<b>Limitations and future plans</b> .....	218
Chapter 5		
	Cryoinjury on LMS – arrhythmia regulation.....	220
<b>5.1</b>	<b>Introduction</b> .....	221
<b>5.2</b>	<b>Methods</b> .....	223
5.2.1	LMS production.....	223
5.2.2	Force measurements.....	223
5.2.3	CamKII inhibition.....	223
5.2.4	Arrhythmia provocation and analysis .....	224

5.2.5	Ca <sup>2+</sup> handling .....	224
5.2.6	Transmural analysis .....	224
<b>5.3</b>	<b>Results</b> .....	225
5.3.1.1	Contraction – AIP .....	225
5.3.1.2	Spontaneous contractions – AIP .....	227
5.3.1.3	Calcium regulation .....	232
5.3.1.4	Transmural differences .....	234
<b>5.4</b>	<b>Discussion</b> .....	239
5.4.1	AIP .....	239
5.4.2	Transmural analysis .....	240
<b>5.5</b>	<b>Limitations and future work</b> .....	242
<b>5.6</b>	<b>Conclusions</b> .....	243
Chapter 6		
	Cryoinjury on LMS - EV application .....	244
<b>6.1</b>	<b>Introduction</b> .....	245
<b>6.2</b>	<b>Methods</b> .....	247
6.2.1	EV isolation .....	247
6.2.2	LMS production .....	247
6.2.3	EVs delivery optimisation.....	247
6.2.4	Confocal analysis .....	250
6.2.5	Force measurements.....	250
6.2.6	RT-qPCR-molecular analysis .....	250

<b>6.3</b>	<b>Results</b> .....	<b>252</b>
6.3.1	Exosomes .....	<b>252</b>
6.3.1.1	<b>Optimisation of the delivery method</b> .....	252
6.3.1.2	<b>EVs concentration</b> .....	252
6.3.1.3	<b>Contractility LMS – EVs application</b> .....	254
6.3.1.4	<b>Gene transcription analysis</b> .....	258
<b>6.4</b>	<b>Discussion</b> .....	<b>260</b>
6.4.1	Exosomes .....	<b>260</b>
6.4.1.1	<b>Delivery method – EV concentration</b> .....	260
6.4.1.2	<b>Contractility upon EV treatment</b> .....	261
6.4.1.3	<b>Molecular response of the LMS</b> .....	262
<b>6.5</b>	<b>Limitations</b> .....	<b>264</b>
<b>6.6</b>	<b>Conclusions</b> .....	<b>265</b>
Chapter 7		
	General Discussion .....	266
<b>7.1</b>	<b>Overview</b> .....	<b>267</b>
<b>7.2</b>	<b>Strengths &amp; Limitations</b> .....	<b>270</b>
<b>7.3</b>	<b>Implications</b> .....	<b>273</b>
<b>7.4</b>	<b>Future work</b> .....	<b>275</b>
7.4.1	LMS metabolic stability.....	<b>275</b>
7.4.1.1	<b>Reactive oxygen species</b> .....	275
7.4.2	Increase in LMS culture time.....	<b>276</b>



<b>7.5 Conclusion.....</b>	<b>278</b>
Chapter 8	
References.....	279
Chapter 9	
Appendices.....	352

# Table of Figures

Figure 1.1-IPSC technology. _____	37
Figure 1.2- 3D iPSC-CMs models. _____	39
Figure 1.3- Graphical representation of cardiac fibre distribution in the left ventricle. _____	44
Figure 1.4-LMS culturing systems. _____	47
Figure 1.5- Schematic representation of sarcomeres. _____	56
Figure 1.6-Substrate metabolism. _____	61
Figure 1.7-O <sup>2</sup> concentration in culture vessels. _____	69
Figure 2.1-Necessary equipment and setup needed to be prepared prior to heart harvesting. _____	78
Figure 2.2-Rat heart dissection steps. _____	82
Figure 2.3-Human tissue dissection and preparation for slicing. _____	84
Figure 2.4-Fibre orientation and tissue holder attachment. _____	87
Figure 2.5-Culture set up. _____	91
Figure 2.6-Multielectrode array (MEA) dish used to analyse LMS conduction velocity. _____	94
Figure 2.7-Force transducer set up. _____	97
Figure 2.8-Analysis of sarcomere length (SL). _____	105
Figure 2.9-Schematic representation for live imaging of mitochondrial membrane potential. _____	112
Figure 2.10-Laser diffraction set up for sarcomere length (SL) measurements. _____	115
Figure 3.1- Overview of radiolabelled energy metabolic pathways in the heart. _____	124
Figure 3.2-Ion-exchange chromatography separation method (Dowex). _____	127
Figure 3.3- Slicing solutions assessment. _____	130
Figure 3.4-Thinner LMS (200µm). _____	133
Figure 3.5-Tissue holders. _____	134
Figure 3.6-Lipid media substitution. _____	137
Figure 3.7- Oxygen analysis on LMS. _____	138
Figure 3.8-The effect of preload on cultured LMS. _____	140
Figure 3.9-Representative images of $m\Delta\Psi$ in LMS stained with TMRM. _____	143

<i>Figure 3.10-Mitochondrial assessment of the LMS under different preload conditions.</i>	144
<i>Figure 3.11-Mitochondrial assessment on human cultured LMS.</i>	145
<i>Figure 4.1- Schematic representation of the areas of interest in a cryoinjured LMS.</i>	161
<i>Figure 4.2-Schematic representation of the arrhythmia provocation assay.</i>	164
<i>Figure 4.3-Schematic representation of the assay used to acutely assess multiple injuries on healthy LMS.</i>	166
<i>Figure 4.4- Schematic representation of the imaging positions in regard to the injury.</i>	169
<i>Figure 4.5-CV measurement of freshly prepared rat LMS.</i>	172
<i>Figure 4.6--Viability assessment (LIVE/DEAD staining) of 24h cultured rat LMS.</i>	175
<i>Figure 4.7- TUNEL assay staining of cultured LMS to investigate tissue damage in the inner cell layers of the tissue.</i>	177
<i>Figure 4.8-Experimental design of the acute injury induction.</i>	179
<i>Figure 4.9-Contraction analysis after acute injury of the rat LMS.</i>	180
<i>Figure 4.10-Image processing for automated sarcomere length analysis.</i>	182
<i>Figure 4.11-High throughput sarcomere length analysis.</i>	184
<i>Figure 4.12-Contraction force was measured at maximum isometric stretch on cultured LMS as a measure of viability and functionality.</i>	186
<i>Figure 4.13- Baseline LMS contractility was assessed after 24h of culture.</i>	187
<i>Figure 4.14-Cultured LMS were treated with a proarrhythmic protocol of fast pacing (FP) ± isoproterenol (FP ISO).</i>	189
<i>Figure 4.15-Calcium transient analysis of LMS after 24h of culture. LMS were stained with Fluo-8AM which act as a calcium indicator.</i>	191
<i>Figure 4.16-Cultured LMS were treated with a proarrhythmic protocol and spontaneous calcium release (SCR) events were analysed during rest (in absence of electrical stimulation).</i>	193
<i>Figure 4.17-Wave properties of the spontaneous foci in cultured LMS.</i>	195
<i>Figure 4.18-Cultured LMS were stained for caveolin-3, a protein that localises in t-tubules (TT).</i>	198
<i>Figure 4.19-Connexin 43 immunohistological analysis. Cultured LMS were stained for connexin 43 (green), which localises in gap junction at the intercalated discs (ID).</i>	199

<i>Figure 4.20-Collagen quantification of cultured LMS. LMS were stained for collagen I and visualised in a confocal microscope.</i>	201
<i>Figure 4.21-Sarcomere length (SL) measurements of cultured LMS. LMS were stained for <math>\alpha</math>-actinin (green) and visualised in a confocal microscope.</i>	202
<i>Figure 4.22- Baseline contractility of human LMS after 48h in culture. LMS contractility was measured at 2.2<math>\mu</math>m of SL.</i>	204
<i>Figure 4.23- Cultured human LMS were treated with a proarrhythmic protocol of fast pacing (FP) <math>\pm</math> isoproterenol/caffeine (FP ISO).</i>	206
<i>Figure 5.1-Contractility analysis on cultured LMS treated with CamKII inhibitor (AIP).</i>	226
<i>Figure 5.2-Arrhythmia counting after arrhythmia provocation on 24h cultured LMS.</i>	229
<i>Figure 5.3- Pearson's chi-squared analysis of arrhythmias to determine the % of LMS developing arrhythmias irrespective of their level of arrhythmogenicity.</i>	230
<i>Figure 5.4-Arrhythmia latency (the time interval between the stimulation pause and the first spontaneous contraction).</i>	231
<i>Figure 5.5- Ca<sup>2+</sup> analysis of control and cryoinjured LMS treated with CamKII inhibitor, AIP.</i>	233
<i>Figure 5.6-Transmural differences of spontaneous arrhythmia development between treated and untreated groups under ISO or/and fast pacing stimulation.</i>	236
<i>Figure 5.7-Transmural Ca<sup>2+</sup> analysis of LMS after AIP treatment.</i>	237
<i>Figure 5.8-Transmural analysis of contraction amplitude and kinetics in control.</i>	238
<i>Figure 6.1-EV delivery on LMS.</i>	249
<i>Figure 6.2-Optimisation of EVs on LMS.</i>	253
<i>Figure 6.3-Contractility analysis of healthy LMS treated with EVs for 24h.</i>	255
<i>Figure 6.4- Contractility analysis of the cryoinjured LMS treated with EVs for 24h.</i>	256
<i>Figure 6.5- Contractility analysis at maximum isometric stretch of the healthy and cryoinjured LMS treated with EVs for 24h.</i>	257
<i>Figure 6.6- RT-qPCR data for Ki-67, Collagen 1, <math>\alpha</math>- Smooth Muscle Actin (A-SMA), and SERCA2.</i>	259

## List of acronyms

<b>ACE</b>	angiotensin converting enzyme
<b>AIP</b>	autocamtide-2-related inhibitory peptide
<b>ANOVA</b>	one-way analysis of variance
<b>AP</b>	action potential
<b>ARDS</b>	acute respiratory distress syndrome
<b>ARVC</b>	arrhythmogenic right ventricular cardiomyopathy
<b>ATP</b>	adenosine triphosphate
<b>Bcl-2</b>	B-cell lymphoma 2
<b>BDM</b>	2,3-Butanedione 2-monoxime
<b>BSA</b>	bovine serum albumin
<b>BZ</b>	border zone
<b>CaM</b>	Ca <sup>2+</sup> liganded calmodulin
<b>CaMK</b>	Ca <sup>2+</sup> /calmodulin-dependent protein kinase
<b>cAMP</b>	cyclic adenosine monophosphate
<b>CICR</b>	Ca <sup>2+</sup> induce Ca <sup>2+</sup> release
<b>CMs</b>	cardiomyocytes
<b>CoA</b>	acyl-coenzyme A
<b>CoCl<sub>2</sub></b>	cobalt chloride
<b>CPA</b>	cyclopiazonic
<b>CPC</b>	cardiac progenitor cells
<b>CPM</b>	counts per minute
<b>CPT</b>	carnitine palmitoyltransferase
<b>CRYO</b>	cryoinjured
<b>cTnI</b>	cardiac Troponin I
<b>CTR</b>	control
<b>CV</b>	conduction velocity
<b>Cx</b>	connexin
<b>DADs</b>	delayed after-depolarizations
<b>DCM</b>	dilated cardiomyopathy
<b>DMEM</b>	Dulbecco's Modified Eagle Medium
<b>DMSO</b>	dimethyl sulfoxide

<b>DNTs</b>	deoxyribonucleotides
<b>EADs</b>	early after-depolarizations
<b>E-C</b>	excitation-contraction
<b>ECM</b>	extracellular matrix
<b>ECs</b>	endothelial cells
<b>EHT</b>	engineered heart tissue
<b>ENDO</b>	endocardium
<b>eNOS</b>	endothelial nitric oxide synthase
<b>EPI</b>	epicardium
<b>ET-1</b>	endothelin-1
<b>EV</b>	extracellular vesicles
<b>FA</b>	fatty acids
<b>FAO</b>	fatty acid oxidation
<b>FBS</b>	fetal bovine serum
<b>FBs</b>	fibroblasts
<b>FCCP</b>	carbonyl cyanide-p-trifluoromethoxyphenylhydrazone
<b>FGF</b>	fibroblast growth factor
<b>FP</b>	fast pacing
<b>G6P</b>	glucose 6-phosphate
<b>GLUTs</b>	glucose transporters
<b>H<sub>2</sub>O<sub>2</sub></b>	hydrogen peroxide
<b>HF</b>	heart failure
<b>HIF<math>\alpha</math></b>	hypoxia induced factor alpha
<b>HRE</b>	hypoxia responsive elements
<b>HSP70</b>	heat shock protein 70
<b>I/R</b>	ischemia/reperfusion
<b>ICaL</b>	L-type Ca <sup>2+</sup> current
<b>ICU</b>	intensive care unit
<b>ID</b>	intercalated discs
<b>IJM</b>	imageJ macro language
<b>IL</b>	interleukine
<b>iNOS</b>	nitric oxide synthase
<b>IP3</b>	Inositol trisphosphate

<b>iPSC</b>	induced pluripotent stem cells
<b>ISO</b>	isoproterenol
<b>Ito</b>	transient outward K <sup>+</sup> current
<b>LDH-<math>\alpha</math></b>	lactate dehydrogenase-alpha
<b>LMS</b>	living myocardial slices
<b>LTCC</b>	L-type Ca <sup>2+</sup> channel
<b>M199</b>	Medium 199
<b>MAMs</b>	mitochondrial associated membranes
<b>MCU</b>	mitochondrial Ca <sup>2+</sup> uniporter
<b>MEA</b>	multielectrode array
<b>MES</b>	mechano-electric response
<b>MGC</b>	mechanically gated channels
<b>MHC</b>	myosin heavy chain
<b>mitoBKCa</b>	calcium-activated potassium channel
<b>MLC2</b>	myosin light chain
<b>MLP</b>	muscle specific LIM protein
<b>MMCs</b>	mechanically modulated channels
<b>MPTP</b>	mitochondrial permeability transition pore 3-(4,5-dimethylthiazol-2-yl)-5-(3-carboxymethoxyphenyl)-2-(4-sulfophenyl)-2H-
<b>MTS</b>	tetrazolium
<b>m<math>\Delta\Psi</math></b>	mitochondrial membrane potential
<b>NADH</b>	nicotinamide adenine dinucleotide
<b>NCX</b>	Na <sup>+</sup> /Ca <sup>2+</sup> exchanger
<b>Nf-K<math>\beta</math></b>	nuclear factor kappa beta
<b>NO</b>	nitric oxide
<b>NRF-1</b>	nuclear respiratory factor 1
<b>Nrf2rf2</b>	nuclear factor-like 2
<b>NRG-1</b>	neuregulin-1
<b>NRVMs</b>	neonatal rat ventricular myocytes
<b>NTA</b>	nanoparticle tracking analysis
<b>O<sub>2</sub></b>	oxygen
<b>O<sub>2</sub><sup>•-</sup></b>	superoxide radical
<b>OXPHOS</b>	oxidative phosphorylation

<b>PaO<sub>2</sub></b>	partial oxygen pressure in the blood
<b>PBS</b>	phosphate-buffered saline
<b>PCr</b>	phosphocreatine
<b>PDK</b>	1(pyruvate dehydrogenase kinase, isoform 1
<b>PETT</b>	polyethylene terephthalate
<b>PFA</b>	paraformaldehyde
<b>PGC1<math>\alpha</math></b>	peroxisome proliferator-activated receptor gamma coactivator 1-alpha
<b>PHDs</b>	prolyl hydroxylase domain enzymes
<b>PKA</b>	protein kinase A
<b>PLA</b>	polylactic acid
<b>PIGF</b>	placental growth factor
<b>PPAR<math>\alpha</math></b>	peroxisome proliferator-activated receptor alpha
<b>PV</b>	pressure-volume
<b>ROS</b>	reactive oxygen-species
<b>RXR</b>	retinoid X receptor
<b>RyR2</b>	ryanodine receptor 2
<b>SC</b>	spontaneous contractions
<b>SCR</b>	spontaneous Ca <sup>2+</sup> release
<b>SEC</b>	size-exclusion chromatography
<b>SEM</b>	standard Error
<b>SERCA2<math>\alpha</math></b>	sarcoplasmic Ca <sup>2+</sup> -ATPase 2 $\alpha$
<b>SL</b>	sarcomere length
<b>TATS</b>	axial tubules
<b>TCA</b>	tricarboxylic acid
<b>TdT</b>	terminal deoxynucleotidyl transferase
<b>TMRM</b>	tetramethylrhodamine, Methyl Ester
<b>TRP</b>	transient receptor potential
<b>TT</b>	t-tubules
<b>UV</b>	ultraviolet light
<b>VDAC</b>	a voltage-dependent anion channel
<b>VEGF</b>	endothelial growth factor
<b><math>\alpha</math>-SMA</b>	alpha smooth muscle actin



# Chapter 1 Introduction

Here, we will discuss the significance of translational models in cardiac preclinical research, and their advantages and disadvantages. We will summarize the aspects that *in vitro* models need to have in order to better recapitulate the *in vivo* conditions of the heart, with emphasis on mechanical load, cell metabolism and oxygenation. Finally, we will also explain the benefits of using living myocardial slices (LMSs) for *in vitro* studies, their so far development, and their possible utilization in various applications.

## **1.1 Cardiovascular models**

The processes involved in normal cardiac physiology or pathology are often difficult to unravel or interpret. Over the years, cardiac models have provided an important tool to better understand cardiac biology. The role of these models serves mainly three purposes: a) to define the important physiological processes and investigate how they are involved in the progression of disease, b) to develop new treatments and c) to test for drug safety and toxicity (Savoji et al., 2019). Indeed, accurate and relevant cardiac models are able to predict cardiac toxicity up to 70% at preclinical stage, while human clinical trials are still necessary to reveal long term adverse effects (Olson et al., 2000). In this section we will describe the current cardiac *in vivo* and *in vitro* models that have been developed, their applications and benefits - limitations.

### **1.1.1 *In vivo* models**

Animal models are one of the first research models used to study human physiology (Ericsson et al., 2013). Small animals like mice and rats have been extensively used, due to their easy handling and housing, short gestation time and cost-effective maintenance. The most important feature of them though, is that they can be genetically manipulated and provide a high throughput system in comparison to large animal models. Since genetic manipulation was developed in mice (Cre-Lox system), around the 1980s, these small rodents gained great

attention in cardiovascular research. The method was later developed in other animal species including rats (Orban et al., 1992), cats (Wongsrikeao et al., 2011) and dogs (Hong et al., 2009). However, these larger species were used less frequently, due to their longer reproductive cycle and life span. Genetic modification did not only allow to study the role of genes in pathophysiology but was also used to mimic cardiac diseases. Among others, mice that were engineered by deletion of the myofilament proteins, e.g. muscle LIM protein (MLP), showed signs of dilated cardiomyopathy in the first 4-6 months (Dos Remedios et al., 2003). Additionally, deletion of myosin-binding protein C, cardiac-type (cMyBP-C) showed development of hypertrophy which progressively resulted in heart failure (de Lange et al., 2013). Besides gene editing, diseased animal models have also been developed by altering the environmental conditions, administering pharmacological agents or applying injury during percutaneous or surgical procedures. A widely established method to mimic myocardial infarction in mice and rats is by coronary artery ligation. This method requires anaesthesia of the animal, surgical intervention and time for cardiac remodelling to occur, when heart failure progression is studied (Kumar et al., 2016). Similarly, hypertrophy can also be developed by ascending aortic banding in the heart (Barretti et al., 2017). Other environmental disease triggers include high fat (Calligaris et al., 2013) or salt diet (Tobian, 1991) to induce obesity or hypertension, respectively. Finally, pharmacological agents such as chronic administration of doxorubicin or isoproterenol also showed to induce heart failure due to drug toxicity or excessive  $\beta$ -adrenergic stimulation (Krennek et al., 2009; Lohse et al., 2003; Mitry and Edwards, 2016; Zhu et al., 2008).

Despite the wide use of small animal models, their main disadvantage is the relevance of the data acquired to humans, because of their distinct differences in cardiac architecture, heart rate, oxygen consumption, contractility, protein expression and genetic background (Hamlin and Altschuld, 2011). More relevant models can be seen in larger mammals such as dogs, pigs, and

sheep. Studies in dogs have shown to be more relevant to human physiology and disease development. In dogs heart disease can be either induced as described above or can derive endogenously in specific canine breeds. Arrhythmogenic right ventricular cardiomyopathy (ARVC) can often be seen in Boxers, with high levels of arrhythmic events, histological changes, fat tissue replacement and high occurrence of sudden cardiac death (Basso et al., 2004), while dilated cardiomyopathy is prominent in Golden Retrievers (Tsang et al., 2016). Pigs are also widely used for their similarities to human heart size and arterial anatomy, without excessive collateral coronary circulation which is often a problem in canine models (Lelovas et al., 2014; Yoran et al., 1982).

Despite the benefits and relevance to human biology, large mammals are costly, impose several ethical restrictions, they are not ideal for genetic modification and provide a low throughput model that requires specialised facilities and staff. For these reasons, *in vitro* models were developed for studying human disease by using tissue culture, tissue engineering, and biochemical assays.

### **1.1.2 *In vitro* models**

#### **1.1.2.1 *Ex vivo* heart tissue**

*Ex vivo* heart preparations including papillary muscles, cardiac wedges or whole hearts have had a central role in cardiac research. Multiple studies evaluated the role of cardiac mechanics (De Tombe and Little, 1994; Hibberd and Jewell, 1982), and electrophysiological changes upon pharmacological stimulation (Chen et al., 2006). However, many of these preparations require a sophisticated perfusion system or Langendorff devices to support cardiac viability. These experimental set ups usually allow a limited number of samples, e.g. one heart per Langendorff device, which significantly limits the throughput of the model. Additionally, these models can only be kept for acute studies since their viability and contractility significantly

drops after only a few hours (Bell et al., 2011; Kappler et al., 2019; Fotios G Pitoulis et al., 2020).

### **1.1.2.2 Primary isolated cells**

Isolated primary cells, cell lines or pluripotent stem cell-derived cardiomyocytes (induced iPSC-CMs or embryonic ESC-CMs) are the main sources of cardiac cells to study *in vitro*. Primary cardiac cells were first cultured over 100 years ago (Burrows, 1912; Mitcheson et al., 1998) and they are still widely used. Cardiac cell isolation includes an enzymatic digestion of the tissue usually by applying collagenase, in order to disintegrate the extracellular matrix (ECM) and release the cells in the culture medium. Next, these cells are cultured on flat culturing containers (flasks or petri dishes), treated with ECM proteins for cell adherence.

Primary isolated cells can be obtained from either healthy or diseased human or animal sources, allowing the study of functional and molecular differences between the two, and helping to identify potential therapeutic targets. They also provide a medium throughput platform where one heart can provide multiple cells which can later be split in many different conditions. Most importantly, primary isolated cells can derive from fully mature animal hearts or human hearts which better recapitulate human physiology and have higher translational potential. Despite their many benefits, primary isolated cardiomyocytes have been known for quickly de-differentiating during culture, losing their mature phenotype and their rod shape, developing plasma membrane extensions like filopodia, and expressing foetal genes including c-kit (often present in progenitor cells) and GATA-4 (Mitcheson et al., 1998; Zhang et al., 2010a). These changes can occur hours after cell plating and thus the cells are used within the first 1-3 days upon isolation (Bird et al., 2003; Li et al., 2014). Similar changes have also been seen in other cardiac cell types such as fibroblasts. Fibroblasts often turn into myofibroblasts in culture, a

phenomenon usually seen under pathological conditions, followed by enhanced ECM secretion, tissue stiffening and  $\alpha$ -smooth muscle actin ( $\alpha$ -SMA) expression (Hinz et al., 2004).

### **1.1.2.3 Cell lines**

Cell lines, on the other hand, are immortalised cells that offer great availability, unlimited expansion capacity, have standardised genetic composition and behaviour, and are easy to use (Pan et al., 2009). Common cardiac cell lines can be found for fibroblasts, smooth muscle cells, endothelial cells and cardiomyocytes. Usually the development of these lines requires immortalisation, which means that cells have to be genetically modified or be derived from proliferative tumour tissue (Davidson et al., 2005). These cells do not fully represent the *in vivo* cardiac physiology and often deviate from the normal function and structure of the cardiac cells (Pan et al., 2009).

### **1.1.2.4 Induced pluripotent stem cell - cardiomyocytes**

Finally, the development of induced pluripotent stem cell cardiomyocytes (iPSC-CMs), paved the way for new regenerative and drug testing studies. In this method, donor specific somatic cells can be reprogrammed into a state of pluripotency by expressing key transcriptional factors such as Oct4, Sox2, cMyc, and Klf4 (Gonzalez and Huangfu, 2015; Takahashi and Yamanaka, 2006). These cells can then be differentiated into any somatic cell of interest. This methodology was firstly published in 2006 and has been extensively used, accounting for more than 24000 citations (Takahashi and Yamanaka, 2006) to date. iPSCs are an important tool for regenerative medicine, since the technology could resolve tissue compatibility problems by acquiring cell material from the same patients and expand them in adequate numbers for tissue regeneration purposes (Medvedev et al., 2010). This high throughput model is also useful to model disease *in vitro*, by acquiring cells (e.g. skin fibroblasts) from patients with cardiac

disorders. These cells can be turned into iPSC-CMs while retaining their disease genetic profile.

At the beginning of their discovery, iPSCs gave great hope for organ regeneration and tissue replacement, attracting the interest of many fields including the cardiac field. Soon, the scientific community realised that this was a more complicated task, which required further investigation of cell differentiation to reach full maturity, which was difficult to achieve in many tissue types (Gherghiceanu et al., 2011). Unfortunately, in the cardiac field, iPSC-CMs were also lacking the adult cardiac phenotype with underdeveloped contractile and electrical apparatus, neonatal morphology and foetal gene expression (Feinberg et al., 2013; Goversen et al., 2018). iPSC-CMs are usually mononucleated in comparison to CMs and their shape is different, with round morphology and limited anisotropy (Denning et al., 2016; Yang et al., 2014a). The immature structural phenotype is also followed by disorganised sarcomeres with short sarcomere length and reduced levels of important structural proteins, including myosin heavy chain (MHC6-7) and titin (Denning et al., 2016). Along with the disorganised sarcomeres, other cellular structures are underdeveloped including the sarcoplasmic reticulum, the ion channel transporters and the mitochondrial organisation, which all resemble a neonatal phenotype (Savoji et al., 2019). In iPSC-CMs the low levels of SERCA, inward rectifier potassium current (IK1) and connexin 43 alter the action potential morphology and reduce the conduction velocity (Goversen et al., 2018; Pesl et al., 2017; Veerman et al., 2017). Additionally, the reliance of the cells on glycolysis instead of fatty acid oxidation is another indication of their immature function. Mitochondria are usually underdeveloped and small in size, localised around the nucleus (perinuclear), with lack of intrafibrillar and subsarcolemmal localisation that is always present in adult CMs (Jiang et al., 2018; S. Li et al., 2018).

To overcome this problem, soon it was recognised that other elements besides gene expression were necessary for iPSC-CMs maturation. Co-culturing (Tulloch et al., 2011), metabolic

triggering (Feyen et al., 2020), oxygenation (Ward and Gilad, 2019) and mechano-electric stimulation (Black et al., 2009) are some of the most important environmental cues to enhance cell maturation in cardiomyocytes. The addition of triiodothyronine (T3) (Yang et al., 2014b), ascorbic acid (N. Cao et al., 2012) and neuregulin-1 $\beta$  (Zhu et al., 2010), significantly improved cell maturation. Electrical stimulation was also found to significantly improve sarcomere structure by increasing the sarcomere length to 2.2 $\mu$ m, increasing mitochondrial density by 30% and enhancing the presence of transverse tubules (Ronaldson-Bouchard et al., 2018).



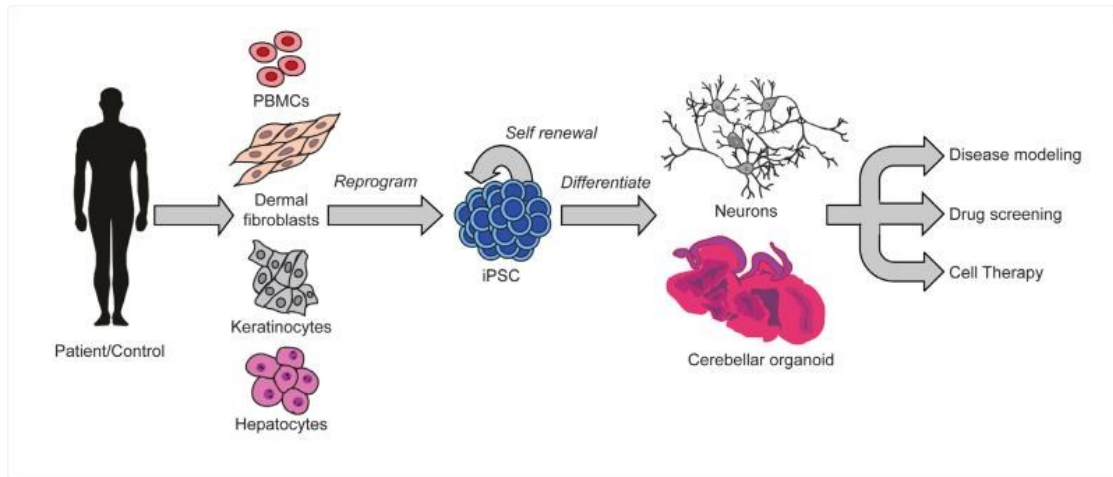


*Figure 1.1-IPSC technology. These cells can derive from somatic human cells and reprogrammed to a pluripotent state. Pluripotent cells can be then expanded in high cell numbers and differentiated in any cell type including cardiomyocytes. This technology is a useful tool for disease modelling, drug screening and regenerative therapies. Figure adjusted from (Bedada et al., 2016)*

### **1.1.2.5 3D *in vitro* models**

To better simulate the *in vivo* anatomical structure and apply mechanical load, iPSC-CMs were cultured in a 3D environment. There were 4 main approaches used for this purpose: 1) Cells encapsulated in hydrogels (Zimmermann et al., 2006, 2002), 2) cells attached in pre-fabricated structures (Macqueen et al., 2018), 3) cells attached on decellularized native ECM (Ott et al., 2008), and 4) stacking of 2D cell sheets to create tissue layers (Shimizu et al., 2003). The most popular 3D structure was developed in 1997 (Eschenhagen et al., 1997) with the embedding of cardiac embryonic cells in a collagen mixture that solidified between two fixed probes. This method allowed the fabrication of engineered heart tissues (EHTs). After culture, the EHTs could be transferred on a force transducer so that force measurements and functional evaluation could be applied. This methodology was further improved by fabricating EHTs on flexible silicon posts that could bend upon tissue contraction and provide mechanical afterload to the cells. This model could better mimic the native myofilament alignment and respond to a number of pharmacological interventions (Schaaf et al., 2011).

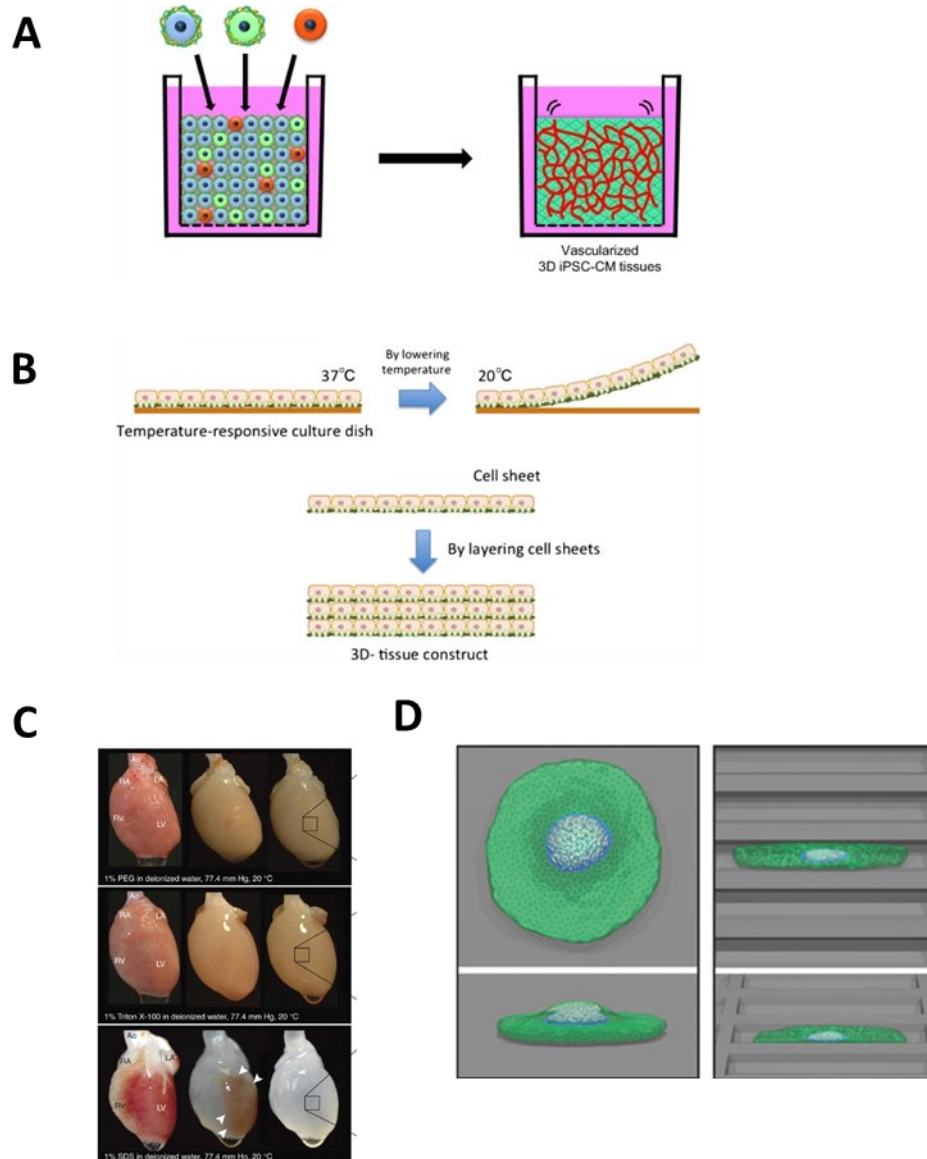







Figure 1.2- 3D iPSC-CMs models. A) Cells encapsulated in hydrogels (Amano et al., 2016). B) Cell sheet technology (Masuda and Shimizu, 2016). C) Application of cells on decellularized tissue (Ott et al., 2008). D) Culture of cells on prefabricated/patterned surfaces (Masuda and Shimizu, 2016).

The EHTs hold promise for drug testing and treatment applications; however, they cannot fully acquire the adult mature phenotype seen *in vivo*. Along with their immature phenotype, the model needs to be better optimised to support cell viability throughout the whole tissue, the thickness of which can range from mm-cm (Nguyen et al., 2019). Efforts to improve nutrient and oxygen diffusion are made by incorporating endothelial cells in the EHT, which can form tubes. In another report, the fabrication of EHTs with increased surface area within the EHT, can improve oxygen and nutrient diffusion in the inner parts of the hydrogel (Majid et al., 2020). Additionally, one difficulty for fabricating EHTs is that they require big cell numbers, that are usually difficult to acquire or expensive to produce, since they require complex bioreactor systems (Huang et al., 2018). The perfect model that fits all types of studies does not exist and the choice of model should depend on the experimental question and design (Table 1). However, there is a constant effort to optimise and improve the experimental models, especially their relevance to the native *in vivo* environment. Recently, increased emphasis has been given on models that can recapitulate the *in vivo* cardiac multicellularity (Wang et al., 2018), ECM composition (Pagliarosi et al., 2020), electromechanical stimulation (Santoni et al., 2018), and cardiac metabolism (Feyen et al., 2020). The importance and application of these elements in different culturing systems will be discussed in the following sections.

Table 1.1- Strength and limitation of different in vitro models. “+” indicates a beneficial impact of the model compared to other, whereas “-” indicates disadvantageous impact of the model compared to others. Table adjusted from (Fotios G Pitoulis et al., 2020).

Features	Isolated myocytes	Papillary muscles	Whole-hearts	Engineered heart tissue	Myocardial slices
					
Proximity to in vivo cardiac operation	+	++	++++	++	+++
Throughput	++++	+	-	++	+++
Causality degrees	++++	++	++	++	++
Cost	+++	++	-	+	+++
Capacity for long term experiments (culture)	+	++	-	++++	+++
Personalized assays	-	-	-	+++	-

## 1.2 Living myocardial slices

One of the recently emerged models that are closer to the *in vivo* heart physiology is the living myocardial slices (LMSs). LMSs are finely cut ventricular tissue sections of 200-400 $\mu$ m thickness that are produced using vibrating microtomes that allow only minimal tissue damage. This methodology results in an *in vitro* model of intermediate complexity with preserved multicellularity, structural, electrophysiological, metabolic and functional properties (Camelliti et al., 2011a; Kang et al., 2016; Wang et al., 2015). Camelliti *et al.*, 2011b showed that LMSs produced from humans had normal electrophysiological responses with conduction velocity, transmembrane potential and calcium transients similar to the ones seen in whole hearts. LMS metabolism remained stable during culture with increased glycolysis and glucose oxidation (Camelliti et al., 2011b).

### 1.2.1 Development of the model

Living tissue slices were firstly described 70 years ago with the technology having already been used in organs such as the brain, kidney and lungs (Bauer et al., 2000; Burdette and Wilhelmi, 1946; Crain, 1966). In the heart the first reported case of cardiac slices came out in 1946, with the aim of studying oxygen consumption under haemorrhagic shock in the presence or absence of different metabolic substrates (Burdette and Wilhelmi, 1946). Since then, several reports were published using this technique under the name of heart slices (Kaneko et al., 2012a), organotypic slices (Brandenburger et al., 2012a; Habeler et al., 2009b; Kang et al., 2016), precision cut slices (Bussek et al., 2009; Ruegg, 1994) or left ventricular myocardial slices (Wang et al., 2014; Yamashita et al., 2004a; Yasuhara et al., 1996). Regardless of their name, the idea behind the research model was the same: to section the cardiac tissue in thin pieces and allow for short- and long- term experimentation. In the beginning, this idea was vaguely shaped, and studies used a wide range of cutting techniques such as manual tissue

cutting or utilised more sophisticated equipment, the microtomes. This had as a result the production of slices with variable tissue thickness and with ambiguous O<sub>2</sub> diffusion in the core of the tissue. This issue was soon resolved when studies showed that tissue thickness of approximately 300µm was adequate to provide oxygenation to the inner layers of the slices (Biochemistr et al., 2007; Carmeliet and Jain, 2000; Yamashita et al., 2004a). Inconsistencies in slicing orientation added another variable to this technique. Transverse slicing (perpendicular to the long ventricular axis of the left ventricle/across the endo- and epicardium) was a useful tool to study transmural changes within the same slice (He et al., 2019; Wen et al., 2018); however, according to later findings on the cardiac fibre orientation, it was shown that transverse slicing transected the fibres and decreased cell viability (Buckberg and Hoffman, 2014; Sengupta et al., 2006). This happens because, the muscle fibre orientation of the left ventricle changes gradually from a right-handed helix in the sub-endocardium to a left-handed helix in the sub-epicardium. Unlike the transmural change in fibre orientation, cardiomyocytes are always aligned in parallel to the epicardial surface and to each other in organised fibre bundles (Fig 1.3). Therefore, cutting the slices in the epicardium-tangential plane is the best method to minimise tissue damage. Indeed, viability experiments by our lab, showed that less than 3% of total cells are damaged, with most of them residing on the surface of the slice (Watson et al., 2017).

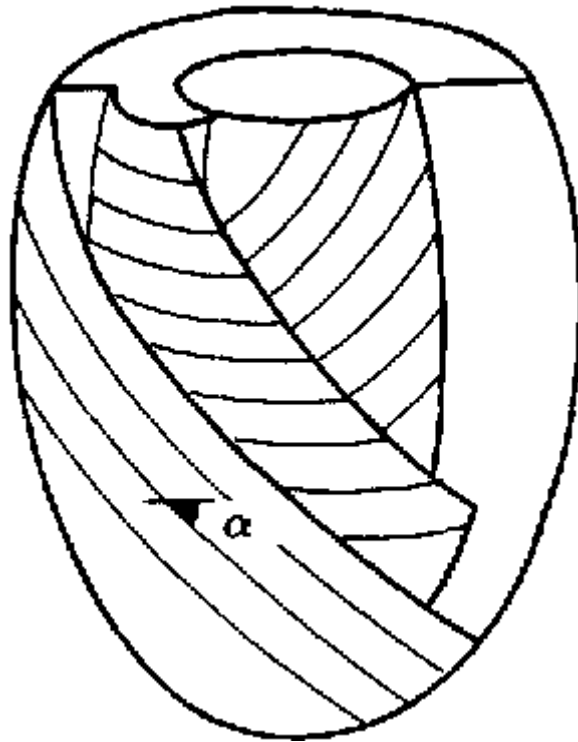


*Figure 1.3- Graphical representation of cardiac fibre distribution in the left ventricle. Cutting the heart across the ventricle would cause increase cardiac damage in comparison to cutting along the fibres, following the fibres' orientation. Image adjusted from (Bovendeerd et al., 1992).*



### 1.2.2 LMS culture

Similar to other *ex vivo* tissue preparations, LMSs were vastly used for short term experiments. The model was initially used to study tissue metabolism with regards to oxygen consumption in the presence of SERCA blockers (Thapsigargin) (Takaki et al., 1998) and investigating myocardium aging and its sensitivity to glycosides using radiolabelled substrates (Katano et al., 1984). Electrophysiological studies of the LMSs showed electrical stability of the freshly prepared slices, using patch clamp recordings in new-born rat hearts (Bnrnashev et al., 1990). Multielectrode arrays and fluorescent dyes validated these findings in adult human, rodent and pig LMSs (Borile et al., 2014; Brandenburger et al., 2012b; Camelliti et al., 2011a; Pillekamp et al., 2007; Wang et al., 2014).

Prolonged culture of the LMSs was attempted by a number of different methodologies, which all tried to fulfil the same aim: to provide adequate oxygenation to the LMS. Among others, the rolling tube and the shaken well plate were two of the most popular ones (Morin et al., 1999; Olinga et al., 1997). However, the big breakthrough was made in 1991 with the development of the liquid interface method. In this method the slice is placed on a semi-porous membrane and on top of a well plate. The wells are filled with media so that the slice can absorb nutrients from the bottom of the well and oxygen from the top (Habeler et al., 2009a; Stoppini et al., 1991) This technique was initially developed for brain slices, but it was later adapted for other systems, such as the heart (Brandenburger et al., 2012c; Kaneko et al., 2012b; Kang et al., 2016; Thomas et al., 2016). This method proved to better preserve slice viability and gained popularity because it was also an easy, practical and cost effective technique (Stoppini et al., 1991). Despite its wide popularity, it was later shown to result in significant reduction of contractility (Brandenburger et al., 2012b; Perbellini et al., 2017), increased proliferation of stromal cells and cardiac de-differentiation followed by loss of sarcomeric proteins (MLC2) (Brandenburger et al., 2012a).

One of the most important missing elements of the liquid interface system was that the LMS remained unloaded and without electrical stimulation. As in other *in vitro* studies, such as in iPSC-CMs engineered heart tissues, electromechanical stimulation was shown to increase cell maturation, as seen by improvements of cell structure, myofilament anisotropy, active force and electrophysiologic function (increase of SERCA2a and (Morgan and Black, 2014), ion channel KCNJ2 gene expression (Jiang et al., 2018). In these models, the EHTs were fixed in flexible posts of variable elasticities that could directly affect myocardial maturation (Mannhardt et al., 2016). In case of the adult LMS, mechanical stimulation was induced by using custom-made adjustable stainless-steel stretchers that could be used to vary the length of the LMS. The percentage of LMS stretch was determined by measuring the SL using the laser diffraction method (Watson et al., 2019). The use of stretchers allowed control of the cardiac preload but kept the afterload constant so isometric contraction was obtained. In other systems, as described by Fischer *et al* (Fischer et al., 2019), the use of a flexible spring on one side of the LMS could provide afterload, but the preload could not be precisely regulated. In both cases though, cardiac viability and contractility were preserved for up to 3 days in rodents and up to 5 days in rabbits (Watson et al., 2019), whereas in human tissue contractility was preserved for up to 4 months (Fischer et al., 2019) (Fig 1.4).

In the last decade, LMS technology has been greatly improved, allowing long term culture of adult cardiac tissue, with preserved contractile and electrical function (Fotios G Pitoulis et al., 2020). This was a big achievement since long term culture of isolated CMs always resulted in de-differentiation after the first days of plating, a condition followed by a decrease in maturation, increase of foetal gene expression and loss of function (Zhang et al., 2010b). This advancement on adult cardiac tissue culture paved the way for successful drug discovery and toxicity testing on human healthy or diseased samples, making the model an excellent translational tool (Kang et al., 2016; Meyer et al., 2010; Fotios G Pitoulis et al., 2020).

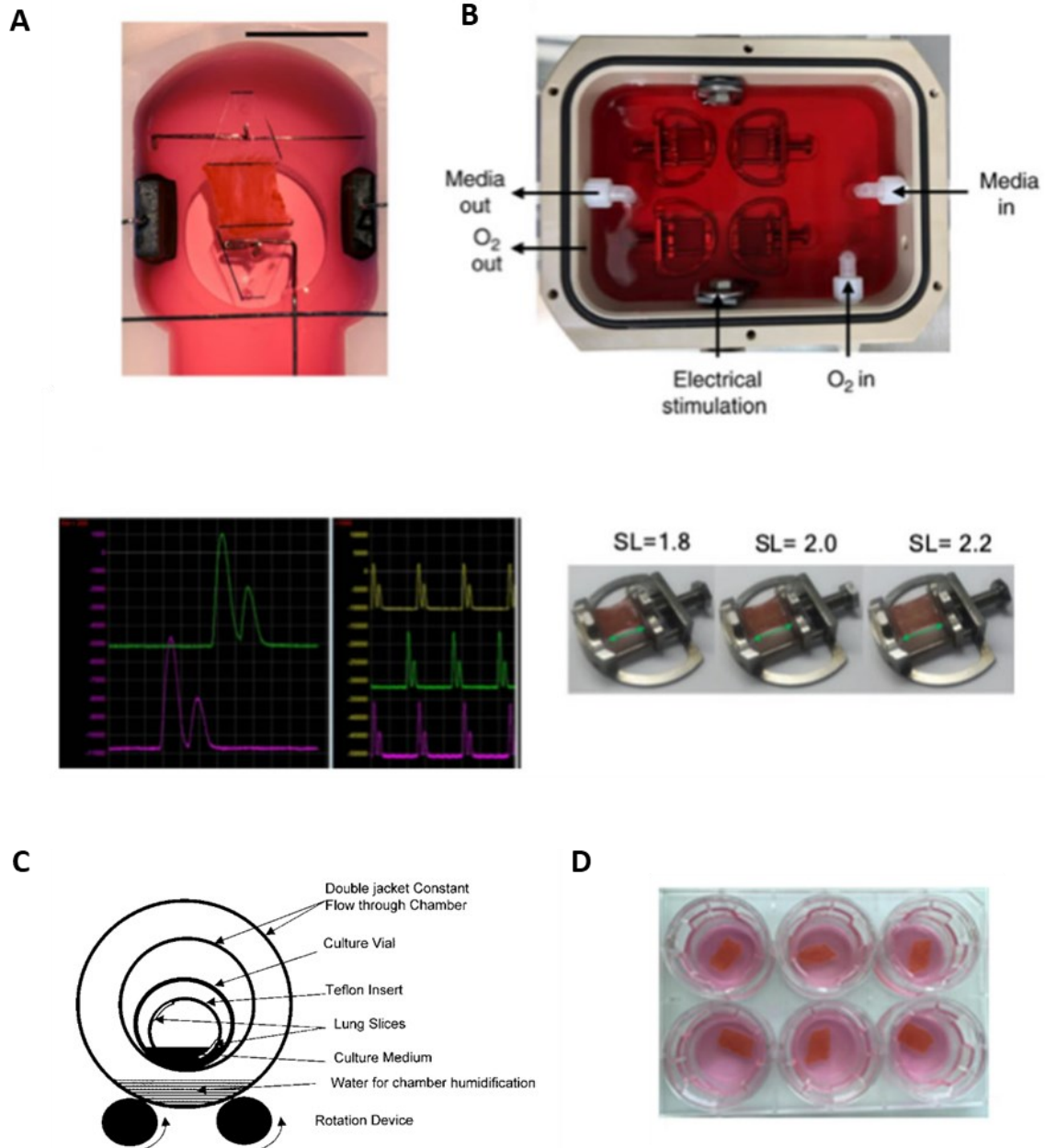


Figure 1.4-LMS culturing systems. A) Chamber culturing system with flexible posts developed by Fischer et al. (Fischer et al., 2019). B) Chamber culturing system with LMSs on stretchers with fixed posts, developed in our lab (Watson et al., 2019). C) Rolling tube system where the slice is temporarily exposed to the media and oxygen as the tube rotates. (Morin et al., n.d.). D) Liquid interface system, where the slices are exposed in the air for oxygen and the media (bottom) for nutrient absorption (Watson et al., 2019).

## 1.3 Applications of LMSs

### 1.3.1 Extracellular vesicles

So far LMSs have been used in a number of studies, investigating human electrophysiology, metabolism and cardiac contractility. Another field that was also explored was the application of embryonic cell transplantation on heart slices and their regenerative potential. Interestingly, cell transplantation of embryonic cells on mice/rat/human neonatal heart sections showed structural integration after 1-2 months of culture (Habeler et al., 2009b, 2009a). Nowadays, regenerative attempts of cell transplantation have shown to increase cardiac function, but with minimal cell retention (Hong et al., 2014). This increase in function cannot derive from the newly transplanted cells and therefore it was suggested that paracrine secreted factors of the transplanted cells were the reason of functional improvement such as cell proliferation (vasculature) and reduction of inflammation (Nakanishi et al., 2008; Van Den Akker et al., 2013). Apart from hormones and neurotransmitters, the cells secrete various types of membrane vesicles, called extracellular vesicles (EVs). Initially these vesicles were believed to be just waste carriers; however, they were later proven to have more diverse functions. EVs carry a variety of cargo ranging from proteins and lipids to DNA and miRNAs. The secretion of EVs is conserved throughout evolution from more simplistic organisms such as bacteria to plants and humans (Deatheragea and Cooksona, 2012; Robinson et al., 2016; Schorey et al., 2015) and they act as signalling agents in either normal or pathological processes (Colombo et al., 2014; Lo Cicero et al., 2015; van Niel and Raposo, 2018).

The exact EV content, mechanism of action and cell target are yet to be determined, since there is little information on how they exert their actions on the heart. So far, studies have shown that exosomes derived from cardiac progenitor cells (CPCs) have an antiapoptotic role when administered *in vitro* (Chen et al., 2013; Youn et al., 2019) or *in vivo* after ischemia/reperfusion

in rodents (Agarwal et al., 2017). Other studies emphasise that CPCs EVs enhance endothelial cell proliferation and tube formation (Agarwal et al., 2017; Vrijssen et al., 2016b; Youn et al., 2019), while CPCs EVS have also been shown to decrease scar formation (Smith et al., 2007).

The majority of these studies have been performed on monocultures of either cardiomyocytes or endothelial cells, but no studies on multicellular preparations have been conducted *in vitro*. LMSs could provide an ideal multicellular platform to test EVs and their global effect on cardiac tissue, since both molecular and functional assessments can be performed on this model.

### **1.3.2 *In vitro* model of local injury**

Several models have been used to mimic cardiac pathology *in vitro*, especially myocardial infarction. One of the most common models is the ischemia/reperfusion (I/R) model that uses healthy cells in culture in the absence of oxygen and glucose (Chen and Vunjak-Novakovic, 2018). Models focusing on hypertrophy by activating different oncogenes such as c-fos, c-myc, c-jun, and Egr-1, or heat shock proteins (HSP70), result in overexpression of hypertrophy-inducing genes such as ANP, BNP, and  $\beta$ -MHC (Rysä et al., 2018). Pharmacological induction of hypertrophy utilises agents such as phenylephrine (Jain et al., 2018), angiotensin II (Gélinas et al., 2018), noradrenaline (Güven, 2018), endothelin-1 (Spannbauer et al., 2019), and isoproterenol (Zlabinger et al., 2019). Finally, more recent methods are based on iPSC-CMs technologies with cells derived from heart failure patients.

All the above examples describe interventions that affect cell populations in separate wells and therefore different conditions are present in different samples. In the *in vivo* environment though, changes occur in the same heart where healthy and necrotic tissues coexist and interact with each other (Janse et al., 1979). This is of great importance, since it has been shown that areas with intermingled healthy and diseased cells are the epicentre of disease development as

seen in the border zone (BZ) upon ischemia (Picard et al., 1999). This area is characterised by high heterogeneity levels of healthy and diseased cells, an area which progressively remodels and gives rise to excessive fibrosis and contributes to heart stiffening (Kung et al., 2018; Myerburg et al., 1977).

A smart model to study spatial changes in cardiac function was developed in zebrafish and was based on the local tissue damage using freezing probes (Chablais et al., 2011a; Yu et al., 2018). This cryoinjury model was initially developed in order to control infarct size and better monitor heart healing and regeneration. The same strategy was adopted by many others working in regenerative medicine and applied to either zebrafish or small mammals like mice (Smith et al., 2007; Ewout J Van Den Bos et al., 2005a). Results from these studies showed great reproducibility of infarct size, induction of fibrosis, fibroblast activation and reduction of cardiac function similar to that seen in experimental animals of coronary ligation (Chablais et al., 2011b; González-Rosa et al., 2011a; Ewout J Van Den Bos et al., 2005a). Even though the technique has been primarily used *in vivo*, there was an attempt in 2017 to replicate it *in vitro* by using cardiac organoids to study cardiac regeneration on immature heart tissues (Holly K Voges et al., 2017). The reproducibility of infarct size, the similar cellular response seen *in vivo*, and the cost-effective manner of inducing tissue damage makes the model a great choice to use with LMS. Cryoinjured LMSs can provide a high-resolution *in vitro* model where microscopic electrophysiological changes can be measured together with functional changes in contractility, along with further structural characterisation.

### **1.3.2.1 Local injury and CamKII activation**

Recently, cryoinjured hearts have also been used as models to better understand heart electrophysiology upon cell death. Cryoinjury induces  $\text{Ca}^{2+}$  alternans initiation in injured hearts, with high prevalence in the BZ area (Tomek et al., 2019). It is well established that  $\text{Ca}^{2+}$

is one of most important second messengers in the heart and changes in the intracellular  $[Ca^{2+}]$  can lead to acute or chronic changes in cardiac function (Maier and Bers, 2002). Increase of  $[Ca^{2+}]$  can affect various classes of  $Ca^{2+}$ -regulated enzymes, one of which is the  $Ca^{2+}$ /calmodulin-dependent protein kinase (CaMK) family (Braun and Schulman, 1995). These are serine-threonine kinases that are regulated by the  $Ca^{2+}$  ligand calmodulin (CaM). They are expressed in various tissues, with CamKII being ubiquitously expressed at high levels in neuronal areas (Sovari, 2016). Activation of CamKII is regulated by increased levels of  $Ca^{2+}$ , oxidative stress and glucose, resulting in hypertrophy, E-C coupling changes, arrhythmias, cell death and heart failure (Pellicena and Schulman, 2014; Zhang and Brown, 2004). Its ability to phosphorylate a wide range of ion transporters such as RyR, phospholamban, SERCA2a, and L-type calcium channels makes it a potent target for treatment or regulation in the myocardium (Peuch et al., 1979; Simmerman et al., n.d.; Xu et al., 1993) Inhibition of CamKII by using inhibiting peptides and genetically modified cells or animals improves cardiac function with respect to inflammation (Weinreuter et al., 2014), arrhythmogenicity (Weinreuter et al., 2014) and apoptosis (Vila-Petroff et al., 2007). In order to better understand how tissue damage affects arrhythmogenicity on LMS, a CamKII inhibitor could be used in the cryoinjured model.

## 1.4 Recapitulate the *in vivo* environment in *in vitro* models

Despite the improvements of the LMS model, there are still limitations that need to be overcome, before application of different treatments. LMS loss of function in culture is still one of the main pitfalls of the model; such loss of function usually occurs after a few days in culture in our system and therefore it is important to be further optimised. The most successful way to functionally preserve the LMSs *in vitro* is by providing all the necessary environmental conditions that are present *in vivo*, a strategy that was also adapted in an effort to mature the iPSC-CMs. Therefore, in the following sections we will discuss the importance of electrical stimulation, mechanical load, metabolism and *in vitro* oxygen regulation. These factors are chosen as potential contributors for LMS preservation in culture.

### 1.4.1 Electrical stimulation

*In vivo* excitation contraction is a process initiated in the sinus node from specialised pacemaker cells with high automaticity. These cells can self-initiate depolarization in a rhythmic fashion, which is then propagated through the atrioventricular node, His bundle and Purkinje fibres to reach the rest of the atria and ventricles. Without external electrical triggering the cells in atria and ventricle cannot initiate contraction in physiological conditions. The cardiomyocyte anisotropy, continuous network and presence of gap junctions also contributes to the heart's conduction system (Kléber and Rudy, 2004).

In most of the *in vitro* systems, the presence of pacemaker cells and/or native cell organisation are missing (Ruan et al., 2016). Hence, external excitation is provided through field electrical stimulation, that is able to depolarise the cells (membrane potential becomes less negative) (Fried et al., 2009). Depolarisation of the cardiomyocytes initiates the action potential by activating a number of ion channels. In short, the action potential begins with the rapid influx of  $\text{Na}^+$  in the cell, followed by the opening of voltage-gated L-type  $\text{Ca}^{2+}$  channels (Santana et



al., 2010; Shih, 1994). This initial  $\text{Ca}^{2+}$  entry in the cells is adequate to activate the intracellular  $\text{Ca}^{2+}$  stores in the sarcoplasmic reticulum, by opening the ryanodine receptors RyR. Opening of the RyR leads to further  $\text{Ca}^{2+}$  release, which completes the so-called mechanism of  $\text{Ca}^{2+}$  induced  $\text{Ca}^{2+}$  release (CICR) (Woodcock and Matkovich, 2005). The big increase in cytoplasmic  $\text{Ca}^{2+}$  can activate the myofilaments by binding to troponin C and initiate contraction (Williams et al., 1992). Removal of  $\text{Ca}^{2+}$  can occur via different mechanisms including the sarcoplasmic reticulum  $\text{Ca}^{2+}$  ATPase (SERCA) (Bers et al., 2003) and  $\text{Na}^+/\text{Ca}^{2+}$  exchanger (NCX) (Hilgemann, 2004).

Providing the right combination and level of these stimuli to *in vitro* models and in particular to iPSC-CMs has been previously shown to be beneficial and improve cell maturation (Maroli and Braun, 2020). Electrical field stimulation on iPSC-CMs induced global excitation-contraction response and significantly improved cell differentiation, by upregulating cardiac specific genes including SERCA, Kv4.3 (potassium voltage-gated channel), alpha myosin heavy chain ( $\alpha\text{MHC}$ ), and Cx43 (Chan et al., 2013; Ma et al., 2018). In other muscle types such the skeletal muscle electrical stimulation also improved their function and reduced deterioration and muscle atrophy (Sheffler and Chae, 2007; Tandon et al., 2009).

As with other *in vitro* models the presence of pacemaker cells in LMSs is also missing. Therefore, external electrical stimulation is necessary to preserve the electrical and conduction system of the cardiomyocytes. Indeed, application of electrical stimulation could significantly improve viability and contractility in culture as shown by our lab and others (Fischer et al., 2019; Watson et al., 2017).

#### **1.4.2 Mechanical load**

Acute as well as prolonged responses to mechanical stimuli differ between healthy and diseased tissue. That can be seen in overloaded hearts with hypertension that exhibit cardiac dysfunction,

as well as in unloaded hearts that experience atrophy and loss of cardiac mass (Diakos et al., 2014; Oh and Cho, 2020). This contrast in mechanical responses shows that there is a fine balance between mechanical load and physiological function that needs to be preserved. In the LMS system, mechanical load was not considered as an essential culture element for tissue preservation, until recently, with the development of stretchers, bioreactor systems and new culture designs (Fischer et al., 2019; Perbellini et al., 2017; Watson et al., 2019). All of these methods tried to provide either preload or afterload in order to stimulate and preserve tissue function *in vitro* and prolonged the LMS culture time and tissue viability. Indeed, electromechanical stimulation managed to increase tissue viability, preserve contractility, metabolism and Ca<sup>2+</sup> handling. It also managed to preserve connexin 43 density and conduction velocity, with high electrical stability and reduction in arrhythmia presence *in vitro* (Watson et al., 2019). These functional changes were followed by preservation of tissue structures such as t-tubules, cell size and gene expression of key structural elements (Watson et al., 2019).

The importance of providing mechanical stimulation was also known in other *in vitro* systems. EHTs were also mechanically stimulated by placing them on flexible posts (increased afterload). This treatment showed to significantly improve the cell's structure and contractility (Machiraju and Greenway, 2019; Ruan et al., 2016). Additionally, plating the iPSC-CMs on ECM with variable elasticity and composition (changes in afterload) could also cause changes in cell maturation during development (Stoppel et al., 2016), which also affected mechanotransduction in cardiomyocytes, through integrin activation (Garoffolo and Pesce, 2019; Ruan et al., 2016).

The above observations clearly demonstrate the importance of mechanical load in many *in vitro* models; however, it is still not known what are the optimal mechanical conditions that enhance or preserve tissue maturation. To better understand mechanical load it is necessary to look at the acute and prolonged effect of mechanical load on cardiomyocytes.

#### 1.4.2.1 Mechanical stretch – acute responses

It was early recognised by Otto Frank and Ernest Henry Starling that mechanical load directly affects cardiac output, a mechanism that is known today as the Frank – Starling law or as the Heart law (Shiels and White, 2008). This theory explains how CMs respond to different preload conditions, whereby increase in muscle length (or ventricular volume) results in enhanced tissue contraction, a regulatory system that works on a beat to beat basis (Allen and Kentish, 1985; Fuchs and Smith, 2001). Along with the muscle stretch upon increased preload, the sarcomeres within the myofibrils are also stretched. The sarcomeres consist of thin and thick filaments that are bound to the z lines. The thin filaments are composed of three different types of protein: actin, tropomyosin, and troponin, while the thick filaments are comprised of myosin protein complexes (Sequeira and van der Velden, 2015). The sarcomere length (distance between two consecutive z lines) during rest in unloaded CMs is only  $\sim 1.8\mu\text{m}$  in healthy cells (Guccione et al., 1997). When the muscle is stretched, the distance between the thin filaments increases, while the double thin filament overlap progressively decreases (Shiels and White, 2008). When this overlap reaches SLs between  $2.0\text{--}2.2\mu\text{m}$ , then the muscle reaches the maximum active force, since longer SL reduces the myofilament overlap and decreases the active tension (Fig 1.5) (Gordon et al., 1966; Sequeira and van der Velden, 2015).

In many *in vitro* systems the SL or % of stretch is used as a way to define the preload conditions, since direct force measurements in culture are not always feasible. There have been many studies using this stretching method; however, there is not enough information on the physiological and pathological chronic stretching conditions that needs to be applied *in vitro* to mimic heart physiology or pathology in *in vitro* systems. This is very important since prolonged increase in mechanical load does not only have an acute effect on sarcomeres but it can also cause irreversible changes on cardiac function.

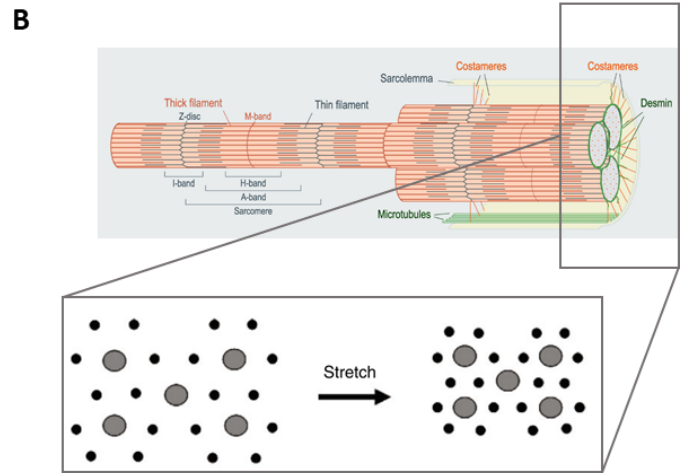
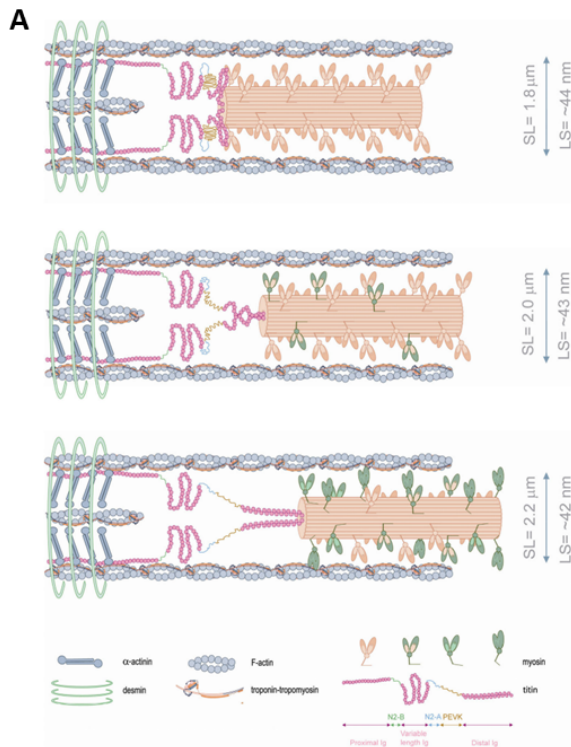


Figure 1.5- Schematic representation of sarcomeres. A) Structural changes in sarcomeres upon stretch (Sequeira and van der Velden, 2015). B) Myofilament lattice spacing theory, where increase of stretch brings the thin and thick filaments closer together (Shiels and White, 2008).

#### **1.4.2.2 Mechanical load – chronic adaptations in pathology**

Patients with chronic increase in cardiac load exhibit deleterious effects on their cardiac function. Patients with increased afterload, where the arterial pressure is elevated, initially respond with a compensatory release of catecholamines and other hormones to sustain cardiac function (Schirone et al., 2017), but later develop contractile, electrophysiological, metabolic, and structural abnormalities. Increased afterload (hypertension) in the heart, if untreated, often leads to hypertrophy, caused by cardiomyocytes adding new sarcomeres in parallel, and eventually results in concentric increase of ventricular mass (Grossman and Paulus, 2013). Hypertensive patients with increased ventricular preload can also experience cardiac death, which is associated with protein dysregulation/synthesis, resulting in accumulation of unfolded proteins, activation of the unfolded protein response and apoptosis (Dickhout et al., 2011). Hypertension is also associated with endothelial remodelling and permeabilization of the capillary wall, increase of cytokines and chemokines, which all contribute to the increase of inflammation (Ghigo et al., 2014). Finally, fibrosis is one of the most frequent adverse effects of hypertension, that affects cardiac structure and function (Berk et al., 2007). Activation of fibroblasts induces excess production of extracellular matrix proteins such as collagen I and II. Increased interstitial fibrosis, in turn, affects the tissue passive stiffness and rate of relaxation, and leads to impairment in diastolic function.

These structural and functional changes eventually lead to heart failure, where the heart is unable to employ the Frank-Starling mechanism due to loss of length-dependent activation. This observation has been seen both in humans and experimental models including dogs with congestive HF (Komamura et al., 1993) and spontaneously hypertensive rats (Hallbäck et al., 1975).

### **1.4.3 Metabolism**

Cardiac metabolism is essential for heart function and maturation. Changes in bioenergetics have been observed in a number of pathological conditions, with a decrease in energy production, accumulation of metabolites, substrate preference, mitochondrial dysfunction, and foetal metabolic switch in gene expression. Metabolic regulation has also been studied for the maturation of iPSC-CMs, with encouraging results when adult fatty phenotypes are adopted. Better understanding of the heart metabolism will provide valuable information for better regulating cell metabolism *in vitro* and preserve cardiac function and energetics.

#### **1.4.3.1 Metabolism in the healthy heart**

In the adult heart under normoxic conditions more than 95% of ATP derives from oxidative phosphorylation (OXPHOS) in mitochondria, while the rest 5% comes mainly from glycolysis. The majority of ATP, 60-70%, is being used to fuel tissue contraction and the remaining 30-40% for various pumps, especially SERCA (Barry, 2004; Ingwall, 2002). The heart either uses energy in the form of ATP, or stores energy in the form of phosphocreatine (PCr). With a smaller molecular weight, phosphocreatine can easily diffuse through the mitochondrial membranes and into the cytosol (Beer et al., 2002). Despite the storage of ATP as phosphocreatine, energy can be easily depleted upon continuous mechanical work in the heart. Therefore, cardiac function strongly depends on the continuous supply of ATP (Neubauer, 2007). The main substrate that is responsible for the majority of the total ATP production is fatty acids (FA). Full oxidation of FA account for 70-90% of the total ATP production, while next comes glucose, lactate and ketone bodies (Barry, 2004; Gertz et al., 1988; Wisneski et al., 1985). FA utilisation from the cells can be divided in 3 sections: FA uptake into the cytosol, FA transport in mitochondria and FA oxidation. Although FA can enter cells passively through a flip-flop mechanism (reorientation of lipids from one bilayer to the other in the membrane),

their active uptake is facilitated by transport proteins such as CD36 (Van Der Vusse et al., 2000). In the cytosol, free FAs are esterified to fatty acyl-coenzyme A (CoA) by carnitine palmitoyltransferase (CPT) I, located in the outer mitochondrial membrane, and then metabolised through the Krebs cycle and OXPHOS (Doenst et al., 2013; Van Der Vusse et al., 2000). One of the most abundant FA in the human body is palmitic acid accounting for 20–30% of total fatty acid in the body and can either be supplied from our diet or synthesised *de novo*. Besides metabolism and energy production, lipids also play an important role in membrane structure and are necessary for cell maintenance (Carta et al., 2017).

Glucose provides another substrate for ATP production which relies less on O<sub>2</sub> consumption. Glucose sources in cardiomyocytes can derive exogenously by active translocation through glucose transporters (GLUTs), including GLUT1 and GLUT4, or endogenously from glycogen stores (Aerni-Flessner et al., 2012; Dale Abel, 2004). Glycogen stores comprise <40% of glucose derived ATP in rats, making active transportation an important element in glucose ATP production (Henning et al., 1996). Upon uptake in the cytosol, glucose is rapidly phosphorylated to glucose 6-phosphate (G6P), which subsequently enters many metabolic pathways with a final conversion to pyruvate and production of NADH and a small amount of ATP. If pyruvate cannot enter mitochondria, then it gets converted to lactate in the cytosol and causes acidosis. In the presence of O<sub>2</sub> the pyruvate enters the mitochondrial matrix and gets oxidised into acetyl-CoA, which later enters the Krebs cycle to generate GTP (or ATP), CO<sub>2</sub>, and reducing equivalents of NADH<sub>2</sub> (Doenst et al., 2013). During glucose oxidation, the production of reducing agents of NADH<sub>2</sub> and FADH enter the electron transport chain for OXPHOS, producing high levels of ATP (Fig 1.6). Full oxidation of glucose or FA yield a different amount of ATP. Glucose oxidation results in 38 ATP molecules while utilising 6 O<sub>2</sub>, whereas FA (palmitate) can yield 129 molecules of ATP at expense of 31 O<sub>2</sub> (Lodish et al.,

2000). That means FA produce much more energy, but they are less efficient in O<sub>2</sub> utilisation, since they require more molecules to complete FA oxidation (FAO).



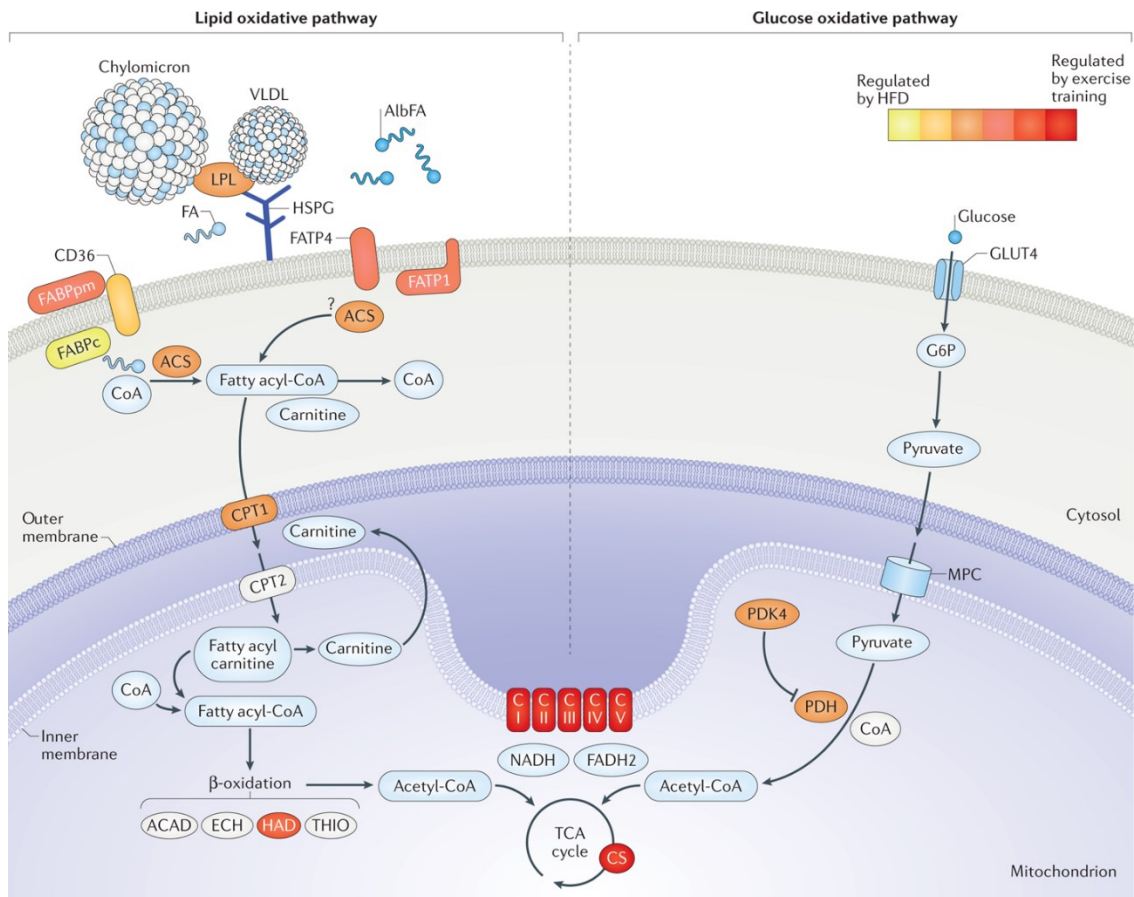


Figure 1.6-Substrate metabolism. Glycolysis occurs in the cytoplasm producing pyruvate which later enters mitochondria for fully oxidation. FA enter the cells either through diffusion or by transport proteins and transferred in the mitochondria where they undergo  $\beta$ -oxidation to enter in the Krebs cycle (TCA cycle) and later in OXPHOS (Fritzen et al., 2020).

### **1.4.3.2 Metabolism in heart failure**

It is well established that cardiac metabolism can be reprogrammed in response to pathological conditions and it is characterized by increased reliance on glucose consumption and a significant decrease in FAO (Doenst et al., 2013; Young et al., 2001). In small mammals, the shift from FAO to glycolysis is associated with downregulation of transcriptional factors for FAO and mitochondrial biogenesis, such as peroxisome proliferator-activated receptor alpha (PPAR $\alpha$ ) and peroxisome proliferator-activated receptor gamma coactivator 1-alpha (PGC1A) (Lehman and Kelly, 2002). These changes resemble a foetal metabolic profile in the heart, accompanied with transcriptomic changes in glucose transporting genes, PDK2 and PDK4, GLUT1, GLUT4, with upregulation of the neonatal form of glucose translocators GLUT1 and downregulation of the adult form GLUT4 (Razeghi et al., 2001). Under ischemic conditions both GLUT1 and GLUT4 are upregulated, followed by a 2-3 fold increase in glucose uptake (Szablewski, 2017). This reliance in glycolysis for ATP production is an important adaptation especially in heart failure caused by chronic ischemic cardiomyopathy where O<sub>2</sub> supply is limited (Burkhoff et al., 1991; Korvald et al., 2000). Metabolic changes in other types of cardiomyopathy, such as hypertrophy, are also seen, with ATP reserve reduction (PCr/ATP ratio), followed by further depletion as the disease progresses (Ingwall, 2008; Kolwicz et al., 2013; Liao et al., 1996; Neubauer, 2007).

### **1.4.3.3 Mitochondria in response to mechanical load**

As mentioned before, ATP production and utilisation is highly related to cardiac contractility. High efficiency of ATP transfer from mitochondria to sarcomeres is ensured by close apposition of the two organelles (Glancy et al., 2015; Vendelin et al., 2005). Apart from sarcomeres, mitochondria are in close contact with other important organelles, such as the sarcoplasmic reticulum, in areas that are called *mitochondrial-associated membranes*, or MAMs. MAMs are believed to be areas of ion regulation and Ca<sup>2+</sup> transfer that regulate

mitochondrial function and metabolism (Raturi and Simmen, 2013; Rutter and Pinton, 2014).  $\text{Ca}^{2+}$  entry in the mitochondria is associated with increased mitochondrial function and ATP production by activating key enzymes in the Krebs cycle (Gherardi et al., 2019).  $\text{Ca}^{2+}$  uptake in mitochondria is attributed mainly through the outer mitochondrial membrane via a voltage-dependent anion channel (VDAC), while the mitochondrial  $\text{Ca}^{2+}$  uniporter (MCU), located in the inner mitochondrial membrane, regulates  $\text{Ca}^{2+}$  transportation to the inner mitochondrial matrix (Tarasova et al., 2019). Even though the role of  $\text{Ca}^{2+}$  is well described in the cytosol in response to mechanical load, little is known of its role in mitochondrial mechanotransduction. In an effort to understand mitochondrial function and cell contractility Takaki *et al*, used contraction inhibitors, such as BDM (2,3-Butanedione 2-monoxime) and  $\text{Ca}^{2+}$  uptake inhibitors (by the sarcoplasmic reticulum), such as cyclopiazonic acid (CPA). They found that oxygen consumption during cell shortening is affected by  $\text{Ca}^{2+}$  handling, while smaller changes were observed when  $\text{O}_2$  consumption under inhibition of cross-bridge cycling was measured (Takaki et al., 1998; Yamashita et al., 2004b).

The role of mitochondria upon mechanical stimuli has also been highlighted in a study of isolated mitochondria from neural cells. In this study mechanical stimuli increased the opening probability of calcium-activated potassium channel (mitoBKCa) (Walewska et al., 2018). The channel has been identified in other cell types as well, such as in ventricular cells, rat skeletal muscle, and the brain (Frankenreiter et al., 2017; Kicinska et al., 2016; Paucek et al., 1992; Walewska et al., 2018).

#### **1.4.3.4 Metabolism in LMS**

LMS metabolism has not been thoroughly investigated. Reports on LMS metabolism have shown that the tissue has an active metabolic phenotype, with OXPHOS and glucose catabolism being evaluated (Camelliti et al., 2011c; Neri et al., 1984). However, there are

hardly any reviews on FAO. The first reports came out in 2019, with a focus on evaluating the metabolic status on several tissue slice models by using transcriptomic analysis on cultured slices. The study showed that after culture there was a decrease in the transcription of metabolic genes, in particular those that were implicated in FAO, such as the PPARs and LXR/RXR. These signalling pathways are implicated in FA uptake and metabolism and are key regulatory elements in the heart (Bigaeva et al., 2019).

With respect to LMS mitochondria, there were also very limited studies investigating the morphology and function. The first study investigating the mitochondrial structure came out in 2015, which showed that mitochondrial structure could be maintained after 4h of culture, as measured by electron microscopy (Wang et al., 2015). In 2019 our lab also published that LMS cultured for 24h had preserved their ATP production and mitochondrial content in a similar way to freshly prepared LMSs (Watson et al., 2019). However, there are still no functional evaluation of the mitochondria and their response to different culture conditions.

#### **1.4.4 Oxygenation**

In highly oxidative tissues such as the heart, O<sub>2</sub> availability is very important and has been extensively studied with emphasis on ischemia/reperfusion. Ischemia in 3D models such as the LMS, was always a matter of interest since the absence of tissue circulation makes these models vulnerable to ischemia. LMSs are also a 3D model and its thickness was always a concerning topic with respect to its adequate oxygenation or ischemic core.

##### **1.4.4.1 Cellular responses under ischemia**

Myocardial infarction is one of the leading causes of death and is most usually a consequence of artery occlusion/stenosis (Crossman, 2004). Cessation of blood flow in the heart deprives the cells from both O<sub>2</sub> and nutrients, creating a hostile environment of acidification, ionic imbalance, nutrient deprivation and accumulation of metabolic debris (Stavrou et al., 2001). As a result of reduced O<sub>2</sub> the heart changes its metabolic reliance from OXPHOS and FAO and turns to O<sub>2</sub> efficient metabolic mechanisms such as anaerobic glycolysis (Lopaschuk and Stanley, 1997). Anaerobic glycolysis results in pyruvate production, which cannot enter mitochondria in the absence of O<sub>2</sub> and therefore gets converted to lactate that is confined in the cells as there is no blood supply to remove it. That has as a consequence the decrease of pH (R. A. Harris, 2013). Energy depletion under ischemia reduces cellular ATP, inactivates important ATPases such as SERCA and therefore reduces Ca<sup>2+</sup> uptake from the sarcoplasmic reticulum leading to sarcoplasmic Ca<sup>2+</sup> overload (Giorgi et al., 2018; Marban et al., 1987). Accumulation of Ca<sup>2+</sup> induces changes in mitochondria and causes opening of the mitochondrial permeability transition pore (MPTP), which depolarises the mitochondrial membrane potential and increases mitochondrial apoptosis and necrosis (Kalogeris et al., n.d.). This chain of reactions eventually leads to irreversible cellular changes and cell death that give rise to cardiac dysfunction.

#### **1.4.4.2 O<sub>2</sub> dependent molecular changes**

O<sub>2</sub> depletion during ischemia has a distinct role in disease progression, different from that of nutrient depletion. In the heart O<sub>2</sub> availability and consumption is essential. Along with the brain, the heart is one of the most O<sub>2</sub> demanding organs, consuming 8–15 ml O<sub>2</sub>/min/100g and 70 ml O<sub>2</sub>/min/100g during vigorous exercise (Abe et al., 2017). Under hypoxia cells undergo various types of responses on the transcriptional, translational and post-translational level. Hypoxia genes related to angiogenesis, via VEGF- $\alpha$  (Tuder et al., 1995), erythropoiesis, via erythropoietin (Semenza and Wang, 1992), metabolism via PDK 1 (pyruvate dehydrogenase kinase, isoform 1), or LDH- $\alpha$  (lactate dehydrogenase-alpha) (Kim et al., 2006; McClelland and Brooks, 2002) and inflammation through iNOS (Melillo et al., 1995) are significantly altered. One of the first molecules that are regulated under O<sub>2</sub> presence/absence is the hypoxia induced factor alpha (HIF $\alpha$ ). HIF $\alpha$  is regulated at translational level. In the presence of O<sub>2</sub> (normoxic conditions), HIF $\alpha$  is localised in the cytoplasm and is hydroxylated through an O<sub>2</sub>-dependent manner, facilitated by prolyl hydroxylase domain enzymes (PHDs) (Watts and Walmsley, 2019). This modification leads to HIF $\alpha$  degradation through the ubiquitin-proteasome system. When O<sub>2</sub> is low (hypoxia) HIF $\alpha$  translocates to the nucleus, where it forms a heterodimer with HIF $\beta$  and together they bind to hypoxia responsive elements (HRE) (Semenza, 2014). HIF1- $\alpha$ , one of the member of HIF $\alpha$  family, is also known for its effect on endothelial cells, where it enhances the expression of VEGF and inducible nitric oxide synthase (iNOS), which are both known to facilitate angiogenesis (Bosch-Marce et al., 2007). Despite extensive research on HIF1- $\alpha$  in cardiac function, there is still controversy on its protective/deleterious action.

#### **1.4.4.3 Hyperoxygenation**

A less appreciated area is the impact of increased O<sub>2</sub> levels in the heart, which, as described below, can also lead to malfunction. In the human body O<sub>2</sub> levels are being regulated by lung

function and vascular system, but in *in vitro* models vascular regulation is absent and therefore precise regulation depends only on the culturing system.

Hyperoxygenation is the condition whereby the person receives higher levels of O<sup>2</sup> which often occurs in hospitalised patients. In particular, there is a need for O<sup>2</sup> ventilators in people with respiratory failure, cardiac arrest, stroke, sepsis and traumatic brain injury so that O<sub>2</sub> and CO<sub>2</sub> levels are adequately restored (Brugniaux et al., 2018). Out of the total ventilated patients in ICU (intensive care unit), up to 32% are hyperoxygenated (Kraft et al., 2018). Hyperoxia in critically ill patients was also directly associated with poor hospital outcome (Helmerhorst et al., 2015). Given that hyperoxia is given through medical ventilators, initial studies focused on studying its effect on the lungs. High O<sub>2</sub> levels in the lungs increases the levels of ROS production and leads to development of oedema and inflammation (Han et al., 2018; Pannu, 2016; Sato et al., 2016). In neonates it also affects lung development, while in adults it can cause acute respiratory distress syndrome (ARDS) (Qin et al., 2018). *In vivo* rabbit models of cardio-pulmonary bypass showed that hearts perfused in hyperoxic conditions are prone to developing myocardial oxidative stress, inflammation, and ventricular dysfunction (Peng et al., 2019).

Taken together, these data suggest that proper O<sub>2</sub> regulation is essential for the physiological function in the heart, since excessive lack or availability can lead to detrimental effects on cardiac function and development.

#### **1.4.4.4 Media Oxygenation *in vitro***

O<sup>2</sup> regulation *in vitro* is regulated by the culturing systems. O<sup>2</sup> levels in water-based solutions can be affected by several conditions including cell density, cell type, O<sub>2</sub> consumption rate, O<sub>2</sub> solubility, temperature and height of the media column (Fleischaker and Sinskey, 1981; Martin and Vermette, 2005; McLimans et al., 1968; Place et al., 2017; Van Winkle et al., 2012).

According to Fick's first law, diffusive O<sub>2</sub> flux is proportional to the difference in concentration between either side of the medium (the gas liquid interface and the bottom of culture well) and inversely proportional to the thickness of the media (Krogh, 1919). This means that changes in media volume or changes in media oxygenation can affect the dissolved O<sub>2</sub>. In practise O<sub>2</sub> diffusion in deeper layers is lower than at the surface of the media.

Cardiac cells are highly oxidative and therefore they require high levels of oxygenation; however, there are hardly any studies investigating the physiological levels of O<sub>2</sub> in different cell culture systems, including 3D tissue cultures, engineered heart tissues, microfluidics or conventional 2D cultures and cell suspensions. Instead, typically, short term cardiac maintenance utilises direct solution/media oxygenation using O<sub>2</sub> diffusers to saturate the solution, whereas long term cultures are based on 20% of atmospheric O<sub>2</sub> (Al-Ani et al., 2018; Place et al., 2017). O<sub>2</sub> diffusion in the media also depends on humidity, altitude, cell O<sub>2</sub> consumption and O<sub>2</sub> supply in the media. Parameters like these are rarely reported in the literature and therefore accurate judgement of the oxygenation levels cannot be made. This can lead in inconsistencies in experimental models and generation of misleading data.



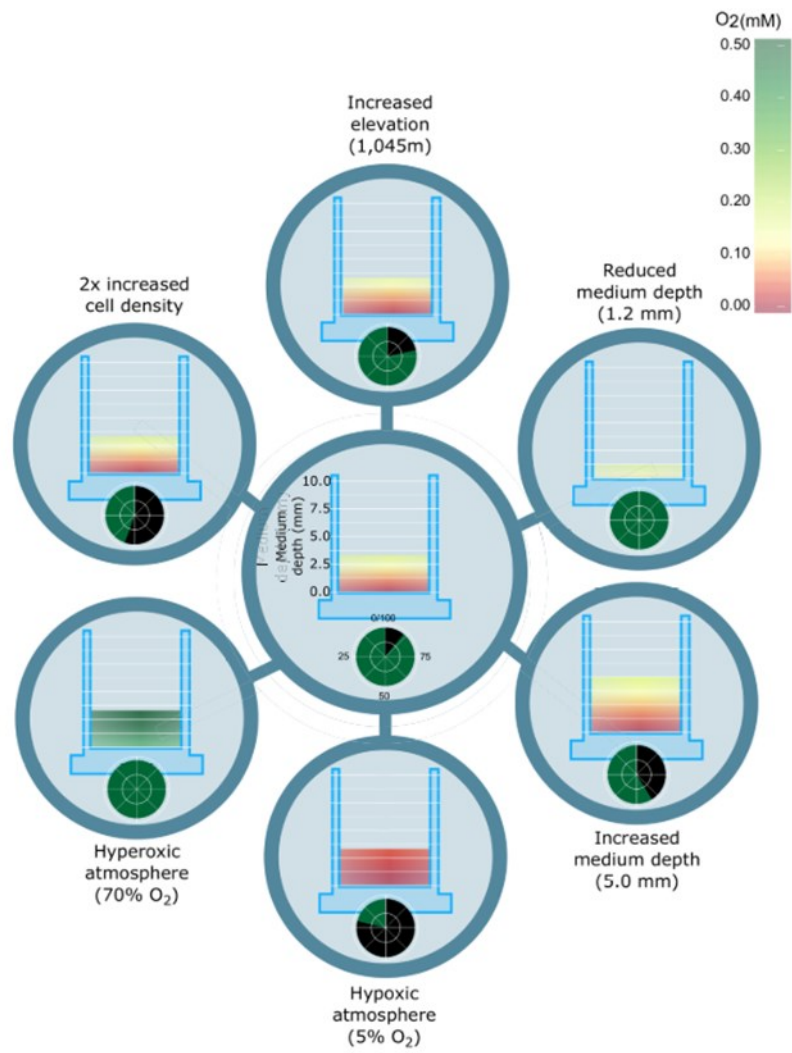


Figure 1.7- $O_2$  concentration in culture vessels. Dissolved  $O_2$  concentration depends on media volume (height), cell density and metabolism, atmospheric  $O_2$  concentration and elevation.

## 1.5 Hypothesis

In summary, there have been several *in vitro* models to study cardiac physiology, but only a few can recapitulate the cardiac complexity and maturation. LMS is a promising model to study mechanical, structural, and functional changes upon injury, since they retain cardiac multicellularity, ECM, and contractility under acute and prolonged culture. Despite the significant improvements of the model there are still unexplored areas that require further characterisation, to deliver an *in vitro* model with high sensitivity and reproducibility for the elucidation of changes occurring in disease development.

Studies on tissue damage have already revealed important humoral, molecular and mechanical changes which are responsible for cardiac remodelling and heart failure. Healthy LMSs have also be used to study cardiac function as well as evaluate the changes seen in failing LMS. However, there is little evidence on the progression of the disease during the early stages of tissue damage, especially with regards to spatial mechanical changes and calcium regulation that give rise to early arrhythmias.

Therefore, in this project it was hypothesised that LMSs can be used as a useful model to study local tissue damage and unravel structural, functional, and electrophysiological mechanisms involved in disease progression.

To investigate this, different hypotheses and aims were set out:

- 1) Optimisation of slicing and culturing conditions can further enhance LMS viability *in vitro* (Chapter 3).

Aims: ▶Define the right slicing solution and LMS thickness.

▶Evaluate Media oxygenation levels and supplementation.

▶Define the right mechanical load and how that affects contractility and bioenergetics on LMS.

2) Local cell death affects contraction and electrophysiological stability of LMSs (Chapter 4).

Aims: ▶Apply cryoinjury on healthy rat LMSs and culture them for the remodelling to occur.

▶Analyse global LMS contractility and arrhythmogenicity using a force transducer.

▶Evaluate local ionic changes by measuring cytoplasmic calcium using optical mapping.

▶Study local mechanical alterations by evaluating the SL, collagen deposition, connexin density and t-tubule organisation. .

3) Cryoinjured LMSs can provide a valuable tool to study the role of CamKII in the development of arrhythmias upon injury (Chapter 5).

Aims: ▶Evaluate the role of a known  $\text{Ca}^{2+}$  regulator, CamKII, at global and cellular levels using contractility and optical mapping techniques.

4) Cryoinjury on LMSs can reveal functional changes upon EV application (Chapter 6).

Aims: ▶Administrate EVs on healthy and cryoinjured LMSs and assess the consequences on contractility and molecular profiles.

# **Chapter 2**

## **General methods**

This chapter includes all the necessary material and methods used to address the proposed hypothesis and aims. The protocols are explained in detail in this section and briefly in the respective chapters. Small modifications on commercially available or widely used procedures were required to address the different needs of tissue handling and assessment and were included in the description when necessary.

## **2.1 Source of cardiovascular tissue**

This project involved the use of animal tissue, derived from rats, but human tissue was also utilised whenever available.

### **2.1.1 Rat tissue**

All animal experiments performed according to the institutional and national regulations. The use of living cardiac tissue was approved by Imperial College London and the procedures described here were completed following the United Kingdom Animals (Scientific Procedures) Act 1985. Animals were killed following guidelines established by the European Directive on the protection of animals used for scientific purposes.

### **2.1.2 Human tissue**

Human heart failure tissue was provided by the Cardiovascular Research Centre Biobank at the Royal Brompton and Harefield NHS Foundation Trust, UK (NRES ethics number for biobank samples: 09/H0504/104+5; Biobank approval number: NP001-06-2015 & MED\_CT\_17\_079). Each human sample used in this study was obtained upon informed consent. Even though the size of the received tissue varied between patients, on average the inferior 1/3 of the heart was acquired.

Unused human donor hearts, rejected for heart transplantation, were provided by the NHS Blood and Transplant organisation, UK (REC reference 16/LO/1568).

## **2.2 Living myocardial slice preparation**

Slicing and culturing of the LMSs were previously published by our laboratory (Watson et al., 2017), however further refinements were applied to improve the method's reproducibility and enhance LMS variability.

### **2.2.1 Preparation of the slicing solution**

The solution is based on classic Tyrode's composition, with the addition of the excitation-contraction uncoupler, BDM (VWR, USA) and high potassium concentration. The solution was cooled in the freezer for 40min, just before ice crystals start to form, and then the pH was adjusted to 7.4, with addition of NaOH (2M) (Sigma-Aldrich, USA). For detailed description of the slicing solution see Table 2.1.

Table 2.1-Tyrode's solution used during tissue slicing and LMS assessment

Reagents	Concentration (mM)	
	Slicing Tyrode's solution	Recording Tyrode's solution
2,3-Butanedione 2-monoxime (BDM)	30	-
Glucose	1	1
HEPES	10	10
Potassium chloride	6	4.5
Sodium chloride	140	140
Magnesium chloride (1M)	1	1
Calcium chloride (1M)	1	1.8

### **2.2.2 Solution preparation for heart excision**

During heart excision it was important to avoid any blood clotting that could compromise heart function. Therefore, 2x 60ml containers were filled with 50ml of slicing solution and 120IU of Heparin Sodium (1000IU/mL) (Fannin, UK) (120µl in 50mL slicing solution). One of the containers was then cooled in the freezer for 40min and the other was warmed up at 37°C.

### **2.2.3 Preparation of 4% agarose**

4% agarose (Sigma-Aldrich, USA) was added in distilled water and heated in the microwave until boiled and fully dissolved. The mixture was then poured into large glass petri dishes (VWR, USA) until it reached a height of 2-3mm. Once the agarose was cooled and solidified, it was cut in smaller rectangular blocks of 3x2cm. It was crucial that the agarose thickness was homogeneous across all sides of the block, so that when the tissue was attached on it would be on the right position for cutting and excessive tissue damage was avoided. The blocks were kept at 4°C for up to 3 weeks in a parafilm-shielded petri dish.

### **2.2.4 Preparation of the specimen holder**

The agarose block was glued on the base of the specimen holder, using Histoacryl Surgical Glue (B. Braun Medical, UK). To avoid agarose evaporation, the specimen holder was placed inside a closed polythene bag with a small, damped tissue paper inside and kept in the fridge until needed.

### **2.2.5 Preparation of the tissue dissection area**

The tissue dissection area was prepared prior to slicing to minimise delays. A clean bench area was prepared next to the vibrating microtome; the area was sterilised with 70% ethanol and included the following equipment: a large, 15cm petri dish (Corning, USA), a sterile surgical scalpel (Swann-Morton, UK), razor blades (VWR, USA), small tweezers, micro scissors (Fine



Science Tools, Germany), Histoacryl surgical glue (B Braun, Germany), specimen holder with agarose and tissue paper. The organised dissection area can be seen in Fig 2.1d.

### **2.2.6 Calibration of the vibrating microtome**

The vibrating microtome (Campden, UK) and ceramic blade (Campden Instruments, UK) was sterilised with 70% ethanol. The instrument was calibrated and tested for z alignment error. The error should have been  $<1\mu\text{m}$ , to ensure better slicing conditions and minimise tissue damage. If the error was  $>1\mu\text{m}$  then the screws of the blade were adjusted until the error falls  $<1\mu\text{m}$ . If that did not successfully decrease the error, then the blade was replaced. The same blade could be reused up to 1 month. Upon calibration, the holding bath was sterilised with 70% ethanol and mounted onto the vibrating microtome. Once the ethanol has evaporated, the outer part of the bath was filled with ice. The ice was regularly refilled to keep the bath cool at all times.

### **2.2.7 Preparation of the storing bath**

Whenever LMSs were not immediately used after slicing, they needed to be stored in cold oxygenated slicing solution. To prepare the storage area, a large glass 1L container (Ikea, Sweden) was placed on ice and filled with slicing solution. 6 cell strainers (Corning, USA.) were placed in the glass container and secured in place using a custom-made 6-well plate (Corning, USA) with holes in the bottom to allow solution movement. The assembled storage area can be seen in Fig 2.1c-d.

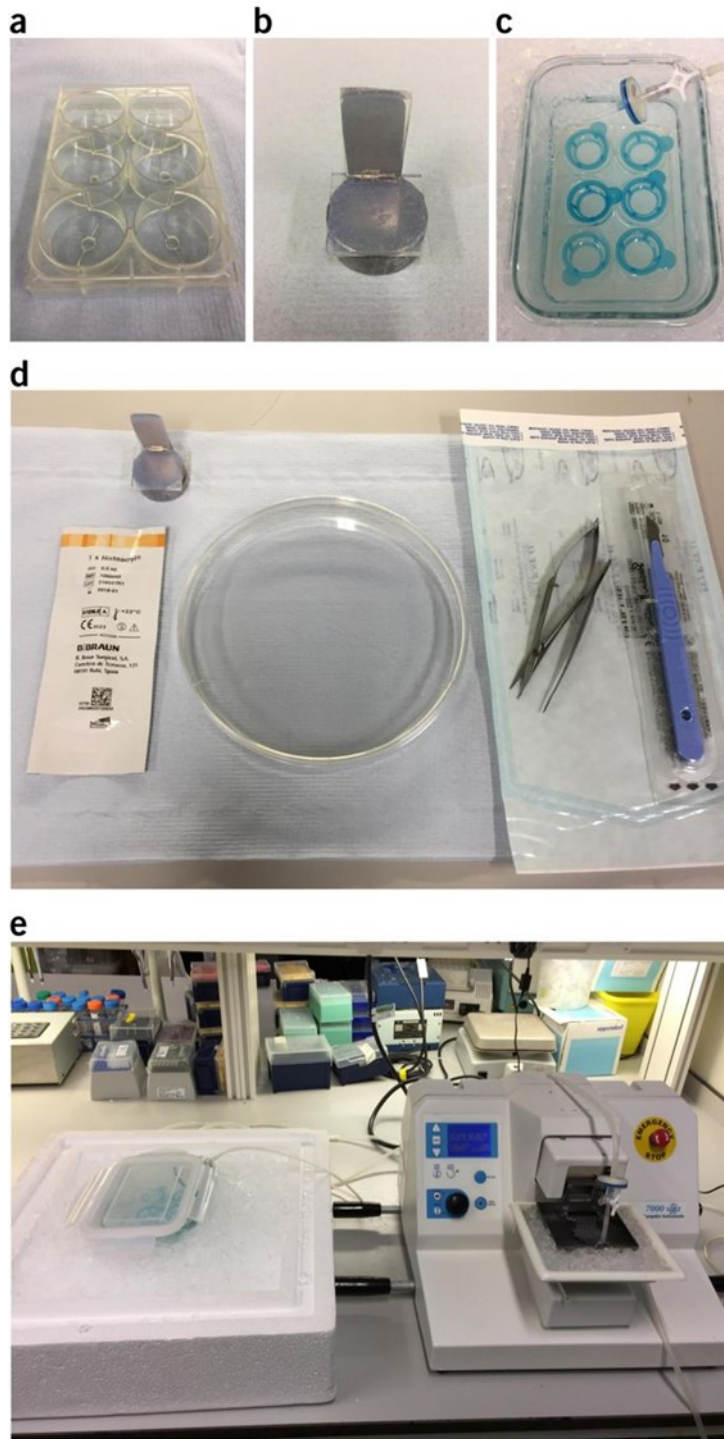


Figure 2.1-Necessary equipment and setup needed to be prepared prior to heart harvesting. a) Customised 6-well plates with holes at the bottom to allow solution perfusion. b) Specimen holder with attached agarose. c) Storage glass bath filled with slicing solution that was oxygenated with 100% oxygen. The bath contained the custom-made 6-well base with holes on the bottom to support the cell containers and allow solution movement. The bath was surrounded with ice to keep the temperature low. Figure from (Watson et al., 2017).

### **2.2.7.1 Collection of rat hearts**

In this project both rat and human tissue were used, however the slicing procedure differed between the two species.

Sprague-Dawley male rats (body weight between 250-400gr) were used in this project. All animals were sacrificed following Institutional and National guidelines. In more details, the rats were initially sedated with isoflurane (Zoetis, USA) (4% isoflurane and 4L/min oxygen). The animal's reflexes were tested and when they showed no response then the animal was ready for cervical dislocation. As a second confirmation of death cessation of circulation was performed. The animal was then placed in the supine position. The sternum was located and the skin area on top of it was removed. After a small incision in the area, the sternum was exposed, and the diaphragm was cut. An incision around the ribs made the access to the lung and heart easier. The heart was then held with one hand and with a gentle incision of the aorta the venae cavae (at the back of the heart) and the pulmonary vessels, the heart was excised. The excision of the heart was done as soon as possible, usually in no more than 30s, so that the heart would not become hypoxic after cessation of circulation.

The isolated heart was placed immediately in heparinised solution at 37°C (see section 2.2), and gently and repeatedly compressed for 5s to remove any excessive blood from the ventricles. The tissue was then placed in the heparinised solution at 0°C, and the same procedure was repeated to accelerate tissue cooling and stop tissue contraction. The heart in the cold solution was kept on ice and quickly transferred to the dissection area.

### **2.2.7.2 Collection of human hearts**

Upon arrival the failing hearts were dissected, and the lower apical part of the heart was placed in 1L of cold cardioplegia solution and transported to the lab on ice. In contrast, the whole heart from healthy donors was received in cold cardioplegia solution and dissection was performed in the lab. Approximately 1.5x1.5cm of tissue block was acquired from each specimen and attached on the specimen holder as described in section 2.2.9.

### **2.2.8 Preparation of tissue for slicing**

The preparation of the tissue block differed slightly between the human and the rat tissue due to differences in size and curvature of the heart.

### **2.2.8.1 Preparation of the rat ventricular block**

The tissue was placed in a 15mm petri dish and covered with heparinised cold slicing solution. The different chambers were identified, and an incision was made between the atria and ventricles, using razor blades (Fig 2.2.a). Upon atrial removal the two ventricular chambers were revealed. The right and left ventricle were distinguished, with the right ventricle had thinner walls and crescent shape. The right ventricle was removed by making an incision along the right ventricular/septal junction using micro scissors. Once the septum was revealed, it was possible to make an incision through the septum starting from the base towards the apex. Once the chamber was opened the tissue was placed at the bottom of the petri dish with the endocardium facing up. Any remained curvature of the tissue was removed by cutting off the lower apical part of the ventricle (1-2mm). Lastly, the septum on either side of the ventricle was removed as well. At that stage, the left ventricle was isolated and flattened and therefore was ready to be mounted on the specimen holder. The process of preparing the isolated flatten left ventricle lasted no more than 5-10min. The faster the procedure the better was the tissue viability. During the dissection time the tissue was always kept under the cold slicing solution in order to avoid cardiac activation and spontaneous contractions. A detailed representation of the procedure can be found in Fig 2.2.

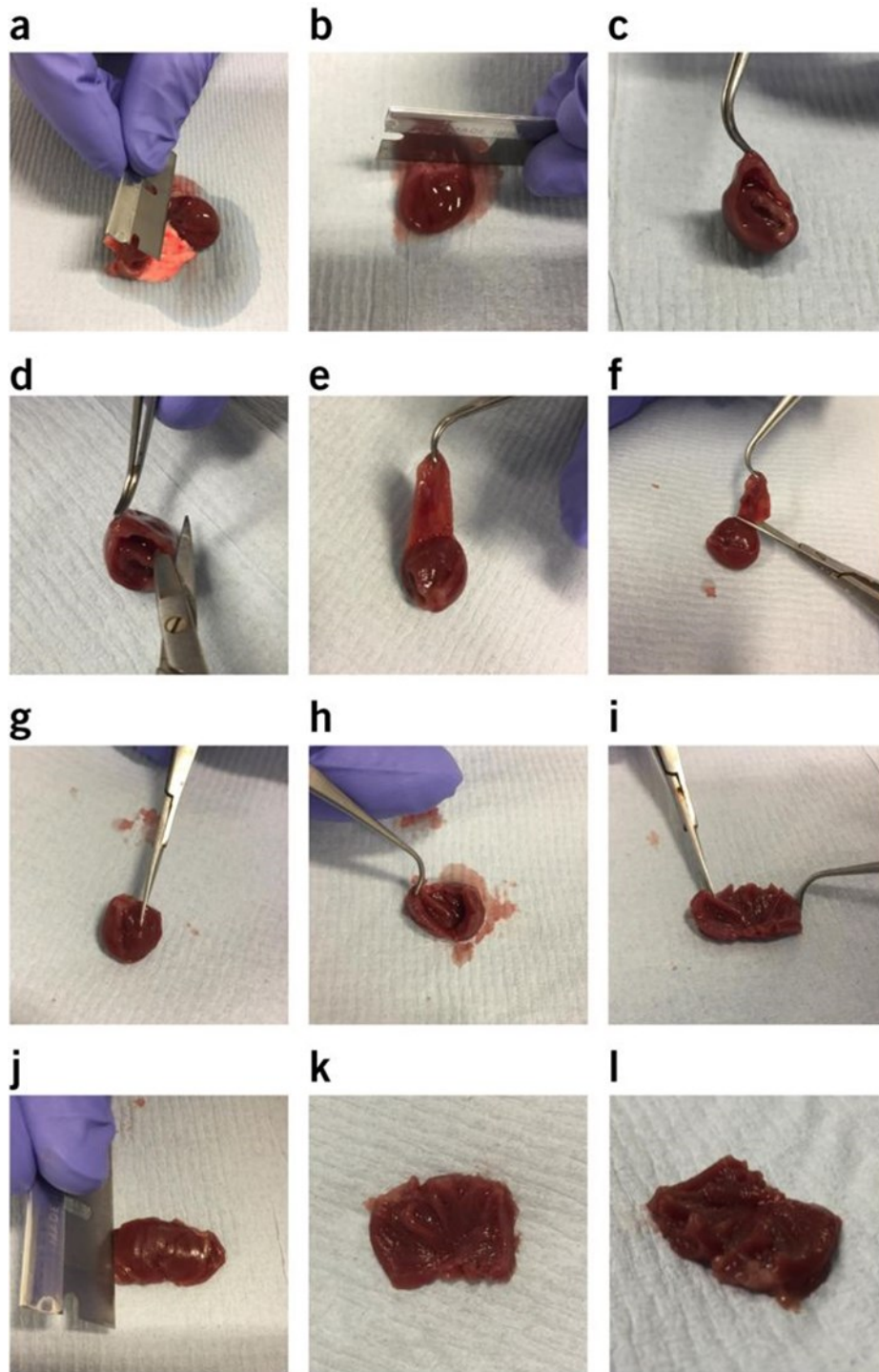


Figure 2.2-Rat heart dissection steps. a) In case lungs were still attached on the heart they were removed using a razor blade, to visualise the atria. b) Removal of the atria and Imm of the basal tissue using a razor blade. c) View of the rat heart from the base, the open ventricles were clearly visible. The right ventricle was determined by its thinner wall and more crescenting shaped. d-f) The wall of the right ventricle was held with a pair of tweezers and removed using microscissors. The tissue was cut along the right ventricular–septal junction. g) An incision was made along the septum and towards the apex. h) The left ventricle opened up. i) Small incisions were made at the apical area of the tissue to further flatten the left ventricle. j) The tissue was turned around so that the epicardium was facing up and the lateral septum area was easily identifiable and easily removed. k-i) The left ventricle was isolated and flatten as shown in the picture. The tissue was always submerged in cold slicing solution. However, for visual reasons all the pictures were taken on dried tissue. Previously published in (Watson et al., 2017)

### **2.2.8.2 Preparation of the human ventricular block**

A 1.5cm<sup>2</sup> tissue block was cut from the left ventricle of the human cardiac tissue and mounted on the specimen holder as described in section 2.2.9. Flattening of the tissue was not necessary with human samples since the size of the tissue was big enough and curvature was minimal. A representation of human tissue preparation for slicing can be found in Fig 2.3.

### **2.2.9 Mounting of the tissue on the specimen holder**

The epicardial surface was lightly blotted on a tissue paper to remove any excessive solution which helped tissue adhesion with the surgical glue. Surgical glue was applied on the surface of the agarose/specimen holder and spread across the surface. The tissue was placed on top of the agarose with the endocardium facing up and the basal area towards the back of the specimen holder. The tissue was lightly pressed down, using a flat spatula, so the entire epicardial surface was in touch with the agarose and the tissue appeared as flat as possible. This was a critical step to make sure that the blade would cut in parallel to the cardiac fibres. Rapidly, the specimen holder was transferred to the microtome bath and secured to the magnetic holder on the bottom of it.

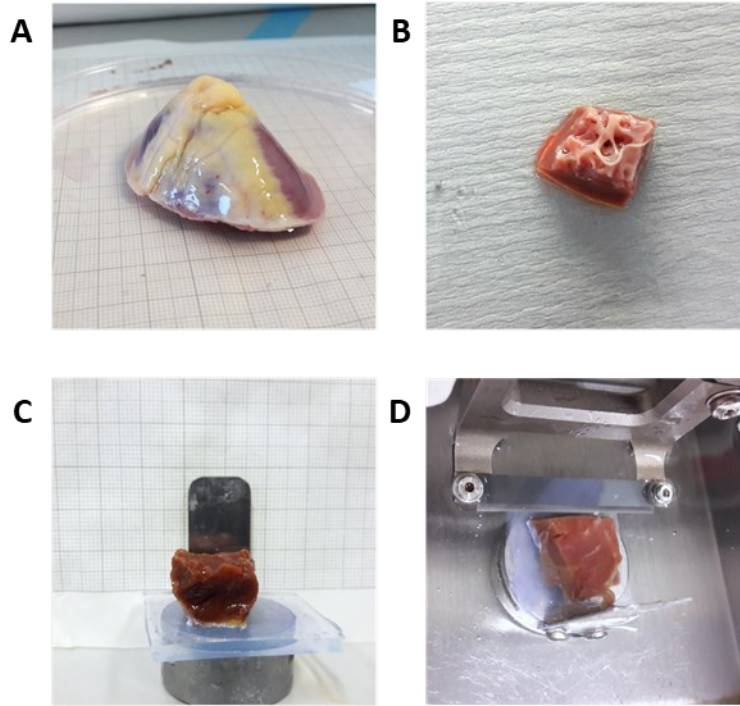


*Figure 2.3-Human tissue dissection and preparation for slicing. A) A failing heart tissue received in the lab. B) A small block of the left ventricle was dissected. C) The tissue block was attached to the base of the specimen holder using surgical glue. D) The specimen holder with the tissue were immediately submerged in the slicing bath.*



### **2.2.10 Slicing of the left ventricular tissue**

The blade of the vibrating microtome was adjusted to the height and position of the tissue. The settings of the microtome were also adjusted to Frequency - 80Hz, Advance speed - 0.03mm/s, Amplitude - 2mm and Tissue thickness - 300 $\mu$ m. These settings have been previously validated within our group (Watson et al., 2017) and are optimal for rat/human tissue heart slices.

Once the LMSs detached from the tissue block were immediately transferred to the storage bath. The LMSs were submerged into the cold slicing solution inside the storage bath and flatten on top of the cell strainers. At all times, the handling and transferring of the LMSs were done using the back of a sterile Pasteur tip to avoid any damage (e.g. handling with forceps).

## **2.3 Fibre alignment**

Cardiac fibres and their laminar sheets are arranged in parallel to the epicardial surface (Legrice et al., 1995; Streeter et al., 1969). However, their angle of orientation changes depending on fibre's transmural, basal or apical position. In order to acquire a homogeneous cell sheet, LMS fibre orientation was assessed under a microscope and an area of homogeneous parallel fibre bundles was identified and cut using a scalpel. The LMSs were cut in a rectangular shape with dimensions of width=7mm and length=9mm using a 1mm graph paper as a guide, which was located under the petri dish. The shape and size of the LMSs were kept consistent in all experiments.

## **2.4 Attachment of tissue holders**

To manipulate and mechanically load the LMSs it was necessary to develop a system that would be able to pull the tissue along the fibres. For that reason, custom made rectangular

tissue holders were designed using an online and free software tool, TinkerCAD (Autodesk, USA). The design was then printed with a 3D printer, Ultimaker 3 (Ultimaker, The Netherlands) using Polyethylene Terephthalate (PETT), T-glase, (Taulman, USA), which is a biocompatible, non-degradable and high-strength material. The slice holders were made in big quantities (approximately 100 at a time), stored in 70% ethanol and dried before use.

Once an LMS was trimmed, the slice holders were attached on either side of it, using surgical glue, perpendicular to the fibre orientation (Fig 2.4). It was important that the tissue holders were placed in parallel to each other so that the applied stretch would be equally applied when stretched.

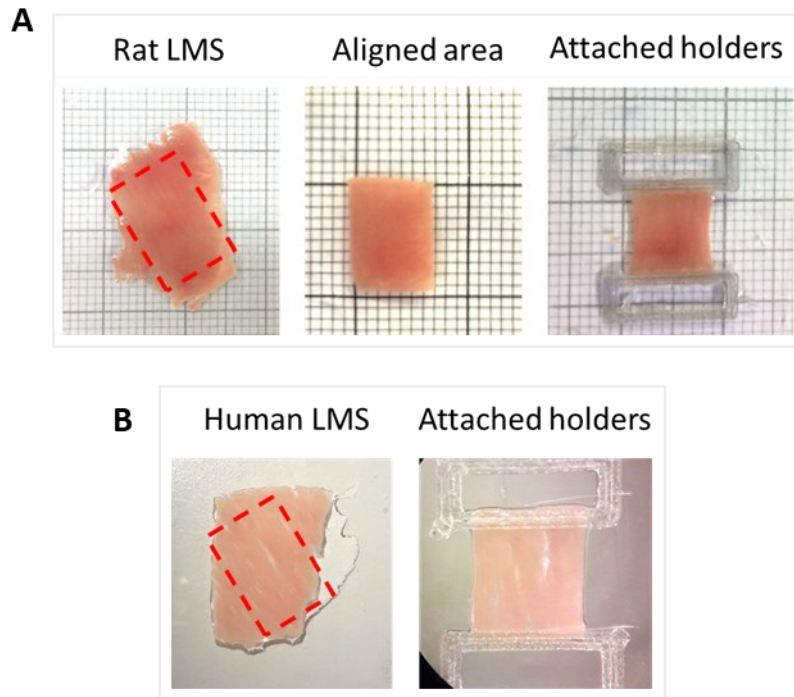


*Figure 2.4-Fibre orientation and tissue holder attachment. A) Freshly prepared rat LMSs were cut so that it contains only homogeneously aligned cardiac fibres. The tissue holders were then attached perpendicularly to the fibres' orientation. B) Freshly prepared human LMSs were prepared the same way as rats.*

## **2.5 LMS size measurements**

After the tissue holders were mounted, the final size of the tissue was measured using a digital calliper (RS components, UK). The length and width of each mounted myocardial slice was required for experiments. The width of the LMS was necessary to allow normalisation of the force generation during contractility assessment. The length of the LMS was required to calculate the % of stretch and therefore determine the applied preload to the LMS.

## **2.6 LMS culturing system**

Culture of LMSs was performed in aseptic conditions. All equipment was bought sterile or autoclaved at 121°C for 20min. Whenever heat treatment was not possible, the equipment was sterilised in 70% ethanol and exposed to ultraviolet light (UV). The tissue harvest and LMS production were conducted on the bench, but the culture assembly was performed in a sterile laminar flow hood. Media contained 3% penicillin and streptomycin (Sigma-Aldrich, USA) to avoid any contamination that might have occurred during the culture system set-up.

### **2.6.1 Culture Medium**

The culture media used was previously described and widely used in previous studies (Brandenburger et al., 2012d; Fischer et al., 2019; Watson et al., 2019). Medium 199 (M199) (Sigma-Aldrich, USA) with Earl's Salts was supplemented with 3% Pen/Strep and 0.001% ITS liquid media supplement (containing 1.0 mg/mL human insulin, 0.55 mg/mL human transferrin and 0.5 µg/mL sodium selenite) at 100x concentration. The type of media used contained physiological levels of glucose, calcium (1.8mM) as well as a variety of vitamins and minerals to aid in the longer preservation of tissue over time. Full composition of M199 can be found

at <https://www.sigmaaldrich.com/content/dam/sigmaaldrich/docs/Sigma/Formulation/m4530for.pdf>. This media is referred as culture media in the following sections.

## **2.6.2 Culture chambers design**

LMSs have been traditionally cultured on a liquid-air interface, so that nutrients can be absorbed from the bottom of the LMS and oxygen from the top. During, this project a new culturing system was developed by our lab members (Watson et al., 2019), that included electromechanical stimulation, oxygenation and media circulation. Electrical field stimulation was provided via carbon electrodes connected to a bipolar stimulator via crocodile clips. A peristaltic pump circulated the media inside the chamber at a rate of 15mL/minute. 5% CO<sub>2</sub>, 95% O<sub>2</sub> was provided either directly inside the media or at the surface of it at rate of 0.5L/min. The mechanical load was induced by stretching the LMS on custom-made stainless-steel stretchers. The stretchers were comprised of a fixed and a movable post. The movable post was attached to a screw which regulated the stretch of the LMS. The whole chamber was sealed with a polycarbonate lid, while the side holes were closed either with O-rings or polycarbonate adaptors. All the chamber components were autoclavable to ensure sterile conditions during culture. Fig 2.5 shows the design of the chamber in detail.

## **2.6.3 Placing LMSs in culture**

The LMSs on stretchers were washed with media solution, so that most of the slicing solution was removed before putting them in the culture media. Each LMS was, then, stretched to the desired average tissue sarcomere length (SL) by turning the screw at the desired length. The chamber was sealed, supplied with 95% O<sub>2</sub>/5% CO<sub>2</sub> and provided with field electrical

stimulation. Rat LMSs were stimulated with Voltage=15V, Width=10mms and Frequency=1Hz.. The media was circulated with a peristaltic pump at a rate of 15mL/minute and finally the chambers were placed in a humidified incubator and cultured at 36°C for 24h.

Human LMSs were, also, cultured in in a similar way to the rats. There were stretched at 2.2 $\mu$ m of SL, which corresponds to higher stretching of 20%, based on previous data generated in the lab. The human LMSs were electrically field stimulated at stronger electrical pulses of Voltage=20V, Width=15mms and Frequency=2Hz

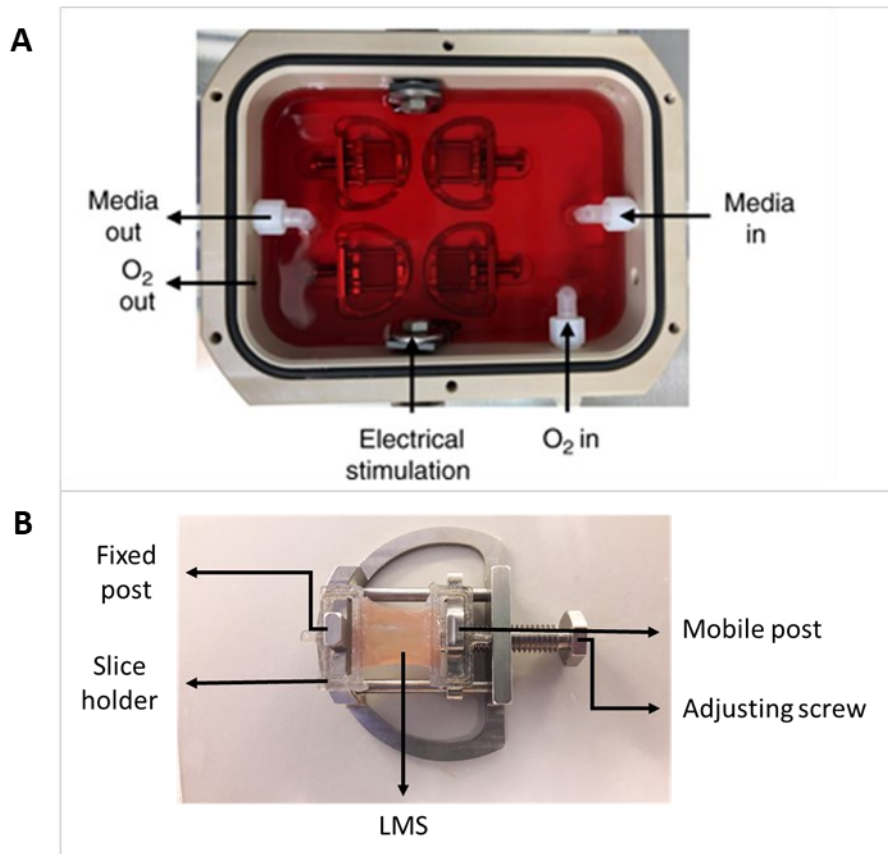


*Figure 2.5-Culture set up. A) Culture chamber representation including LMS, stretchers and media. The arrows indicate the location of each element and the direction of the media/O<sub>2</sub> flow. Figure adjusted from (Watson et al., 2017). B) Representative image of the stainless-steel stretcher with a mounted rat LMS. The stretcher has been designed to allow unidirectional stretch on a slice.*

## **2.7 Assessment of conduction velocity**

### **2.7.1 Recording of Multielectrode array (MEA) signals**

The conduction velocity (CV) was measured using a multielectrode array system (Multi Channel Systems, Germany). This system offers a non-invasive, synchronous and multifocal platform for extracellular CV measurements. A 60EcoMEA multielectrode array dish with 60 golden electrodes, 8 x 8 matrix with 700 $\mu$ m inter-electrode space was used resulting in 4.9 x 4.9 mm recording area. These specifications provided enough surface area and adequate resolution to measure CV in LMS. The LMS fibre alignment was checked under the microscope and one of the edges were cut to mark the fibre orientation, so it was easier to identify is once it was moved on to the MEA dish (see Fig 2.6 for LMS position on the MEA dish). In order to keep the LMS in close contact with the electrodes a stainless-steel washer and circular gauze were placed on top of the LMS to weight them down. The dish was, then filled with 37°C oxygenated recording solution and placed on top of a heating plate, which kept the temperature stable, at 37°C, for the whole duration of the experiment. Electrical stimulation was controlled by MC\_Rack software (Multi Channel Systems, Germany) and point stimulation of 1Hz, 500 $\mu$ s and 1-3 V was applied via the middle electrode of one of the external microelectrode rows. The LMSs were stimulated either longitudinally or transversely to their fibre orientation. The signal was then amplified using MEA1060 amplifier (Multi Channel Systems, Germany) and 10s of LMS stimulation were recorded using MC\_Rack software (Multi Channel Systems, Germany) (Camelliti et al., 2011d).



### **2.7.2 Analysis of CV**

It has been shown that there is a linear relationship between the upstroke of the action potential and the field potential rise, represented as the most negative point in Fig 2.6 (Halbach et al., 2003) and this was used to calculate the CV of the LMS as previously described (Bussek et al., 2012; Camelliti et al., 2011b; Watson et al., 2019).

The recorded files were processed using MC\_Rack software. After the stimulation artifact was removed the new data were saved in a separate folder and then imported in MATLAB (MathWorks, USA.) A custom-made MATLAB code (Chowdhury et al., 2018) that automatically detects the activation time of the LMS under each electrode was utilised. The CV was then calculated by importing the activation times to an excel sheet kindly provided by Prof Cesare Terracciano, based on a previously described analysis method (Meiry et al., 2001).

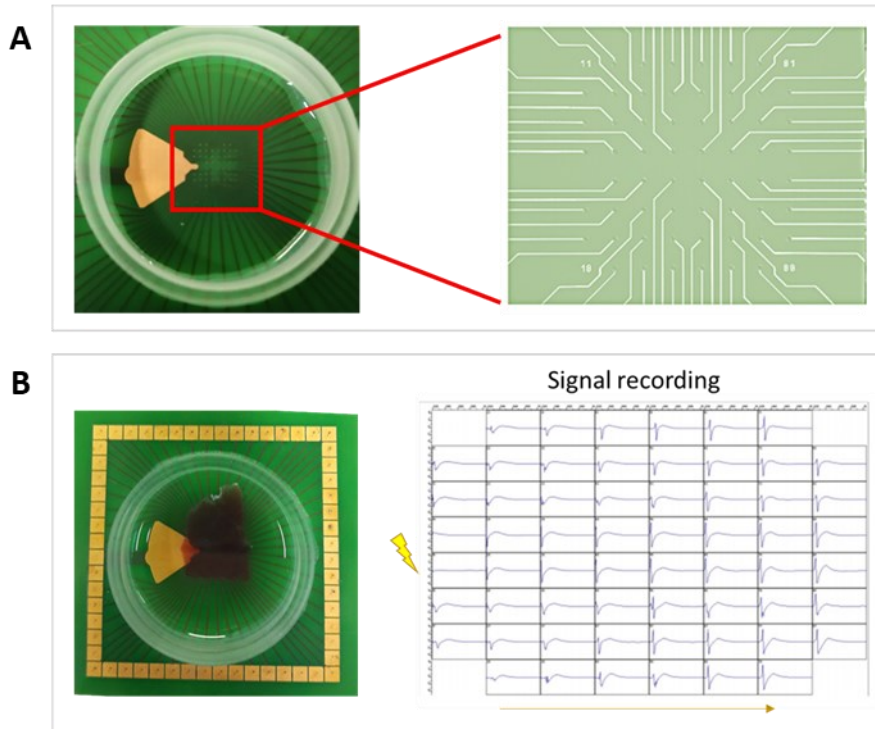


Figure 2.6-Multi-electrode array (MEA) dish used to analyse LMS conduction velocity. A) An MEA dish contained 60 golden electrodes at the centre of the dish. The electrodes are placed in  $700\mu\text{m}$  distance from each other, providing a good resolution for rat or human LMS. B) The LMSs were placed on top of the electrodes, with the fibres' direction running in a known direction. The LMS was point stimulated and tissue response was recorded from the remained the electrodes.

## **2.8 LMS force measurements**

### **2.8.1 Recording LMS contraction traces**

LMS contractility was assessed by using an F30 isometric force transducer (Harvard Apparatus, USA). Two hooks were used to secure the LMS on the system. A fixed hook was placed on the edge of the perfusion bath, while the second hook was attached on the force transducer. A micromanipulator was used to facilitate the movement of the force transducer, which allowed the fine adjustment of the LMS position inside the bath and controlled the mechanical stretch of the LMS.

The LMS was placed inside the perfused bath, the slice holders were secured on the hooks and positioned in parallel to each other to promote homogeneous stretch throughout the tissue (See Fig 2.7). The LMS was continuously perfused with 37°C pre-oxygenated recording Tyrode's solution and stimulated with bipolar electrical field stimulation, of Voltage=10-40V, Width=10-40ms, Frequency=1Hz. The stimulation settings were adjusted depending on the animal species, culture conditions and protocol used. The LMS was stretched in a stepwise manner, allowing 20s interval between each step, to allow the LMS contraction to stabilise. LMS contraction was monitored and recorded throughout the entire experiment using AxoScope software (Molecular Devices, USA).

Maximum contractility was measured by stretching the tissue, in a stepwise manner, until maximum isometric force was recorded. After each stretching step the LMS was left to stabilise for at least 15s before the next step begun. This gradual stretch allowed enough time for the LMS to adjust to the new stretching conditions, while abrupt changes in stretching were avoided to prevent mechanical damage. Excessive stretching led to decrease in contraction amplitude or provocation of arrhythmias, indicating that the LMS had exceeded its maximum contraction.

On the other hand, LMS contraction at physiological stretch (2.2 $\mu$ m SL) was measured by stretching the LMS, in a stepwise manner, to 15% for rats and 20% for human tissue.

### **2.8.2 Analysis of contraction traces**

Recorded traces acquired from AxoScope were analysed using Clampfit software (Molecular Devices, USA). Peak twitch force and contraction kinetics were measured. To measure maximum force the twitches with the largest amplitude were detected and 3 consecutive peaks were analysed and averaged. The twitch force was recorded as displacement, in  $\mu$ m, and then converted to mN using a scaling factor of 0.881 (calculated from calibration of the force transducer). The twitch force was then normalised to the cross-sectional area and reported as mN/mm<sup>2</sup>. The same normalisation was, then, conducted for measuring the resting diastolic force of the LMS. Contractility at basal stretch was measured when the LMS was stretched at sarcomere length of 2.2 $\mu$ m.

In order to assess contraction kinetics, time to peak, time to 50% decay, time to 90% decay and decay constant were measured. Time to peak was defined as the time taken from electrical stimulation to peak force. Time to 50% and 90% decay was defined as the time taken from peak force to 50% and 90% decay, respectively. Decay constant ( $\tau$ ) was calculated by fitting a monoexponential curve to the twitch force decay curve.  $t$  was equal to the time at which the curve was reduced to  $\frac{1}{e}$  times its initial value.

Contraction kinetics were calculated when LMSs were stretched at the same sarcomere length, at basal conditions of SL=2.2 $\mu$ m. LMSs that reached maximum isometric contraction were not used for calculating contraction kinetics.

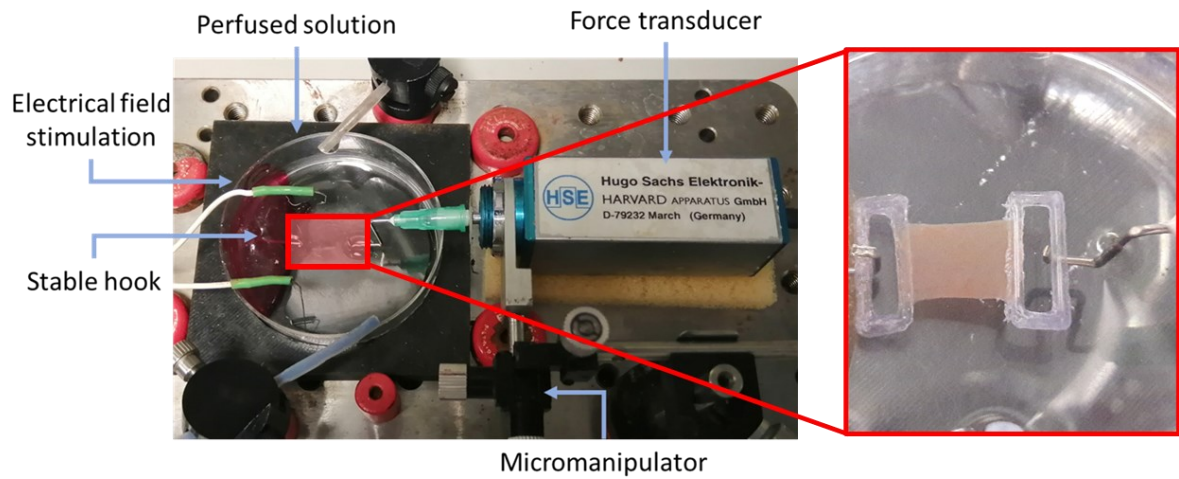


*Figure 2.7-Force transducer set up. The LMSs were secured between a stable hook and a hook attached on the force transducer. A micromanipulator was used to regulate the position of the force transducer and therefore the position/stretch of the LMS. Field stimulation was provided by 2 platinum electrodes and LMSs were always perfused with pre-heated and pre-oxygenated slicing solution during force measurements.*

## **2.9 LMS viability assessment**

LMS viability was tested using two different methods. To measure whole LMS viability a colorimetric method using CellTiter 96® AQueous One Solution Cell Proliferation Assay (Promega, USA) was used. To measure spatial changes in LMS viability LIVE/DEAD Viability/Cytotoxicity for Mammalian Cells Assay (Thermo Fisher Scientific, USA) was used.

### **2.9.1 Whole LMS viability**

This colorimetric method measures metabolically active cells. The reaction is based on the conversion of a tetrazolium compound [3-(4,5-dimethylthiazol-2-yl)-5-(3-carboxymethoxyphenyl)-2-(4-sulfophenyl)-2H-tetrazolium, inner salt, MTS] and an electron coupling reagent (phenazine ethosulfate, PES) into coloured formazan product by NADPH and NADH.

In order to eliminate variation due to tissue volume, a tissue puncher (3mm) was used to produce same-size LMS disks. The disks were blot dry and added to a mixture of 200µl of culture medium + 40µl CellTiter 96 AQueous One Solution reagent in a 96 well plate. The plate was then incubated for 30min at 37°C in a 5% CO<sup>2</sup> humidified incubator, protected from the light. At the end of the incubation the solution of each well was mixed well and 200µl of the supernatant were re-plated in new clean wells. Their absorbance was measured at 490nm using SoftMax Pro 6.4.2 (MolecularDevices, USA).

### **2.9.2 Local changes in LMS viability**

The LIVE/DEAD Viability/Cytotoxicity assay (Thermo Fisher Scientific, US) uses a dual staining to detect the % of viable and dead cells within a sample. The assay provides two colour

fluorescent probes that measure two different aspects of cell viability, plasma membrane integrity (ethidium homodimer-1) and intracellular esterase activity (calcein AM). Cells that have lost their membrane integrity are permeable to ethidium homodimer-1, which enters the nucleus and binds to nucleic acids, thereby producing a bright red fluorescence in dead cells (excitation ~495nm, emission~635 nm). On the other hand, viable cells were detected, when the calcein AM was enzymatically converted by intracellular esterases. Calcein AM is virtually nonfluorescent and cell permeable but it produces an intense uniform green fluorescence in live cells (excitation ~495 nm, emission ~515 nm).

Calcein AM and ethidium stock solutions, 4mM and 2mM respectively, were prepared by adding dimethyl sulfoxide (DMSO) to the vials and mixed well. LMSs were incubated at 37°C in 5% CO<sub>2</sub> humidified incubator for 40min. During the incubation the LMSs were mounted on stretchers, so that tissue deformation was avoided, and placed in 6-well plates with 10ml of media M199 + 2µM Calcein + 4µM Ethidium homodimer-1. At the end of incubation LMSs were washed in phosphate-buffered saline (PBS) and then fixed in 4% paraformaldehyde (PFA) (Alfa Aesar, USA) for 15min at room temperature. LMSs were, then, washed with PBS and prepared for imaging (see detailed description in section 2.12).

LMS viability was visualised using a Zeiss AxioObserver Widefield microscope (Zeiss, Germany). Whole tissue fluorescence was captured at 10x magnification and tiles were used to acquire whole tissue coverage. Widefield microscopy is limited to the assessment of LMS surface viability as it cannot penetrate more than 2 cell layers.

The image was analysed using Fiji software. The proportion of viable and dead cells were calculated and expressed as a % of the total LMS area.

Confocal imaging was also used for higher magnification acquisition imaging. Images were visualised using a Zeiss LSM780 confocal laser scanning microscope (Zeiss, Germany) and

analysed with Fiji software. A z-stack of images was acquired so that multiple layers can be observed. Detailed analysis is described in section 2.12.

### **2.9.3 TUNEL assay DNA fragmentation analysis**

The localisation of apoptotic cells was determined by using the In situ BrdU-Red DNA Fragmentation (TUNEL) Assay Kit (Roche, Switzerland). This method targets both double and single stranded DNA that usually occurs at the final stages of apoptosis due to DNase activity. Enzymes such as the terminal deoxynucleotidyl transferase (TdT) catalyses the polymerisation of deoxyribonucleotides (dNTs) to the free 3'-OH termini of the DNA. The added dNTs contain deoxyuridine which labels the DNA and therefore detects DNA breaks.

To perform the kit on the LMSs it was necessary to produce thinner slices which could be stained and visualised in the confocal microscope. Therefore the 24h cultured LMSs were fixed as described in section 2.10 and subsequently added in a well that contained a solution of 30% sucrose (Sigma, USA) in PBS. The LMSs were incubated for about 30min until the tissue sunk to the bottom of the well. That step was necessary to minimise crystallisation during tissue cooling. The excess sucrose solution was then removed by tabbing the LMSs on a tissue paper. The LMSs were placed on a Tissue-Tek Cryomold Mould (Agar Scientific, UK) and OCT Compound (Agar Scientific, UK) was added to provide the necessary support to the tissue. The mould was placed in cold isopropanol so that the OCT could solidify. The iced block was then attached to the specimen holder and placed on a cryostat and sliced at 12 $\mu$ m slices. The slices were attached on slides and let dry for at least 30min before stored at -80 Co. The sliced LMS were then stained with the TUNEL assay following the company's instructions. The stained LMS were visualised on a confocal microscope as described in section 2.12 .



## **2.10 Fixation of LMS**

Fixation of LMSs was necessary to preserve tissue structure for immunohistochemical assessments. The LMSs were, initially, washed in PBS and, then, incubated in 4% PFA (Alfa Aesar, USA) in PBS solution for 15min at room temperature. During fixation, LMSs were mounted on stretchers, so they remain flat. After fixation they were washed in PBS solution, the slice holders were cut with a razor blade and stored in fresh PBS solution at 4°C for up to 4 months.

## **2.11 Immunofluorescence staining**

Immunofluorescence staining is a very informative method that is used to unravel spatial changes in biological samples, quantify protein expression and localisation within cells. The method utilizes fluorescent-labelled antibodies to detect specific target antigens. In brief, a primary antibody recognises and binds to the protein of interest, while a secondary fluorescent antibody binds to the primary and allows the visualisation of the target under a fluorescence or confocal microscope. Since LMSs retain their native cell organisation they are an excellent platform to investigate local changes both within cells and within the highly organised tissue architecture.

Fixed LMSs were used for immunofluorescence staining. In order for the antibodies to reach the inner parts of cells and penetrate within the tissue a permeabilization step was needed. Fixed LMSs were permeabilised in 1.5% Triton X-100 (Sigma-Aldrich, USA), a detergent that permeabilises the lipid membranes. Another important step was to avoid unspecific binding of the antibodies to non-targeted structures. Blocking with serum, milk powder or bovine serum was essential to minimise this effect. For that reason, a specific blocking solution, previously

developed in the lab, was used. Samples were blocked in a solution of 10% fetal bovine serum (FBS) (Thermofisher, USA), 5% bovine serum albumin (BSA) (Sigma-Aldrich, USA) and 10% horse serum (Thermofisher, USA). The permeabilization and blocking components were combined in one solution and were all diluted in PBS. The LMSs were incubated with the permeabilization/blocking solution for 3h at room temperature. At the end of the incubation, the permeabilization/blocking solution was removed, and primary antibody was added and incubated overnight at 4°C. The next day the primary antibody was removed, and samples were washed with PBS solution 3x for 30min. The secondary antibody was, then added and incubated for 2h in room temperature. The samples were again washed with PBS solution 3x for 30min. Finally, the tissue nuclei were stained with Hoechst 33342 dye (Thermofisher, USA) for 15min at room temperature and then washed with PBS solution for 30min. All incubations were done on a rocker so solutions could better penetrate the inner layers of the tissue. All samples were covered with aluminium foil after the addition of the secondary antibodies to avoid bleaching of the fluorophores. The concentration of the primary and secondary antibodies can be found in table 2.2.

The stained samples were placed on microscope slides (Sigma, USA), a drop of PBS was added and a 1mm cover glass (VWR, USA) was placed on top of the sample. The cover glass was placed on the edge of the slide and then slowly released, so that bubble trapping was avoided. Due to surface tension between the cover glass and the wet mounting the LMSs were kept flat, which resulted in quicker image acquisition. The cover glass was sealed with nail varnish and the prepared LMSs were visualised either immediately or within 12h.

## **2.12 Confocal microscopy**

### **2.12.1 Imaging procedure**

Confocal microscopy is a well-established imaging technique that is used for high-resolution three-dimensional visualisation. Confocal microscopy has many advantages over widefield microscopy in that it can control the depth of field, reduce the background information of the out-of-focus plane, and collect serial optical sections from thick samples (St. Croix et al., 2005). This is an essential element for the imaging of LMS, since they are comprised of multiple cell layers and extracellular matrix. Confocal microscopy was carried out at the Facility for Imaging by Light Microscopy, Imperial College London with the assistance of Mr. Stephen Rothery. A Zeiss LSM780 confocal laser scanning microscope with 7 laser lines (Argon multiline 458/488/514nm 25mW, Diode 405nm 30mW, HeNe 543nm 1mW, HeNe 594 2mW and HeNe 633nm 5mW) and 34 detectors (34 Channel GaAsP detection (System) was used for imaging. Zen Black software (Zeiss, Germany) was used to control the microscope and acquire the images. Images were captured using either a 10x objective (EC Plan Neofluar 10x/0.3 air, working distance 5.2mm), a 20x objective (Plan Apochromat 20x/0.8 air, working distance 0.55mm) or a 40x objective (EC Plan Neofluar 40x/1.3 oil, working distance 0.21mm). During all experiments, laser power, gain and digital offset were optimised using the range indicator, to ensure best image quality and minimise photo-bleaching and saturation. In experiments that required intensity quantification, these parameters remained constant to make sure that results could be comparable. Usually a z-stack of images were acquired, in order to collect data from inner cell layers. Despite the ability of the microscope to access the inner layers of 3D objects the tissue density and light scattering within the LMS made imaging possible only on the outer layers of the tissue.

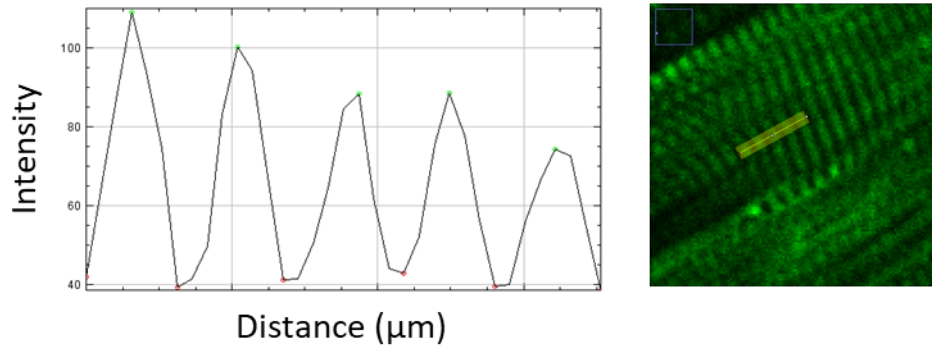
## **2.12.2 Confocal image analysis**

Image analysis was conducted in Fiji (ImageJ, USA), either using built in plugins and macros or by using custom made macros with the help of Mr. Stephen Rothery. The scope of the experiment and the methodology used to analyse the images is described below.

### **2.12.2.1 Analysis of sarcomere length**

To measure the sarcomere length of cardiomyocytes, the LMSs were stained with  $\alpha$ -actinin.  $\alpha$ -actinin is densely localised on the Z-disks of striated muscles. The distance between two consecutive z-lines determines a sarcomere and therefore the sarcomere length of a cell. Z-stacks of images were acquired using a 20x objective so sarcomeres from different cell layers can be included. A z-stack of images was acquired from at least 3 different areas within one LMS. In each z-stack at least 25 different cells were measured. On the area of injury, where most cells were destroyed, samples were acquired from all the possible positions with positive sarcomeric signal. To analyse the sarcomere length a line was drawn across 5 consecutive sarcomeres in parallel to the longitudinal axis of the cardiomyocyte. A custom-made macro designed by Mr Stephen Rothery, by using ImageJ Macro language (IJM), was used to calculate the distance between consecutive peaks and the average distance of 5 consecutive peaks was measured. For cryoinjured LMSs the areas used to calculate the SL derived from the injury, the border zone (middle), the border zone (side) and away from the injury. Fig 2.10 summarises image acquisition and SL analysis.

## Sarcomere distance measurement



*Figure 2.8-Analysis of sarcomere length (SL). The LMSs were stained with  $\alpha$ -actinin and individual cells were assessed for their SL. The SL was determined by measuring the distance between the peak intensity of 5 consecutive sarcomeres. Analysis was conducted using Fiji.*

### **2.12.2.2 Collagen quantification**

For collagen detection LMSs were stained with pro-collagen I and visualised at red spectrum, at wavelength of 555nm. To evaluate the amount of collagen on the surface and deeper cell layers a z stack was acquired at 20x magnification. To accurately select only collagen structures, the image was processed by thresholding the collagen I, using the Moments thresholding function on Fiji (Tsai, 1995). The area of the cardiomyocytes, stained with  $\alpha$ -actinin, was also calculated after thresholding the area using the Huang thresholding function on Fiji (Wang, 1995). The amount of collagen was calculated as the percentage of area contained collagen to the percentage of area contained cardiomyocytes ( $\text{area of collagen I} / \text{area of cardiomyocytes} \times 100$ ). This calculation prevents misinterpretation due to variability in tissue abundance and homogeneity within a sample.

Table 2.2-Deatalied list of antibodies used in this project and their respective concentrations

<b>Primary antibodies</b>			
Alpha-actinin	Mouse	1:1500	Sigma (a7811)
Collagen I	Rabbit	1:1000	Abcam (ab34710)
Caveolin 3	Mouse	1:500	Beckton Dickson BD Biosciences
Connexin 43	Rabbit	1:2000	Sigma-Aldrich
HIF-1alpha	Mouse	1:200	Abcam (H1alpha67)
HIF-1alpha	Rabbit	1:500	Abcam (ab179483)
Isolectin-B4	Biotin conjugated	1:1000	Life technologies
Vimentin	Chicken	1:3000	ThermoFisher Scientific
<b>Secondary antibodies</b>			
Alexa 488	Donkey, Anti-mouse	1:1000	ThermoFisher Scientific
Alexa 555	Goat, Anti-rabbit	1:1000	ThermoFisher Scientific
Alexa 647	Goat, Anti-chicken	1:1000	ThermoFisher Scientific
<b>Nuclear staining</b>			
Hoechst 33342		1:1000	ThermoFisher Scientific

## 2.13 LMS Ca<sup>2+</sup> handling

To detect intercellular calcium changes a chemical Ca<sup>2+</sup> indicator was used, Fluo8-AM (Abcam, USA). This is a cell permeable dye that binds to intracellular Ca<sup>2+</sup> resulting in increase in fluorescence, >150 times higher. Once inside the cardiomyocytes, the molecule undergoes de-esterification to form a membrane impermeable fluorescent dye. To facilitate better solubility of the dye to the media, pluronic F-127 (Thermo Fisher Scientific, USA), a non-ionic, surfactant was used. The Ca<sup>2+</sup> handling experiments were performed by Dr Eef Dries.

Cultured LMSs were carefully removed from the culture chamber and incubated for 15 min at 37°C with the 10µM Fluo8-AM in recording Tyrode's solution + 0.01 % pluronic F-127 (Thermo Fischer Scientific, USA) + 10 mM BDM + 10 µM blebbistatin. LMSs were incubated on stretchers, so that SL was maintained, and under electrical field stimulation of Voltage=15V, Width=10ms and Frequency=1Hz.

### 2.13.1 Optical mapping

After incubation, LMSs were transferred to an upright microscope (Nikon Eclipse FN1, Japan) and perfused with pre-oxygenated 37°C recording Tyrode's solution + 10mM BDM and 10µM blebbistatin to prevent motion artefacts. Excitation of Fluo-8AM was done using a LED light source at 470 nm and emission signals recorded at wavelength of 495nm with a 10x objective. Baseline Ca<sup>2+</sup> transients were recorded by field stimulating the LMSs at 1Hz, Voltage=15V, Width= 20ms. Calcium transients were recorded in a 2048 x 512pixel image at 154 frames/second during a 5 second period using HCLImage Live software (Hamamatsu, Japan). Subsequently, the LMSs were conditioned with a pro-arrhythmic pacing protocol for 2 min (described in section 2.10.3) under the presence of 1µM isoproterenol. After 2 min, pro-arrhythmic pacing was stopped, and spontaneous Ca<sup>2+</sup> release (SCR) events were detected in a 2048 x 512 pixel image at 125 frames/second during a 20 seconds period.



### 2.13.2 Ca<sup>2+</sup> event analysis

Raw imaging data were firstly analysed using Fiji software and later, traces were further processed using the Clapmfit software.

Calcium transients were analysed after background subtraction on Fiji. To measure Ca<sup>2+</sup> transient amplitude the ratio of peak fluorescence (F) normalized to baseline values (F<sub>0</sub>) was calculated. For the kinetics, a profile plot was generated and saved as a .txt file. The .txt file was analysed in Clampfit, where the traces were processed in the same way as contractility.

The analysis of SCR events was performed after background subtraction and using custom-made macros in Fiji. For each LMS, the number of SCR foci, the latency time, the distance to the nearest SCR foci, the speed of SCRs, the distance and angle of SCR propagation were analysed. The number of foci was quantified as the number of spots with spontaneous Ca<sup>2+</sup> release at rest and reported as the number of events/mm<sup>2</sup>/second. The latency time was quantified as the time interval between cessation of stimulation and the occurrence of the first SCR event. The number of SCR was analysed manually using Fiji software, and the areas of interest were saved for further analysis such as determining the latency time. To evaluate the spatial relationship between the SCR foci, the nearest distance between SCR foci was calculated by using a plugin function at Fiji software called “NND (nearest neighbour distances calculation)”. The wave distance was calculated by manually measuring the distance between the beginning and end of a Ca<sup>2+</sup> wave.

## **Mitochondrial membrane potential**

### **2.13.3 Assessment of the mitochondrial membrane potential**

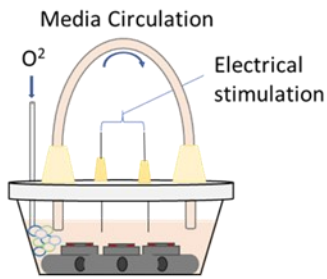
Mitochondrial membrane potential was assessed in both fresh and cultured LMS. Acute LMSs were prepared as described previously in section 2.2 and mounted on stretchers. Cultured LMSs were already prepared for the staining. Mitochondrial membrane potential ( $m\Delta\Psi$ ) on viable LMSs was assessed by staining the tissue with Tetramethylrhodamine, Methyl Ester (TMRM) (ThermoFisher, USA). The cell-permeant dye accumulates in active mitochondria with intact membrane potential depending on their  $m\Delta\Psi$ . At low concentrations, non-quenching mode, the signal of the dye appears bright (high intensity) indicating that the cells contain healthy active mitochondria. On the other hand, low intensity indicates that the cells have lost their  $m\Delta\Psi$  and their cells have reduced their metabolic function. The dye can also be used in high concentrations, in the quenching mode, with reverse function; however, in these experiments the non-quenching state was used. The LMSs were incubated in a circular custom-made box, provided with electrical stimulation, media circulation and oxygenation. The incubation solution contained 100ml of Media M199 + 3%Pen/Strep + 0.001% ITS + 25nM of TMRM. The LMSs were incubated for 40min.

### **2.13.4 Widefield imaging**

The stained LMSs on stretchers were placed on a 35mm glass-bottom dish (Ibidi, Germany). In order to position the LMS close to the objectives of the inverted widefield microscope, the stretcher with the LMS was placed upside down with the bottom of the stretcher facing up (See Fig 2.11). The dish was filled with 2ml of warm, 37°C, Media M199 + 3%Pen/Strep + 0.001% ITS. The acquisition settings were optimised to avoid TMRM bleaching and maximise imaging quality. The same acquisition settings were used for all subsequent experiments to allow

intensity comparisons between conditions. TMRM was excited at 555nm, while emission was recorded at 578nm, as recommended by the manufacturer. In order to record changes in  $m\Delta\Psi$ , a time series function was used, and images were recorded every 2 s. The LMSs were left to stabilise for 30s and then 10 $\mu$ M Carbonyl cyanide-p-trifluoromethoxyphenylhydrazone (FCCP) (Sigma-Aldrich) was added to uncouple the mitochondrial oxidative phosphorylation. The FCCP was used to calculate the percentage of TMRM fluorescence compared to fluorescence that was produced when the  $m\Delta\Psi$  was abolished. A schematic representation of the experimental design can be seen in Fig 2.11.

24h LMS incubation  
in TMRM media



Up-side down position of  
the stretcher for microscopy



TMRM intensity  
recording

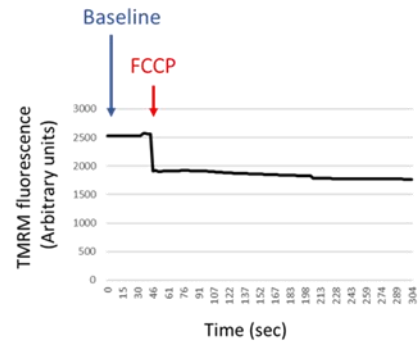


Figure 2.9-Schematic representation for live imaging of mitochondrial membrane potential. 24h cultured LMSs were incubated in TMRM culture media solution for 40min on stretchers. Stained LMSs were visualised on an inverted Widefield microscope and therefore, the stretchers were positioned up-side down to allow better optics. The fluorescence during basal conditions or after addition of a mitochondrial membrane uncoupler, FCCP, were measured.

### **2.13.5 Analysis of the $m\Delta\Psi$**

The files were analysed using Fiji software. LMS intensity at each time point was measured using a plug in designed by Mr Stephen Rothery, the values were later processed in Excel Microsoft software (Microsoft, USA). TMRM fluorescence was calculated by averaging the LMS intensity for the first 30s recording, while TMRM fluorescence of collapsed  $m\Delta\Psi$  was measured by averaging the LMS intensity for the first 60s after FCCP addition. The fold change of fluorescence before and after the addition of FCCP was calculated. See Fig 2.11 for representative traces of TMRM fluorescence.

## **2.14 Laser diffraction**

To simulate different preload conditions on the LMSs it was necessary to determine % of LMS stretch and its correlation to the average SL of the cardiomyocytes. For this reason, the SL of the slice fibres was measured by using the laser diffraction method. This method originates from Sandow's experiments (Sandow, 1936), who found that striated muscles act as a network when they are exposed to a beam of light, resulting in a diffracted light pattern (Fig 2.12.A). Since then many investigators have used this method to measure sarcomere length in both skeletal muscle (Lieber et al., 1984; Roche et al., 2015) and cardiac muscles (Carlsen et al., 1961; Leung, 1982).

The whole set-up was placed in a matt black box to reduce reflections of the laser beam and background light. A HeNe laser (Lasos, Germany) with a wavelength of 633nm was positioned vertically, 2cm above the LMS sample. The LMS was mounted on a stretcher and placed in a petri dish filled with Tyrode's slicing solution. The light beam was directed to the LMS and projected 20.9cm away from it, a distance that was optimised to maximise the light peaks spacing, without significantly compromising light density and allowing more accurate

measurements. The light was diffracted creating 3 different lines that were projected on a white paper, marked with a known distance measurement. The equation described by Cross (Cross et al., 1981) was used to calculate the sarcomere length based on the distance between the zero and the first order band. The diffracted light was captured with a Logitech C920 HD camera and light density were analysed using Fiji software. Excel software was used to analyse the results. The same LMS was used to calculate the SL under different % of stretch. The calculation of SL was determined following the following equation (Cross et al., 1981) in Fig 2.10.

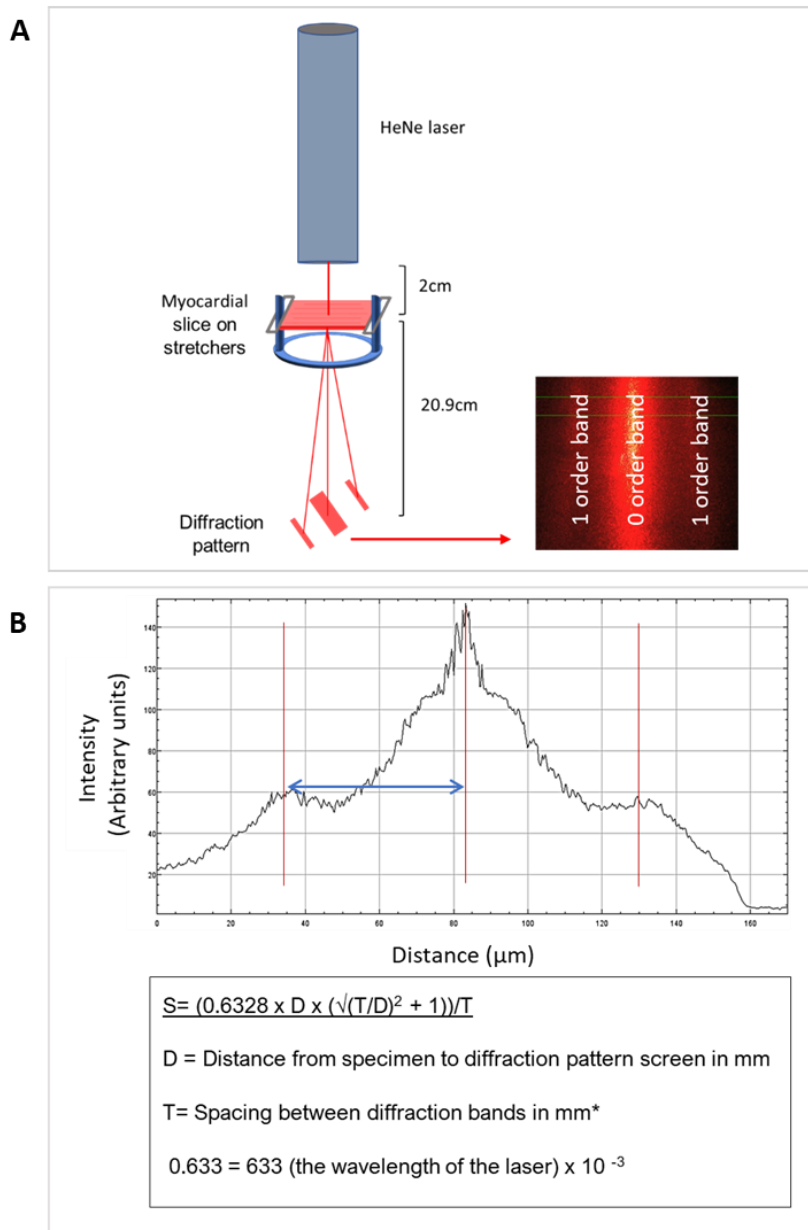


Figure 2.10-Laser diffraction set up for sarcomere length (SL) measurements. A) The laser source and the LMS sample were placed in the optimal position so that the diffracted bands are clearly visualised and separated from each other to allow accurate measurements. B) The laser intensity was visualised using Fiji and the diffracted lines were identified. The distance between the first order bands was measured and then the distance was calculated using the presented formula.

## **2.15 3D printing**

3D printing helped designing custom made tools that were integrated into the LMS work. Custom made objects were designed using the online free to use TinkerCAD tool (Autodesk, USA) and they were printed using an Ultimaker 3 (Ultimaker, The Netherlands). The materials used for this project were either T-glase (Taulman, USA), for designing tissue holders, or of Polylactic acid (PLA) (RS, UK), for designing smaller incubation chambers.

## **2.16 Lipid supplementation on culture media**

### **2.16.1 Preparation of palmitate for LMS culture**

LMSs were also cultured under the presence of long chain fat chain acids, palmitic acid. 10mM Palmitate was prepared by weighting 2.56gr of palmitic acid (Sigma, USA) and put it in a glass beaker. 2ml of 100% ethanol was added to the weighting boat, to scrape of the remaining palmitate and finally the beaker was placed in a water bath at 70°C, until the palmitic acid was dissolved. 1.38gr of potassium carbonate anhydrous (Sigma, USA) was dissolved in 1ml of ddH<sub>2</sub>O. The potassium solution was then slowly added to the palmitic acid, covering the whole area of the beaker bottom. The mixture was heated at 70°C for 3h until all the water evaporated. 100ml of 0.9% sodium chloride was added to the mixture and left at 70°C in the water bath until the solution became transparent. The resulted palmitate solution had 100mM concentration. In order for the palmitic acid to become soluble in the media, it was necessary to bind it to BSA. For that reason, 5.61 gr of pure BSA powder (Sigma, USA) was dissolved in 45ml of media. The mixture was stirred and heated on a heated stirrer up to 37°C. Higher temperature would denature the proteins. 5ml of palmitate solution was then heated to 70°C and slowly added to the 37°C BSA solution. The final solution should be transparent. When



there was denaturation of the proteins due to high temperature or incomplete binding, the solution appeared opaque and was discarded.

## **2.17 Statistics**

Normally distributed data are represented as Mean  $\pm$  Standard Error (SEM). In case of not normally distributed data, the Median  $\pm$  95% Confidence interval was reported. Statistical analysis of two groups was performed with a T-test, whereas for more groups One-way analysis of variance (ANOVA) was chosen. For One-way ANOVA comparisons a Tukey's post-hoc analysis was used. In case multiple samples and variables were considered a 2-way ANOVA was used. The number of replicates is presented as N/n=biological replicates (animals)/technical replicates (LMS).

# **Chapter 3**

## **LMS characterisation**

### 3.1 Introduction

Although the idea of using living tissue sections was developed years ago, it has only been the last decade that popularity of this technique has increased (Fotios G Pitoulis et al., 2020). With the development of new technologies for tissue slicing and culturing, tissue slices became highly viable and were successfully retained *in vitro* for longer periods of time (Fischer et al., 2019; Watson et al., 2019, 2017). This was an important milestone for adult cardiac research since previously used methods of primary isolated cardiomyocytes did not allow studying cells for a long period of time without cell de-differentiation *in vitro* (Mitcheson et al., 1996; Zhang et al., 2010b). This is not a surprising outcome since cell culture monolayers can rarely resemble the physiological conditions seen *in vivo*.

On the other hand, LMSs benefit from their multicellularity, preserved architecture, native ECM and cell composition, elements that are all necessary for the physiological function of the heart. Such complex systems require equally complex and refined culturing methods that can provide all the necessary environmental cues that can be seen in the human mammalian body.

Even though LMSs were initially cultured in an air liquid interface culture system it was soon found that this method could not effectively sustain high contractility and viability of the cardiac tissue (Watson et al., 2019). In 2019 our lab and others (Fischer et al., 2019; Watson et al., 2019) published a new culturing system with electromechanical stimulation that proved to be essential for successful LMS preservation in culture. LMS contractility was significantly improved and proved to be superior to the liquid interface culture system (Watson et al., 2019, 2017). To better refine this *in vitro* system both the slicing and culturing conditions were revisited. LMSs were also characterised for their physiological function after culture.

One of the most important parameters of the LMS is tissue thickness. Tissue thickness dictates oxygen and nutrient distribution through passive diffusion, since active perfusion through the

vasculature cannot be supported after slicing the tissue. The most commonly used thickness for LMSs is 300µm; however, in the literature there is a wide range of tissue thickness used in cardiac or other tissue samples ranging from 100 to 500µm (Chalisova et al., n.d.; Morin et al., 2002, 1999; Watson et al., 2017). Preparing thinner slices (<300µm) could aid in increasing the yield of slices per tissue and therefore, increase the throughput of the method. Additionally, thinner slices could improve oxygen diffusion and enhance tissue contractility.

The heart is constantly under diastolic and systolic pressure. It has been shown that changes in pressure can alter cardiac function and lead to either hypertrophy or atrophy depending on the nature and duration of the stimuli (Diakos et al., 2014; Kahan and Bergfeldt, 2005). Therefore, regulating mechanical load can also modulate myocardial function *in vitro*.

It was hypothesised that changes in slicing and culturing conditions can further enhance LMS viability *in vitro*.

The aims of this chapter are to:

- 1) Define the right slicing solution and LMS thickness.
- 2) Evaluate media oxygenation levels and supplementation.
- 3) Define the right mechanical load and how that affects contractility and bioenergetics on LMS.

## **3.2 Methods**

### **3.2.1 Slicing solution preparation**

The effect of different slicing solutions was assessed by preparing 3 different solutions, Tyrode's slicing solution, Media M199 and Media M199+extra buffer. Tyrode's slicing solution was prepared as described in section 2.2.1. Media M199 was used either as purchased (buffered NaHCO<sub>3</sub> at 2.2gr/L) or extra buffer (buffered NaHCO<sub>3</sub> 3.7gr/L) (Sigma, Germany) was added. In all solutions 30mM BDM was added to prevent tissue contraction during slicing. Media M199 and Krebs's solution were cooled at 4°C before any pH measurement was performed.

### **3.2.2 Tissue slicing**

Tissue slicing was performed on male rats. A full description of the protocol can be found in section 2.2.

Whenever applicable, thinner LMSs were produced by lowering the tissue thickness settings on the vibrating microtome to 200µm.

### **3.2.3 Tissue holder**

Hand-made tissue holders were made out of 0.25mm insulated silver wires (PTFE-insulated) (Goodfellow, UK). This material was used since it was light weighted, non-toxic and with an easily adjustable shape. The wire was shaped in a rectangular shape of 10mm in length. Because the silver wire holders did not hold the glue after the first application, multiple coats of Histoacryl were applied so that the LMS could attach.

3D printed tissue holders were designed and printed as described in section 2.4.

### **3.2.4 LMS culture**

LMSs were cultured as described in section 2.6.

### **3.2.5 Contractility**

Contractility at maximum isometric stretch was assessed using a force transducer as described in section 2.8.

### **3.2.6 LMS viability**

LMS viability was assessed using the MTS protocol, CellTiter, as described in section 2.9.1.

### **3.2.7 Media glucose quantification**

To identify LMS glucose uptake and lactate production, medium samples were collected, before and after 24h culture. Culture media was filtered using 0.5 Centrifugal Filter (Merckmillipore, USA), in order to remove large proteins, >10kD (mostly BSA and lipids bound to it), that could interfere with the glucose and lactate detection. Samples were immediately frozen and stored at -80°C. To quantify glucose consumption, an enzymatic based (oxidase/peroxidase) method was used (Glucose (GO) Assay Kit, Sigma, Germany). The assay was performed according to the manufacturer's instructions. Similarly, lactate production was measured by using L-Lactate Assay Kit (Colorimetric/Fluorometric) (Abcam, United Kingdom), which is also based on enzymatic conversion of lactate to a colorimetric and fluorometric substance. In both kits, absorbance was measured by using a microplate reader at 540nm (glucose) and 570nm (lactate).

## 3.2.8 Radiolabelled palmitate/glucose detection

### 3.2.8.1 Palmitate consumption

Palmitate oxidation was determined by measuring the release of  $^3\text{H}_2\text{O}$  derived from  $^3\text{H}$ -palmitate metabolism through the electron transport chain as previously described (Barr and Lopaschuk, 2000; Lopaschuk et al., 1994). LMSs were cultured in culture media containing 2% BSA (Sigma-Aldrich), 0.1mM palmitate and 1.85 MBq of Palmitic Acid/150ml media, [9,10- $^3\text{H}$ (N)] (PerkinElmer, USA). The palmitate was heated at  $70^\circ\text{C}$  to become liquid and added at the same time with the  $^3\text{H}$  palmitate so that both types have equally opportunity to bind to the BSA in the media. The LMSs were cultured for 24h as described in section 2.6.3. In the beginning of the experiment 4ml of media were collected before their exposure to the LMS. During culturing,  $^3\text{H}_2\text{O}$  was released into the incubation media. Media samples were, also, collected and stored at  $-20^\circ\text{C}$  at the following timepoints: baseline, 30min, 1h, 2.5h, 5h, 18h, 24h.

The incubated media contained both produced  $^3\text{H}_2\text{O}$  and remained  $^3\text{H}$ -palmitate, which were later separated via Folch extraction. A volume of 1.88ml of chloroform (Fisher Scientific, USA): methanol (Honeywell, USA) (1:2 v/v) solution, 625ml chloroform and 625 $\mu\text{l}$  KCl-HCl solution (2M KCl, 0.4M HCl) were added to 0.5ml of cultured media. The mixture was rotated on an SB3 Stuart rotator at 40 rpm for 10min and left in the hood for 1h, to allow the different layers to separate. The top aqueous layer was then removed with a glass pipette-bulb, while the organic (bottom) layer was discarded. The extracted solution was mixed again with 1ml chloroform, 1ml methanol and 0.9ml KCl-HCl solution and then placed on the Stuart rotator for 10min at 40rpm. The mixture was, then, left for separation to occur in the hood for 1h. The top aqueous phase was once again removed and 0.5ml (in duplicate) of it was added into a scintillation vial containing 10 mL of Ecolite liquid scintillation cocktail (MP Biomedicals, USA). The radioactivity of the sample was counted, in counts per mole (cpm), using the Tri-

Carb 2800TR Liquid Scintillation Analyzer (PerkinElmer, USA). As a negative control spiked media (media that was not exposed to LMS) were extracted to determine the background noise. As a positive control non extracted spiked media was added directly into scintillation vials to determine the activity of the buffer.

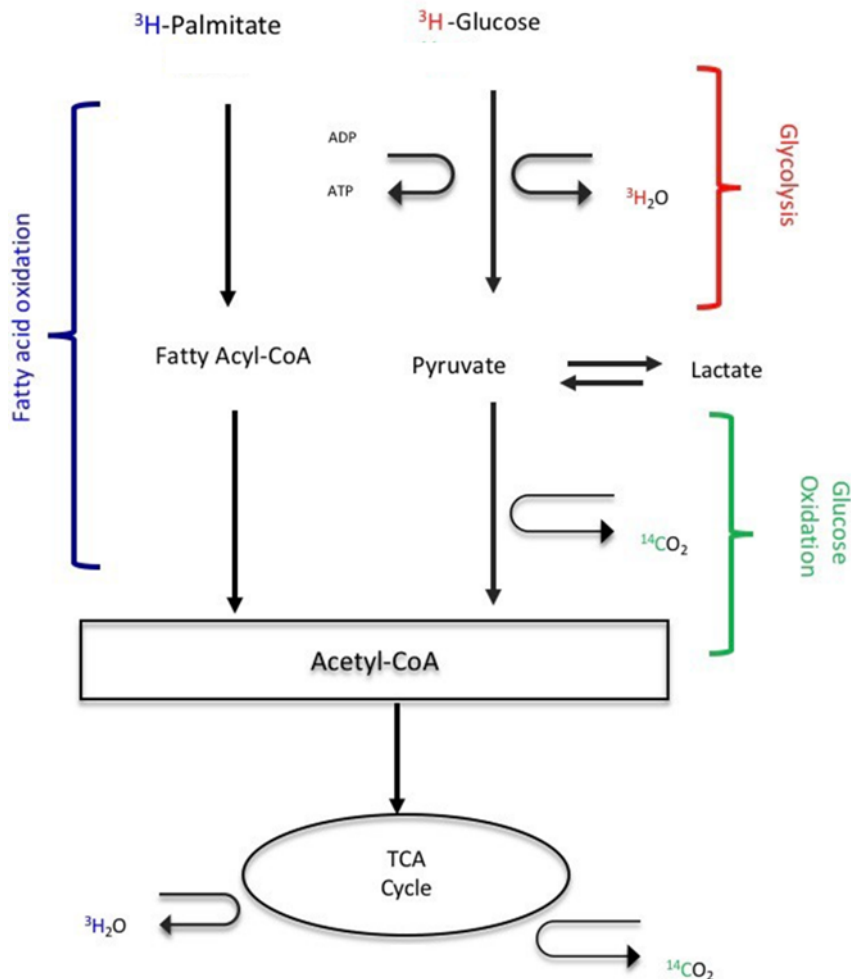


Figure 3.1- Overview of radiolabelled energy metabolic pathways in the heart. Adapted from (Sci. Guid. to Card. Metab., 2016).



### 3.2.8.2 Calculation of palmitate radioactivity

For each sample the analyser performed two identical measurements and therefore the average measurement (in counts per minute-cpm) was calculated. The average cpm of the negative control (background) was subtracted from the sample cpm. Palmitate oxidation rate was calculated using the following equations:

Total Palmitate oxidation per (nmol/cell number/hour)

=

$17.1 * (Aver. sample\ cpm - Aver. background\ cpm) / Counts\ per\ mole\ palmitate / Cell\ count /$   
*Hours*

The dilution factor of 17.1 was due to the dilution of the buffer aliquot during the extraction protocol (Lopaschuk and Barr, 1997).

### 3.2.8.3 Glucose consumption

Glycolytic rates were determined through the conversion of  $^3\text{H}$ -glucose to  $^3\text{H}_2\text{O}$  via enolase which converts 2-phosphoglycerate to phosphoenolpyruvate and releases  $\text{H}_2\text{O}$  as a by-product (Fig 3.1).

LMSs were incubated in 150ml of culture media contained 0.074 MBq of Glucose, D-[5- $^3\text{H}$ (N)] (PerkinElmer). The LMS culture is described in detail in section 2.6. Culture media before adding of the LMSs was collected as a control. During culture  $^3\text{H}_2\text{O}$  was released into the incubation media. At the end of incubation, the media contained both the produced  $^3\text{H}_2\text{O}$  and the remained  $^3\text{H}$ -glucose. These two were separated later using the ion-exchange chromatography separation (Dowex) method (Hammerstedt, 1973; Støttrup et al., n.d.; Teslaa and Teitell, 2014; Walborg and Lantz, 1968). The  $^3\text{H}_2\text{O}$  was separated from the  $^3\text{H}$ -glucose using a Dowex 1x4 chloride form and 100-200 mesh (Sigma, UK) anion exchange column.

The Dowex compound was prepared by adding 250 g of Dowex resin into a solution containing 1.25M NaOH and 1.61M boric acid. The mixture was then mixed gently, and the beads were repeatedly washed with distilled H<sub>2</sub>O until the mixture reached pH 7.5. The exchange columns were prepared in glass Pasteur pipettes (VWR, USA). The bases of the pipettes were filled with glass wool (Fig 3.2A) and placed in a rack (Fig 3.2B). The glass pasteur pipette was filled up to 2/3 with Dowex. The columns were, then, washed twice with dH<sub>2</sub>O and allowed to drain. Scintillation vials were filled with 10ml of scintillation fluid, Ecolite liquid scintillation cocktail, (MP Biomedicals, USA), and placed underneath the columns to collect samples. 200 µL of the collected incubation media from each sample were added to the Dowex column, and incubated for 15 minutes, allowing the <sup>3</sup>H-glucose to bind to the column and <sup>3</sup>H<sub>2</sub>O to be eluted into the vials. 1ml of dH<sub>2</sub>O was added to the dowex columns to wash down any residual samples. The scintillation vials were collected after the columns were fully drained and the radioactivity (cpm) was measured using a Tri-Carb 2800TR Liquid Scintillation Analyzer (PerkinElmer).

In addition, a media sample at time zero was run through the dowex column (negative control) and another one was added directly into scintillation vials (positive control).

#### **3.2.8.4 Calculation of glucose radioactivity**

For each sample the analyser performed two identical measurements and therefore the average measurement (in cpm) was calculated. The average cpm of the negative control (background) was subtracted from the sample cpm. Glycolytic rates were calculated using the following equation:

Total glycolytic flux per (nmol/cell number/hour):

$$= (\text{Aver. sample cpm} - \text{Aver. n cpm}) / \text{Counts per mole glucose} / \text{Cell count} / \text{Hours}$$

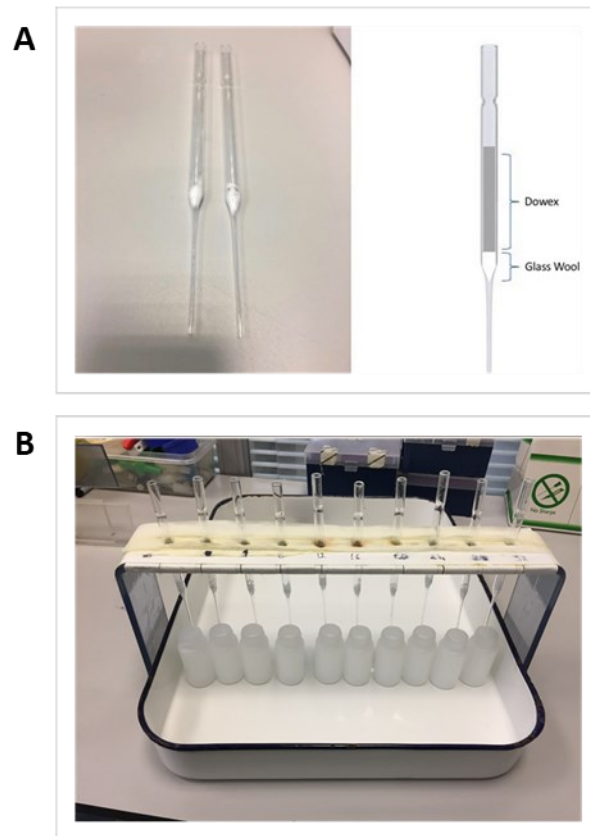


*Figure 3.2-Ion-exchange chromatography separation method (Dowex). A) Glass pipets filled with glass wool and Dowex material. B) Design of a rack holding 10 glass pipets. The glass pipet ends were inserted into scintillation vials, where the separated samples were collected.*

## **Hypoxia measurements**

Hypoxia was measured by staining the LMSs using HIF1- $\alpha$  antibodies (Abcam, ab179483, US), rabbit, 1:500. Z-stacks were recorded as described in section 2.12. The same number of z-stacks were used in all samples so that mean intensity could reveal differences only based on HIF1- $\alpha$  fluorescence. The z-stacks were flattened using z-projection and mean intensity was recorded from individual cells.

### **3.2.9 Media oxygenation**

Oxygen concentration in the media was measured by using an oxygen meter (Mettler-Toledo International, Switzerland). The device was calibrated as specified by the company, by measuring the atmospheric oxygen levels which resulted in 100% of oxygen saturation. Subsequently the probe was inserted in the culture media perfused with 95% O<sub>2</sub>, 5% CO<sub>2</sub> directly in the media, above the surface of the media or not perfused at all. Multiple measurements were taken during the time of 15h. The media was placed inside an incubator and warmed up to 37°C at all times.

### **3.2.10 Sarcomere length measurements**

The sarcomere length of freshly prepared LMSs was measured using the laser diffraction method as described in section 2.15.

### **3.2.11 Mitochondrial membrane potential**

Mitochondrial membrane potential was measured by using a mitochondrial membrane dye, TMRM, on both rat and human LMS, as described in section 2.14.

## 3.3 Results

### 3.3.1 Slicing solution

In order to determine the optimal slicing solution for rat LMSs three different solutions were used, Tyrode's solution, Krebs solution and media M199 solution. Tyrode's solution was perfused with 100% O<sub>2</sub>, whereas Krebs solution and media M199 were perfused with a mixture of 95% O<sub>2</sub> and 5% CO<sub>2</sub>, based on their buffers.

The effect of temperature and oxygenation were evaluated and therefore, the pH in M199 media was measured at both RT and 4°C in the presence or absence of oxygenation. The temperature did not significantly alter the pH of the media which remained at 7.8 in both RT and 4°C. However, oxygenation reduced the pH of the media in both temperatures. After oxygenation RT media pH decreased in 7.2 and similarly in 4°C media the pH decreased at 7. Both values were below the physiological pH range of 7.35 – 7.45 (Hopkins and Sharma, 2018). To correct for the low pH, extra buffer, NaHCO<sub>3</sub>, was added which increased the pH to 7.4.

To test if different slicing solutions affect tissue viability, LMS contractility was measured on freshly prepared samples. Neither M199 or M199 with higher buffer concentration increased contractility (active force) compared with Tyrode's solution, as seen in Fig 3.3D. Similar results were observed on LMSs sliced with Krebs solution. Krebs solution was used because it contains the same type of buffer as M199 but it has less nutrients as the Tyrode's solution. As a positive control normal Tyrode's solution was used, which showed to have the higher contractility values over the other conditions.

A

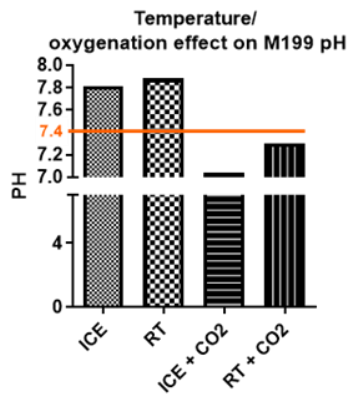
Tyrode's solution	
Composition	Concentrations (mM)
NaCl	140
KCl	6
Glucose	10
HEPES	10
MgCl <sub>2</sub>	1
CaCl <sub>2</sub>	1.8
BDM	30

Medium 199	
	<b>M4530</b>
	[1x]
	g/L
<b>COMPONENT</b>	
<b>Inorganic Salts</b>	
CaCl <sub>2</sub> • 2H <sub>2</sub> O	0.2
Fe(NO <sub>3</sub> ) <sub>3</sub> • 9H <sub>2</sub> O	0.00072
MgSO <sub>4</sub> (anhydrous)	0.09767
KCl	0.4
KH <sub>2</sub> PO <sub>4</sub>	—
Na • Acetate (anhydrous)	0.05
NaHCO <sub>3</sub>	2.2
NaCl	6.8
Na <sub>2</sub> HPO <sub>4</sub> (anhydrous)	—
NaH <sub>2</sub> PO <sub>4</sub> (anhydrous)	0.122
<b>Amino Acids</b>	
L-Alanine	0.025
L-Arginine • HCl	0.07
L-Aspartic Acid	0.03
L-Cystine • 2HCl	0.00011
L-Cysteine • HCl • H <sub>2</sub> O	0.026
L-Glutamic Acid	0.0668
L-Glutamine	0.1
Glycine	0.05
L-Histidine • HCl • H <sub>2</sub> O	0.02188
Hydroxy-L-Proline	0.01
L-Isoleucine	0.02
L-Leucine	0.06
L-Lysine • HCl	0.07
L-Methionine	0.015
L-Phenylalanine	0.025
L-Proline	0.04
L-Serine	0.025
L-Threonine	0.03
L-Tryptophan	0.01
L-Tyrosine • 2Na • 2H <sub>2</sub> O	0.05766
L-Valine	0.025
<b>Vitamins</b>	
Ascorbic Acid • Na	0.000566
D-Biotin	0.00001
Calciferol	0.0001
Choline Chloride	0.0005
Folic Acid	0.00001
Menadione (sodium bisulfite)	0.000016
myo-Inositol	0.00005
Niacinamide	0.000025
Nicotinic Acid	0.000025
p-Amino Benzoic Acid	0.00005
D-Pantothenic Acid • ½Ca	0.00001
Pyridoxal • HCl	0.000025
Pyridoxine • HCl	0.000025
Retinol Acetate	0.00014
Riboflavin	0.00001
DL-α-Tocopherol Phosphate • Na	0.00001
Thiamine • HCl	0.00001
<b>Other</b>	
Adenine Sulfate	0.01
Adenosine Triphosphate • 2Na	0.001
Adenosine Monophosphate • Na	0.0002385
Cholesterol	0.0002
Deoxyribose	0.0005
Glucose	1.0
Glutathione (reduced)	0.00005
Guanine • HCl	0.0003
HEPES	—
Hypoxanthine	0.0003
Phenol Red • Na	0.0213
TWEEN 80	0.02
Ribose	0.0005
Thymine	0.0003
Uracil	0.0003
Xanthine • Na	0.000344
<b>ADD</b>	
L-Glutamine	—
Sodium Bicarbonate	—

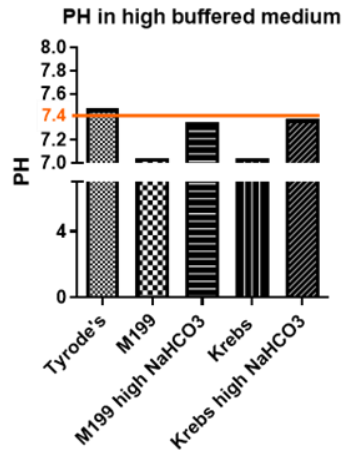
**Medium 199 with increased buffer (NaHCO<sub>3</sub>)**

1g/L < NaHCO<sub>2</sub> < 2.2g/L < 5% CO<sub>2</sub>  
 NaHCO<sub>2</sub> > 3.7g/L → 10% CO<sub>2</sub>

B



C



D

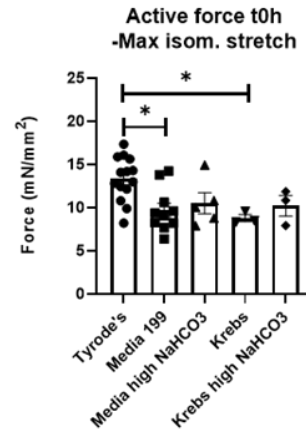


Figure 3.3- Slicing solutions assessment. A) Slicing solution composition. B) The effect of medium M199 temperature and oxygenation on pH regulation. C) Correction of media pH with higher buffer concentration. D) LMS contractility in different slicing solution at 40°C.  $N/n_{Tyrodes}=4/14$ ,  $N/n_{M199}=3/10$ ,  $N/n_{M199\ high\ NaCO_3}=4/14$ . One-way ANOVA was used for statistical analysis.  $N/n$ =biological replicates (animals)/technical replicates (LMS).

### 3.3.2 LMS thickness

In absence of vascular perfusion, oxygen and nutrient availability depends on passive diffusion. The tissue thickness of the LMS could affect nutrient distribution and therefore reduce tissue viability. To assess if thinner LMSs can improve tissue viability the left ventricle was sliced in 200 $\mu$ m thick LMSs and tissue functionality was tested on freshly prepared and cultured LMS. Thinner LMSs produced 40% more tissue samples (~7 LMS) compared to 300 $\mu$ m LMSs (~5 LMS). Freshly prepared and cultured LMSs showed no differences in active force between the different groups (Fig 3.4A); however, thinner LMSs resulted in higher variability as shown by the standard deviation, which in both t0h (STDEV<sub>300 $\mu$ m</sub>=3.8, STDEV<sub>200 $\mu$ m</sub>=6.7) and t24h (STDEV<sub>300 $\mu$ m</sub>=3.24, STDEV<sub>200 $\mu$ m</sub>=5.7) was double than the one seen in 300 $\mu$ m thick LMS. Additionally, thinner LMSs developed arrhythmic events, with high automaticity in absence of electrical stimulation, especially after 24h, which made contractility measurements difficult to acquire (Fig 3.4B).

### 3.3.3 LMS tissue holders

LMS manipulation was performed by using handmade tissue holders made out of silver wire. Histoacryl glue was added to attach the LMS to the tissue holders. The first application of glue was too weak to successfully adhere the tissue holders and therefore multiple glue coats were necessary. This increased the attachment surface area of the tissue holder; however, it also created an uneven glue coating (Fig 3.5A). LMSs frequently detached from the silver wire tissue holders and for that reason 3D printed tissue holders were designed. The holders were made out of PETT filament and were able to improve LMS attachment, with significantly reduced detachment problems. To assess toxicity of the new material, LMSs were cultured for 24h and tissue contractility was assessed. The 3D tissue holders showed no signs of toxicity

when compared to freshly prepared LMS. They additionally resulted in significantly higher contractility (active force) after 24h in culture compared with the silver wire holders, Fig 3.5B.



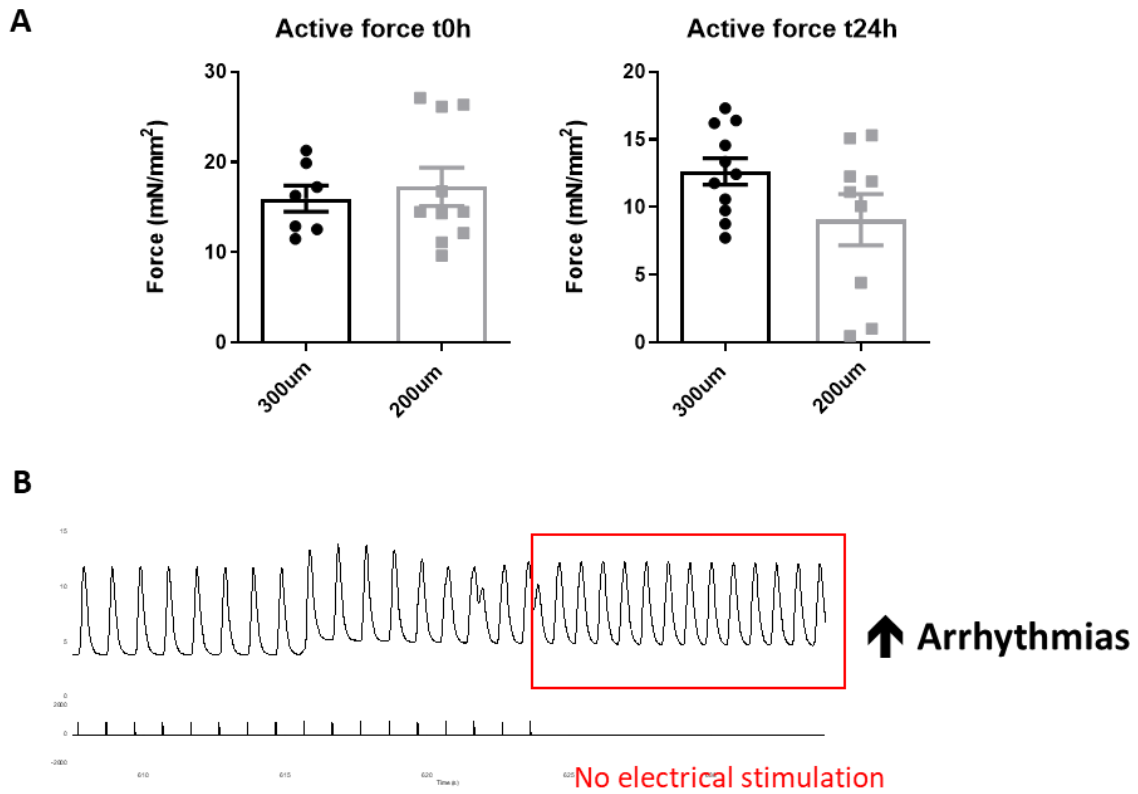
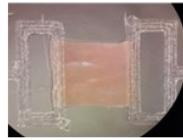
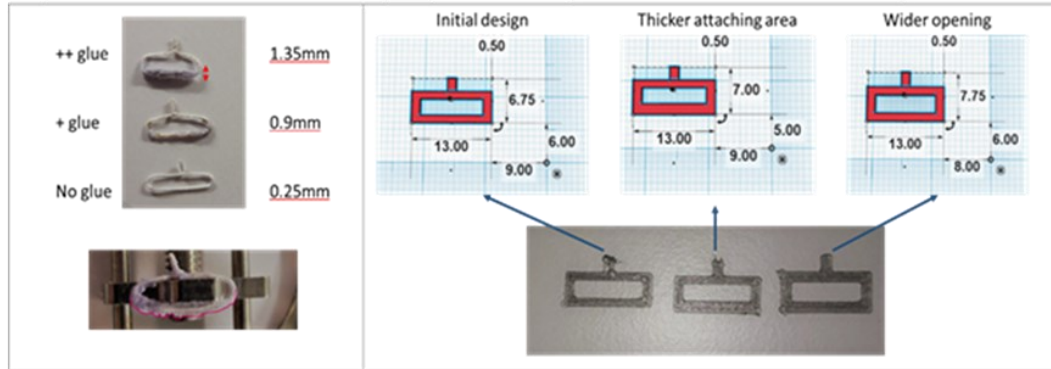


Figure 3.4-Thinner LMSs (200 $\mu$ m). A) LMS active force at maximum isometric stretch. B) Representative image of LMS contractility traces, with signs of arrhythmias.  $N/n_{300\mu\text{m}}=7/7-11$ ,  $N/n_{200\mu\text{m}}=5/10-11$ . A t-test analysis was used for statistical analysis.  $N/n$ =biological replicates (animals)/technical replicates (LMS).

**A**

Silver insulated  
handmade holders

3D printed T-glase  
holders



**B**

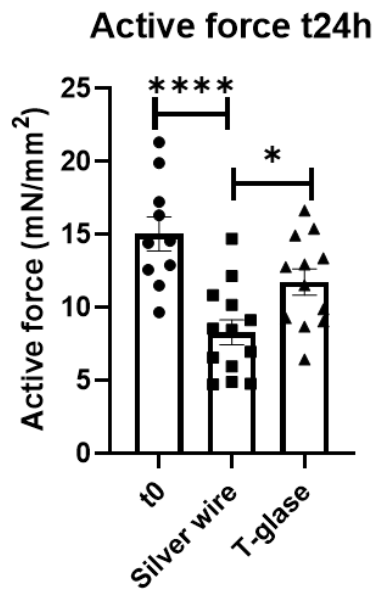


Figure 3.5-Tissue holders. A) Handmade silver wire tissue holders with accumulated tissue glue show inhomogeneous glue distribution. The designs of the new PETT (T-glase) tissue holders can be seen on the right side of the image. Three different designs were printed with differences in the attachment and gap areas. B) Active force measured after 24h of culture at maximum isometric stretch.  $N/n_{t0}=10/10$ ,  $N/n_{silver\ wire}=7/13$ ,  $N/n_{T-glase}=7/12$ . One-way ANOVA was used for statistical analysis.  $N/n$ =biological replicates (animals)/technical replicates (LMS).

### 3.3.4 Tissue culture - Media lipid supplementation

FA are the main energy source for cardiomyocytes and therefore palmitic acid was introduced to the culture media as preferred substrate for ATP production. In order to define the appropriate concentration a dose response experiment was performed on freshly prepared LMS. Acute exposure to palmitic acid on the LMSs showed a reduction of viability starting from concentrations of 1mM and higher, with 2mM reaching statistical significance (Fig 3.6A). Different palmitate concentrations were also tested after 24h culture. LMSs cultured in concentration above 0.1mM showed significant decrease in active force and therefore further experiments were done with the maximum tolerable palmitate concentration of 0.1mM.

FA utilisation was assessed at the end of the LMS culture by measuring lactate production and glucose reduction in the culture media. Both initial and culture levels were evaluated. Glucose levels before and after culture remained unchanged in both LMS control culture media or media supplemented with 0.1mM palmitate. Lactate levels were significantly elevated after 24h of culture in both types of media in comparison to t0h; however, no significant changes were observed between control media and supplemented media after 24h culture (Fig 3.6D). A more sensitive method of measuring FA oxidation is by using radiolabeled substrates in the media. LMS metabolism of both glucose and palmitate started at high levels for the first 3h and then drastically declined and stayed stable for 24h. Glucose levels remained at detectable levels, while palmitate consumption was completely halted at 5h of culture (Fig 3.6E).

These experiments were performed at Oxford University in collaboration with Dr Colleen Lopez and Prof Carolyn Carr. LMS preparation and culture was done by me, while metabolic analysis was conducted by Dr Colleen Lopez.

### 3.3.5 Tissue culture – LMS O<sub>2</sub> levels

Initial culture conditions included direct oxygenation inside the media to ensure adequate oxygenation of the cardiac tissue through the inner cell layers. However, to better define the O<sub>2</sub> levels in the culture chambers, an oxygen meter was used to determine the O<sub>2</sub> levels (%) in relationship to the atmospheric O<sub>2</sub> levels. Oxygenation directly in the media resulted in highly elevated levels of O<sub>2</sub> (200-300%), which was 5 times higher than the normal O<sub>2</sub> levels (56% corresponding to 75-100 mmHg). Therefore, alternative oxygenation ways were tested such as oxygenation only at the surface level of the media, outside of the solution. This method kept the oxygen levels at physiological levels (90mmHg or 56% O<sub>2</sub> saturation) (Fig 3.7B), without significantly affecting the pH of the media (Fig 3.7D). These experiments were done in collaboration with other lab members, Waseem Hasan (BSc student) and Dr Sam Kit Anan (postdoctoral researcher).

O<sub>2</sub> and nutrient diffusion in 3D tissue constructs is of great importance to avoid hypoxic and necrotic areas in the inner layers. To assess whether there was hypoxia, freshly prepared and cultured LMSs were stained against HIF1- $\alpha$  protein. LMSs treated with cobalt chloride (CoCl<sub>2</sub>) were used as positive control of HIF1- $\alpha$  activation. Cultured LMSs showed similar levels of HIF-1 $\alpha$  intensity as freshly isolated LMS, as shown in Fig 3.7A. CoCl<sub>2</sub> images showed increased levels of HIF-1 $\alpha$  fluorescence compared to freshly prepared or cultured LMS.

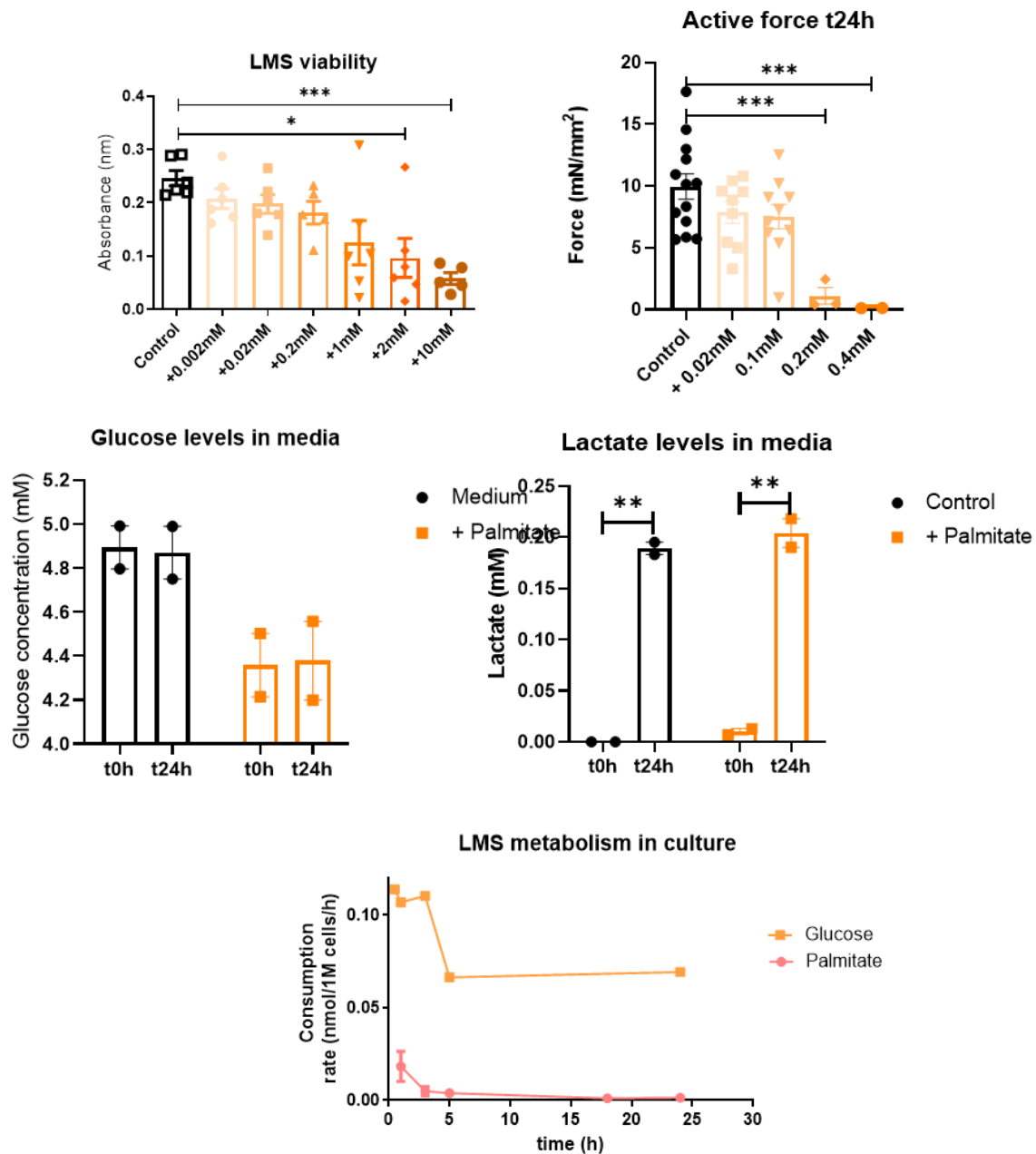


Figure 3.6-Lipid media substitution. A) LMS viability after palmitate dose response on freshly prepared tissue.  $N/n=2/6$ . B) LMS contractility after 24h culture under different palmitate concentration.  $N/n_{control}=7/123$ ,  $N/n_{0.02mM}=5/9$ ,  $N/n_{0.1mM}=5/10$ ,  $N/n_{0.2mM}=2/3$ ,  $N/n_{0.4mM}=1/2$ . C-D) Glucose and lactate levels in media using commercial detection kits.  $N/n=2/2$ . E) Radiolabelled analysis of glucose and palmitate consumption during LMS culture.  $N/n_{palmitate}=3/3$ ,  $N/n_{glucose}=1/1$ . One-way ANOVA and 2-way ANOVA were used for statistical analysis of the graphs A/B and B/C respectively.  $N/n$ =biological replicates (animals)/technical replicates (LMS).

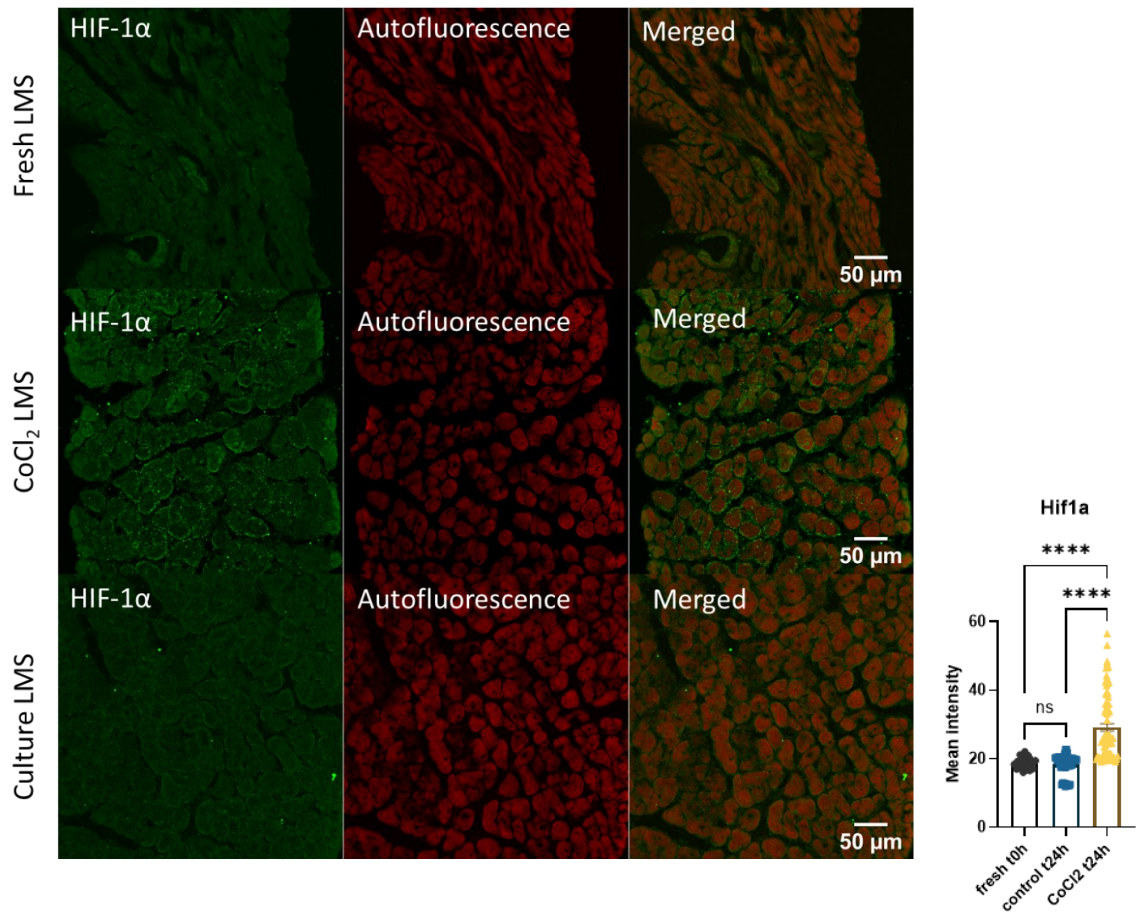
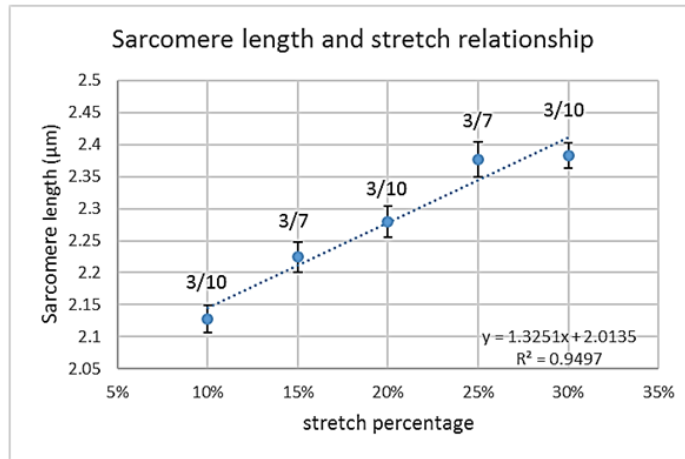


Figure 3.7- Oxygen analysis on LMS. A) Freshly isolated and cultured LMSs stained for HIF1- $\alpha$ . As a positive control CoCl<sub>2</sub> treated LMSs was used. N/n=2/2. B) O<sub>2</sub> level assessed on the culture media at 37°C under perfusion inside the media, on the surface of the media and in absence of oxygenation. C) The pH on these conditions was also evaluated. N/n=1/1. N/n=biological replicates (animals)/technical replicates (LMS).

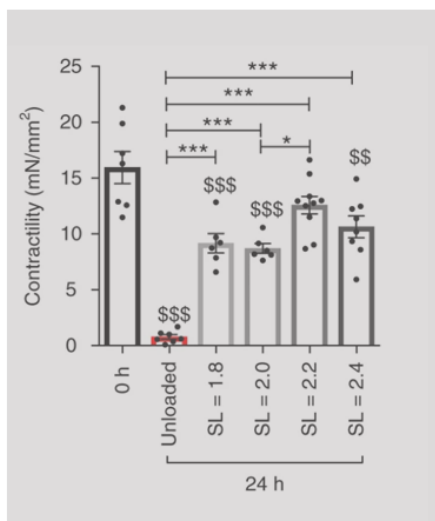
### 3.3.6 Tissue culture- Mechanical stimulation

Previous studies by Watson et al (Watson et al., 2019) showed that stretch can affect tissue functionality after 24h of culture (Watson et al., 2019). To validate and reproduce the data, the SL of freshly prepared LMSs was measured under different preloads by using the laser diffraction method. Fig 3.8A shows linear relationship between the stretch and tissue's SL. Three different stretching conditions were further tested in culture, the unloaded condition (SL=1.8 $\mu$ m or 0% stretch), the physiological load (SL=2.2 $\mu$ m or 15% stretch) and the overload condition (SL=2.4 $\mu$ m or 30% stretch). Freshly prepared LMSs responded as expected with an increase of active force generation as the stretch increases, following the Frank-Starling Law (Rysä et al., 2018). Cultured LMSs in different preloading conditions showed that samples cultured with 15% of stretch (2.2 $\mu$ m of SL) had significantly higher active force under maximum isometric stretch, compared to the other conditions. Similar results were also obtained by Watson et al (Watson et al., 2019).

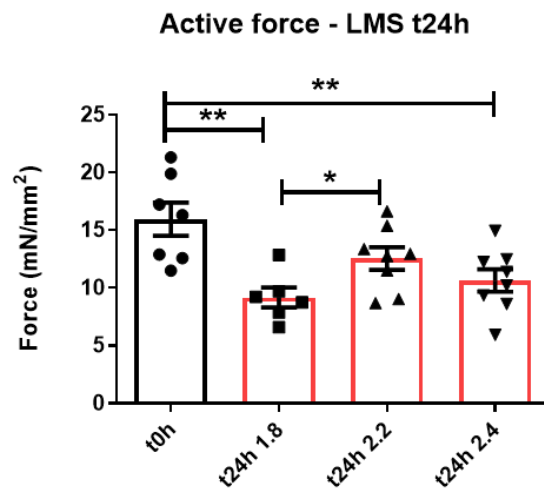
**A**



**B**



**C**



**D**

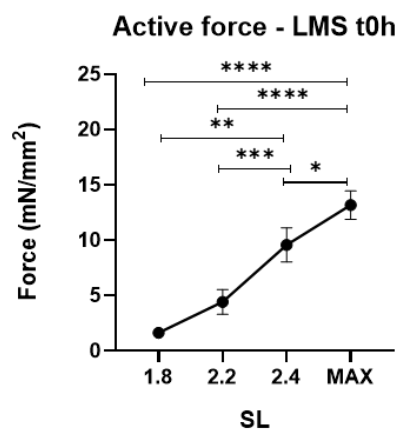


Figure 3.8-The effect of preload on cultured LMS. A) Laser diffraction experiments were done to define the relationship between stretch and SL in freshly prepared LMS. B-C) Cultured LMSs in different preload conditions were reported by Watson et al (Watson et al., 2019) (grey graph) and reproduced for this project. D) Relationship between active force and SL in freshly prepared LMS.  $N/N_{t24h}=6-7/6-8$ ,  $N/nt_{0h}=2/10$ . One-way ANOVA was used for statistical analysis.  $N/n$ =biological replicates (animals)/technical replicates (LMS).



### 3.3.7 Metabolic response to different preloads

To better understand if the contractility phenotype of cultured LMSs is also mirrored in the bioenergetics of the LMS, mitochondrial function was assessed by using a live cell dye, TMRM. The staining was done in a non-quenching mode by using low levels of TMRM concentration. In this mode increase in fluorescence indicates more hyperpolarised  $m\Delta\Psi$ , resulting in higher intensity (Joshi and Bakowska, 2011; Perry et al., 2011). Subsequent application of FCCP depolarises the mitochondria, reduces TMRM fluorescence, which helps to better define the background levels (Fig 3.9B-C). Fig 3.10A shows raw intensity levels of TMRM on freshly prepared LMSs stretched at different preload conditions. The increase of stretch is followed by an increase in the raw fluorescence of TMRM. As stretch increased, there was also, an increase in fluorescence difference before and after application of FCCP. The fold change of fluorescence over FCCP was also calculated to correct for non-specific cytoplasmic staining. The corrected values of fluorescence revealed that overstretched LMSs had higher levels of fluorescence compared with unstretched LMSs (Fig 3.10B). The same measurements were also performed in cultured LMSs (Fig 3.10D). However, cultured LMSs showed no significant differences between the different stretching conditions when their raw intensity data were analysed. Analysis of fold change over FCCP, also, showed similar results (Fig 3.10C-D).

Difference in fluorescence between the freshly prepared and cultured LMSs was also, observed: the latter had more hyperpolarised mitochondria compared to freshly prepared LMS. This indicates that the culture affects mitochondrial function after 24h. This observation was especially apparent in unloaded and physiologically loaded LMSs with levels of fluorescence similar to overloaded LMS.

Autofluorescence of both freshly prepared and cultured LMSs was tested, by recording fluorescence in absence of TMRM.

Whenever possible, human tissue was used, and  $m\Delta\Psi$  was measured in either healthy (donor) or diseased (transplanted-Heart Failure) cardiac tissue. Failing LMSs showed lower fluorescence compared with healthy donors, which indicates that their mitochondria were less polarised (Fig 3.11).

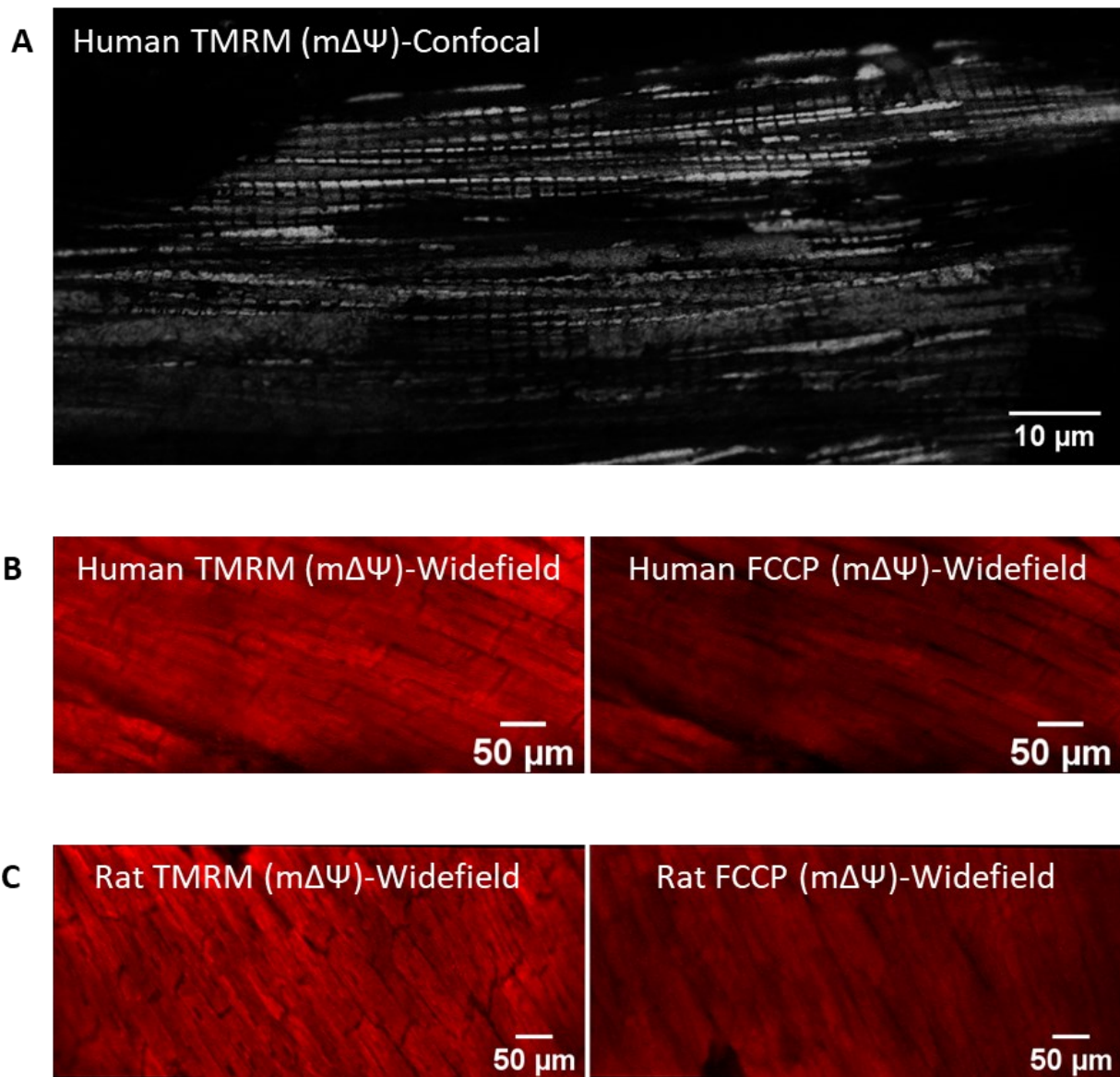


*Figure 3.9-Representative images of  $m\Delta\Psi$  in LMSs stained with TMRM. A) Representative confocal image of human  $m\Delta\Psi$ . B) Representative widefield images of human  $m\Delta\Psi$  of intact mitochondria (Left) and uncoupled mitochondria (Right). C) Representative widefield images of rat  $m\Delta\Psi$  of intact mitochondria (Left) and uncoupled mitochondria (Right).*

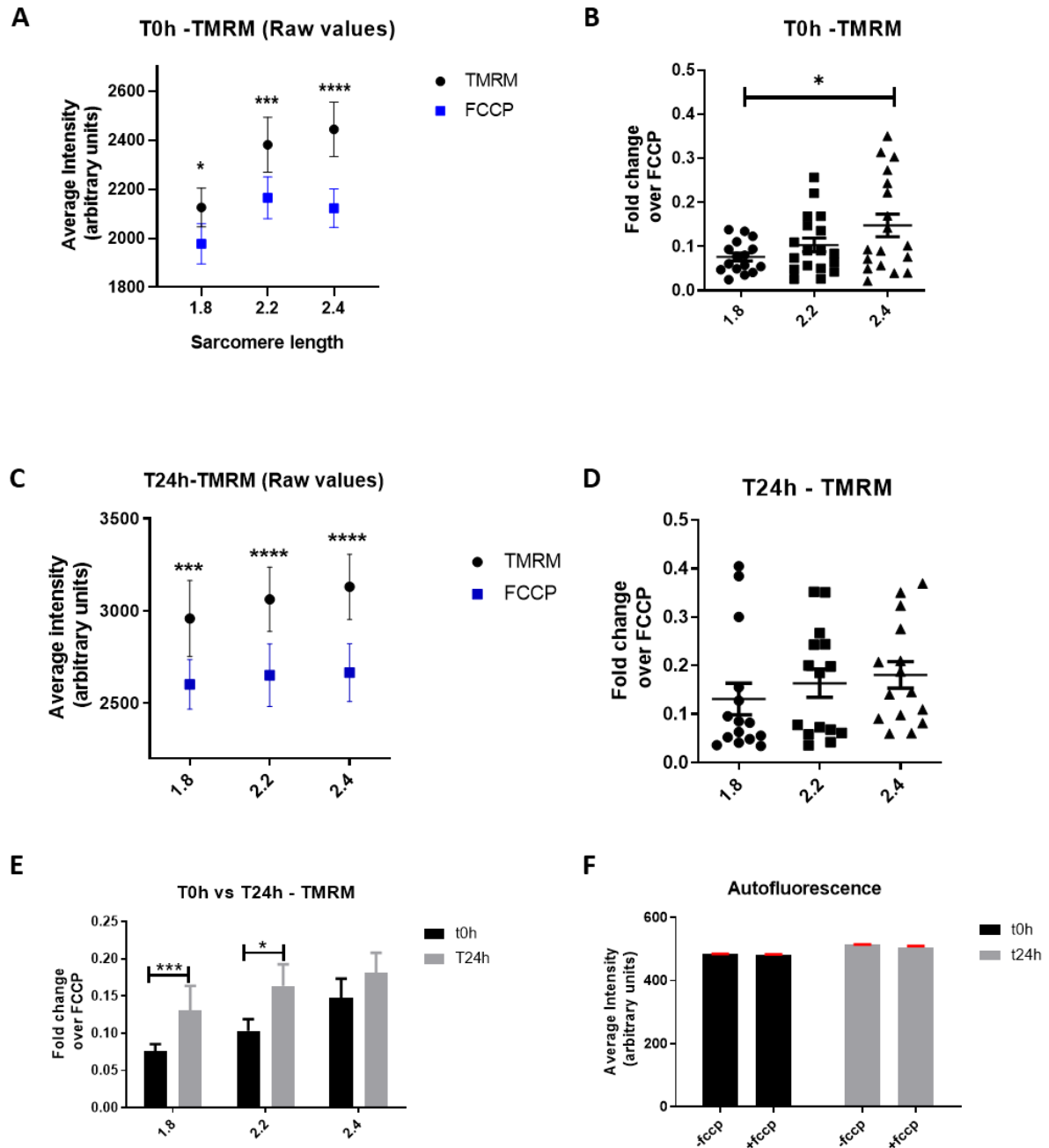


Figure 3.10-Mitochondrial assessment of the LMSs under different preload conditions. A-B) Freshly prepared LMS TMRM fluorescence. Data are shown as raw data (A) and normalised to FCCP fluorescence (B). N/n=10/16-18. C-D) Cultured LMS TMRM fluorescence. Data are shown as raw data (C) and normalised to FCCP fluorescence (D). N/n=10/15. D) Comparison between freshly prepared and cultured LMS fluorescence. E) Autofluorescence of LMSs in absence of TMRM. N/n=2/2. 2-way ANOVA was used in paired analysis, while one-way ANOVA was used for the rest of the graphs. N/n=biological replicates (animals)/technical replicates (LMS).

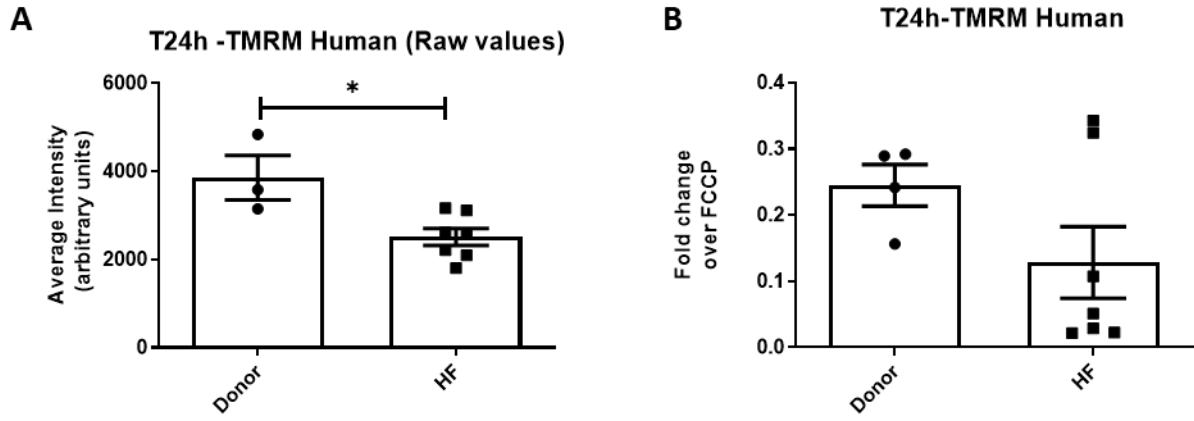


Figure 3.11-Mitochondrial assessment on human cultured LMS. The LMSs derived either from healthy (donor) or failing hearts (HF) cultured at  $2.2\mu\text{m}$  SL.  $N/n_{\text{donor}}=1/3$ ,  $N/n_{\text{HF}}=3/7$ . An unpaired  $t$ -test analysis was used for statistical analysis.  $N/n$ =biological replicates (animals)/technical replicates (LMS).

## 3.4 Discussion

LMS technology has only started to gain popularity in the past 10 years generating a variety of different protocols depending on the tissue type or application. In order to establish and optimise the method for studies on rat and human hearts both the slicing and culturing conditions were evaluated. This chapter shows that the slicing thickness and solution play an important role in tissue viability and functionality. The role of media oxygenation was also highlighted with new findings proving that the cultured LMSs were adequately oxygenated. Finally, the role of mechanical stretch in culture was further investigated finding that LMS response in contraction increased with an increase in stretch. This was also followed by a subsequent increase in their  $m\Delta\Psi$ . After 24h culture, though, these stretch related changes in  $m\Delta\Psi$  were abolished.

### 3.4.1 Tissue slicing

Traditionally slicing solutions used for acute cardiac tissue experimentation include Krebs and Tyrode's solutions (Di Diego et al., 2013; He et al., 2019). Both solutions are comprised of basic salts and ions essential for the physiological function of the heart. However, none of them could retain cardiac contractility and viability for prolonged periods of time. On the other hand, media formulations and especially M199 has been proven to better support myocardial contractility and viability over time in culture. M199 is a nutritionally rich medium, more complex than DMEM (Dulbecco's Modified Eagle Medium) and is widely used in cell cultures (Nelson et al., 2013; Weiss et al., 1980). It contains a variety of vitamins and amino acids that are essential to reduce reactive oxygen species, especially in conditions of extreme stress (Rodrigo et al., 2013). Amino acids are also important in cardiac stress, since they can be used as alternative metabolic substances, as seen in ischemia conditions (Drake et al., 2012). The media is, also, cost-effective and therefore a suitable choice when large quantities are needed,

as in our culturing model. For this reason, it was selected as an alternative slicing solution that could potentially better preserve tissue viability during slicing. The slicing procedure includes solution oxygenation to avoid tissue hypoxia during slicing. However, the results showed that M199 medium pH was significantly impacted by oxygenation with 95%O<sub>2</sub>/5%CO<sub>2</sub> at 4°C. The decrease of pH under these conditions was successfully regulated at 7.4 by adding more buffer. However, this was not enough to improve LMS contractility after 24h in culture, where in fact Tyrode's solution was significantly superior to both M199 medium and Krebs solution. Krebs solution was used as a second control, with similar composition to Tyrode's solution but different buffer, bicarbonate, the same as M199 medium. This was used as an intermediated solution with the same ion concentrations to Tyrode's but containing M199's buffer, bicarbonate.

Even though that M199 was chosen for its high content of vitamins and amino acids, it seems that these were not enough to improve tissue viability. In a metabolic inactive tissue it is widely accepted that pH and temperature are two of the most important homeostatic regulators, since they control enzyme conformation, enzyme function, metabolism and oxygen consumption (Chitwood et al., 1979; Fromm, 1975). Tyrode's solution contains HEPES as a buffer, which can accurately maintain the pH at lower temperature and it shows excellent buffering at pH 7.4-7.8 (Baicu and Taylor, 2002). Therefore, it was concluded that Tyrode's solution was a better slicing solution and was used for all subsequent experiments.

### **3.4.2 Tissue thickness**

The optimal slice thickness can vary and it depends on the tissue type, metabolic requirements, cell density and tissue architecture (Parrish et al., 1995). In the heart a variety of LMS thicknesses have been previously suggested, ranging from 150 (Halbach et al., 2006) to 500 µm (L Janssen et al., 1999; Pertsov et al., 1992). There have also been reports estimating the

maximum tissue thickness using computational models to be of 200µm (McMurtrey, 2016), which can support oxygen and nutrient diffusion without a drop in tissue viability (Carmeliet and Jain, 2000). However, there were no official reports to standardise the optimal slice thickness, in respect to tissue functionality and sustainability in culture. Here it was shown that LMSs thinner than 300µm can be produced, handled and be acutely functional. However, they quickly deteriorate, after 24h in culture, resulting in variable contractility values and often develop spontaneous contractions.

This is believed to occur because thinner LMSs have less cell layers compared to 300µm LMSs and therefore, the ratio of viable inner cell/damaged surface cells is smaller and may favour spontaneous activities originating from the damaged cells. Unavoidable cell damage on the surface of the LMS account for around 40% of the LMS surface as shown by previous lab members (Watson et al., 2017), but usually this is a negligible amount of damage, 2.6%, when compared to the total cells number of cells on the LMS. These measurements were calculated on 300µm LMS, however similar analysis in 200µm LMSs showed that there is a 4% of total damage. Probably cell death is not the only reason for LMS instability in culture and there must be other factors such as oxygen/nutrient diffusion or mechanical properties of the tissue. It is therefore concluded that thinner LMSs are not advised to be used for long term experiments.

*Table 3.1-Cell death calculation in different LMS thicknesses*

Total # of cells in a <b>300µm</b> LMS (LMS volume=7x7x0.2mm)	583519
Total # of dead cells in both sides of the LMS	152000
<b>% of dead cells</b>	<b>2.6%</b>
Total # of cells in a <b>200µm</b> LMS (LMS volume=7x7x0.2mm)	389012
Total # of dead cells in both sides of the LMS	152000
<b>% of dead cells</b>	<b>4%</b>



### 3.4.3 Oxygenation

As a key substrate in the bioenergetics of cells, O<sub>2</sub> availability and biodistribution dictates metabolic efficiency, gene expression and viability (Simon and Keith, 2008). Regulation of *in vitro* oxygenation is often overlooked and heavily rely on culture incubators provided with 20% atmospheric O<sub>2</sub>. In the present study, direct oxygenation of the media proved to be hyperoxic (300% O<sub>2</sub>, 480 mmHg), considering that physiological *in vivo* blood O<sub>2</sub> levels are approximately 40-90 mmHg (represented as 25-56% O<sub>2</sub> saturation in our measurements) (Malatesha et al., 2007; Thilo-Körner et al., 1992). Hyperoxia is being known to induce cell differentiation and specifically fibroblasts activation and transition into myofibroblasts (Sen et al., 2006). High oxygen levels encourage cells to utilise oxidative phosphorylation which is the main metabolic pathway for ROS production such as H<sub>2</sub>O<sub>2</sub> (hydrogen peroxide) and O<sub>2</sub><sup>•-</sup> (superoxide radical) initiated in the mitochondrial electron transport chain (Brueckl et al., 2006; Giordano, 2005). Changing from direct oxygenation of the media to oxygenating the air above it reduced O<sub>2</sub> levels and improved reproducibility of the system.

### 3.4.4 Fatty acid media supplementation

Even though the importance of FAO has long been known in cardiovascular metabolism, many *in vitro* studies use only glucose as the major substrate for energy production (Louch et al., 2011). In physiology though metabolism is a more complex system that requires a number of different available metabolites such as FA, glucose, ketones and amino acids (Pascual and Coleman, 2016; Taegtmeyer et al., 2008). In many cases the heart's metabolism needs to adapt by changing substrate utilisation to either physiological, such as exercise, or pathological conditions, such as diabetes (Gibb and Hill, 2018). These adaptations depend on many factors: a) the availability of FA (Vickers and Fisher, 2004); b) the availability of competing energy substrates (glucose, lactate, ketones, amino acids); c) energy requirements of the heart

(increased function requires higher level of ATP); d) oxygen levels in the heart; e) FA uptake, esterification, and mitochondrial transport (Lopaschuk et al., 1994; Stanley et al., 2005).

To enhance FA metabolism on the LMS, the culture media was enriched with FA, which then can be used for FAO and therefore increase ATP levels and improve cardiac function after culture. For this reason, one of the most abundant saturated fatty acids found in the human body, palmitic acid, was chosen. Palmitic acid accounts for 20–30% of total fatty acids in humans and can be provided either by our diet or synthesized endogenously via lipogenesis (Akhtar Khan et al., 2017; Carta et al., 2015). Palmitic acid could be successfully bound to BSA, making it soluble in the water-based media and therefore accessible to cells for metabolism. In physiology, palmitic acid concentration varies from 0.3–4.1mM (Abdelmagid et al., 2015), but the current viability studies showed that concentrations above 0.1mM significantly decreased LMS viability. Palmitic acid can be toxic in high quantities as shown in numerous studies, with lipid droplet accumulation, mitochondrial swelling, decrease of ATP production, ROS production and increased cell apoptosis (J. Cao et al., 2012; Chen and Yin, 2011; Fukai and Ushio-Fukai, 2011; Park et al., 2014). The selected working concentration in this study did not show any functional changes; however, palmitate supplementation was not enough to increase FA oxidation as measured either by biochemical or radioactive studies (section 3.3.5). LMSs still heavily based their ATP production on glycolysis or glucose oxidation, which is a less effective way of energy production since it only yields 2–37 ATP molecules in comparison to palmitic acid oxidation ( $\beta$ -oxidation) which provides 106 ATP molecules (Lodish et al., 2000).

### **3.4.5 Electro-Mechanical stimulation**

Cardiomyocyte maturation is a complex and still partially understood process and often the centre of regenerative and developmental biology. Two major environmental contributors that

have shown to improve differentiation or retain maturation are mechanical and electrical stimulation (Bajaj et al., 2010; Bhana et al., 2010; Fischer et al., 2019; R. A. Li et al., 2018). Electrical stimulation is physiologically provided in the heart via pacemaker cells which are responsible for generating electrical impulses (action potentials) which are later propagated across the tissue (Boyett et al., 2000). *In vitro* systems, though, are deprived of such cells and therefore excitation is traditionally provided through point or field electrical stimulation (Stoppel et al., 2016). This trigger alone has been shown to activate pathways related to mitochondrial function (cytochrome C), cardiac maturation (GATA4), calcium handling (CamKI) and oxidative stress (NRF-1, nuclear respiratory factor 1) (Passier et al., 2000; Stoppel et al., 2016; Xia et al., 1998). It also enhances cardiac metabolism and improves the contractile machinery and conduction velocity by increasing expression and organisation of MHC (Myosin heavy chain), Cx43 (Connexin 43), creatine kinase-MM, and cTnI (cardiac Troponin I)(Radisic et al., 2004; Stoppel et al., 2016). As in many other *in vitro* 3D culture systems, electromechanical stimulation was a vital element in our culturing system that could better preserve myocardial function (Watson et al., 2019).

Mechanical stimulation has been proved to enhance cell maturation, in iPSC-CMs, improving their cell structure and function in a variety of 2D and 3D models (R. A. Li et al., 2018; Pasqualini et al., 2016). Substrate stiffness, fixed preload or afterload, as well as biodynamic stretching are some of the mechanical triggers that have been introduced *in vitro* (Leychenko et al., 2011; Zhang et al., 2007). In this study fixed mechanical load (preload) significantly improved viability in comparison to unloaded LMSs as previously shown in our lab (Watson et al., 2019). The % stretch plays a crucial role in LMS functionality after 24h culture. Physiological levels should be used for long term LMS culture to avoid tissue deterioration.

Mechanical load plays an important role in preserving excitation contraction coupling, supported by enhanced microfibrillar architecture and turnover (Simpson et al., 1996), activity

of stretch activated ion channels (Sigurdson et al., 1992; Youm et al., 2005), and the organization of focal adhesions (Shakp et al., 1997; Youm et al., 2005).

Mechanical load can also affect cardiac bioenergetics. Acute exposure of cardiomyocytes to stretch increased gene expression of metabolic markers as well as protein kinases and ATP production (Kalifa et al., 2008; Rysä et al., 2018). Long term exposure to pathological load conditions have the opposite effect and eventually reduce metabolic function of the heart, by reversing its gene transcription back to a foetal gene programming which relies to glucose oxidation instead of FAO (Gibb and Hill, 2018). In this study it was also hypothesised that physiological stretch provides the optimal conditions for mitochondrial function. However, my data in combination with the lab's published reports (Watson et al., 2019) show that mitochondrial function is not following the observed contractility trends. Measurements of mitochondrial membrane potential showed that increased stretch progressively polarises the mitochondrial membrane potential, which indicates higher mitochondrial function. This is expected since increased cardiac function is usually followed by increased bioenergetics and ATP production complying with high demand (Bittl and Ingwall, n.d.; Kalifa et al., 2008). However, 24h of culture dissipates the mitochondrial membrane differences between the different stretching groups, even though contractility is improved only in 15% of static stretch (2.2 $\mu$ m in SL). This means that other parameters must influence high LMS functionality at this stretching condition.

Previously published studies investigating the transcriptome of cultured LMSs showed that titin and muscle specific LIM protein (MLP) were involved in mechanotransduction and hypertrophy (Anderson and Granzier, 2012; Knöll et al., 2002). In the study published by Watson et al (Watson et al., 2019), the complex of titin and MLP was upregulated under physiological preload, particularly at 2.2 $\mu$ m SL, with significant increased expression of MLP over unloaded LMS, 1.8  $\mu$ m SL. Significantly increased expression was also observed in

costameres under physiological stretch, an important element of lateral force transmission (Danowski et al., 1992). A study in isolated neonatal cardiomyocytes (NRVMs) showed that stretch-induced responses are mediated through proinflammatory responses. In these studies, interleukine 1 and 8 (IL1, IL8) and nuclear factor-like 2 (Nrf2) became activated mediating oxidative stress response signalling. After the first 12h of stretch, inflammation genes were downregulated, including nuclear factor kappa ( $\text{Nf-K}\beta$ ), Endothelial Nitric Oxide Synthase (eNOS) and inhibition of retinoid X receptor (RXR). This study reveals the importance of oxidative stress response upon acute and prolonged mechanical stress emphasising the role of Nrf2 as a protective, antiapoptotic and anti-hypertrophic elements necessary for mechanotransduction (Rysä et al., 2018).

### 3.5 Limitations and Future work

LMS optimisation has opened new opportunities for adult tissue culture and provides a more representative model to study cardiac interactions in a multicellular and organised platform. Since the use of LMSs in culture is a relatively new practice in the scientific community there are many areas that could benefit from further improvement, as has been done in other *in vitro* models of isolated primary cells or iPSC-CMs.

One of the most important elements that is missing is the regulation of LMS's metabolism and in particular enhancement of FAO. This is the main source of energy and results in significantly higher yield of ATP which is necessary for tissue contraction. In this study the effect of palmitate supplementation was utilised as a main source of FA, as well as a fatty acid mixture (data not shown), both of which were unable to trigger FAO in culture. Many other lipids have been used by other groups on cardiac cells, with oleic acid being one of the most interesting ones because of its cardioprotective effects (Joris and Mensink, 2016; Perdomo et al., 2015). FA supplementation is usually accompanied by addition of proteins, such as BSA, to solubilise the lipophilic fats in a water based medium. Commercially available lipid mixtures have now been introduced and can be purchased at a low cost, which should improve reproducibility of the FA mixtures and reduce LMS culture variability. Other ways to regulate metabolism is by altering metabolite availability, such as glucose, FA, ketones, amino acids, which can shift substrate utilisation (Hawley et al., 2000). Regulating hormone concentration can also affect metabolic regulation. Thyroid hormones are shown to affect cholesterol and carbohydrate metabolism through alterations of gene expression and cross-talk with other nuclear receptors, including peroxisome proliferator-activated receptor (PPAR) (Mullur et al., 2014). Insulin is another hormone that plays a key role in triggering glucose utilisation and stimulating FA synthesis (Qaid and Abdelrahman, 2016).

Hormones and adrenergic stimulation are also essential elements that are missing from the culture, since slicing procedure cuts off the connected innervation. It has been observed in our lab that these extra supplements can improve cardiac contractility over time (recent and unpublished observation).

As mentioned in the discussion, mechanical stretch is necessary for contractile function. In our model static stretch was used by placing the LMSs in custom made stretchers. It has been proposed by our lab and others that biodynamic stretch that allow physiological levels of pre- and afterload would better preserve cardiac function and viability over longer periods of culture. For this reason, bioreactors can be utilised; however, this is a low throughput method that requires expensive instruments to operate. It is important to redesign the LMS culture system and create a multichannel system that can support multiple LMSs in a controlled and sterile manner. An additional element that could improve the LMS culture is real time contraction monitoring. This is a major advantage of the bioreactors which is achieved by integrating a force transducer to the culture system. Real time monitor of contractility can give valuable information on the progression of the treatment at all times.

If these two elements are improved, then it is highly likely that preservation of the LMSs in culture will improve as well, opening new research opportunities such as longer treatments and cell transfection.

### 3.6 Conclusions

This chapter demonstrates the importance of evaluating and optimising the slicing and culturing technique. In this project the protocols used have been based on already published data used by our lab and others, but further adjustments seem to be important for improving the LMS model. In more detail, it was shown that LMS thickness is an important element that should be considered when culturing LMSs for longer times (24h). Attention should also be given to the culture conditions where oxygen levels should remain in physiological levels. The use of oxygen meters should be considered to determine the O<sub>2</sub> levels in each set up. Despite regulating the O<sub>2</sub> levels and FA availability, LMSs did not show any evidence of FAO and further experimentation is essential to improve LMS metabolism. Finally, it was also showed that LMS response to different preloads affect tissue functionality, SL and mitochondrial function. Following the Frank-Starling Law, freshly prepared LMSs increased their active force as the stretch increased. In similar way the m $\Delta\Psi$  also, increased with increase in stretch. However, this pairing between active force and m $\Delta\Psi$  was lost after culture. LMSs reduced their contractility under unloaded and overloaded conditions, whereas the m $\Delta\Psi$  increased in all conditions regardless of their stretching condition.



**Chapter 4**

**Cryoinjury on LMSs -**

*a model to study local cell responses to*

*myocardial injury*

## 4.1 Introduction

Even though disease development is usually multifactorial, studying the contribution of single stimuli is important and necessary to understand disease progression and find new therapeutic targets (Poulter, 1999; Slanzi et al., 2020). *In vitro* disease models have been widely used for this purpose (Benam et al., 2015; Hoes et al., 2019; Slanzi et al., 2020; “Tissue-engineered disease models,” 2018). In *in vitro* disease models, the user has the ability to choose the trigger of their interest and therefore isolate it from other confounding factors that occur *in vivo*. In the cardiac field one of the most common simulated diseases is myocardial infarction, because of its high prevalence in the human population affecting 32.4 million people worldwide (Hassan et al., 2019). In animal models myocardial infarction is often simulated by performing surgical coronary artery occlusion (Lindsey et al., 2018a) or by using an alternative method of local cardiac ablation (Bise et al., 2020; Chablais et al., 2011a). Artery occlusion is thought to be a more representative method similar to human pathophysiology of cardiac infarction, since it has similar effects of oxygen and nutrient deprivation on the left ventricle, which in turn is the main cause of cell death after ischemia in human hearts (Kumar et al., 2016; Lutgens et al., 1999). However, the artery occlusion model often lacks reproducibility due to variability of induced injury size, which often stems from either structural variability of the animal’s heart, animal species or even human error/inexperience of the user (Bøtker et al., 2018; Lindsey et al., 2018b). Recently, cell death induced by cryo-ablation of the left ventricle has been proved to be a useful tool that can bypass several inconsistencies already seen in the occlusion model. Therefore, this is an attractive technique with tight control over injury size, high reproducibility and additional control over the injury location. Until now, cryoinjury studies have been, primarily, focused on regenerative studies where injury size and subsequent recovery is an important factor for assessing regenerative efficacy (Feng et al., 2017; González-Rosa et al., 2011a; Marín-Juez et al., 2016; Schnabel et al., 2011). However, recent studies have shown

that cryoinjury could also be a useful tool to study tissue response to cell death and cell electrophysiology (Tomek et al., 2019).

LMSs serve as a great platform for cryoinjury, since it is a 3D model with native cell organisation, ECM composition, multicellularity that can be easily manipulated (Camelliti et al., 2011b; Watson et al., 2017). These characteristics make it an ideal model for functional and electrophysiological analysis. Investigation of all these parameters is of great importance to better understand and create links between the trigger and the response of the tissue upon cell death. The lack of nutrients or oxygen deprivation in this model makes it suitable for studies that focus on the mechanical effect of apoptotic cells on tissue functionality/arrhythmogenicity.

To our knowledge there is no report of an *in vitro* cryoinjury model using adult animal tissue. Therefore, the novelty of this method lies on the use of LMSs to mimic local cell death by cryoinjury and the study of tissue response at structural, electrophysiological, and molecular levels.

It is hypothesised that the local cell death on the LMSs induces functional and electrophysiological changes, representative of cardiac disease

To validate the hypothesis, the following aims were set to:

- 1) Apply cryoinjury on healthy rat LMSs and culture them for the remodelling to occur.
- 2) Analyse global LMS contractility and arrhythmogenicity using a force transducer.
- 3) Evaluate local ionic changes by measuring calcium traces.
- 4) Study local mechanical alterations by using microscopic approaches.

The following sections focus on the cellular, mechanical and functional responses of the LMSs upon local tissue damage.

## **4.2 Methods**

### **4.2.1 LMS preparation**

LMSs were prepared from both rodent and human hearts. Male Sprague-Dawley rats, with a body mass of 250-500g were used in this study, while human cardiac tissue was obtained from healthy donors or heart failure patients. The slicing procedure is described in detail in section 2.2.

### **4.2.2 Application of cryoinjury**

To induce injury a stainless-steel circular rod with 3mm diameter was used. The rod was cooled for at least 10 min in dry ice, at a temperature of approximately  $-78.5^{\circ}\text{C}$ . The injury was applied on the corner of the LMS for 3sec. The location was chosen so that different areas can be assessed locally as shown in Fig 4.1. Before removal of the probe the area was superfused with slicing solution at room temperature so that the temperature of the rod increases and detaches easily from the LMS without any rupture of the tissue. The cryoinjured LMS was then used either for acute studies or mounted on stretchers for tissue culture as described in section 2.6.3.

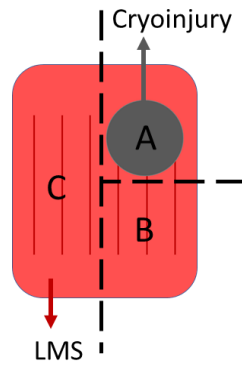


*Figure 4.1- Schematic representation of the areas of interest in a cryoinjured LMS. The location of cryoinjury allowed the study of different areas within the tissue such as the cryoinjury (A), the areas along the cryoinjury (B) and the healthy areas (C).*

### **4.2.3 Conduction velocity (MEA)**

Freshly prepared LMSs were assessed for their CV on a multielectrode array system. The system contained multiple electrodes which can be used simultaneously for electrical point stimulation and recording of the tissue's electrical response. Baseline CV of a healthy LMS was initially assessed. The LMS was then removed from the MEA dish, cryoinjured and placed in the MEA dish again for further measurements. The acquisition and analysis of MEA data are described in detail in section 2.7.

### **4.2.4 Viability**

Viability of the cryoinjured LMS was assessed by using the LIVE/DEAD Viability/Cytotoxicity method described in detail in section 2.9.2. Additionally, the In situ BrdU-Red DNA Fragmentation (TUNEL) Assay Kit was used as an alternative method to detect apoptotic cells. Staining of the LMS with TUNEL assay is described in detail in section 2.9.1.

### **4.2.5 Arrhythmogenicity assessment**

To evaluate LMS arrhythmogenicity, an *in vitro* tissue provocation protocol was designed. To elevate the incidence of SCR and spontaneous contractions (SC) a fast pacing protocol was used in the presence or absence of  $\beta$ -adrenergic stimulation, 1 $\mu$ M isoproterenol (Sigma, Germany), mimicking human stress induced tachycardia.

#### **4.2.5.1 Arrhythmia provocation protocol for LMS**

Cultured LMSs were carefully removed from the stretchers, placed on a force transducer, and perfused with 100% oxygenated recording Tyrode's solution at 37°C. Field electrical stimulation was applied at Frequency=1Hz, Voltage=40V and Width=40ms. The LMSs were progressively stretched by 15% , corresponding to a physiological stretch of 2.2 $\mu$ m SL, as

previously shown in our lab (Watson et al., 2019). This intermediate stretching condition allowed observation of changes so that both increase and decrease of contractility could be recorded upon LMS treatment. This would be impossible if the LMS was stretched at maximum stretch, since the tissue cannot increase contraction amplitude above maximum isometric stretch. Additionally, a defined stretch degree was necessary to allow comparisons of kinetics between conditions, since stretch has found to be affected in different preloads (Hoffman and Penefsky, 1962; Von Lewinski et al., 2004). Once the LMS reached a stretch of 15%, they were left to stabilise for 2min, for baseline measurements, and subsequently subjected to progressive increase of stimulation frequency until they reached a frequency of 5Hz. Each stimulation frequency was maintained for a minimum of 15 seconds. At the end of the fast pacing protocol the stimulation was halted for 2min, so that spontaneous contractions could be observed. The protocol was, then, repeated at the same LMS, with the presence of a non-selective  $\beta$ -adrenoreceptor agonist, isoproterenol (ISO), 1 $\mu$ M (Sigma-Aldrich, USA). A schematic representation of the protocol can be seen in Fig 4.2.

For calcium analysis the LMSs remained on stretchers and were directly placed on the microscope as described in section 2.13. Cultured LMSs were challenged with the fast pacing protocol in the presence of 1 $\mu$ M ISO (Sigma, Germany) and spontaneous events were recorded for 30s during rest (no electrical stimulation).

#### **4.2.6 Arrhythmia analysis – Spontaneous contractions**

To be able to make comparisons both baseline and treated condition were measured in each LMS. Baseline contraction was analysed as described in section 2.8. Then, the number of spontaneous contractions were counted upon ischemia provocation and within the 2min of rest, after the electrical stimulation was halted. The time between the last stimulation and the first spontaneous contraction described the latency of spontaneous events. Latency indicates the tendency of the tissue to develop arrhythmias.

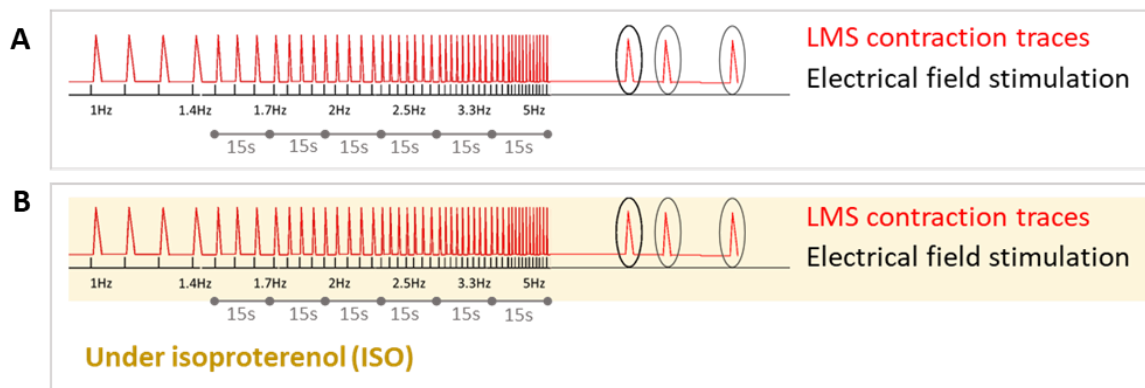


Figure 4.2-Schematic representation of the arrhythmia provocation assay. A) The LMS was stabilised at basal stretch of  $2.2\mu\text{m SL}$  and then a fast pacing protocol was established starting from 1Hz and progressively reaching 5Hz. The stimulation was then halted, and spontaneous contraction (SC) were recorded. B) The protocol was repeated on the same LMS in the presence of a non-selective  $\beta$ -adrenoreceptor agonist,  $1\mu\text{M ISO}$ .



#### 4.2.7 Acute assessment cryoinjury – multiple injuries

To assess the acute response of LMSs to multiple, subsequent cryoinjuries, freshly prepared LMSs were mounted on the FT as described and stretched progressively at SL of 2.2 $\mu$ m. Baseline contraction was recorded for 2min so that the LMSs could equilibrate to the new stretching condition. The warm recording solution was then removed from the perfusion bath so that the cold rod could effectively damage the LMSs, without getting warm from the surrounding Tyrode's solution. Cryoinjury was, then, induced on the side corner of the LMSs for 3sec. The attached rod on the LMSs was detached after perfusing the area with warm slicing solution. The bath was subsequently filled with warm slicing solution and contractility was recorded for 4 min. The procedure was repeated 4 times so that almost half of the LMS area was cryoinjured. During the injury it was important to keep the LMSs on the same position and avoid movements or ruptures, since that would affect tissue contraction and mask the effect of the injury. A schematic representation of the experimental design can be found in Fig 4.3.

For accurate comparisons, control healthy LMSs were also subjected in the same procedure with the difference that the rod used was at room temperature.

Contraction amplitude and kinetics were measured as described in section 2.8.2.

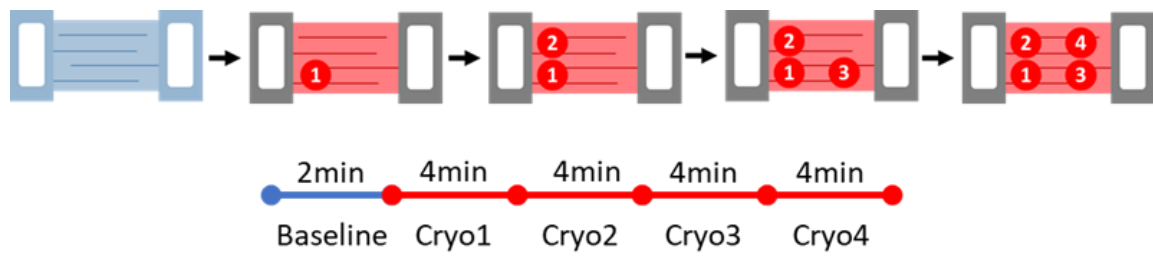


Figure 4.3-Schematic representation of the assay used to acutely assess multiple injuries on healthy LMS. The LMSs were mounted on the force transducer and baseline contraction was recorded. A cryoinjury was, then, induced at the bottom left side of the LMS. Cryo-LMSs were left to stabilize for 4min and then another cryoinjury was induced on the top left side of the LMS. The protocol was repeated until 4 cryoinjuries were induced.

#### **4.2.8 LMS culture**

Rat healthy and cryoinjured LMSs were cultured for 24h as described in section 2.6, while human LMSs were, also, cultured as described in section 2.6.3.

#### **4.2.9 LMS Ca<sup>2+</sup> handling**

Global and local Ca<sup>2+</sup> handling was assessed by loading the LMSs with a Ca<sup>2+</sup> indicator, Fluo-8 and visualised under the microscope. Ca<sup>2+</sup> transients and Ca<sup>2+</sup> waves were analysed as described in section 2.13.

#### **4.2.10 Sarcomere length**

Immunohistochemical assessment was used to measure the SL in LMSs. LMSs were fixed and stained as described in section 2.12.2. The sarcomeres were labelled with alpha actinin and visualised in a confocal microscope.

The SL of the cultured LMSs was analysed using Fiji software as described in section 2.12.2.1.

#### **4.2.11 High throughput image analysis of sarcomere length**

##### **4.2.11.1 Preparation of acutely injured LMSs and image acquisition**

Structural analysis upon acute application of cryoinjury was performed on freshly prepared LMSs. The tissue was prepared and mounted on stretchers. They were stretched at physiological stretch of 2.2µm in SL, placed in culture chambers and incubated for 10min at 37°C in culture media with electrical stimulation as described in section 2.6, so that they recover from the slicing and start contracting. The LMSs were then cryoinjured with different degrees of injury (1-4 application of injury). The injured LMSs were then incubated at 37°C for 10min to allow them to stabilise and were subsequently fixed at 4% PFA as described in section 2.10. They were, then, fixed labelled with  $\alpha$ -actinin as described in section 2.11 and visualised using a Zeiss LSM780 confocal laser scanning microscope with a 40x objective. The

images were acquired at 2048x2048 resolution and single snaps were recorded in the areas shown in Figure 4.4. These areas were chosen to distinguish spatial differences of a cryoinjured LMS.

#### **4.2.11.2 High throughput image analysis**

High throughput image analysis focusing on the evaluation of SL has been previously reported in single cells (Bub et al., 2010; Pasqualin et al., 2016), but rarely applied on whole tissue preparations. However, a recently published methodology was reported by Morris *et al.*, 2020. The group published a free-to-use matlab code that can batch analyse a large number of images based on  $\alpha$ -actinin staining or any other staining that labels the sarcomeres. Before running the code the images were pre-processed on Fiji software in order to remove any noise or unwanted debris and to better isolate the areas of intact sarcomeres. This was an important step, especially since LMSs exhibit dead cells on their surface due to their mechanical preparation which could interfere with the analysis. For that reason, the analysis was focused on cells located in deeper layers, where the cells were mostly unaffected from the slicing procedure. The pre-processing included subtraction of the background (value:20), scaling down the resolution to 512x512 (to allow faster image processing) and trainable weka segmentation. The trainable weka segmentation is a Fiji plugin that can be trained to recognise specific structures depending on their shape or image properties. The plug in was trained to recognise the sarcomeres from the areas of randomly shaped objects with high intensity or blurred areas. Because of the high number of images, the pre-processing was batch analysed, by creating a macro with the help of Mr Stephen Rothery. The cleared processed images were then uploaded to the matlab code (<https://github.com/Cardiovascular-Modeling-Laboratory/zlineDetection>). The produced data were then analysed using R coding. This analysis was done in collaboration with another PhD student, Georgios Sioutas.

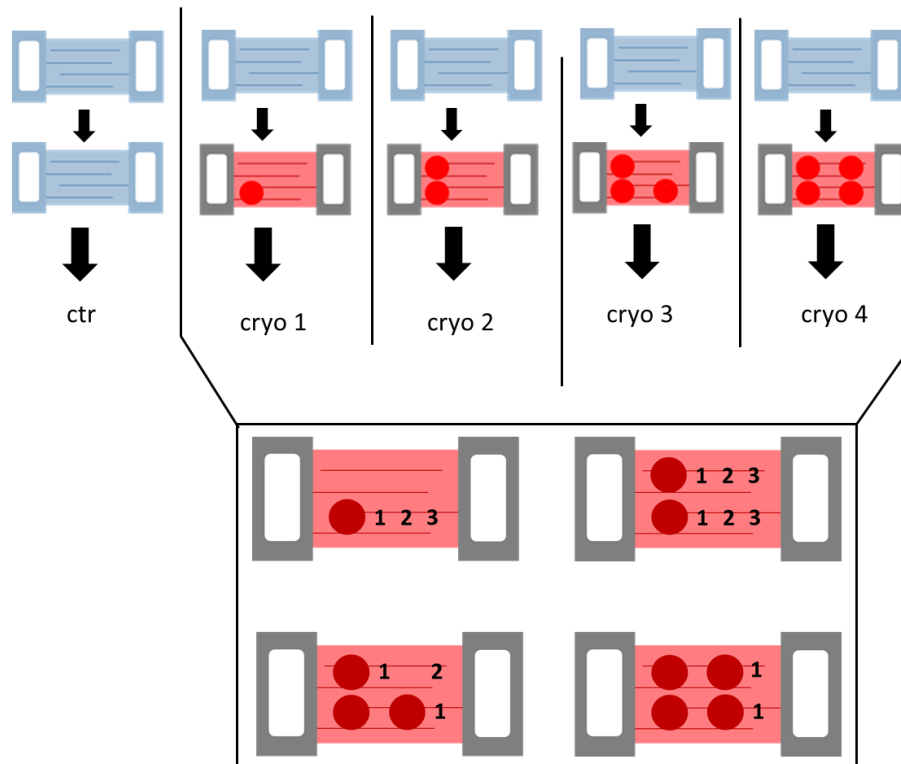


Figure 4.4- Schematic representation of the imaging positions in regard to the injury. The numbers indicate the vicinity of the areas to the injury, with the number 1 being the closest and number 3 further away from the injury.

#### **4.2.12 Collagen I detection**

Immunohistochemical staining was used to quantify collagen deposition. Cultured LMSs were co-stained with  $\alpha$ -actinin and collagen I to calculate the % of collagen on an LMS. A detailed analysis of the staining method and collagen analysis can be found in section 2.12.2.2.

#### **4.2.13 Connexin 43 quantification**

Immunohistochemical analysis was used to identify and quantify connexin 43, an important structural protein of gap junctions, on cultured LMSs. The tissue was fixed and stained as described in sections 2.10-2.11. The acquired images were analysed using Fiji software. Connexin 43 localises at the intercalated disks of the cardiomyocytes; however, it has been shown that it can, also, be found on the lateral sides of the cells (Burstein et al., 2009). Therefore, both the density and localisation were evaluated. The density was evaluated by selecting the labelled areas by thresholding and then calculating the surface area. The area of connexin 43 was normalised to the total area of the tissue. Localisation of connexin 43 on either side of the cardiomyocytes was manually analysed by counting the areas on the short or long axis of the cardiomyocytes. The ratio between these two groups was used to investigate changes in lateralisation of the protein (Burstein et al., 2009).

#### **4.2.14 Transverse and axial tubular network analysis**

Sarcolemma, transverse, and axial tubules (TATS) were visualized by immunostaining by targeting caveolin-3. Confocal images were collected and analysed using Fiji. TATS signals within the cell margins were identified against the background by thresholding. The outer sarcolemmal membrane was subtracted from the images. Next the images were further processed to skeletonize TATS signals. TATS density was quantified as the number of signal-positive pixels over all pixels within the cell margins.

## **4.3 Results**

This section contains representative data collected from healthy rat hearts and healthy or diseased human hearts. Both structural and functional assessments were used to investigate the early effect of cryoinjury on healthy cardiac tissue, focusing on tissue contractility and arrhythmogenicity.

### **4.3.1 Cryoinjury characterisation**

#### **4.3.1.1 Conduction velocity**

LMS CV was quantified before and after cryoinjury using multielectrode array dishes. Both the longitudinal (signal propagation along the fibers) and transverse (signal propagation across the fibers) CV velocity was calculated. Baseline CV was  $70.90 \pm 7.48$  cm/s and  $28.97 \pm 3.68$  cm/s for longitudinal and transverse propagation, respectively. Upon cryoinjury the longitudinal CV was significantly reduced by 55%, while the transverse CV remained unchanged (Fig 4.5). Therefore, cryoinjury managed to immediately reduce the longitudinal CV upon application indicating that the duration of cryoinjury was effective enough to cause cell death. Schematic representation of the local CV shows no signal on the area of injury and therefore the signal acquired on the opposite side of the electrical stimulation was reached transversally and not longitudinally. This type of signal propagation locally reduced the CV on the area below the injury and created CV heterogeneity.

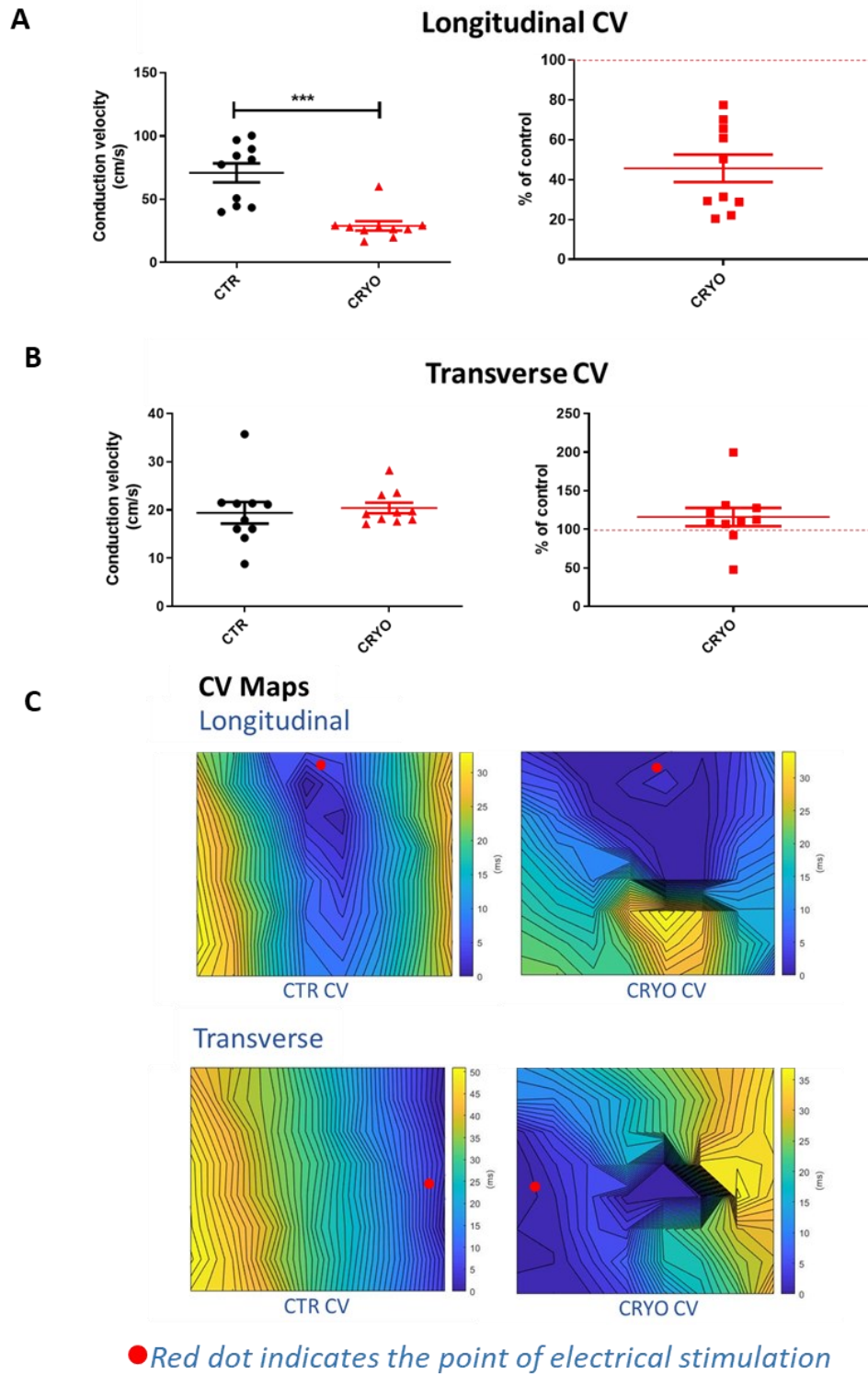


Figure 4.5-CV measurement of freshly prepared rat LMSs. A) Peripheral CV of healthy control (CTR) and injured (CRYO) LMSs. The longitudinal CV was significantly decreased by 55% compared to baseline, while the transverse CV remained unchanged. B) CV maps illustrate local changes CV within a LMS. Cryoinjury created a local barrier that changed signal propagation within the tissue.  $N/n=3/10$ . Paired  $t$ -Test was used between CTR and CRYO, \*\*\*= $P$  value  $\leq 0.001$ .  $N/n$ =biological replicates (animals)/technical replicates (LMSs).



#### 4.3.1.2 LMS viability - local changes in LMSs

Cryoinjury resulted in cell death on the site of application. The affected area consisted of two colours, a bright red which localised at the centre of the injury (6%) and a surrounding yellow area (6%) (Fig 4.6). Yellow indicates the areas with colocalization of red (dead) and green (viable) areas. The area with the mixed population will be referred as the border zone (BZ) in this project, because of its proximity to injury and resemblance in cell viability that has also been seen *in vivo* (Duran et al., 2012). The sum of the injured and BZ area accounted for 12% of the total LMS surface.

Intensity analysis of the cryoinjury showed that the BZ of the diseased rat LMSs had higher intensity values of calcein-AM, compared to the surrounding tissue. Higher intensity is thought to be caused either by increase in cell viability or due to changes in tissue curvature. Tissue curvature results in higher cell number per area and therefore increases the total fluorescence intensity.

Further analysis of cell viability was done to evaluate the level of injury throughout the whole tissue thickness. For this reason, TUNEL assay staining was used to visualise DNA fragmentation, which helped to discriminate between viable and dead cells in fixed and cryo-sectioned LMSs. LMSs were sectioned either longitudinally or transversely in order to visualise the inner and outer layers of the LMS and investigate the depth and limits of the injury in a microscopic level. Fig 4.7 shows representative images of the TUNEL staining. The red spots indicate compromised cell nuclei with DNA fragmentation, the green spots indicate the nuclei, and the blue areas indicate the tissue (autofluorescence). The first observation was that the staining for DNA fragmentation co-localised with the nuclear staining and therefore specifically targeted the DNA, without any significant off target staining (Fig 4.7). Fig 4.7B shows a transversely sectioned LMS, with dead cells running across the whole tissue thickness,

proving that the damage was not only limited to the surface of the LMS but also, penetrated all the inner tissue layers of the LMS creating an injury throughout the whole tissue thickness. Fig 4.7A shows a longitudinally sectioned LMS (inner layers of the LMS), where the dead cells located in an area with clear limits. This observation was different from what was seen with the LIVE/DEAD staining, where the border zone consisted of a mixture of metabolically active and dead cells. These data suggest that the cryoinjury caused a localised and well-defined injury area of cells that were metabolically, structurally, and genetically compromised, while the border zone was composed of a mixture of dead/viable cells without any changes in their DNA integrity.

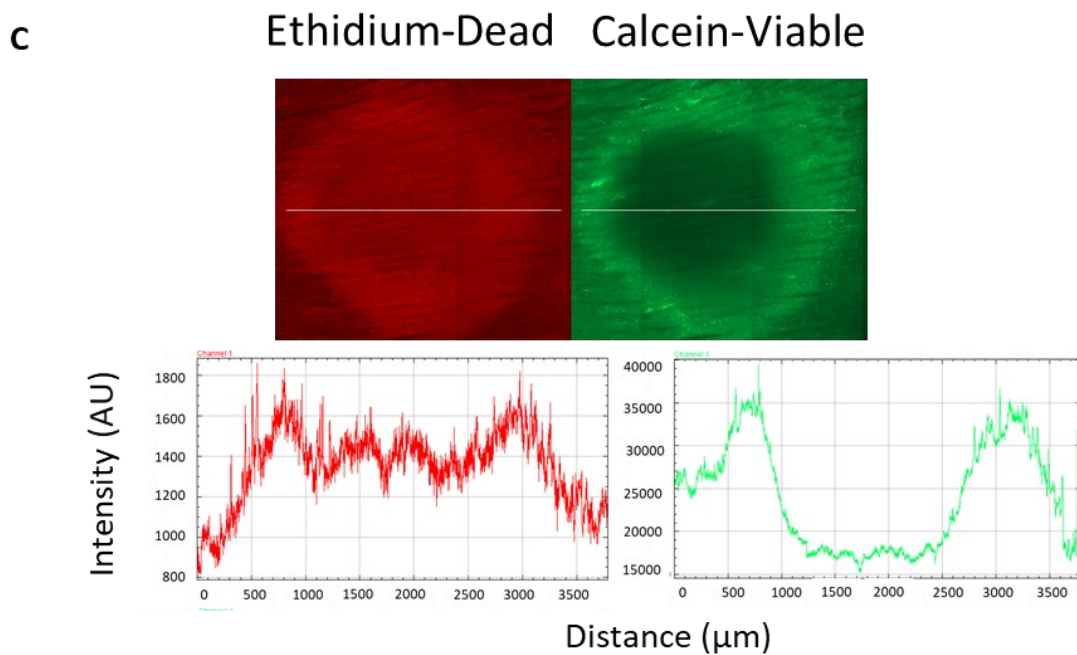
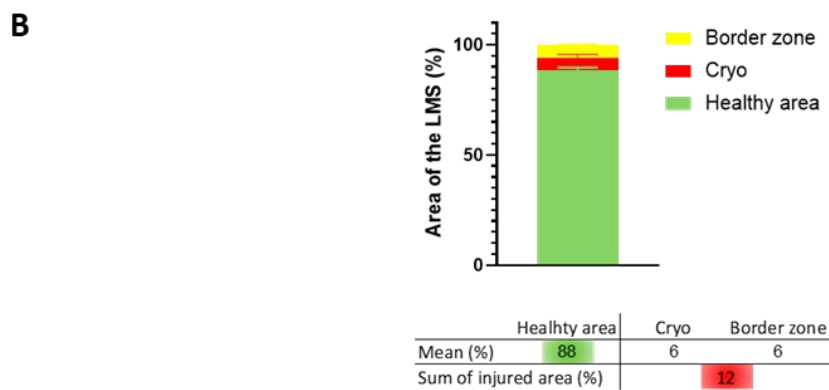
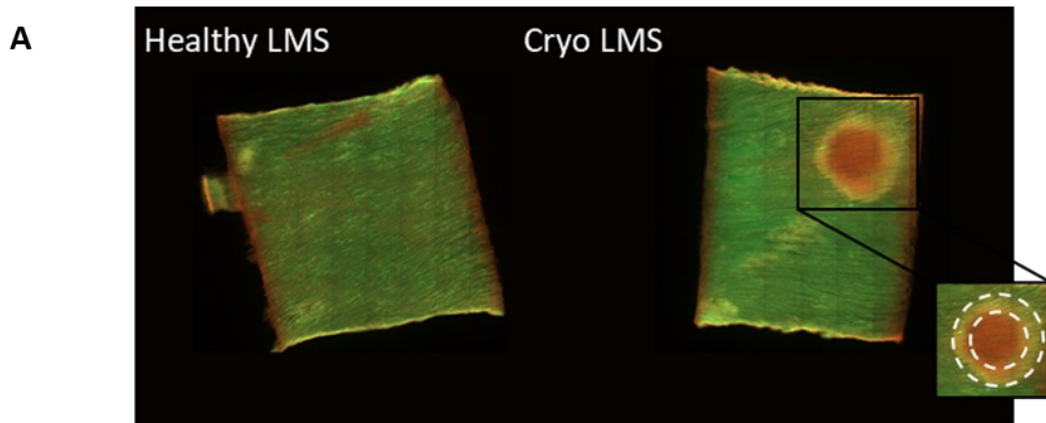
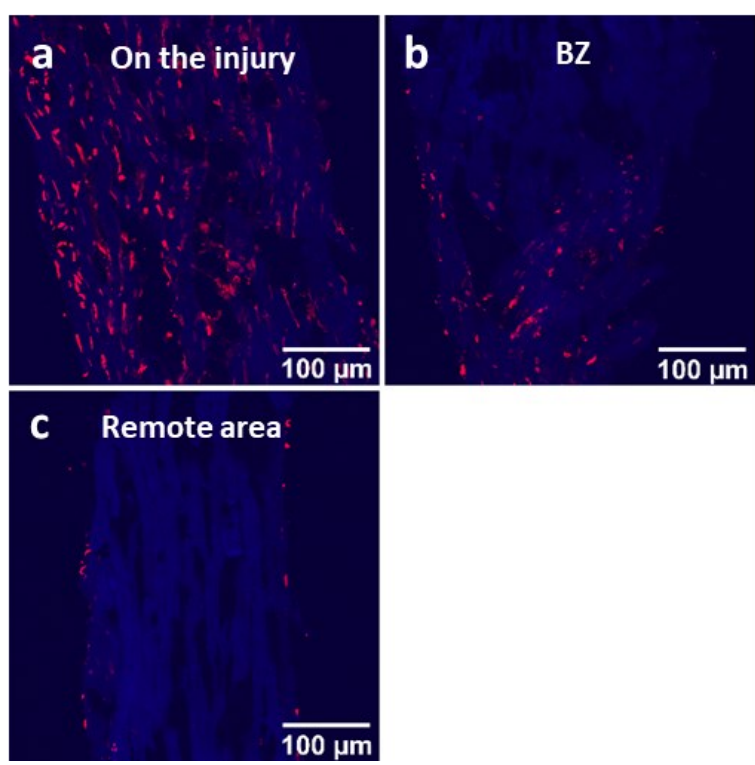
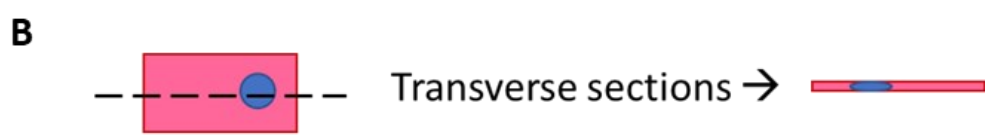
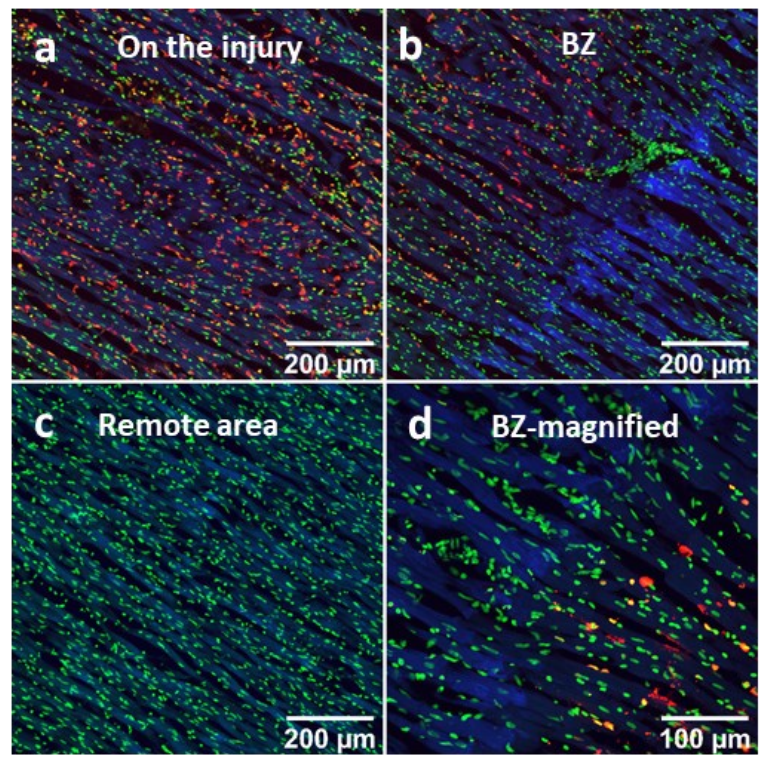
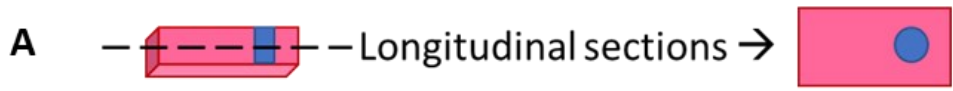


Figure 4.6--Viability assessment (LIVE/DEAD staining) of 24h cultured rat LMSs. A) Viable cells were stained with Calcein-AM (green) and dead cells were stained with Ethidium (red). The area of injury was further analysed, and two different areas were detected. The red area was defined as highly necrotic, whereas the yellow revealed a mixed population of viable and dead cells and therefore was defined as the border zone. B) Quantification of the different areas (healthy, dead, BZ) after image analysis. C) Further segmentation of the channels and intensity measurements across the injury. Higher levels of intensity were present on the BZ. The images were acquired with a widefield microscope and analysed in Fiji. N/n=1/4. N/n=biological replicates (animals)/technical replicates (LMSs).



*Figure 4.7- TUNEL assay staining of cultured LMSs to investigate tissue damage in the inner cell layers of the tissue. Areas with DNA fragmentation were stained in red, nuclei with green and the rest of the tissue with blue (tissue autofluorescence). A) Longitudinal sections of a LMS showed regional change of DNA fragmentation. On the injury (a) there was an extensive necrotic area with high levels of DNA damage, on the BZ (b) the injury appeared to have defined limits next to injury and the healthy area showed no evidence of DNA fragmentation in the inner layers of the LMS. B) The LMS was cryo-sectioned cross-sectionally so that all layers throughout the whole width of the LMS can be visible. The staining revealed that the injury affected the whole depth of the LMS and not only the surface layers (a-b). The healthy area (c) did not contain an extensive number of damaged cells and only few surface cells were damaged. The images were acquired with a confocal microscope and analysed in Fiji.*

## 4.3.2 Acute effects of cryoinjury

### 4.3.2.1 Contraction

To investigate the level of damage and its effects on tissue function LMS contractility was measured before and after acute application of injury. Freshly prepared LMSs were progressively damaged, while being on the force transducer, and their contraction amplitude and kinetics were evaluated. Fig 4.8A shows a schematic representation of injury process and traces from both control and injured LMSs during the injury protocol. Analysis of the traces showed that LMS contraction amplitude (active force) remained stable after tissue injury even when the LMSs was 44% injured (4<sup>th</sup> application of cryoinjury). On the contrary, the passive force (passive tension) progressively increased after each application of injury. Analysis of the decay time of contraction showed that relaxation time (time to 90% decay) was significantly increased after cryoinjury. In accordance with that the decay constant was significantly decreased, meaning that the injured LMSs were relaxing slower compared to control LMSs (Fig 4.9E-F). Time to peak and time to 50% decay remained unchanged.

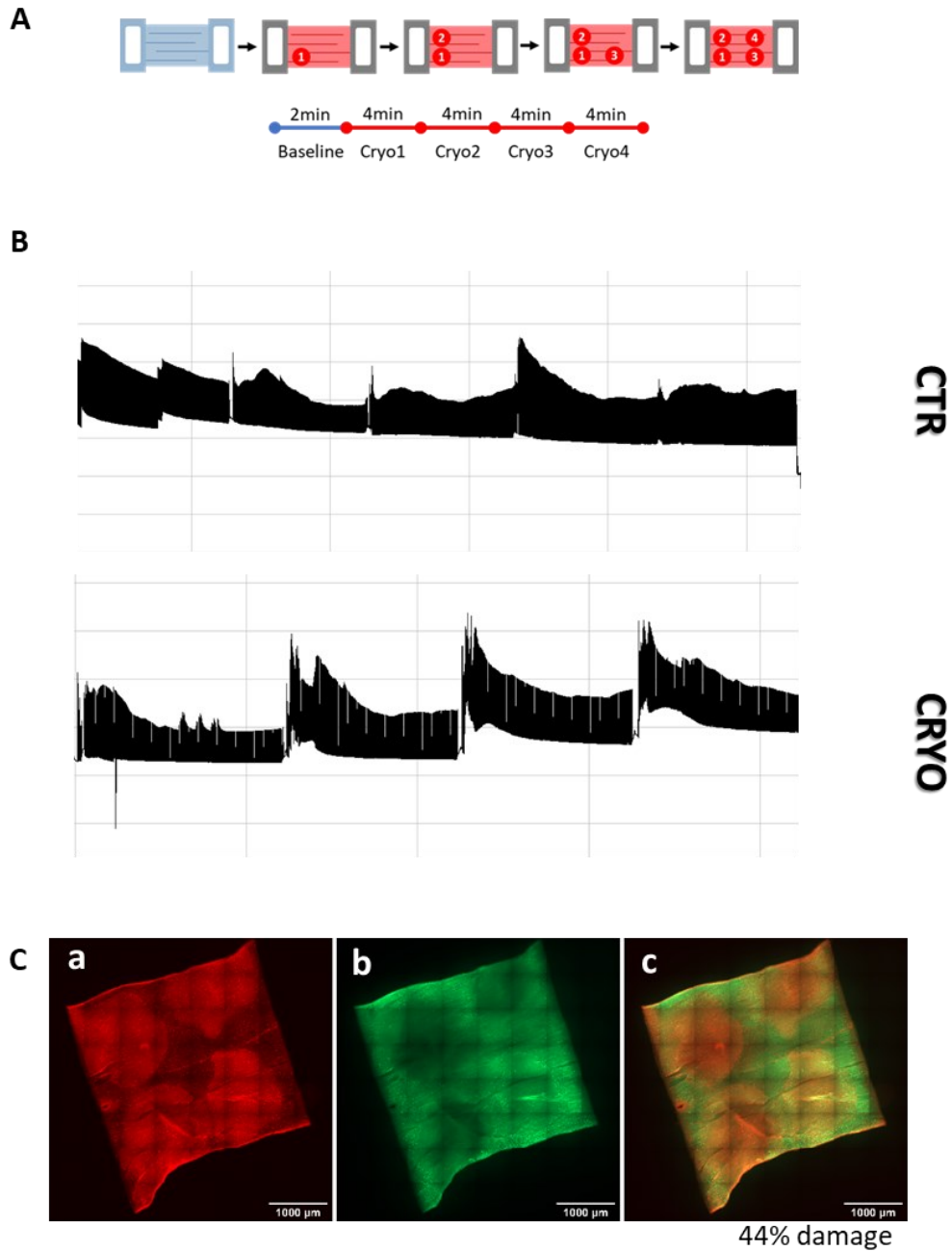


Figure 4.8-Experimental design of the acute injury induction. The LMS was placed on the force transducer, stretched at SL of  $2.2\mu\text{m}$  and subsequently injured 4 times. Between injuries the LMS was left to stabilise, and contraction was then recorded. A) Schematic representation of consecutive injuries on an LMS. B) Representative contraction recordings of control (CTR) and cryoinjured LMSs (CRYO). C) Viability staining of LMSs at the end of the experiment reveal a 44% total damage.

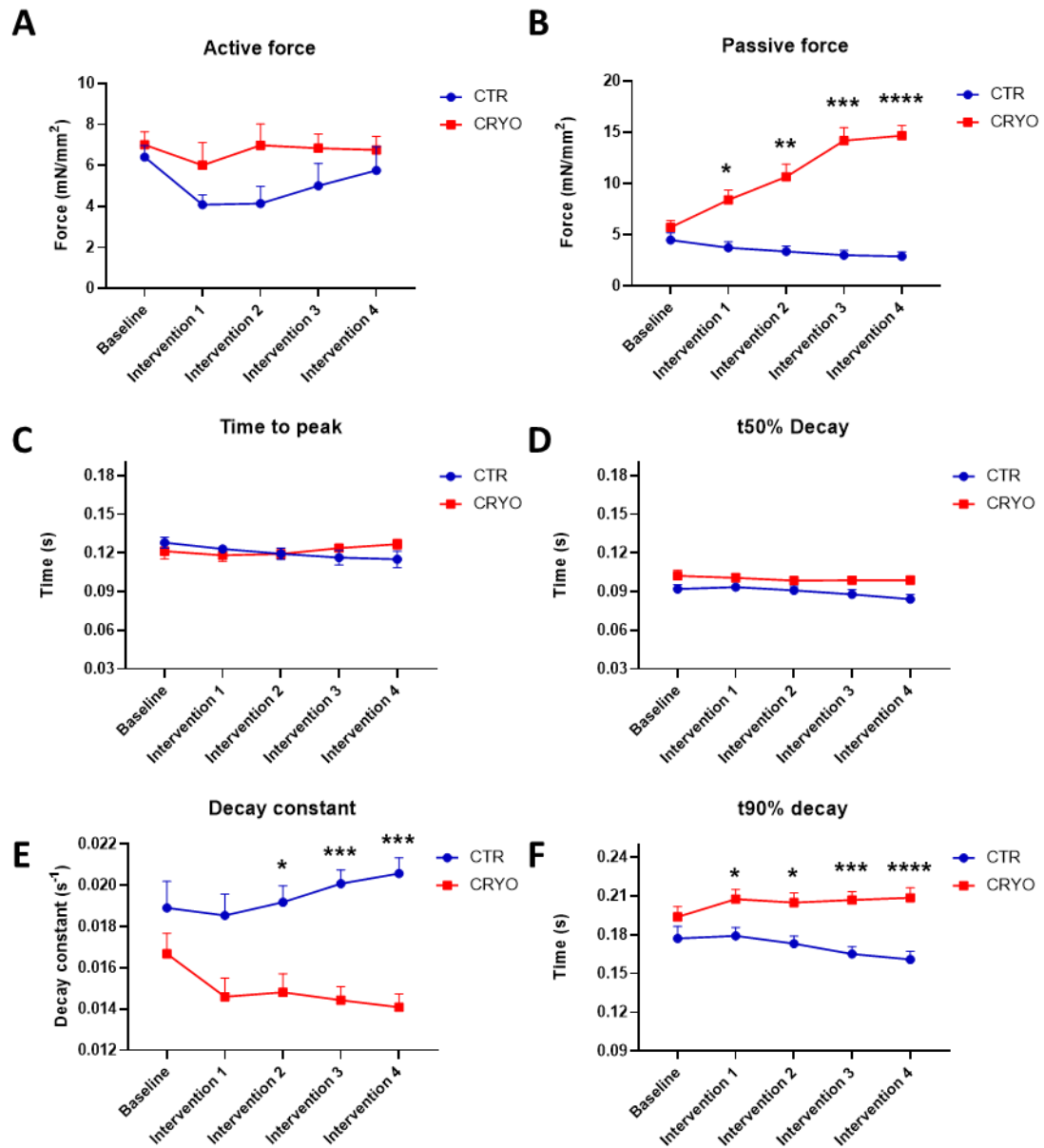


Figure 4.9-Contraction analysis after acute injury of the rat LMSs. Interventions refer to the application of either a cold (CRYO) or room temperature probe (CTR). A) Active force (contraction amplitude) of the LMSs. B) Resting force (passive force) of the cryoinjured LMSs significantly increased after cryoinjury. C-D) Time to peak and time to 50% decay were unaffected by cryoinjury. E-F) Time to 90% decay and decay constant revealed significant changes. Cryoinjury required more time to relax in comparison with control LMSs. 2-way ANOVA was used to compare the control and cryoinjured groups.  $N/n=3/7$ ,  $*$ = $P$  value  $\leq 0.05$ ,  $**$ = $P$  value  $\leq 0.01$ ,  $***$ = $P$  value  $\leq 0.001$ ,  $****$ = $P$  value  $\leq 0.0001$ .  $N/n$ =biological replicates (animals)/technical replicates (LMSs).



#### 4.3.2.2 Sarcomere length

Spatial differences in sarcomere length were evaluated after acute injury of the LMSs. Freshly prepared LMSs were cryoinjured and fixed for analysis. As shown in Fig 4.10, image pre-processing managed to exclude areas of dead, damaged, or unfocused cells, that were presented as highly bright points with disorganised sarcomeres. The remained areas consisted of deeper cell layers that were later analysed using the matlab code. The published matlab code successfully recognised the sarcomeres and calculate the lengths between them (Morris et al., 2020) as shown in Fig 4.10. However, there was high prevalence of values around “0”, which indicated the presence of non-specific detection therefore extreme values  $<0.5$  and  $>3.5$  were excluded from the analysis, since they were far away from the reported normal range of SL, 1.8-2.4 $\mu\text{m}$  (Hofmann and Fuchs, 1988; Kentish and Stienen, 1994).

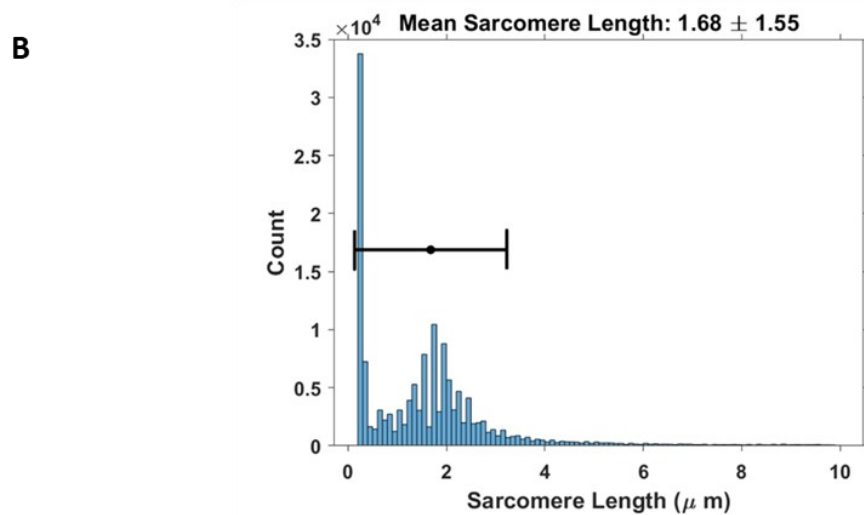
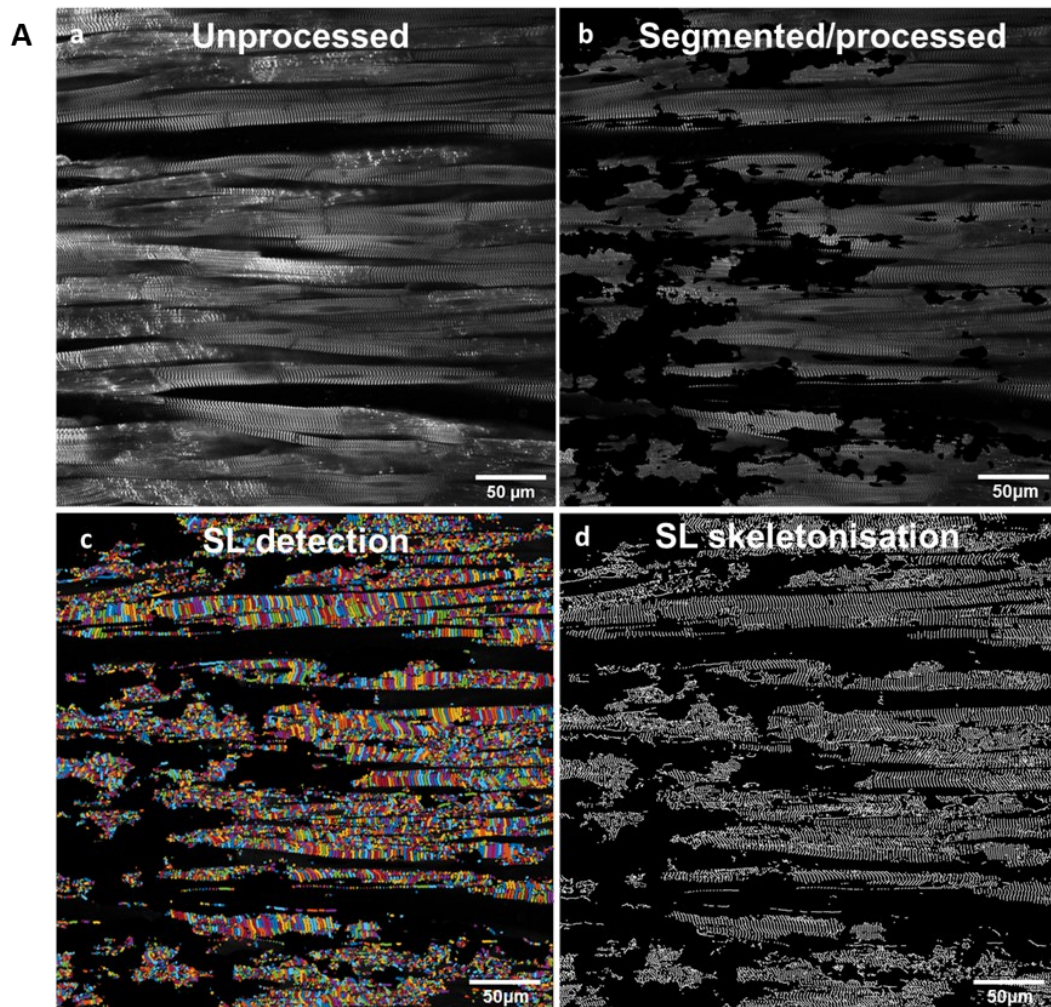
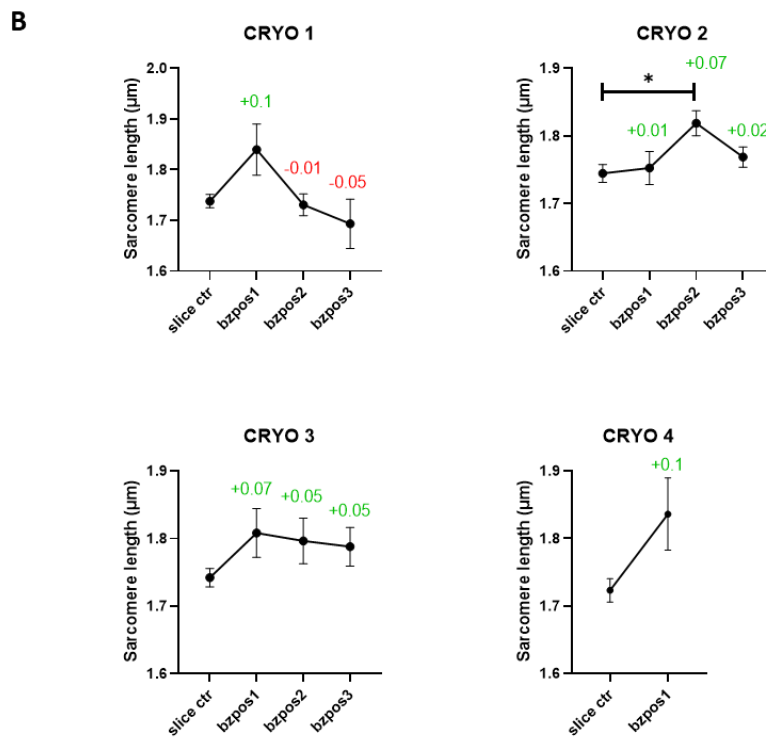
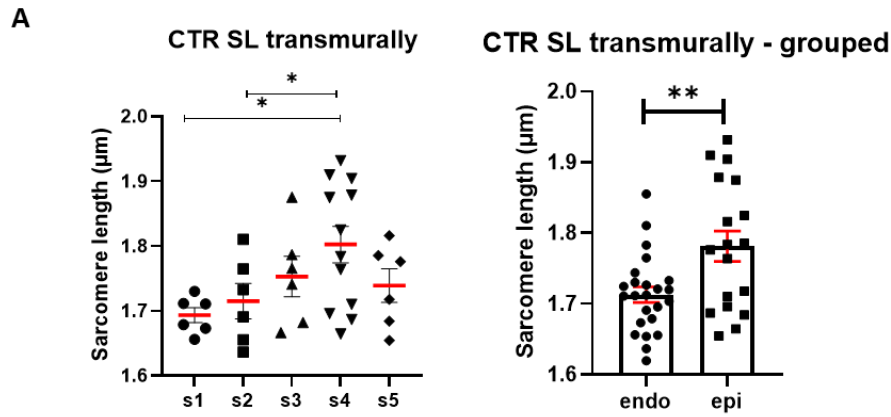


Figure 4.10-Image processing for automated sarcomere length analysis. A) Representative images of unprocessed (a) sarcomeres, labelled with  $\alpha$ -actinin, Fiji processed image (b) for image segmentation, matlab sarcomere detection (c) and sarcomere skeletonization. B) The images were analysed in matlab software and the SL of all the detected sarcomeres was calculated. The resulted values were presented in a histogram, showing the spread, distribution and mean of the SL in each image.

Transmural differences of the left ventricle have been reported by our group and others (Khokhlova et al., 2018; Fotios G. Pitoulis et al., 2020). To evaluate if there are, also, transmural differences in the sarcomeres, analysis was firstly focused on LMSs derived from different areas of the LV. Control LMSs were categorised depending on their slice order, starting from the endocardium (slice 1) towards the epicardium (slice 5). Fig 4.11A shows that midmyocardial/epicardial layers (slice 4) have significantly increased sarcomere length in comparison to endocardial layers (slice 1). This finding suggested that comparison of the controls and the treated cryoinjured samples should be done in respect to their transmural positions. Therefore, cryo groups were paired with control groups from the same transmural areas (e.g. cryo1\_s2 with ctr\_s2). Most of the areas adjacent to the cryoinjury showed an increase in SL in all the different treatments (cryo1-4). More specifically, the area closer to the injury (pos1) was increased by  $\sim 0.1\mu\text{m}$  in all conditions, except of the cryo 2, which showed significant increase at a further position, pos2. The degree of injury (1-4 injury areas) did not affect the level of SL increase as the values did not deviate away from 0.07-0.1  $\mu\text{m}$  in all conditions. These data indicate that cryoinjury locally increased the SL in cryoinjured LMSs regardless of the injury degree.



Treatments	Areas		
	bz_pos1	bz_pos2	bz_pos3
cryo 1	0.1	-0.01	-0.05
cryo 2	0.01	0.07	0.02
cryo 3	0.07	0.05	0.05
cryo 4	0.1		

Figure 4.11-High throughput sarcomere length analysis. A) Differences between transmural layers of the left ventricle. The number (s1, s2, s3, s4, s5, s6) indicates the order of the slices starting from the endocardium (s1) towards the epicardium (s5). The slices were, also, grouped in endo and epi by combining the data from slice1+2 for the endocardium (endo) and slice 4+5 for the epicardium (epi). B) Analysis of the SL in cryoinjured LMSs was also evaluated, focusing on the areas around the injury. The number of areas indicate how close they are to the injury, with pos1 being close and pos3 being far from the injury. The table at the bottom shows mean differences of the areas around the injury in comparison to their respective controls. One-way ANOVA was used to compare the control and cryoinjured groups. N/n=6/6, \*=P value  $\leq 0.05$ . N/n=biological replicates (animals)/technical replicates (LMSs).

### **4.3.3 Chronic effects of cryoinjury**

#### **4.3.3.1 Maximum isometric contraction**

Control and cryoinjured rat LMSs were cultured for 24h and maximum contraction upon isometric stretch was assessed. This condition was chosen as a measurement of viability, since previous observations showed that this was a more accurate and sensitive method than other biochemical or colorimetric methods. Maximum active and passive force did not show any changes after 24h of tissue culture between control and cryoinjured LMSs, which indicates that there were no significant changes in LMS max functionality.

#### **4.3.3.2 Contraction kinetics**

Unlike maximum isometric contraction, which was achieved at various stretching length, contraction kinetics required measurements under the same preload conditions for comparable results. Therefore, control and cryoinjured rat LMSs were cultured for 24h and contraction was measured at physiological stretch of 2.2 $\mu$ m SL. The active/passive force, time to peak and 50% decay time did not significantly differ between the groups. However, relaxation time (90% decay) and decay constant were significantly altered in cryoinjured LMSs, which means that their relaxation was slower than the control LMSs. This observation was in line with previous observations after acute application of cryoinjury.

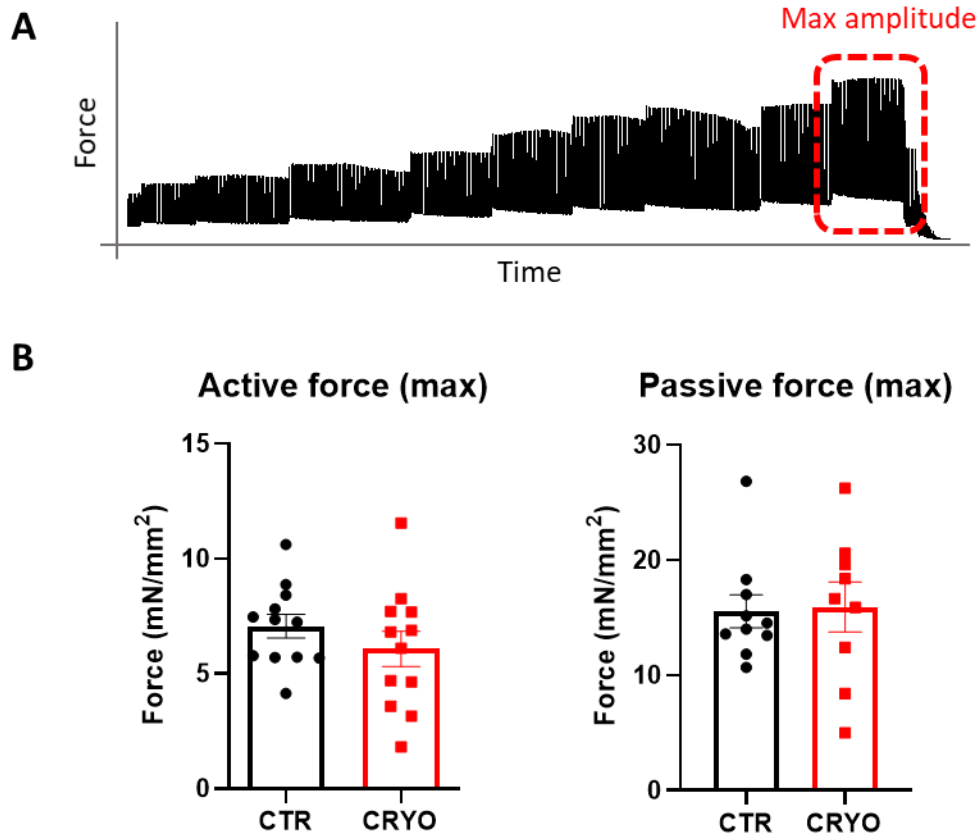


Figure 4.12-Contraction force was measured at maximum isometric stretch on cultured LMSs as a measure of viability and functionality. A) Representative traces of LMS contraction and analysis of maximum generated active force (red selection). B-C) Maximum active and passive force did not show significant changes after 24h of culture. An unpaired t-Test was used for statistical analysis of the groups. No significant differences were detected. N/n=7/12. N/n=biological replicates (animals)/technical replicates (LMSs).

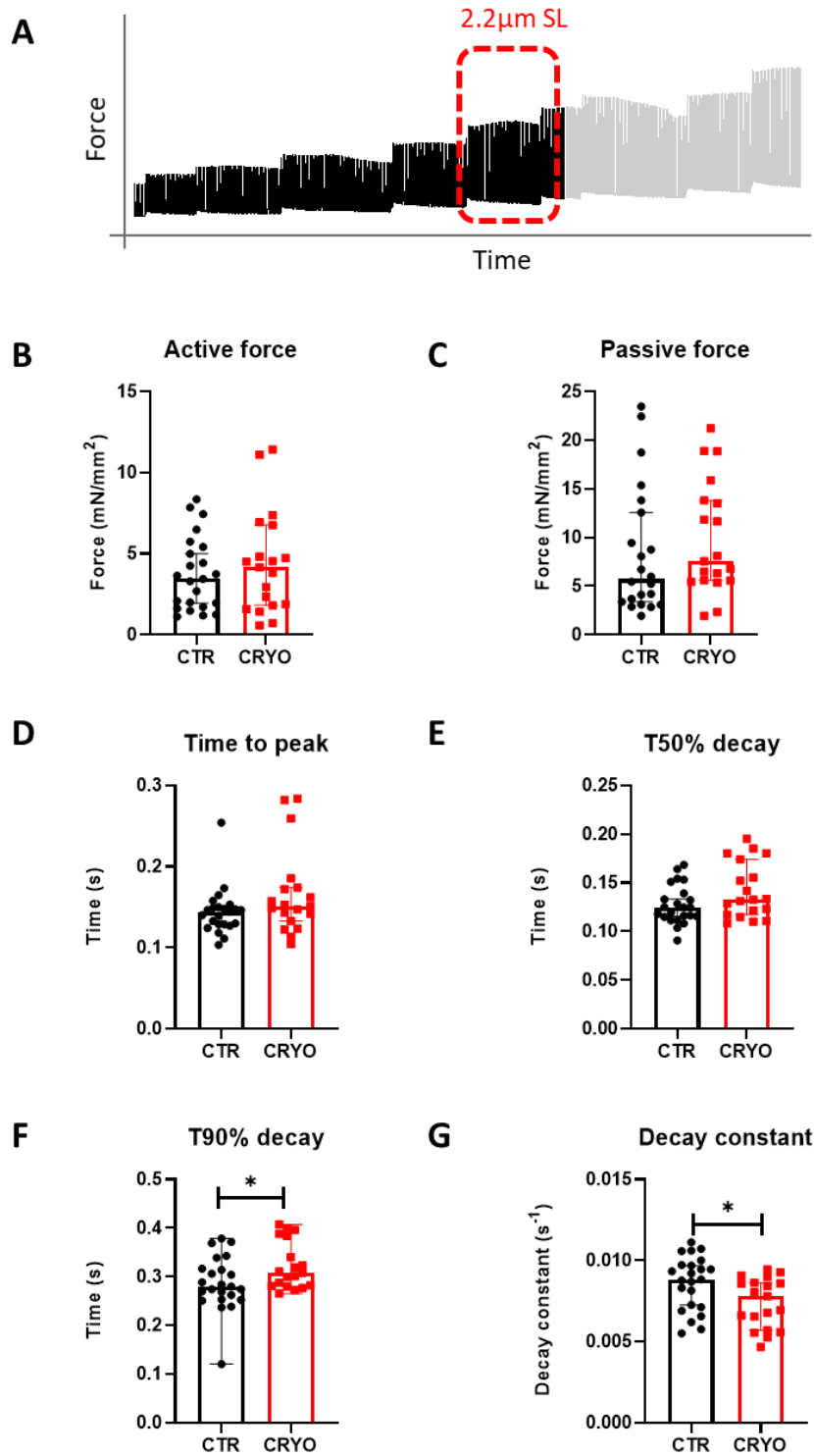


Figure 4.13- Baseline LMS contractility was assessed after 24h of culture. LMSs were placed on the force transducer and stretched at 2.2 $\mu$ m of SL. A) Schematic representation of recorded contraction data and data selection for further analysis. B-F) Contraction amplitude (active force), passive force, time to peak and time to 50% decay remained unchanged between the two groups. F-G) However, decay time was significantly increased, showed by the increase of time to 90% decay and decay constant. Data were not normally distributed and are presented as median and 95% confidence interval. An unpaired *t*-Test was used to compare the two groups. N/n=12/21-22, \*=P value  $\leq$  0.05.

#### **4.3.3.3 Increased LMS arrhythmogenicity**

General observations of contractility in the previous experiments showed the development of spontaneous contractions after 24h of LMS culture in the cryoinjured conditions. In order to better validate tissue arrhythmogenicity a proarrhythmic protocol of fast pacing (FP) in the presence or absence of isoproterenol (FP + ISO), was applied to the cultured LMSs. Cryoinjured LMSs showed increased levels of arrhythmogenicity after fast pacing which became significant after the application of isoproterenol. (Fig 4.14A-B). Out of the LMSs that developed arrhythmias the cryo LMSs showed higher number of spontaneous contractions compared to control, Fig 4.14C-D.

Latency of the tissue was also measured as an additional method of assessing arrhythmogenicity. Again, cryoinjured LMSs required less time to develop spontaneous activation compared with control LMSs, a tendency that became more apparent and significant after the application of isoproterenol.



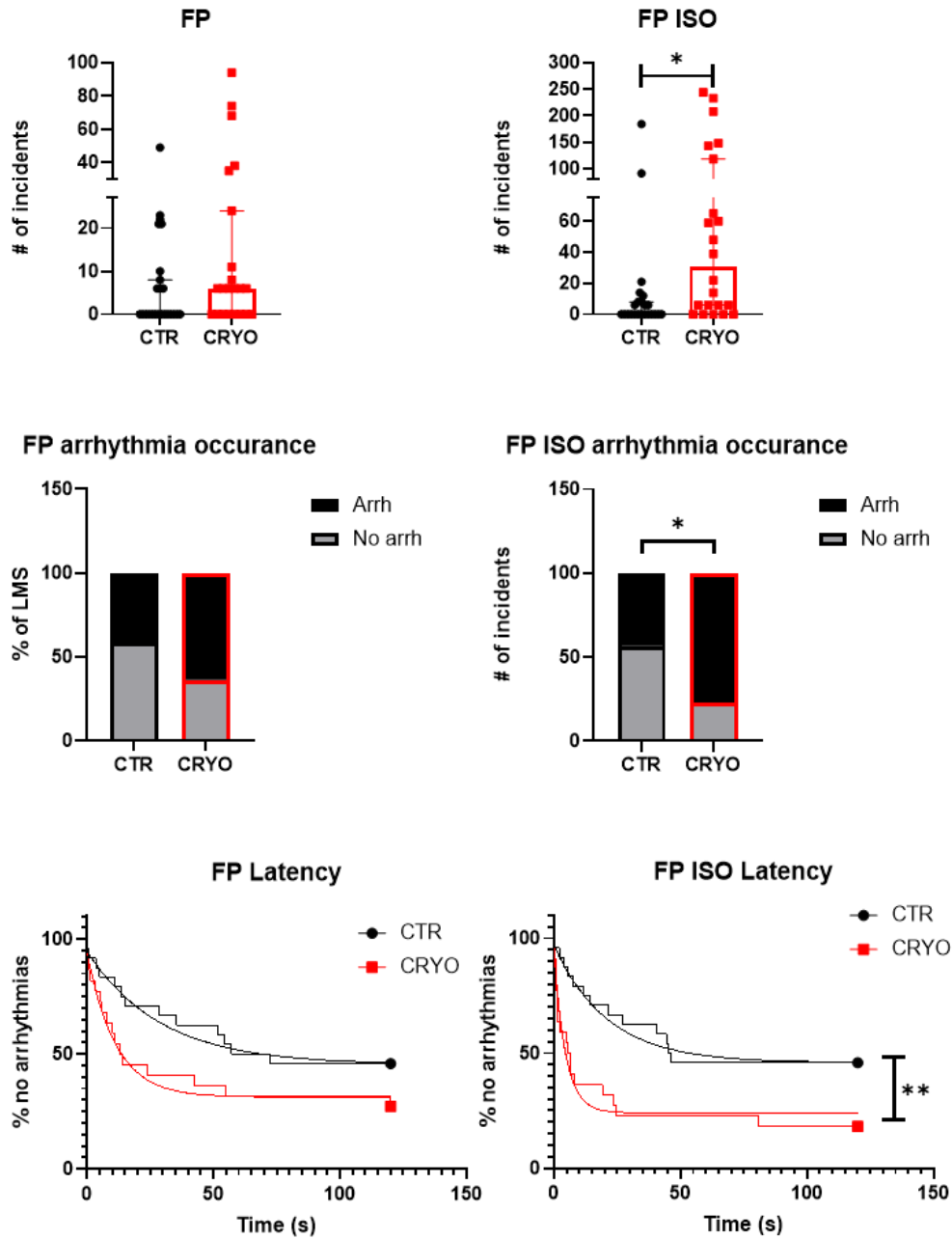


Figure 4.14-Cultured LMSs were treated with a proarrhythmic protocol of fast pacing (FP)  $\pm$  isoproterenol (FP ISO). The electrical stimulation was then halted, and spontaneous contractions were recorded. A-B) FP protocol showed a trend towards higher arrhythmogenic potential of the cryoinjured LMS. The addition of isoproterenol exacerbated the arrhythmogenic potential and cryoinjured LMSs showed significant increase of spontaneous contractions. C-D) The percentage of LMSs that exhibited arrhythmias, irrespective of the arrhythmia degree, were also plotted. Cryo-LMSs showed higher prevalence of arrhythmias, which reached statistical significance after the addition of isoproterenol. (E-D) Spontaneous contractions occurred significantly earlier than the control LMSs, which is presented as reduced latency under FP ISO condition. Data were not normally distributed and are presented as median and 95% confidence interval. Unpaired Mann-Whitey test was used to compare the two groups.  $N/n=12/21-22$ ,  $*=P$  value  $\leq 0.05$ ,  $** P$  value  $\leq 0.01$ .  $N/n=$ biological replicates (animals)/technical replicates (LMSs).

#### **4.3.4 Cytoplasmic Calcium cycling**

Dysfunctional  $\text{Ca}^{2+}$  release, such as SCR events, play an important role in triggering ventricular arrhythmias (Pogwizd and Bers, 2004). To study the association of calcium regulation in cryoinjured LMSs the tissue was stained with Fluo-8AM and  $\text{Ca}^{2+}$  traces were recorded in an upright microscope. Global  $\text{Ca}^{2+}$  transients and single cell  $\text{Ca}^{2+}$  waves were investigated. These studies were done in collaboration with a postdoc researcher, Eef Dries and the majority of experiments were executed by her.

##### **4.3.4.1 Calcium transients and spontaneous calcium events**

Global  $\text{Ca}^{2+}$  transients were measured during electrical stimulation (1Hz). Cryoinjured LMSs showed significantly reduced  $\text{Ca}^{2+}$  transient amplitude with prolonged time to peak, while  $\text{Ca}^{2+}$  decline remained unaffected. To further challenge the tissue a proarrhythmic protocol was performed. When stimulation was halted spontaneous global  $\text{Ca}^{2+}$  transients were recorded. The % of cryoinjured LMSs that developed spontaneous  $\text{Ca}^{2+}$  transients was higher in injured compared with control LMS, as shown in Fig 4.15E. Further analysis of the arrhythmic LMS in both cryoinjured and control LMS showed that cryoinjured LMS had higher frequency of spontaneous global  $\text{Ca}^{2+}$  transients compared with control LMS, Fig 4.15D.

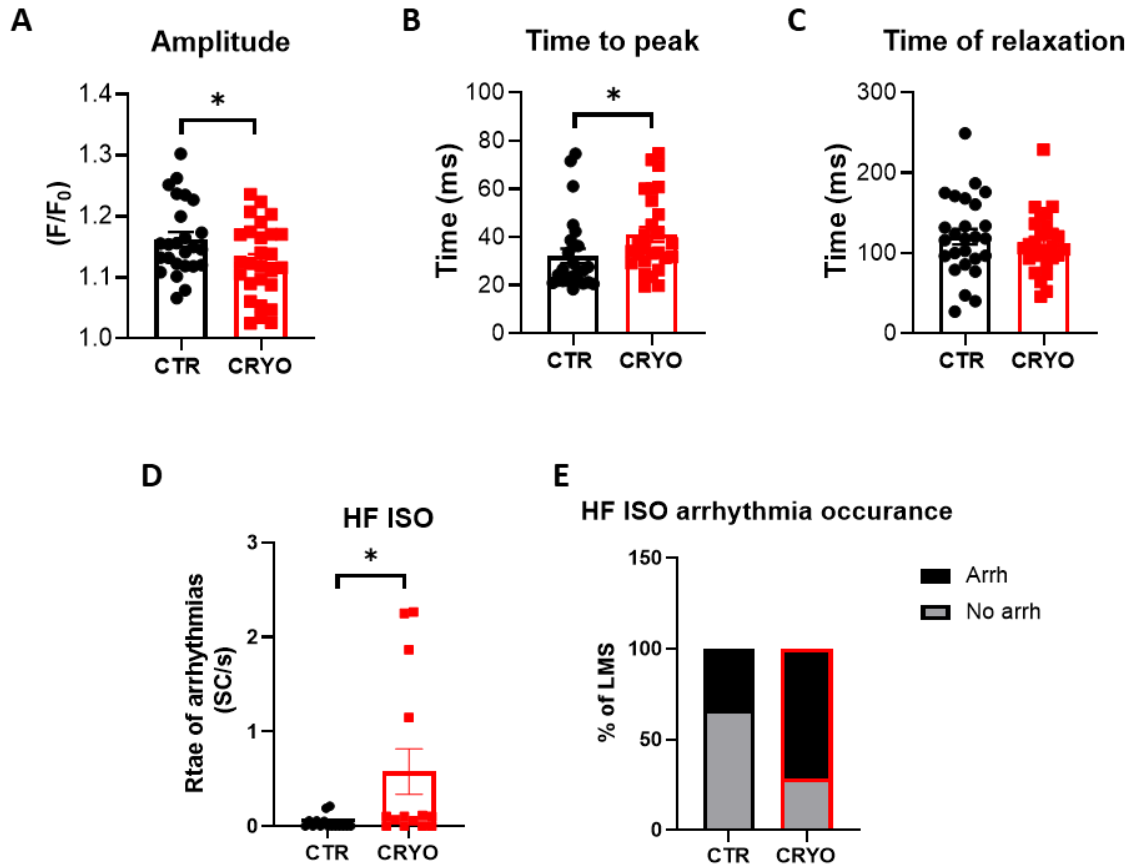


Figure 4.15-Calcium transient analysis of LMSs after 24h of culture. LMSs were stained with Fluo-8AM which act as a calcium indicator. A-C) Cultured LMSs were electrically stimulated, and global tissue calcium transients were recorded. Cryoinjured LMSs showed to have reduced amplitude and slower time to peak. D) The cultured LMSs were, also, subjected to a proarrhythmic protocol, where spontaneous calcium transients (in absence of electrical stimulation) were recorded after halting of electrical circulation. Cryoinjured LMSs showed higher levels of spontaneous  $Ca^{2+}$  transients compared to control LMSs. The arrhythmias were calculated as the number of spontaneous contractions per second. E) The percentage of LMSs that exhibited arrhythmias, irrespective of the arrhythmia degree, were also plotted. Cryoinjured LMSs showed higher prevalence of arrhythmias, without reaching, however, statistical significance. An unpaired t-Test was used for statistical analysis of the groups in figures A-C, whereas data in figure D were analysed with an unpaired Mann-Whitey test, given that they were not normally distributed. Error bars indicate standard error in normal distributions or 95% confidence interval in not normally distributed data. N/n=17/26 \*=P value  $\leq 0.05$ . N/n=biological replicates (animals)/technical replicates (LMSs).

#### 4.3.4.2 Spontaneous Ca<sup>2+</sup> waves in the LMSs

A closer microscopic look in the cellular level of the tissue made possible the detection of spontaneous Ca<sup>2+</sup> waves that originated from single cells during rest (in the absence of electrical stimulation). These waves originated from single areas, called here “foci”, which propagated along the tissue fibers. Fig 4.16A shows two representative images of the Ca<sup>2+</sup> initiation foci in control and cryoinjured LMSs. Cryoinjured LMSs showed to have higher number of spontaneous foci (2x more foci) that were also developed much earlier than in control conditions (Fig 4.16B-C), almost twice as fast as the control foci (CTR mean: 645ms, CRYO mean: 1155ms). The minimum distance between two foci was also measured. Cryoinjured LMSs showed to have significantly closer foci (CTR mean: 102.7µm, CRYO mean: 70.26µm) compare to the control. The majority of the foci were located in close proximity, in distance of no more than 300µm (Fig 4.16E). Further analysis of these foci showed that cryoinjured LMSs contained higher % of foci (larger amplitude in Cryo, Fig 4.16F) that were closer distributed compared (mean distance of 61µm) to the control LMSs. Control samples also contained spontaneous foci; however, the distance between them was sparser, given that their distribution was wider and mean and amplitude were lower as well. The histograms presented in Fig 4.16 were analysed after fitting a Gaussian distribution.

In summary, spontaneous foci appeared after halting of electrical stimulation, which appeared to be more in number and in closer proximity with each other in cryo LMSs.

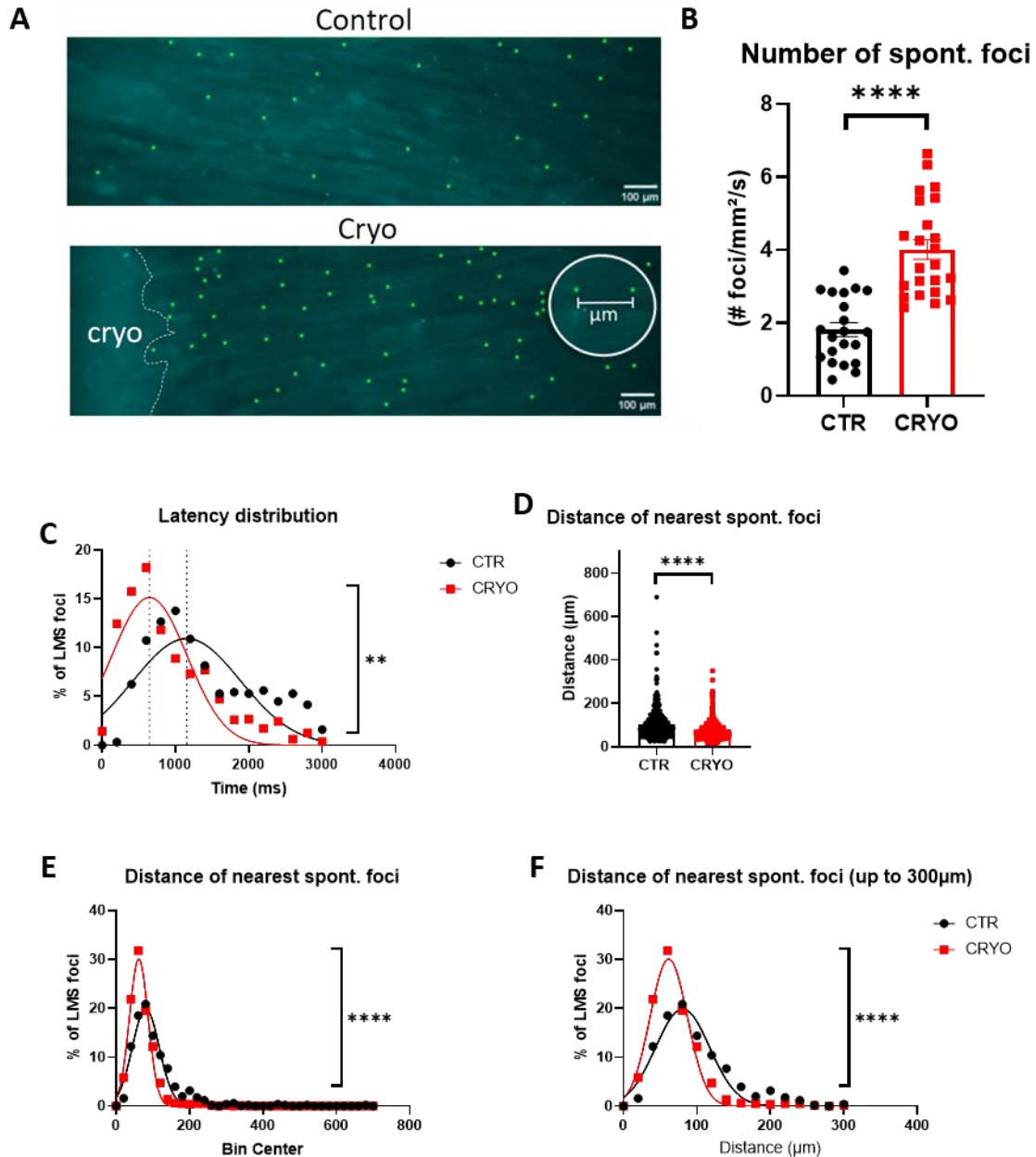


Figure 4.16-Cultured LMSs were treated with a proarrhythmic protocol and spontaneous calcium release (SCR) events were analysed during rest (in absence of electrical stimulation). A) Representative set of images showing the initiation points of spontaneous (spont.) foci (green dots) in control and cryoinjured LMSs. B-C) The number of spontaneous foci was significantly higher and occurred sooner than in control LMSs (latency). D) Analysis of the distance between spontaneous foci showed that cryoinjured LMSs were significantly closer to each other compared to control LMSs. E) Further analysis of the data revealed that most foci were distributed between in 20-300μm distance. F) The distribution curves of the individual groups significantly differed between them. There were more spontaneous foci that were closer distributed in the cryoinjured LMSs compared to the control group. Unpaired t-Test (B), Unpaired Mann-Whitey (D) and Gaussian distribution analysis were used to analyse the data. N/n=19/21 \*\*\*\*=P value  $\leq 0.0001$ . N/n=biological replicates (animals)/technical replicates (LMSs).

#### 4.3.4.3 Spontaneous calcium waves – speed and propagation distance

Irregular local activation in the absence of electrical stimulation has been shown to cause arrhythmias which are often present in diseased cardiac tissue such as the failing heart (Kubalova et al., 2005). To study the role of  $\text{Ca}^{2+}$  waves and their link to the initiation of global spontaneous events, different wave characteristics were evaluated, such as propagation distance, directionality, and wave kinetics.

Spontaneous foci were present in both control and cryo groups with the wave propagation distance not exceeding  $100\mu\text{m}$ , which is the average length of a cardiomyocyte. This observation indicates that the waves in both ctr and cryo conditions happened intracellularly and did not travel to the neighbouring cells. However, cryoinjured LMS waves showed to propagate in longer distances within the cells (Fig 4.17A). The kinetics of these waves were also changed upon cryoinjury with the wave speed being significantly higher in cryoinjured compared to the control LMSs.

The direction of the signal propagation has, also, been reported to be altered in cases of heart failure. While the physiological electrical propagation runs in high speed along the cardiac fibers, failing cardiac tissues exhibit additional lateralisation of electrical propagation, which disrupts electrical synchrony. To test if that was the case in the Cryo group, the direction of the signal propagation was measured. In both groups, the electrical signal propagated in parallel with the fibre orientation ( $0^\circ$ ) and did not exceed an angle more than  $10^\circ$ . Quantification of the cryoinjured LMS fraction showed that there were more LMSs that contained foci with increased angle wave propagation compared with control LMSs.

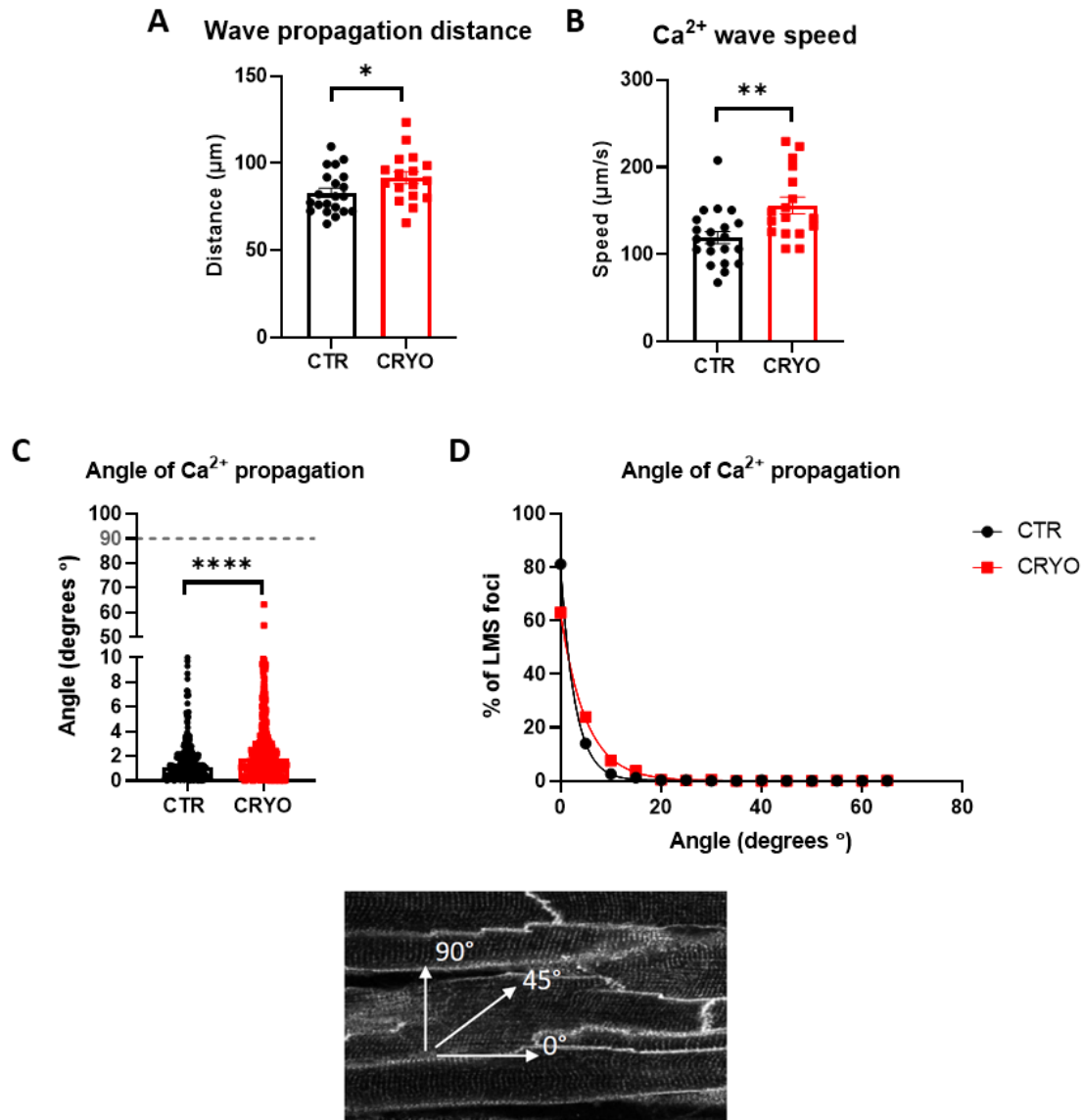


Figure 4.17-Wave properties of the spontaneous foci in cultured LMSs. A-B) Calcium waves in the cryoinjured LMSs propagated faster and over a longer distance compared to control LMSs. C-D) Further analysis of the calcium waves showed that the angle of propagation was close to  $0^\circ$  in control LMSs, indicating that the waves propagated longitudinally, following the fibers alignment. Cryoinjured LMSs had higher number of waves that propagated in bigger angle. An unpaired t-Test (A-C), and Gaussian distribution analysis was used to analyse the data.  $N/n_{ctr}=19/21$ ,  $N/n_{cryo}=14/17$ ,  $*=P$  value  $\leq 0.05$ ,  $**=P$  value  $\leq 0.01$ ,  $****=P$  value  $\leq 0.0001$ .  $N/n$ =biological replicates (animals)/technical replicates (LMSs).

### **4.3.5 Structural analysis**

For further validation of the functional data, structural analysis was, then, performed. This section is focused on sarcomere analysis, and quantification of connexins, caveolin-3 and collagen deposition of the LMSs after 24h of culture and remodelling. These elements have been previously shown to be affected upon cardiac damage and be present in adverse remodelling and heart failure (Hamdani et al., n.d.; Schulz et al., 2015; Travers et al., 2016).

#### **4.3.5.1 T-tubule density**

T-tubule density has been associated with poor cardiac contractility, defective E-C (excitation-contraction) coupling and asynchronous  $\text{Ca}^{2+}$  release (Lipp et al., 1996; Louch et al., 2004). To investigate the role of t-tubules in cardiac arrhythmogenicity upon injury, the density of caveolin 3 was measured. Caveolin 3 is a major structural protein of caveolae and is associated with formation of t-tubules (Galbiati et al., 2001; Woodman et al., 2002). T-tubule analysis showed that the border zone of cryoinjured LMSs had significantly lower amount of caveolin 3 compared to healthy control LMSs, whereas the remote area, away from the injury was not affected Fig 4.18 This is an indication that t-tubules were affected by cryoinjury; however, caveolin staining is an indirect method of studying t-tubules and further validation is needed to fully describe the effects of injury on t-tubules.

#### **4.3.5.2 Connexin 43**

Connexin 43 is a major component for the formation of gap junctions in the heart. Gap junctions are membrane channels that mediate the cell-to-cell movement of ions and small metabolites and therefore are important for the synchronous and coordinated signal propagation between cardiomyocytes (Lo, 2000). Connexin 43 is located on the short axis of the cardiomyocytes and lateralisation of them is been observed in pathological conditions (Fontes et al., 2012; Hesketh et al., 2010). Image analysis of connexin 43 showed that the density or



lateralisation remained unchanged between the control and Cryoinjured LMSs, indicating that gap junction density and localisation was not involved in the development of irregular  $\text{Ca}^{2+}$  events on the LMSs.

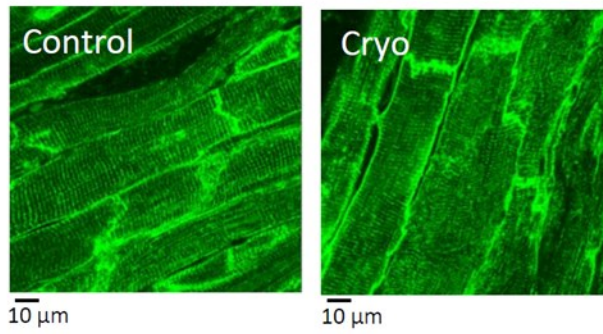
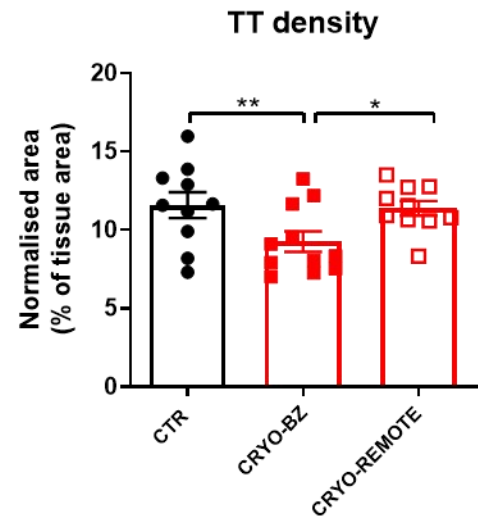
**A****B**

Figure 4.18-Cultured LMSs were stained for caveolin-3, a protein that localises in t-tubules (TT). A) Representative image of t-tubules in cultured control and cryoinjured LMSs. B) Quantification of t-tubule density in cultured LMSs, showing spatial changes between cryoinjured LMSs and healthy tissue. The data were analysed using One-way ANOVA. N/n=6/10, \*=P value  $\leq 0.05$ , \*\*=P value  $\leq 0.01$ . N/n=biological replicates (animals)/technical replicates (LMSs).

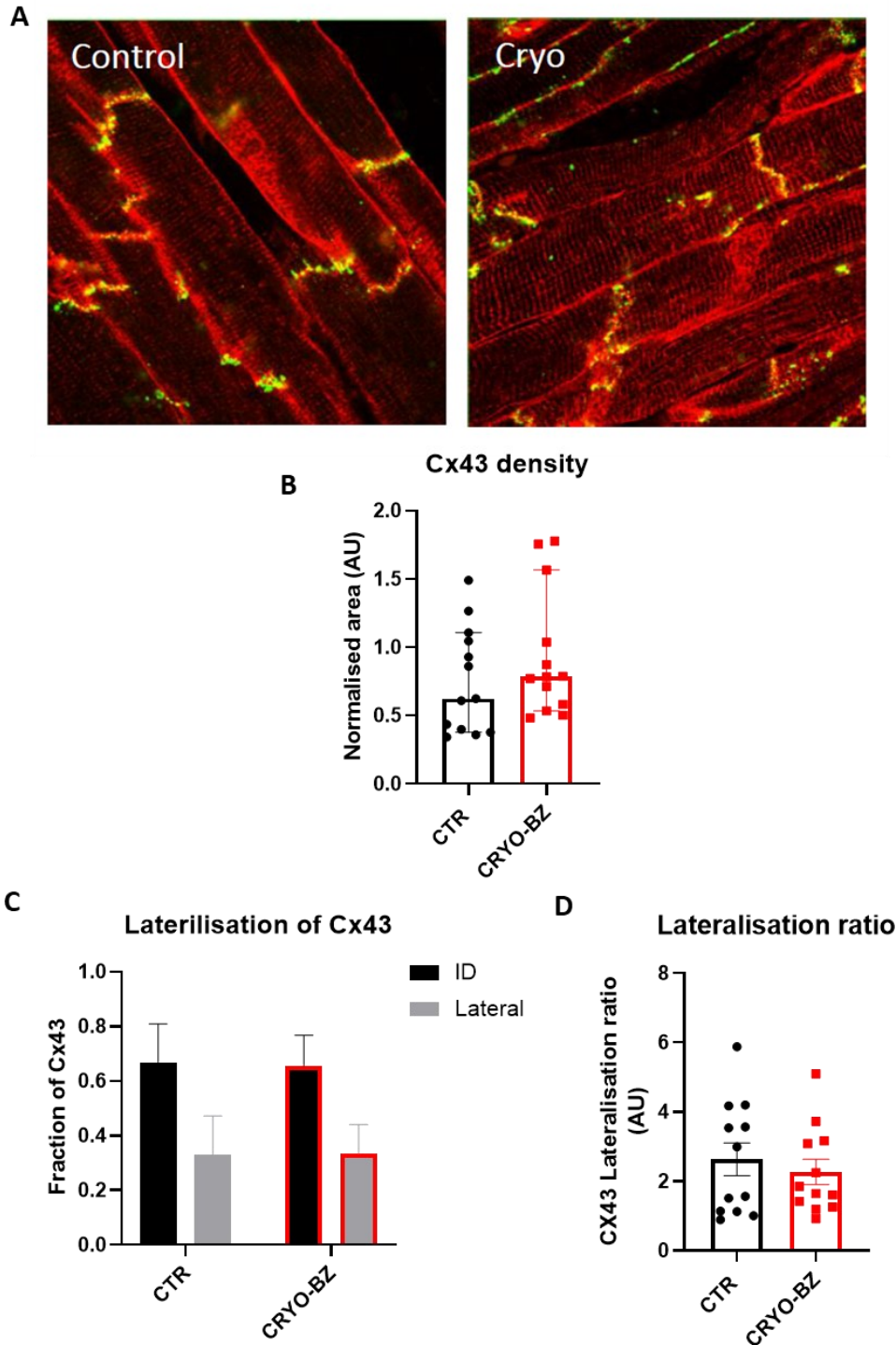


Figure 4.19-Connexin 43 immunohistological analysis. Cultured LMSs were stained for connexin 43 (green), which localises in gap junction at the intercalated discs (ID). Cardiomyocytes were stained, also, for caveolin 3 (red), which was analysed in the previous figure. A) Representative confocal images of control and cryoinjured LMSs. B) Total connexin 43 (Cx43) density was calculated and represented as median and 95% interval confidence. C-D) Connexin 43 lateralisation was, also, analysed by measuring the amount of connexin 43 at the intercalated discs (ID) or the rest of the cell (lateral). Topological anisotropy was also examined by calculating and plotting the ratio of connexin 43 ID/Lateral. Unpaired t-Test (D), Unpaired Mann-Whitey (B) and 2-way ANOVA (C) were used to analyse the data. N/n=6/12. No significance was observed. N/n=biological replicates (animals)/technical replicates (LMSs).

#### 4.3.5.3 Collagen deposition

Fibrosis after myocardial infarction has been one of the most common adverse effects and the scope of many therapeutic strategies in humans. *In vivo* animal studies simulating cardiac infarction, either via artery occlusion or cryoinjury, have shown to increase collagen deposition (González-Rosa et al., 2011a; Mizutani et al., 2016). To evaluate whether collagen secretion was, also, upregulated in cultured LMSs, the tissue was stained for Collagen I, visualised in the confocal microscope and analysed with Fiji software. Collagen deposition on LMSs was evaluated on different areas of the LMSs, the area of injury, the BZ (at the centre of the BZ, at the side of the BZ) and away from the injury (see Fig 4.20B for schematic representation of the analysed areas). The area of collagen was normalised to the total area of the tissue recorded and compared to the healthy LMSs. Fig 4.20 shows that the collagen area was not significantly changed upon cryoinjury after 24h of culture.

#### 4.3.5.4 Sarcomere length after 24h remodelling

Changes in sarcomere architecture were tested by measuring the sarcomere length (SL) of individual cardiomyocytes on the site of injury, the BZ and the area away from the injury. Cultured LMSs were stained for  $\alpha$ -actinin and visualised with a confocal microscope. A low magnification image of the injury reveals that the tissue surrounding the injury had curled up and measurements of this area were not possible. Therefore, SL measurements were done on the area immediately adjacent to the curled area, which was defined as BZ due to close proximity to the injury. The BZ and the area away from the injury did not show any significant changes from the healthy tissue and the mean SL was approximately at 1.8 $\mu$ m in both cases (see Fig 4.2B). The SL on the area of injury showed unphysiological values that exceeded 2.4 $\mu$ m or were smaller than 1.8 $\mu$ m. These values do not belong to the physiological SL range that has been reported in previous studies (Bub et al., 2010).

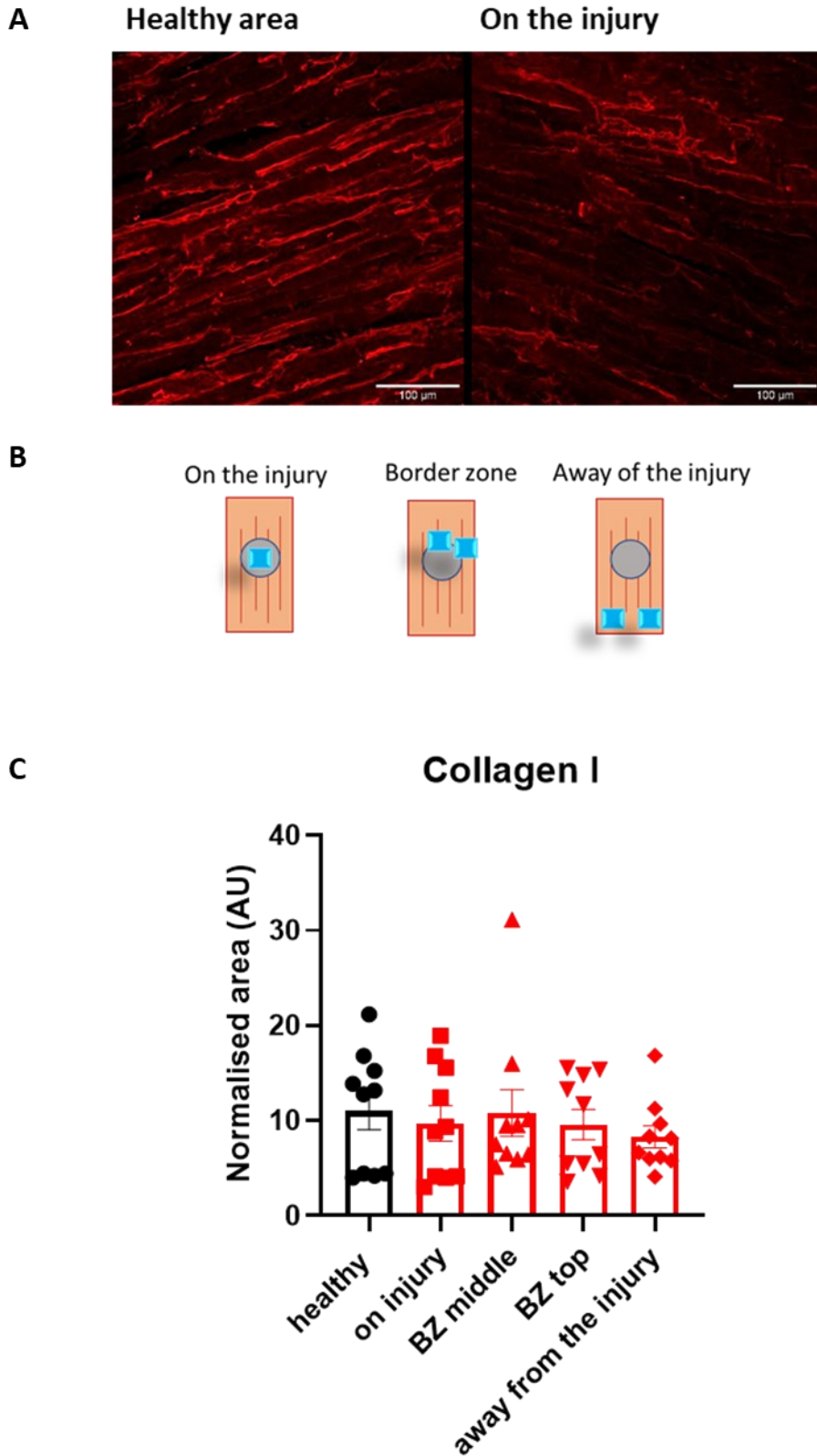


Figure 4.20-Collagen quantification of cultured LMSs. LMSs were stained for collagen I and visualised in a confocal microscope. A) Representative images of stained LMSs with collagen I on healthy and injured LMSs (red). B) Schematic representation of analysed areas. C) Quantification of collagen I in control (black) and cryoinjured LMSs (red). No significant differences were observed between the different groups. One-way ANOVA was used to compare all the groups. N/n=3/10. N/n=biological replicates (animals)/technical replicates (LMSs).

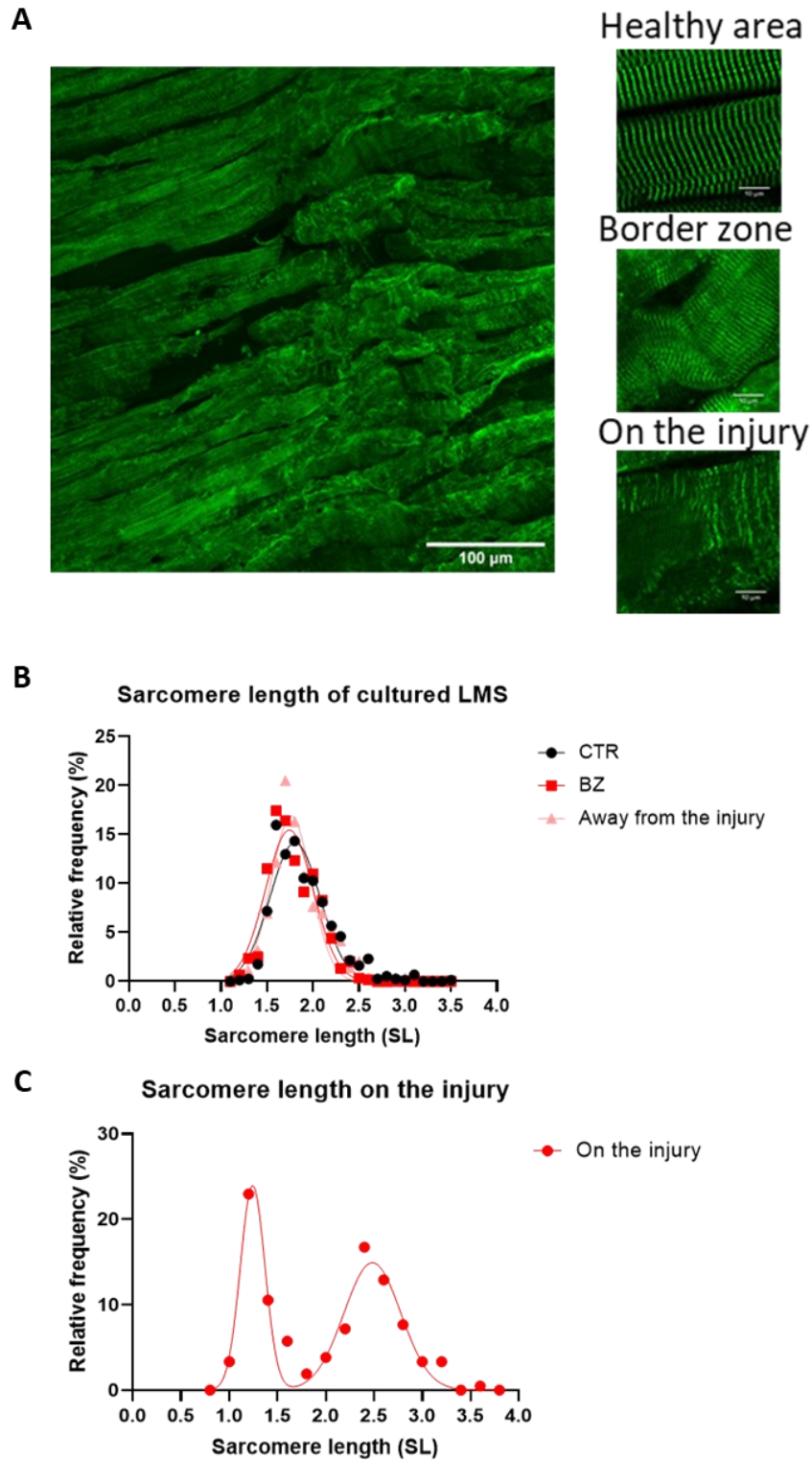


Figure 4.21-Sarcomere length (SL) measurements of cultured LMSs. LMSs were stained for  $\alpha$ -actinin (green) and visualised in a confocal microscope. A) Representative images of stained LMSs near the BZ of cryoinjured LMSs. Isolated and magnified images of all the measured areas are presented on the right side of the panel. B) SL distribution graphs on different LMSs. The BZ and the area away from the injury showed similar distribution to the healthy control LMSs. C) However, the injured area exhibited a highly variable distribution of either very short or very long sarcomeres, represented by the two peaks in the graph. N/n=6/12-30. N/n=biological replicates (animals)/technical replicates (LMSs).

### **4.3.6 Cryoinjury on human LMSs**

To evaluate how a local injury affects the human myocardium, LMSs derived from healthy or failing hearts were produced. Healthy LMSs were cryoinjured, whereas untreated healthy LMSs and failing LMSs were used as a negative and positive control, respectively. The LMSs were cultured for 48h.

#### **4.3.6.1 Contraction of human cryoinjured LMSs**

Contraction of cultured LMSs was measured at baseline stretch conditions at  $2.2\mu\text{m}$  of SL, where the contraction amplitude and kinetics were evaluated. Contraction amplitude (active force) tended to be higher in cryoinjured Donor LMSs (treated group), without any other changes in passive force or kinetics. Failing cultured LMSs (positive control) showed a trend of decreased contraction amplitude and increased passive force compared to healthy and cryoinjured donor LMSs. These results show feasibility of the cryoinjury method on human LMSs and the assessment of it after prolonged culture. Future studies will help understand tissue behaviour upon injury with relevance to human physiology and thus overcoming interspecies differences.

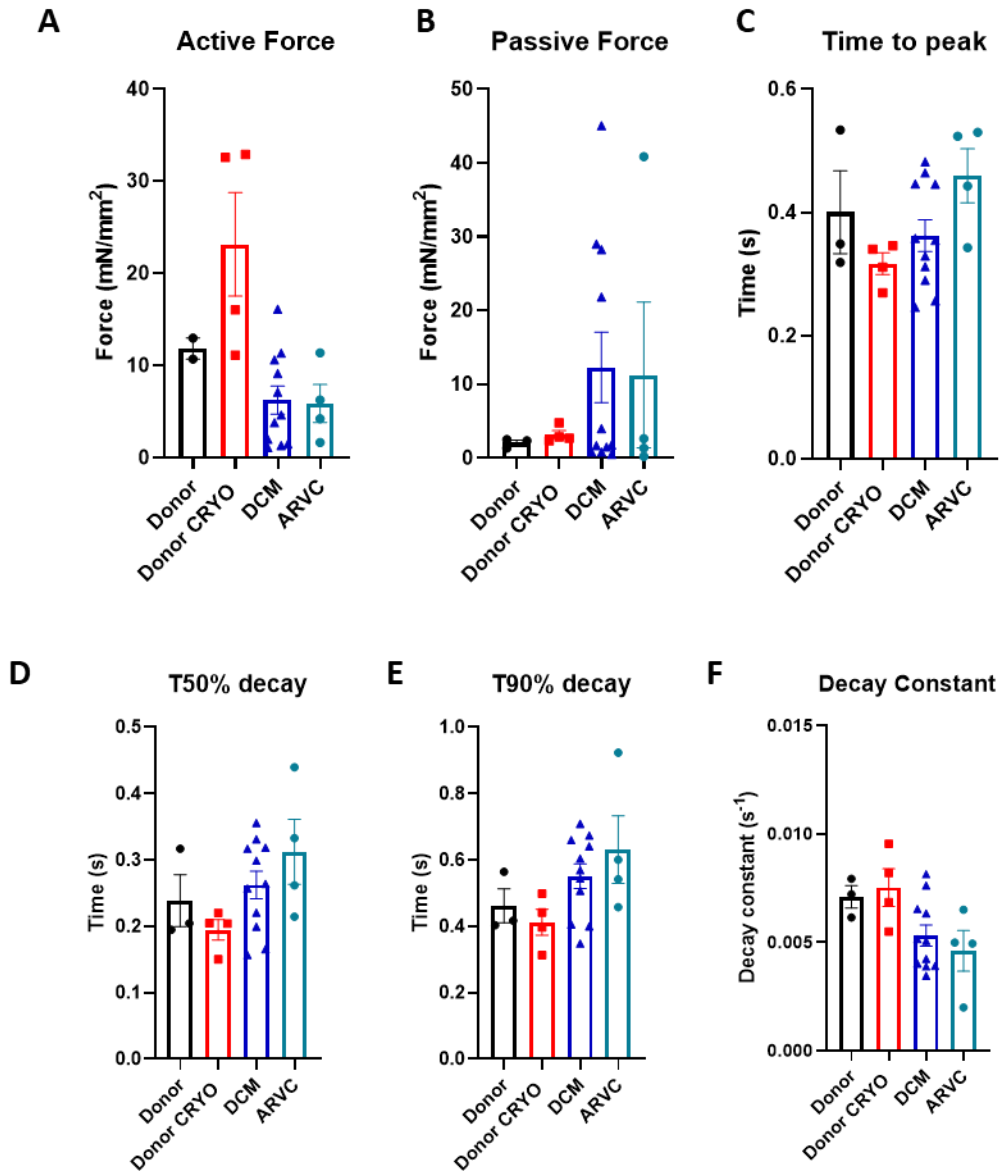


Figure 4.22- Baseline contractility of human LMSs after 48h in culture. LMS contractility was measured at  $2.2\mu\text{m}$  of SL. A) Active force of cryoinjured LMSs showed higher values compared to the control and failing LMSs. On the contrary failing LMSs showed decreased contractility compared to the control LMSs. B) The passive force of the failing LMSs was increased compared to the control and the cryoinjured LMSs. C-F) Contraction kinetics differed between the cryoinjured and failing LMSs, with the cryoinjured LMSs showing faster time to peak, while, the failing LMSs had slower relaxation time. Due to limited n number of the donor LMSs statistics were not performed.  $N/n(\text{donor})=1/3-4$ ,  $N/n(\text{DCM})=2/9$ ,  $N/n(\text{ARVC})=1/5$ .  $N/n$ =biological replicates (animals)/technical replicates (LMSs).



#### 4.3.6.2 Arrhythmogenicity on human cryoinjured LMSs

In order to match the observations seen in animal models with these in humans, a similar arrhythmogenic protocol was applied to human LMSs. Cryoinjured donor LMSs showed no significant increase in arrhythmogenic potential compared to the healthy donor LMSs. However, interesting results were observed from the failing hearts (positive control), which showed a variable trend depending on their pathologies. Failing hearts derived from patients with dilated cardiomyopathy (DCM) had similar arrhythmogenic potential as the donor healthy (negative control) and donor cryoinjured LMSs (treated group). On the other hand, tissue derived from patients with arrhythmogenic right ventricular cardiomyopathy (ARCV) showed a big increase in arrhythmogenic potential after both treatments of fast pacing and isoproterenol stimulation. ARCV LMS latency, also, appeared to be shorter, indicating that arrhythmias occurred much faster than in any of the other LMS groups. These data demonstrate the importance of different pathologies and how they affect arrhythmogenicity. The ARCV proved to be a more robust model to compare the cryo data, due to the high presence of arrhythmias compared to the DCM. Due to small sample numbers, it is necessary to perform more experiments to further validate these observations

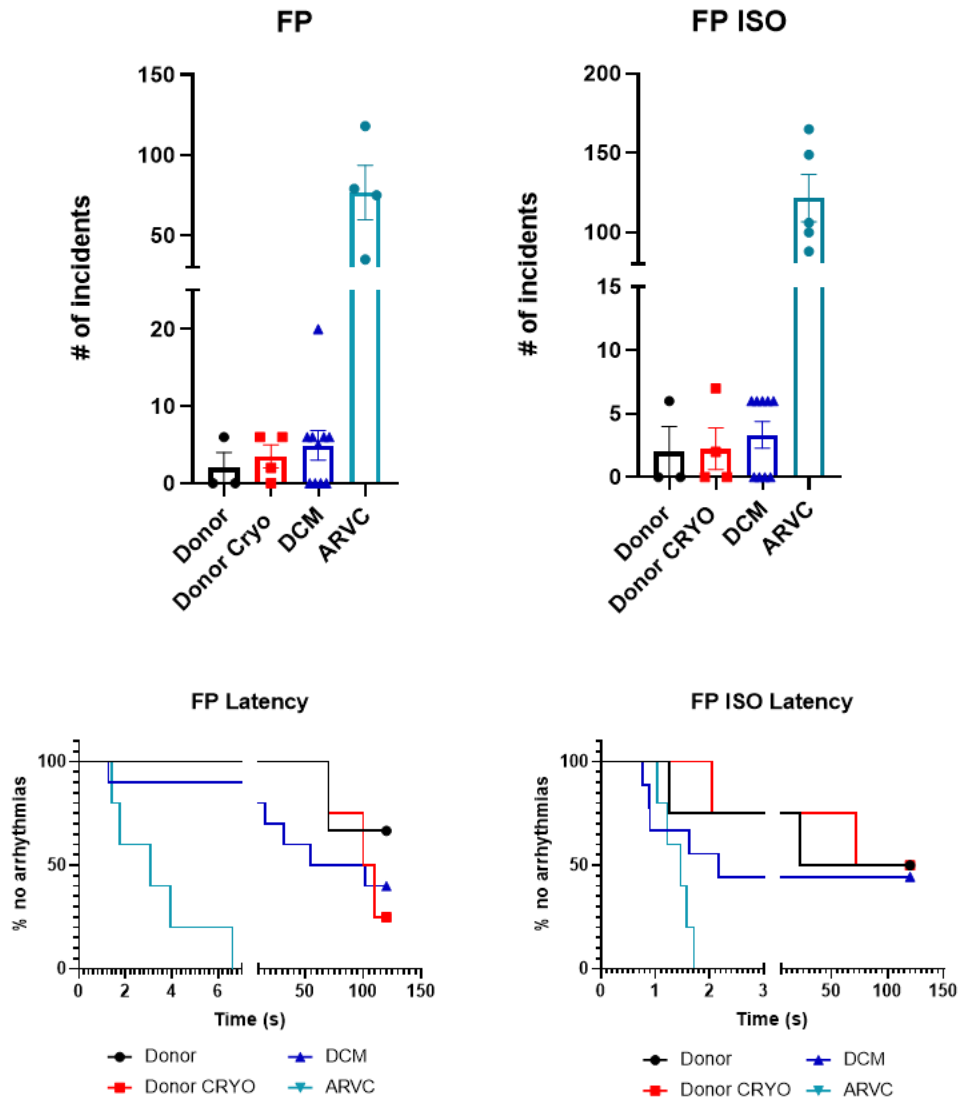


Figure 4.23- Cultured human LMSs were treated with a proarrhythmic protocol of fast pacing (FP) ± isoproterenol/caffeine (FP ISO). The electrical stimulation was then halted, and spontaneous contractions were recorded. Healthy control (Donor) and injured (Donor Cryo) LMSs were tested, while failing heart LMSs were used as a positive control. A) Healthy control and injured LMSs did not show big differences in arrhythmogenicity compared to DCM failing hearts. However, ARVC LMSs showed high arrhythmogenic potential compared to all the other groups, indicating that they represent a useful positive control for arrhythmias. B) Similarly, the latency of injured LMSs did not differ to the control or the DCM failing LMSs. ARVC LMS latency was much shorter than the other groups, indicating that arrhythmias occurred almost immediately after the stop of electrical stimulation. Due to limited n number of the donor LMS statistics were not performed. N/n(donor)=1/3-4, N/n(DCM)=2/9, N/n(ARVC)=1/5. N/n=biological replicates (animals)/technical replicates (LMSs).

## 4.4 Discussion

In this chapter cryoinjured LMSs were characterised for their effect on healthy LMSs and a new diseased model was established, with local and global changes. Cryoinjured LMSs showed to have locally reduced viability and CV without affecting contraction amplitude. Culture of the injured LMSs allowed for remodelling to occur. Cultured injured LMSs showed increased arrhythmia probability both in cellular and global level as seen from contraction and  $\text{Ca}^{2+}$  studies. Sarcomere analysis of the LMSs revealed local differences in SL near the injury with elongated SL on the BZ, indicating differential local mechanical stimulation within the tissue. Finally, cryoinjury on human LMSs demonstrated feasibility of the method on human samples which could be used as a more accurate model to study cardiac injury with translatable potential.

### 4.4.1 Injury size

Infarct size is shown to be significantly associated with overall mortality. In a study published by T D Miller et al (Miller et al., 1995), patients with acute infarcts of size >12%, had 7% mortality rate, in comparison to 0% mortality of patients with <12% infarct size (Miller et al., 1995; Stone et al., 2016). Earlier studies also, confirmed this strong correlation while showing that the majority of people with acute myocardial infarction had cardiac infarction size of around 18%. In order to recapitulate what is happening *in vivo*, a tissue damage of 12% was also induced on LMSs. The use of this size commonly seen in humans and has, also, shown to cause cardiac dysfunction (Arenja et al., 2013). Besides that, this size, also, allows the study of various areas within the LSM (area on the injury, the border zone and the remote or healthy areas), which bigger injuries would not have allowed. The study of different areas is important in order to understand how the residual healthy tissue responds to cell death and remodels over

time. Defining the mechanisms that are involved in these processes gives useful tools and highlights important therapeutic targets.

Further analysis of the injured area showed the existence of two distinct areas with 50% of the injury containing metabolically and structurally compromised cells (dead cells) and the other 50% containing hypercontracted cells with low levels of dead cells. The later population was referred as the border zone (BZ) for distinguishing purposes from the highly necrotic area and because of its similarities in respect to its structure and viability heterogeneity seen in the border zone of human infarcted hearts or animal models (Beyersdorf et al., 1989; Kilic et al., 2006). To better investigate the progression of cell death, TUNEL staining was performed on LMSs, revealing that the damage (DNA fragmentation) was restricted to the area of cryoinjury application. The BZ also showed signs of cell death, such as cell hypercontraction and curvature; however, no DNA fragmentation was observed. These observations indicate that the area of cryoinjury was immediately affected and rapidly underwent cell death, while the adjacent tissue (BZ) responded with a delay to cell death (Garcia-Dorado et al., n.d.).

Studies on apoptosis/necrosis highlight dysregulation of actin and myosin filaments in the cell, as an early response to cells death and therefore cell contraction and dissociation from the extracellular matrix. These observations were also apparent on the BZ of the LMS model upon cryoinjury, enforcing the belief that this area was under the early stages of cell death, in contrast to the area on the injury, which showed features of late apoptosis/necrosis. The loss of cardiomyocytes on the injury, the tissue remodelling of BZ and the heterogenic nature of the whole tissue are significant contributors for the development of arrhythmias and more specifically the development of ventricular re-entrant (De Bakker et al., 1988; Ursell et al., 1985; Wong et al., 2012; Yao et al., 2003)

## 4.4.2 Arrhythmogenicity

### 4.4.2.1 Proarrhythmic triggering

To see if our model also exhibits similar effects of arrhythmogenicity, whole tissue spontaneous contractions were recorded. Since cardiac arrhythmias are not always present in the baseline condition a fast pacing stimulation in the presence or absence of isoproterenol was applied to the cultured LMSs. These conditions challenge the cardiac tissue by increasing the intracellular calcium concentration, activating cyclic adenosine monophosphate (cAMP), protein kinase  $\alpha$  (PKA) and finally  $\text{Ca}^{2+}$ -handling proteins, that make the tissue prone to develop arrhythmias. Similar arrhythmia protocols have been widely used to assess the arrhythmogenic potential of cells or tissues (Calvo et al., 2012; Desantiago et al., 2008). Arrhythmia testing using beta agonists and fast pacing protocols have also been tested in patients (Denis et al., 2014; Segal et al., 2010). Ischemic patients are also prone to develop arrhythmias especially during the first hours/days of the ischemic incidence (Gorenek et al., 2014). Under these conditions, diseased tissue is more susceptible in developing arrhythmias, compared to healthy tissue (Chudin et al., 1999; Harding et al., 1988; Sun et al., 2001; Yatani and Brown, 1989). This study showed that cryo LMSs were more arrhythmogenic, with a shorter latency, which means that they developed more arrhythmias which occurred sooner than in control LMSs. Arrhythmogenicity is also impacted by dysfunctional conduction velocity (Antzelevitch and Burashnikov, 2011). CV on cryoinjured LMSs was affected, with the global longitudinal CV being significantly reduced. Local heterogeneities in the CV were also observed with the CV on the opposite side of the injury and stimulation point being reduced.

#### 4.4.2.2 Connexins

Arrhythmia propagation within the tissue is, also, believed to be modulated by calcium waves. Abnormal  $\text{Ca}^{2+}$  cycling is a critical factor in the development of focal excitations, which can be caused by spontaneous  $\text{Ca}^{2+}$  release (SCR) in the form of intracellular  $\text{Ca}^{2+}$  waves (Shiferaw et al., 2012). Propagation of  $\text{Ca}^{2+}$  waves between cells (intercellular) is believed to occur via a set of ion channel proteins and specialised membrane structures called gap junction. Gap junctions are built out of connexin proteins, which localise mainly in the intercalated disks, even though they can also be found on the lateral side of cardiomyocytes. Gap junctions can provide passage between cells for many substances with a molecular weight  $<1$  kDa, such as cyclic adenosine monophosphate (cAMP), adenosine triphosphate (ATP), Inositol trisphosphate (IP3) (Boyden et al., 2015; Saez et al., 1989). They enable coordinated action potential propagation between cardiomyocytes, create electrical anisotropy and accelerate the longitudinal conduction velocity within the tissue (Kanno and Saffitz, 2001). Connexins 43 is the most abundant structural protein of cardiac connexins and its role in cardiac disease has been extensively studied in both ventricular and atrial tissue (Gourdie et al., 1993; Kanno and Saffitz, 2001; Peters et al., 1993; Sepp et al., 1996). Changes on the expression levels, phosphorylation and localisation of connexin 43 have been linked with increased arrhythmogenic potential in failing hearts and therefore it was further investigated in this study. Immunohistochemical analysis showed no significant differences of protein content or lateralisation, which indicates that the early events of arrhythmias might not be directly linked to gap junction presence. However, further investigation of the protein phosphorylation and more sensitive measurements of protein content (Western blotting) should be done to fully elucidate the role of gap junctions in the development of spontaneous events.

#### **4.4.2.3 Fibrosis**

Myocardial fibrosis is a condition developed by the excess secretion of extracellular matrix. Myocardial infarction and other genetically inherited cardiac diseases can trigger the production of collagen, which in excess can lead in the formation of connective tissue in the areas of injury (Hinderer and Schenke-Layland, 2019). Even though this is initially a protective mechanism which compensates for the loss of cardiomyocytes, it can, also, promote ventricular tachyarrhythmias by creating a vulnerable substrate for reentrant activity (Disertori et al., 2017). Already published studies of *in vivo* myocardial infarction or cryoinjury infarction have shown that after longer remodelling time, lasting for weeks, there was significant increase in fibrosis and collagen secretion (González-Rosa et al., 2011b; Mizutani et al., 2016). However, in this study, collagen deposition was the same in all the different groups and therefore could not have been implicated in the formation of arrhythmic events. Perhaps the culturing time (24h) was not enough to trigger significant collagen secretion from the fibroblasts.

#### **4.4.2.4 SL heterogeneity**

During myocardial infarction, the lack of oxygen and nutrients create a biochemical environment of increased acidosis, potassium concentration, CO<sub>2</sub> and catecholamine release that trigger depolarisation of the resting membrane potential and increase of tissue automaticity (Antzelevitch and Burashnikov, 2011). These biochemical events give rise to further conformational changes on the site of injury where cardiomyocytes undergo cell necrosis and hypercontracture as a results of cell apoptosis/necrosis and excessive release of calcium from the sarcoplasmic reticulum immediately after reperfusion (Garcia-Dorado et al., n.d.; Piper et al., 1998; Ruiz-Meana et al., 1999; Sanada et al., 2011). Following these mechanical changes after acute ischemia there is also an increase of diastolic stiffness, which is accompanied by elevated local tissue shortening and systolic bulge (Garcia-Dorado and Ruiz-Meana, 2000; Pernot et al., 2016; Piper et al., 1998; Theroux et al., 1977). These observations indicate that

acute ischemia locally affects tissue structure and its mechanical properties. Since the application of cryoinjury created similar effects on the LMSs, with extensive cell death on the site of injury and cell bulging on the BZ, it was hypothesised that mechanical changes also occurred both in local and whole tissue level and that these changes are partially responsible for the functional changes seen in tissue contractility. Recording tissue contraction while applying the cryoinjury was a good way of monitoring the early responses of tissue upon cell death. After each application of injury there was an immediate increase in passive tension and local tissue contraction. Local tissue contraction creates heterogeneities in whole tissue level, with areas next to the injury being differentially stretched from the areas away from it. To test this hypothesis, measurement of the sarcomere length (SL) after acute injury was performed. The analysis showed that there were more sarcomeres at the BZ with larger SL, while sarcomeres away from the injury showed no difference or decrease of SL. This indicates that cells could be differentially stretched within the same tissue, with cells close to injury being more stretched than the ones away from it. Local heterogeneity of tissue stiffness and sarcomere length leads to differential mechanical stimulation, a process that plays an important role in the initiation of stretch induced arrhythmias (Franz and Bode, 2003; Quinn and Kohl, 2016; Seo et al., 2009). This phenomenon could be an additional element that can compensate or affects LMS automaticity and development of spontaneous contractions.

### **4.4.3 Contractility**

#### **4.4.3.1 Sympathetic stimulation**

*In vivo* studies of acute cardiac ischemia have demonstrated a strong reduction of cardiac contractility, characterised by lower ejection fraction and incomplete cardiac relaxation (Kléber, 1990; Weisfeldt et al., 1974). In the cryoinjury model active force generation remained unchanged upon injury, even after damaging almost half of the tissue area. This is a strong



indication suggesting that there is a compensatory mechanism which preserves contraction amplitude after damage. One of the most popular reported mechanisms that explains this phenomenon involves the activation of the cardiac sympathetic neurons, which elevate the kinetics and contraction amplitude by noradrenaline secretion and  $\beta$ -adrenergic activation (Schomig, 1990; Ungerer et al., 1996). However, in our system, the mechanical tissue dissection of the left ventricle causes denervation of the LMSs and therefore loss of neural function. Thus, sympathetic stimulation cannot be the reason for the preservation of contraction amplitude.

#### **4.4.3.2 Frank-Starling law**

Structural changes of the tissue and activation of the myofilaments have been shown to alter contraction amplitude. In fact, one of the most important and well accepted theories has been proposed by Otto Frank and Ernest Henry Starling (Frank-Starling theory) (Katz, 2002). The theory suggests that stretch of myocardium results in an immediate increase of myofilament interactions and contractile force. This mechanism could explain the immediate response of the LMSs to local tissue contraction after cryoinjury. Local shrinkage of the cells near the area of injury could induce further strain on the adjacent healthy tissue and therefore, activate more myofilaments. The data suggest that the cells next to the injury had longer SL compared to the areas away from it, suggesting that they may be more stretched. This mechanism could transiently balance the loss function from the dead cells and manages to preserve the contraction amplitude after both acute and prolonged cryoinjury application. Tissue contraction is known not only to increase in amplitude but also slow kinetics (Allen and Kentish, 1985; Milani-Nejad et al., 2013). In cryoinjured LMSs the tissue showed a decrease in relaxation time (90% decay), which is also strengthening the hypothesis that mechanical changes are at least partly responsible for the acute effects seen in contractility preservation.

#### 4.4.3.3 Calcium regulation

In humans the majority (50%) of the patients with heart failure die from dysfunctional pump activity, while the rest suffer from electrical abnormalities leading to life threatening arrhythmias, such as tachycardia or fibrillation (Orn and Dickstein, 2002). Early signs of arrhythmias in patients can stem from altered  $\text{Ca}^{2+}$  handling which later contribute to the development of delayed (DADs) or early after-depolarizations (EADs). These depolarisations can originate either from elevated intracellular  $\text{Ca}^{2+}$  load or spontaneous SR  $\text{Ca}^{2+}$  release (Pogwizd et al., 2001a). Therefore, analysis of the  $\text{Ca}^{2+}$  handling in global and local level is important to elucidate the mechanism of action.

Global  $\text{Ca}^{2+}$  transient amplitude and kinetics are important contributors of tissue contraction and can affect both its amplitude and kinetics. Measuring  $\text{Ca}^{2+}$  concentration in the cardiomyocytes can link changes in contractility and  $\text{Ca}^{2+}$  regulation. Increased  $\text{Ca}^{2+}$  transients indicate higher availability of intracellular  $\text{Ca}^{2+}$ , that is available to bind to troponin and therefore, activate a higher number of myofilaments, producing increased contractile force. However, the current data suggest that  $\text{Ca}^{2+}$  transient amplitude was reduced in injured LMSs, meaning that intracellular  $\text{Ca}^{2+}$  availability is probably not the mechanism involved in contraction preservation. An important detail for these experiments is that the use of a non ratiometric dye, Fluo8-AM, does not allow absolute calculations of  $\text{Ca}^{2+}$  concentration, but instead calculates changes between the baseline and the  $\text{Ca}^{2+}$  release. Therefore, to more accurately draw conclusions, it is essential to include experiments done with Fura-2AM, a ratiometric dye, where  $\text{Ca}^{2+}$  binding to the dye changes its peak absorbance from 380nm to 340 nm and therefore the ratio between the two states determine  $\text{Ca}^{2+}$  concentration (Barreto-Chang and Dolmetsch, 2009; Paredes et al., 2008).

Further investigation of the global  $\text{Ca}^{2+}$  transients showed the presence of spontaneous global  $\text{Ca}^{2+}$  activation upon arrhythmic provocation, which also confirms the previous findings of spontaneous tissue contractions. Collectively, the reduction of  $\text{Ca}^{2+}$  transient amplitude/kinetics and the presence of spontaneous global  $\text{Ca}^{2+}$  transients in the cryoinjured LMSs are in line with the observed disease remodelling seen in animal models and human cardiac pathology (Lou et al., 2012), which means that it reproduces some of the ionic changes of the pathological heart *in vivo*.

Tissue behaviour is a consequence of multiple single cell events. Spontaneous  $\text{Ca}^{2+}$  release in the form of waves often results from  $\text{Ca}^{2+}$  overload. That happens when  $\text{Ca}^{2+}$  homeostasis is being disturbed so that the amount of  $\text{Ca}^{2+}$  entering the myocyte does not match the amount of  $\text{Ca}^{2+}$  leaving the cell. The SR has a central role in regulating  $\text{Ca}^{2+}$  homeostasis, as it is responsible for  $\text{Ca}^{2+}$  release from the SR stores to the cytosol and is able to depolarise the membrane participating in the CICR mechanism (Miura et al., 1999). Under pathological conditions  $\text{Ca}^{2+}$  overload is present. Spontaneous SR  $\text{Ca}^{2+}$  release can elevate cytosolic  $\text{Ca}^{2+}$  resulting in inducing inward current to flow across the sarcolemma and producing transient depolarizations or DADs (Allen et al., 1984; Lederer and Tsien, 1976; Marban et al., 1986). In most cases single DADs have no sufficient amplitude to reach the threshold and initiate an AP; However, when multiple waves arise simultaneously they are capable of triggering an AP (Capogrossi et al., 1987). The formation of synchronised global calcium transients is believed to originate either from direct cell-cell coupling (e.g.  $\text{Ca}^{2+}$  diffusion, mechanical) or indirectly by synchronizing first latency timings (Boyden et al., 2015). In the current study the number of spontaneous  $\text{Ca}^{2+}$  foci upon injury was increased, as well as their density and activity. These observations go in line with already published data which demonstrate that the number of  $\text{Ca}^{2+}$  waves and their activation timing are important contributors for developing spontaneous arrhythmias.

## Conclusions

In this chapter cryoinjury was established as a model to study spatial and temporal changes cardiac function. This methodology has been previously applied in *in vivo* but never exploited in *in vitro* models. LMSs provided us with the opportunity to investigate global and local changes in cardiac functionality, arrhythmogenicity and electrophysiology, by allowing both macroscopic and microscopic evaluation of tissue function. Previous studies on acute cardiac ischemia demonstrate that cardiac function is usually decreased upon myocardial infarction, primarily due to cell death and metabolic/redox imbalances (Burns et al., 2002; Perrelli et al., 2011). Cryoinjury provided a method where only cell death and mechanical changes contribute to subsequent remodelling. Even though there have been studies investigating the local stiffness and passive tension in whole hearts little is known on the effects of it at cellular level, both functionally and structurally. This study revealed that cryoinjury induced cell bulging, which led to the increase of local tissue stretch and subsequent increase of SL. Functional analysis showed that the global developed force was, also, preserved, even after excessive damage of around 40% of the tissue, while relaxation kinetics were prolonged. Changes were also observed in  $Ca^{2+}$  regulation, with reduction of global transient amplitude and kinetics followed by increased automaticity in a single cell level. These single cell responses were also translated in spontaneous whole tissue contractions that were exacerbated after arrhythmogenic triggering.

In conclusion the LMS-cryoinjury model provides a useful tool with multiple electrophysiological similarities with the *in vivo* ischemic models and resembles some important features of human pathophysiology. The fact that metabolic changes are not a part of the model makes it an ideal method to focus on mechanical triggers that are involved in arrhythmia development. LMSs provide an excellent 3D environment of native adult cardiac

tissue which is often missing from other *in vitro* systems and can be used for multiple purposes. Finally, human LMSs can also be utilised for these purposes, which makes it ideal for translational research.

## 4.5 Limitations and future plans

Our method benefits from being highly reproducible, easy to apply and easy to control the location of injury. Apart from the practical advantages it manages to successfully recapitulate key elements of cardiac damage, such as cell bulging on the area of injury, cell death, local conduction obstruction, and increased of arrhythmogenicity.

However, it also bypasses important metabolic and molecular pathways that are induced by extensive hypoxia and nutrient starvation. These can trigger cell death by different molecular pathways, such as programmed cell death, apoptosis, autophagy or necrosis. Different death pathways, also trigger different immune cell recruitment and inflammation (Zhang et al., 2018), which are also important for disease progression and remodelling (Mehta and Li, 1999; Ong et al., 2018). Adding immune cells on the injury could also act as an extra trigger for tissue remodelling and allow the investigation of immune response on the area of injury. Immune response also exacerbate collagen production, which is often observed after myocardial infarction (Frangogiannis, 2014).

Longer culturing time of the LMSs could also provide insightful information about the progression and remodelling of the injured tissue. In our system, the LMSs were cultured for 24h, since longer incubation showed tissue deterioration and loss of functionality in healthy LMSs. However, recent advancements in the culturing system allow longer incubations of the LMSs without changes in contractility and viability, as shown by our lab members and others (Fischer et al., 2019). It allows tissue culturing for at least 3 days and therefore, allows remodelling to progress in later stages. Bioreactor set ups have helped prolonging the culture of cardiac tissue, while also providing constant monitoring of the cardiac function (contractility). This is a very useful tool that can help to identify temporal changes in tissue contractility and arrhythmogenicity. These bioreactors can also provide dynamic stretch, in

comparison to static stretch that was used in this study. This technology was recently developed by a PhD student in the lab, Fotios Pitoulis, who showed feasibility of creating pressure-volume (PV) loops from the contracted tissue and therefore evaluating several contractile features of the LMSs, which can be used to translate this *in vitro* work to the *in vivo* measurement found in patients.

Lastly, investigating the effect of multiple injuries on prolonged cultures of the LMSs would be another useful tool to identify functional differences linked to the injury size, as has already been done in patients with different infarct sizes (Stone et al., 2016).

# **Chapter 5**

## **Cryoinjury on LMSs – arrhythmia regulation**



## 5.1 Introduction

Previous cryoinjury studies have characterised the model for their resemblance to myocardial infarction in *in vivo* experimental models, finding significant similarities in response to myocardial damage such as: extensive local cell death, fibrosis and reduction in ejection fraction (Chablais et al., 2011b; Ewout J Van Den Bos et al., 2005b). The reproducibility and control over the lesion area made cryoinjury an idea model for regenerative applications. Heart regeneration and cell transplantation were extensively studied in cryoinjured hearts and found to be very useful for revealing regenerative mechanisms especially in animals with high regenerative capacity such as the zebrafish (Chablais et al., 2011b; Schnabel et al., 2011; Yu et al., 2018). However, this was not the only application of cryoinjury and further studies showed that the model was also useful for electrophysiological studies. Cryoinjury on mice was frequently used as a quick and reliable model to study cardiac block upon cell death. Studies of this model showed that cryoinjury promoted sustained re-entry arrhythmias in the heart and resulted in ventricular tachycardia (Costa et al., 2012; Roell et al., 2018). Arrhythmias were also present in the cryoinjured LMS model suggesting that it could successfully recapitulate the electrophysiological *in vivo* responses seen in mice. The *in vitro* set up of cryoinjured LMSs allow to further explore and characterise these arrhythmias in macro- and microscopic level. In this study, the role of CamKII was chosen to investigate its involvement in the development of  $Ca^{2+}$  waves and spontaneous contractions. CamKII is known for its presence in arrhythmic and failing myocardium, where it is activated upon sustained  $\beta$ -adrenergic stimulation and  $Ca^{2+}$  overload. CamKII activity can be inhibited by using inhibitors of CamKII phosphorylation, so changes in cardiac function can be observed in absence of CamKII regulation.

Therefore, it was hypothesised that cryoinjured LMSs can provide a valuable tool to study the role of CamKII in the development of arrhythmias upon injury.

To test this hypothesis, inhibition of CamKII phosphorylation was used on healthy and cryoinjured LMSs. The function and  $\text{Ca}^{2+}$  regulation of the treated LMSs were assessed using contractility and optical mapping methods.

## **5.2 Methods**

### **5.2.1 LMS production**

LMSs were prepared from male Sprague-Dawley rats, as described in section 2.2. Cryoinjured LMSs were produced as described in section 4.2.2. Control or cryoinjured LMSs were used immediately or cultured for 24 as described in section 2.6.

### **5.2.2 Force measurements**

To assess LMS functionality, a force transducer was used. The LMSs were mounted and assessed as described in section 2.8.1. Control and cryoinjured LMSs were assessed at intermediate stretch of 15%. The force amplitude, passive force and kinetics were analysed using Clampfit. A detailed description of the analysis can be found in section 2.8.2.

### **5.2.3 CamKII inhibition**

To inhibit CamKII an Autocamtide-2-related inhibitory peptide (myristoylated) (AIP) (Tocris, USA) was used. This peptide inhibitor blocks the catalytic domain and inhibits even the autonomously active form of the kinase (Daniels et al., 2018; Ishida et al., 1995). The selected peptide was also myristoylated to enhance subcellular localisation (Udenwobele et al., 2017). The cultured LMSs (24h) were incubated with 10 $\mu$ M of AIP in custom made small chambers. The small chambers allowed the culture of LMSs in small media volumes of 3ml, in comparison to 250ml used in the normal culture chambers. The small chambers, also, provided electrical stimulation and oxygenation to mimic the physiological conditions used in LMS long term culture. The LMSs were incubated at 37°C for 2h.

#### **5.2.4 Arrhythmia provocation and analysis**

Cultured LMSs were triggered with an arrhythmia provocation protocol, which is described in detail in section 2.4.5.1. Spontaneous contractions were recorded in the force transducer using AxoScope software. The number of spontaneous contractions at rest (no electrical stimulation) were calculated for the duration of 30sec after cessation of electrical stimulation.

#### **5.2.5 Ca<sup>2+</sup> handling**

For Ca<sup>2+</sup> analysis the LMSs remained on stretchers and were directly placed on the microscope as described in section 2.13.1. Cultured LMSs were challenged with a proarrhythmic protocol as described above. Detailed description of the Ca<sup>2+</sup> staining (Fluo-8AM), recording and analysis can be found in chapter 2.13.2. Calcium handling experiments were conducted by Eef Dries.

#### **5.2.6 Transmural analysis**

Due to the slicing procedure, which starts from the endocardium and ends at the epicardium, it is possible to monitor and categorise LMSs from different transmural layers. Contractility, arrhythmia and Ca<sup>2+</sup> data were categorised with respect to their endocardial and epicardial origin. During data analysis, samples derived from the first two LMSs were defined as endocardial and the last 2 LMSs as epicardium, due to proximity to the respective areas.

## **5.3 Results**

To investigate if the developed arrhythmias on cryoinjured LMSs were related with CamKII activation, cultured LMSs were treated with a CamKII inhibitor (AIP) for 2h after tissue remodelling in culture. Subsequently, tissue contraction and  $\text{Ca}^{2+}$  regulation were evaluated.

### **5.3.1.1 Contraction – AIP**

AIP treatment did not affect the amplitude of active or passive force in any of the tested conditions (healthy or cryoinjured LMSs) ; however, kinetics were altered. Comparison between control and cryoinjured LMSs showed significant increase in relaxation time in cryoinjured LMSs. This observation goes in line with previous experiments shown in chapter 4. AIP application on healthy control LMSs caused a significant prolongation of the time to peak and time to relax (50% and 90% of relaxation) (Fig 5.1). Application of AIP on cryoinjured LMSs showed no improvement of cardiac contraction or kinetics.

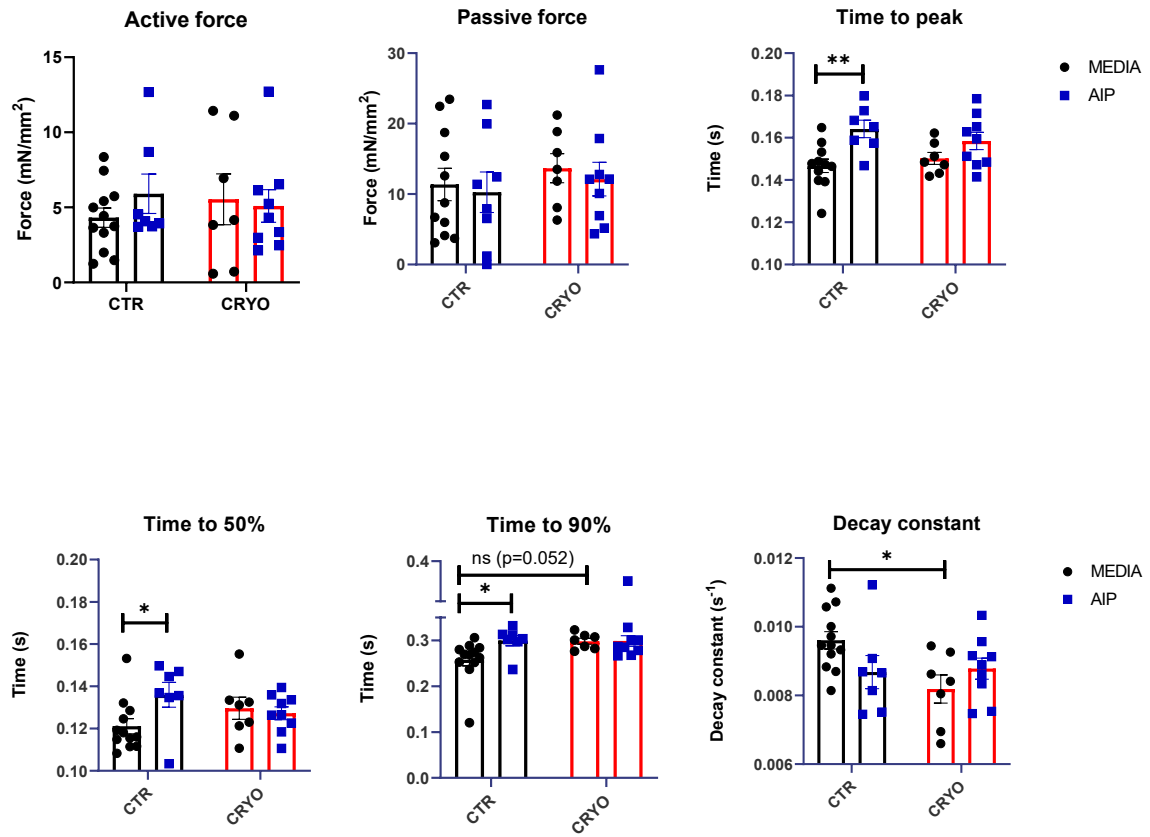


Figure 5.1-Contractility analysis on cultured LMSs treated with CamKII inhibitor (AIP). An unpaired t-Test was used for statistical analysis of the groups. N/n=7-8/7-12, \*=P value ≤ 0.05, \*\* P value ≤ 0.01. N/n=biological replicates (animals)/technical replicates (LMSs).

### 5.3.1.2 Spontaneous contractions – AIP

A provocation protocol was used to evaluate the arrhythmogenic potential of the LMSs after AIP application. Spontaneous contractions under FP stimulation were elevated in cryoinjured samples, whereas treatment with AIP showed a decrease of the arrhythmias, without however, reaching statistical significance, Fig 5.2A. In Fig 5.2B the same data were analysed in a histogram, where changes in data distribution could be observed. The control, control AIP and cryoinjured AIP treated LMSs did not develop significant arrhythmias. On the contrary, the cryoinjured LMSs had a wider distribution and a higher mean, indicating that there were more LMSs developing a higher number of arrhythmias. This observation suggests that AIP reduced arrhythmias in cryoinjured LMSs. Similar effects were, also, observed under the presence of ISO. Cryoinjured LMSs treated with the AIP showed to return to the baseline levels of arrhythmia compared to untreated cryoinjured LMSs. Since these trends did not show significance, more experiments need to be done to draw accurate conclusions on the effect of AIP on injured LMSs.

To better understand the developed arrhythmias, a plot was calculated focusing on the presence or absence of arrhythmias on LMSs. This measurement did not account for the number of arrhythmias and categorise the data on two groups, LMSs that developed arrhythmias and LMSs that did not developed arrhythmias. This categorical analysis shows how likely it is for the AIP treatment and LMS condition to be correlated. Pearson's chi-squared analysis was performed and plotted as shown in Fig 5.3. Fig 5.3A shows comparison between all groups in presence or absence of ISO, whereas Fig 5.3B was designed for statistical analysis, comparing two groups together, using Pearson's chi-squared test. Cryoinjured and control LMSs show significant differences between them as observed in previous experiments; however, under AIP treatment there was a reduction in the number of LMSs that develop arrhythmias upon FP

stimulation, that did not reach statistical significance. Under FP + ISO, AIP treatment did not show any decrease of arrhythmias in cryoinjured or control LMSs.

The latency of these arrhythmias was also calculated as seen in Fig 5.4. Significant differences were observed under fast pacing stimulation + ISO, whereas fast pacing stimulation alone did not reveal any differences. Upon cryoinjury there were more LMSs that developed arrhythmias immediately after cessation of electrical stimulation, compared to control LMSs. Additional treatment of AIP increased the number of control LMSs that developed arrhythmias soon after cessation of electrical stimulation. Latency of cryoinjured LMSs treated with AIP did not show any significant improvement in the latency timings. These observations indicate that AIP treatment did not show any improvement on cryoinjured LMSs but provoked arrhythmias that occurred earlier in healthy control LMSs.



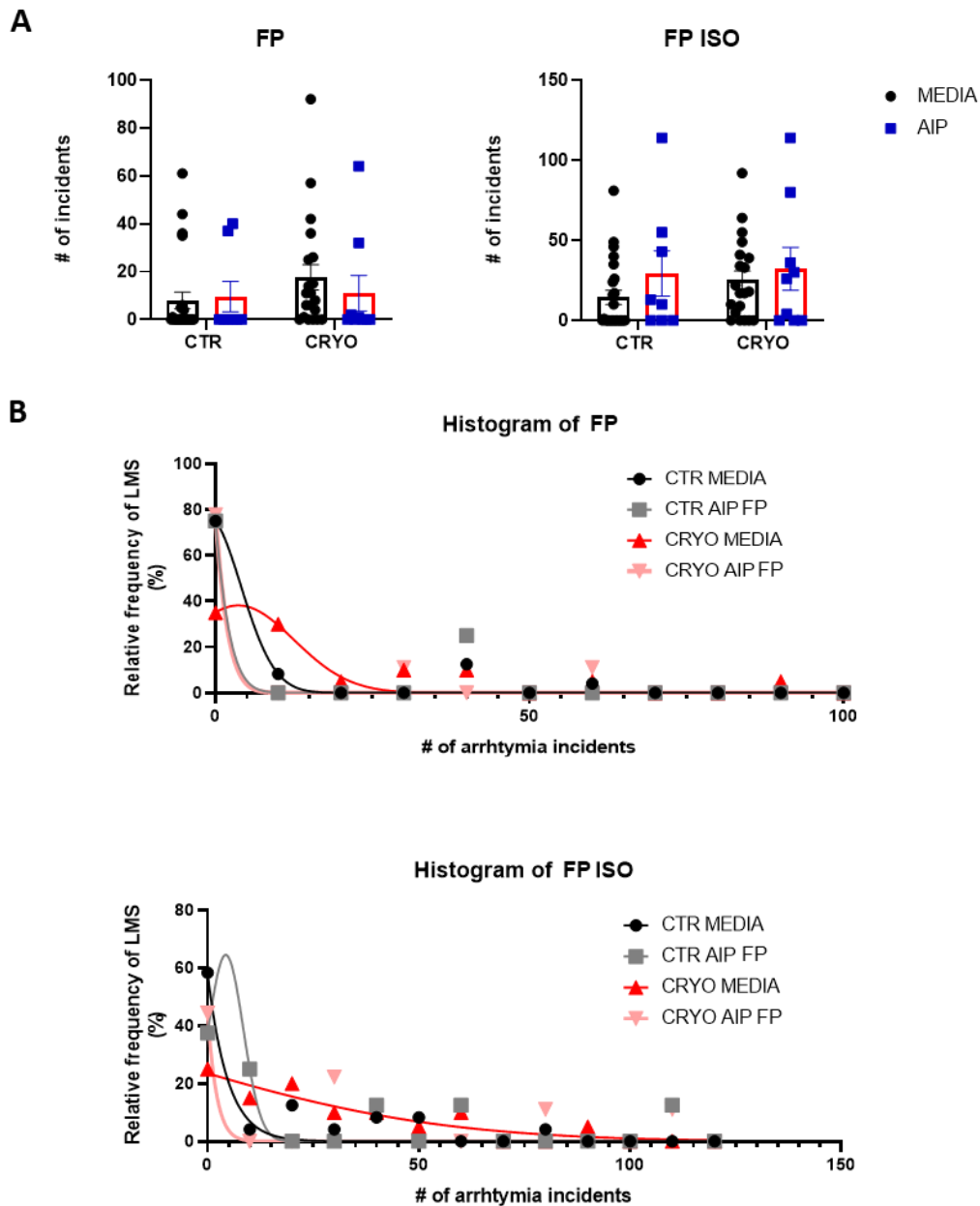


Figure 5.2-Arrhythmia counting after arrhythmia provocation on 24h cultured LMSs. AIP treatment was applied for 2h in control or cryoinjured groups. A) Scatter plot graphs of LMSs treated with ISO and/or FP provocation protocol. B) Distribution analysis of the developed arrhythmias. 2-way ANOVA was used for statistical analysis, no significance was observed,  $N/n_{AIP}=8-9/8-9$ ,  $N/n_{MEDIA}=15-16/20-24$ .  $N/n$ =biological replicates (animals)/technical replicates (LMSs).

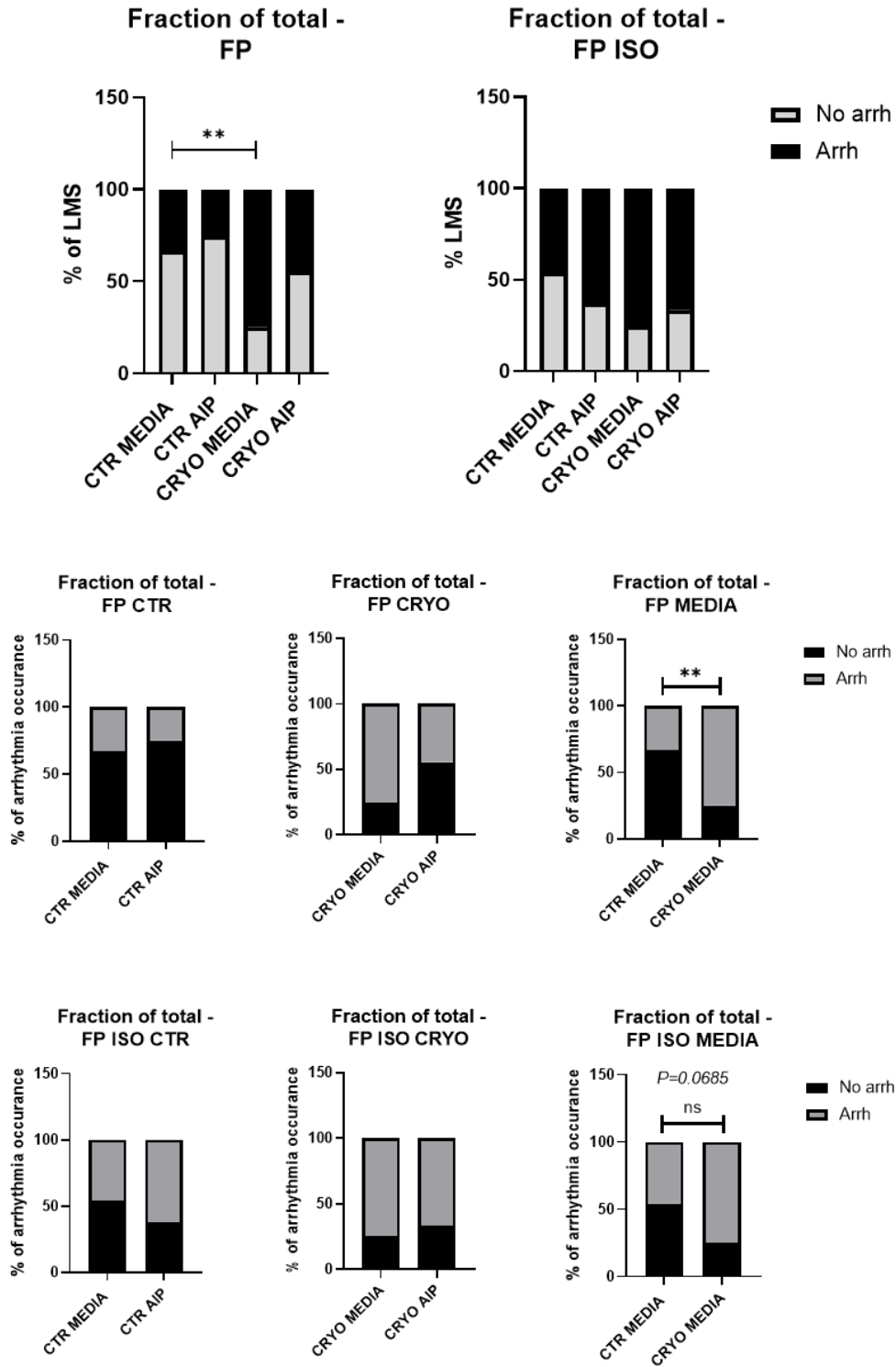


Figure 5.3- Pearson's chi-squared analysis of arrhythmias to determine the % of LMSs developing arrhythmias irrespective of their level of arrhythmogenicity. A) Collective representation of all the groups after FP or FP+ISO. B) Comparison between groups of interest for statistical analysis.  $N/n_{AIP}=8-9/8-9$ ,  $N/n_{MEDIA}=15-16/20-24$ . Fisher's exact test was used for group comparisons. \*\*  $P$  value  $\leq 0.01$ .  $N/n$ =biological replicates (animals)/technical replicates (LMSs).

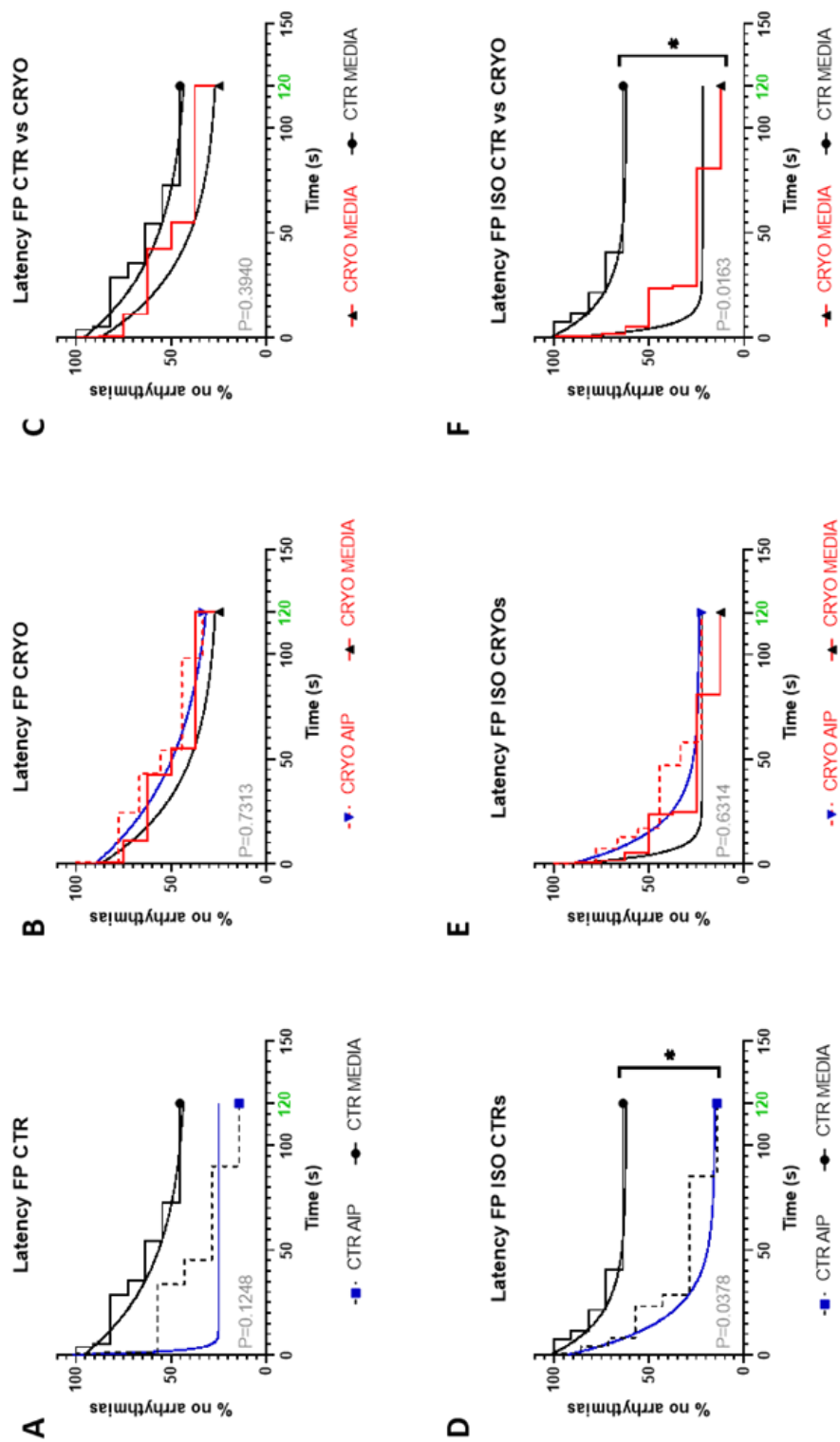


Figure 5.4-Arrhythmia latency (the time interval between the stimulation pause and the first spontaneous contraction). Latency was calculated on samples treated either with ISO or/and fast pacing stimulation. The graphs illustrate the % of LMSs without any arrhythmias against time.  $N/n_{AIP}=8-9/8-9$ ,  $N/n_{MEDIA}=15-16/20-24$ , \*  $P$  value  $\leq 0.05$ .  $N/n$ =biological replicates (animals)/technical replicates (LMSs).

### 5.3.1.3 Calcium regulation

In order to investigate if CamKII is implicated in the developed arrhythmias seen in the cryoinjured model, LMSs were treated with a CamKII inhibitor, AIP, and stained with a  $\text{Ca}^{2+}$  indicator, where  $\text{Ca}^{2+}$  transients and  $\text{Ca}^{2+}$  waves were analysed. These studies were done in collaboration with a postdoc researcher, Eef Dries and the majority of experiments were executed by her.

Analysis of the LMSs under electrical stimulation showed that the  $\text{Ca}^{2+}$  transient amplitude and kinetics did not significantly change upon AIP application, meaning that global calcium regulation was not affected by the CamKII inhibitor. After halting the electrical stimulation, spontaneous  $\text{Ca}^{2+}$  waves were developed and analysed. The number of spontaneous  $\text{Ca}^{2+}$  foci were found to be increased in cryoinjured LMSs. Application of the AIP on injured LMSs showed to significantly reduce the spontaneous foci down to baseline levels, Fig 5.5B. The distance between these foci was also measured. The foci on cryoinjured LMSs were significantly closer to each other in comparison to control LMSs. Treatment with AIP increased the distance between the foci, thus making their distribution more sparse in the tissue, Fig 5.5C. Finally, AIP, also, managed to decrease the wave speed propagation when applied to cryoinjured LMSs. Measurement of the propagation distance showed no significant differences between the different groups, which means that  $\text{Ca}^{2+}$  waves travelled the same distance irrespective of their treatment.

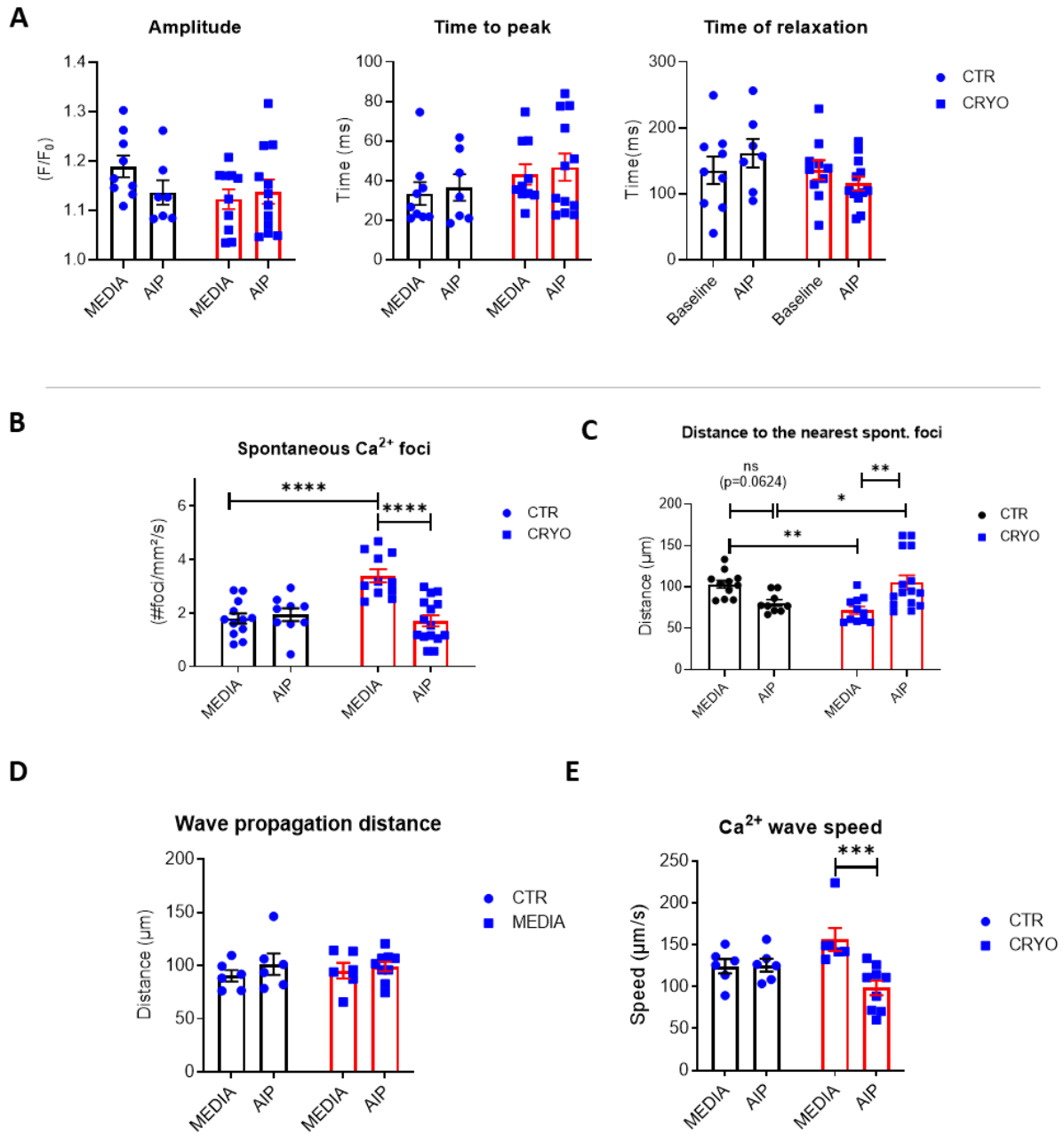


Figure 5.5- Ca<sup>2+</sup> analysis of control and cryoinjured LMSs treated with CamKII inhibitor, AIP. A) Global Ca<sup>2+</sup> amplitude and kinetics under electrical stimulation. B-E) Analysis of the wave propagation at rest (no electrical stimulation). B) Number of spontaneous Ca<sup>2+</sup> foci developed at rest, N/n<sub>control</sub>=6-8/7-9, N/n<sub>AIP</sub>=6-8/10-12. C) Minimum distance between the spontaneous foci, N/n<sub>control</sub>=6-8/7-9, N/n<sub>AIP</sub>=6-8/10-12. D) The distance of the wave propagation within the tissue, N/n<sub>control</sub>=6/6, N/n<sub>AIP</sub>=6/6-9. E) Ca<sup>2+</sup> wave speed N/n<sub>control</sub>=6/6, N/n<sub>AIP</sub>=6/6-9. 2-way ANOVA analysis was used. \* P<0.05, \*\* P<0.01, \*\*\* P<0.001, \*\*\*\* P<0.0001. N/n=biological replicates (animals)/technical replicates (LMSs).

#### 5.3.1.4 Transmural differences

The slicing procedure gives the opportunity to test LMSs from different transmural areas and observe responses related to endo- or epicardial layers of the heart. The data were categorised depending on their transmural area before spontaneous contractions and  $\text{Ca}^{2+}$  events were evaluated.  $\text{Ca}^{2+}$  studies were done in collaboration with a postdoc researcher, Eef Dries and the majority of experiments were executed by her, while contraction measurements were done and analysed by me.

LMSs were analysed during rest for their spontaneous contractions and  $\text{Ca}^{2+}$  waves. Fig 5.6 shows no differences in spontaneous contraction development between endo- and epicardial LMSs with or without AIP treatment. This means that LMSs behaved the same way regardless of their transmural origin. Further analysis of the spontaneous calcium waves developed during rest showed that endocardial injured LMSs had significantly higher number of spontaneous foci compared to the epicardial injured LMSs, Fig 5.7A. Application of AIP reduced the number of spontaneous foci, while it had no effect on epicardial LMSs, Fig 5.7A. In injured endocardial LMSs the distance between spontaneous foci was increased after application of AIP, something that was not observed in epicardial injured LMSs, Fig 5.7C. These data suggest that endocardial LMSs are more prone to arrhythmias than epicardial LMSs after injury, while treatment with AIP seems to be more beneficial in endocardial LMSs compared to the epicardial LMSs.

LMSs were also analysed in whole tissue level looking into global tissue contractility and calcium transients under electrical stimulation. Global  $\text{Ca}^{2+}$  transients showed no significant differences in  $F/F_0$  or kinetics between endocardial and epicardial LMSs.

On the other hand, contractility data showed that epicardial cryoinjured LMSs had higher active force compared to endocardial cryoinjured LMSs. No differences were observed upon AIP treatment in either healthy or injured LMSs.

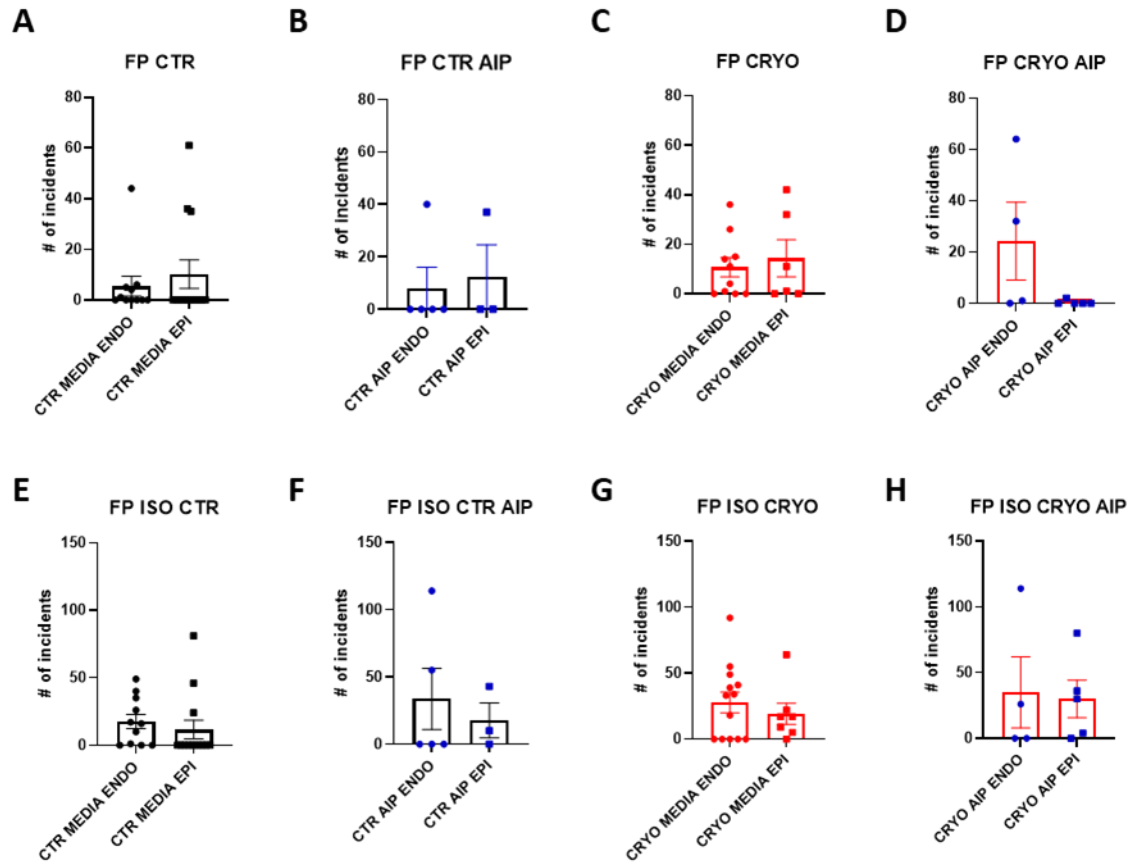


Figure 5.6-Transmural differences of spontaneous arrhythmia development between treated and untreated groups under ISO or/and fast pacing stimulation. A) Fast pacing treated Control LMSs,  $N/n_{endo}=11/11$ ,  $N/n_{epi}=13/13$ . B) Fast pacing treated control + AIP LMSs,  $N/n_{endo}=5/5$ ,  $N/n_{epi}=3/3$ . C) Fast pacing treated cryoinjured LMSs,  $N/n_{endo}=10/10$ ,  $N/n_{epi}=6/6$ . D) Fast pacing treated cryoinjured + AIP LMSs,  $N/n_{endo}=4/4$ ,  $N/n_{epi}=5/5$ . E) Fast pacing + ISO treated control LMSs,  $N/n_{endo}=11/11$ ,  $N/n_{epi}=13/13$ . F) Fast pacing + ISO treated control + AIP LMSs,  $N/n_{endo}=5/5$ ,  $N/n_{epi}=3/3$ . G) Fast pacing +ISO treated cryoinjured LMSs,  $N/n_{endo}=10/10$ ,  $N/n_{epi}=6/6$ . H) Fast pacing +ISO treated cryoinjured + AIP LMSs,  $N/n_{endo}=4/4$ ,  $N/n_{epi}=5/5$ . A *t*-Test analysis was used to analyse the data but no significance was observed in the groups.  $N/n$ =biological replicates (animals)/technical replicates (LMSs).



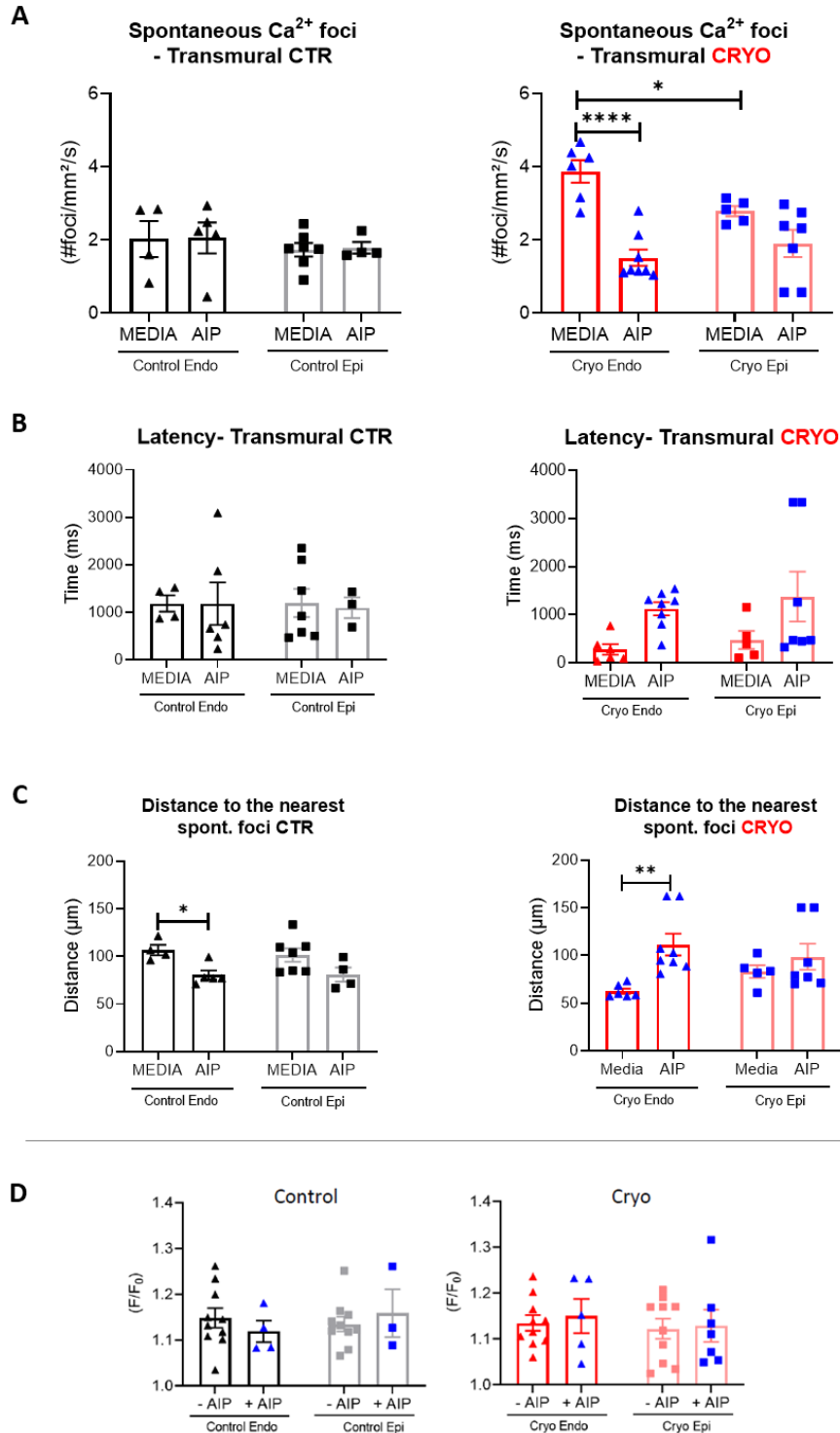


Figure 5.7-Transmural Ca<sup>2+</sup> analysis of LMSs after AIP treatment. A-C) Number and kinetics of spontaneous Ca<sup>2+</sup>foci developed at rest (no electrical stimulation), in control LMSs in absence,  $N/n_{control}=8/12$ , and presence of AIP  $N/n_{control}=8/9$  subcategorized in endocardium and epicardium. D) Global Ca<sup>2+</sup> transients under electrical stimulation in control and cryoinjured LMSs in absence,  $N/n_{control}=8/10$ ,  $N/n_{cryo}=10/20$ , and presence of AIP,  $N/n_{control}=6/7$ ,  $N/n_{cryo}=8/12$ , subcategorized in endocardium and epicardium. A 2-way ANOVA was used for statistical analysis. \*  $P<0.05$ , \*\*  $P<0.01$ , \*\*\*  $P<0.001$ , \*\*\*\*  $P<0.0001$ .  $N/n$ =biological replicates (animals)/technical replicates (LMSs).

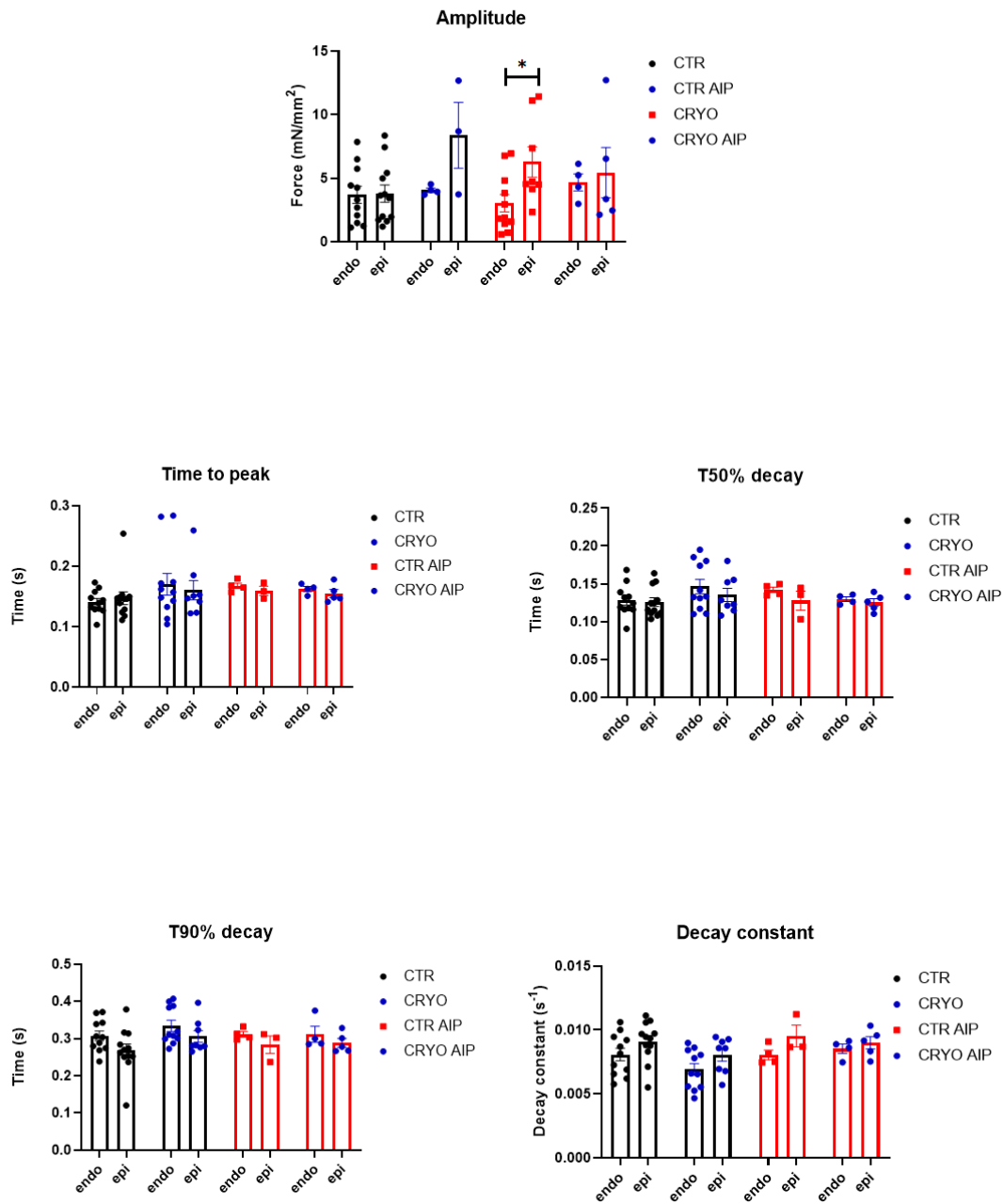


Figure 5.8-Transmural analysis of contraction amplitude and kinetics in control.  $N/n_{control}=5-8/11-12$ ,  $N/n_{cryo}=6-7/8-11$ , and AIP LMSs,  $N/n_{control}=3-4/3-4$ ,  $N/n_{cryo}=3-5/3-5$ . 2-way ANOVA was used for statistical analysis. \*  $P<0.05$ .  $N/n$ =biological replicates (animals)/technical replicates (LMSs).

## 5.4 Discussion

This chapter shows that cryoinjured LMSs is a useful *in vitro* model to study global and local arrhythmia development, in a 3D and multicellular environment. CamKII inhibitor, AIP, showed that it can reduce the number, latency and speed of  $\text{Ca}^{2+}$  waves, without significantly affecting myocardial contraction. Interestingly,  $\text{Ca}^{2+}$  wave reduction was more pronounced in endocardial LMSs compared to epicardial tissue, revealing the presence of transmural differences in CamKII activity under pathological conditions.

### 5.4.1 AIP

Our data demonstrate that inhibition of CamKII in cryoinjured LMSs reduced the arrhythmic potential. These results were both observed in a single cell (spontaneous  $\text{Ca}^{2+}$  foci) and whole tissue level (spontaneous tissue contractions), placing CamKII as one of the possible contributors of the arrhythmia development upon cell death on LMSs. Consistent with these results other studies have showed that CamKII can induce arrhythmias when activated, by phosphorylating the RyR and causing  $\text{Ca}^{2+}$  leak from the SR (Mustroph et al., 2018; Sag et al., 2011). CamKII also targets the L-type  $\text{Ca}^{2+}$  channel (LTCC), phosphorylates its  $\beta 2\text{a}$  subunit so that the channel enters a highly active gating mode accompanied with frequent and long openings. This can eventually lead to an increase in opening probability and prolongation of the action potential (Abiria and Colbran, 2010). CamKII can dynamically increase the  $I_{\text{Ca}}$ , a phenomenon termed as *facilitation* (Anderson et al., 1992; Xiao et al., 1994; Yuan and Bers, 1994). Higher  $\text{Ca}^{2+}$  influx promotes SR  $\text{Ca}^{2+}$  overload, DADs and oscillations in membrane potential that can subsequently induce arrhythmias (Couchonnal and Anderson, 2008).. Collectively, EADs induced by ion transporter alterations on membrane potential and DADs can increase the probability of arrhythmias, including fibrillation and ventricular arrhythmias, often seen in heart failure (Pogwizd et al., 2001b). Inhibition of CamKII has been shown

elsewhere to reduce SR  $\text{Ca}^{2+}$  leak, abbreviate APD and reduce arrhythmias. The reduction of arrhythmias goes well with our observations, while the mechanism of action as reported earlier requires further validation on the LMS model.

#### **5.4.2 Transmural analysis**

LMS slicing allows to study different ventricular areas and help to reveal spatial changes within the same tissue, while also keeping the cells in their native environment and thus avoiding enzymatic tissue digestion used in previous transmural studies (Khokhlova et al., 2018; Stankovicova et al., 2000).

The presence of electrical heterogeneity of the cells in the left ventricle has been widely reported in many studies (Vaverka et al., 2018). Focusing on the electrical properties, cardiomyocytes derived from different transmural areas exhibit different action potential duration, morphology, and response to stimulation rate. It is generally accepted that cells originating from the epicardium have shorter APD, while cells from the endocardium have longer APD, resulting in a gradient of APD across the wall. This heterogeneity is attributed to differences in ion channel expression ( $I_{\text{to}}$  and  $I_{\text{CaL}}$ ) and accounts for activation delays and synchronized ventricular repolarization in the healthy myocardium (Bányász et al., 2003; Litovsky and Antzelevitch, 1988). Furthermore, differences are also seen in the mechanical properties of the tissue, where epicardium and mid-myocardium seem to have higher active and passive force upon high strain (Fotios G. Pitoulis et al., 2020). Differences in structural proteins were also seen at chapter 4, with SL was longer in the mid-myocardium/epicardium compared to endocardial LMSs.

In these experiments transmural analysis of damaged tissue showed that LMSs derived from the endocardial area developed more spontaneous  $\text{Ca}^{2+}$  foci compared to epicardial LMSs. Additional inhibition of CamKII also showed more significant reduction of the spontaneous

Ca<sup>2+</sup> events in endocardial LMSs compared to epicardial LMSs. Given that endocardial cardiomyocytes have smaller I<sub>to</sub> amplitude compared with the epicardial cells, it would be interesting to further investigate the correlation CamKII inhibition in LMSs I<sub>to</sub> activity. Already published studies on animal models have shown that CamKII regulates I<sub>to</sub> by phosphorylating the Kv4.2 and of Kv1.4 channels and thus resulting in enhancement of I<sub>to</sub> (Wagner et al., 2009). On the other hand, inhibition of CamKII using AIP showed to significantly accelerate current inactivation and slowed recovery from inactivation (Sergeant et al., 2005). CaMKII enhancement of I<sub>to</sub> could also play an important role for reactive oxygen-species (ROS) induced arrhythmogenesis. ROS oxidise and activate CamKII, while they are also responsible for the induction of arrhythmias favouring early afterdepolarisations, which are often linked to activated I<sub>to</sub> (Wagner et al., 2011; Zhao et al., 2012). To see if this mechanism is also present in the cryoinjured LMSs, more experiments need to be performed and measure ROS production, I<sub>to</sub> activity and CamKII protein expression.

## 5.5 Limitations and future work

Spontaneous  $\text{Ca}^{2+}$  transients, sparks and waves were linked to ectopic beats by measuring spontaneous LMS contractility in the absence of electrical stimulation. However, due to multiple differences in the experimental setups and use of different LMSs samples for each experiment there were no significant correlations between spontaneous  $\text{Ca}^{2+}$  events and contractions. To minimise the variability between samples and better understand how spontaneous single  $\text{Ca}^{2+}$  events lead to global ectopic beats dual recording of  $\text{Ca}^{2+}$  and action potential could be utilised.

Additional protein analysis of CamKII (phosphorylation and total expression) could greatly strengthen the functional findings of our results. Protein analysis would also be useful for determining the levels of Kv4.2 and Kv1.4 in the transmural experiments to better understand their role in  $I_{to}$ . Finally, patch clamp experiments would, also, give valuable information on the effect of CamKII inhibition and help clarify the differential effect of CamKII in endo- and epicardium.

## 5.6 Conclusions

This chapter demonstrates that the use of cryoinjured LMSs can provide a versatile tool to study arrhythmogenicity and transmural heterogeneity. Characterisation of the cryoinjury described at chapter 4 revealed an arrhythmogenic profile of spontaneous global tissue contractions, altered mechanical tissue properties and  $\text{Ca}^{2+}$  regulation. Inhibition of CamKII showed to decrease the spontaneous  $\text{Ca}^{2+}$  events in cryoinjured LMSs, an effect that interestingly had higher potency on endocardial cryoinjured LMSs. Transmural differences were also observed in other studies that focused on electrophysiological and structural responses (Cordeiro et al., 2004; Fotios G. Pitoulis et al., 2020), which further strengthens our results. Surprisingly, CamKII inhibition did not affect global spontaneous contractions, which indicates that there must be additional mechanisms that lead to the initiation of ectopic beats in the LMSs.

Exploiting the use of the cryoinjury model *in vitro* can provide informative insights of the tissue response under stress, with spatial and temporal analysis that will aid understanding disease progression in a multicellular context relevant to the heart's physiology

# **Chapter 6**

## **Cryoinjury on LMSs - EV application**



## 6.1 Introduction

Models of *in vivo* cryoinjury have already contributed towards gaining great insights of heart regeneration either by studying the intrinsic heart regeneration capacity or by applying exogenous therapies such as cell transplantation or other pharmacological interventions (Bise et al., 2020; Li et al., 1999; Sakai et al., 1999; Schnabel et al., 2011). One of the most interesting regenerative factors can be found in exosomes secreted from multipotent and pluripotent cells (Beez et al., 2019). EVs are lipid bilayer-delimited particles that are naturally secreted by the cells. They can range in size from 40nm to 1 $\mu$ m and can be further divided in different categories depending on their size and origin (Kalluri and LeBleu, 2020). They contain a variety of different cargoes including proteins, metabolites, and nucleic acids, namely mRNA, noncoding RNA species, and DNA. Among other cells, mesenchymal stem cells and progenitor cardiac cells have been shown to exert significant cardioprotective and regenerative effect on the injured heart (Laher et al., 2018; Vrijnsen et al., 2016a).

Most of the studies on the EVs have been performed on primary isolated cells, cell lines or immature iPSC-CMs, which do not fully represent the *in vivo* physiology. Additionally, *in vivo* studies of EVs showed poor EV retention in the heart and systemic diffusion of the particles to the peripheral circulation. Until these technical problems of EV delivery are overcome, LMSs provides a great *in vitro* system where EVs, cells and or other particles can be delivered and retained on top of the LMSs. The effect of the EVs can be assessed in physiological or pathological adult myocardium where cell multicellularity is preserved. LMSs provide a useful tool for regenerative studies without the need of animal surgery procedures and control over the EV delivery. To mimic cell death and apoptosis seen in ischemic hearts the cryoinjured LMS model is utilised, where both functional and molecular assessments can be performed.

Therefore, it was hypothesised that cryoinjured LMSs can reveal functional changes upon EV application on cryoinjured LMSs.

To test this hypothesis, healthy and cryoinjured LMSs will be treated with EVs and their functionality will be assessed using contractility and molecular techniques.

## **6.2 Methods**

### **6.2.1 EV isolation**

The EVs were isolated, analysed and stained at the UMC Utrecht, Netherlands at the Sluijter lab. The EVs were derived from human cardiomyocyte progenitor cells (hCPC) which were isolated according to the protocol of Van Vliet *et al.*, 2008 using size-exclusion chromatography (SEC) (Böing *et al.*, 2014) to isolate particles of the correct size, 20nm-10µm, according to the protocol of Mol *et al.*, 2017. After isolation, EVs were resuspended in PBS and the particle concentration was measured using a nanoparticle tracking analysis (NTA) method. For uptake studies the EVs were stained with a membrane dye, PKH26 Red Fluorescent Cell Membrane Labelling Dye (Sigma, Germany) by using the protocol suggested by the manufacturer. To remove the excess unbound dye, the vesicles were run over the SEC column after staining. The vesicles were stored for up to a maximum of 6 days after isolation at 4°C before they were used on LMSs.

### **6.2.2 LMS production**

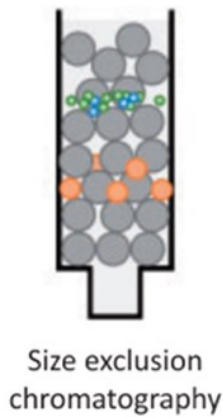
LMSs were prepared from male Sprague-Dawley rats, as described in section 2.2. Cryoinjured LMSs were produced as described in section 4.2.2. Control or cryoinjured LMSs were used immediately or cultured for 24 as described in section 2.6.

### **6.2.3 EVs delivery optimisation**

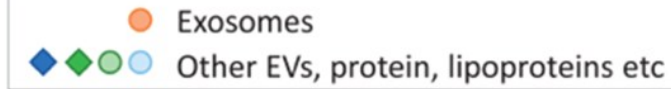
EVs concentration and delivery was optimised to ensure adequate incorporation on the LMSs and minimum loss in the surrounding culture media. To optimise the EVs concentration the transwell method was used. In more details, LMSs were cut in small disks using a 3mm in diameter tissue puncher and placed on top of cell strainers (Corning, USA). The bottom of the well was filled with culture media solution, until the level of the cell strainer was reached, so

that the LMSs could absorb nutrients from it. The top of the LMSs was filled with two different concentrations of EV solution,  $1.65 \times 10^{10}$  (5 $\mu$ l) and  $3.35 \times 10^{10}$  (10 $\mu$ l total volume), and three time points of 15min, 30min and 60min incubation were used. The EVs were mixed with culture media solution before delivery in ration 2:1 (media:EVs). Since the EVs were diluted in PBS, a mixture of PBS and media was used as a vehicle (control samples). The LMSs were incubated in a humidified 95% O<sub>2</sub>/5% CO<sub>2</sub> at 37°C.

Once the EVs concentration and volume were determined the EVs delivery was repeated in a different set up designed for long term culture of 24h. For long term cultures, the LMSs were mounted on stretchers as described in section 2.6.3 and placed inside the culture chambers. The chambers were filled with media up to the level of the LMSs. It was important that the media did not cover the LMSs and only touched the bottom side of the tissue. The chamber was then, assembled with oxygen and media circulation attached and placed the incubator at 37°C. The lid was slightly opened and 10 $\mu$ l of EVs + media mixture ( $3.35 \times 10^{10}$ ) were added on top of the LMSs. Upon EVs addition the chamber was not moved to avoid EVs diffusion in the media. The LMSs were left in the incubator for 30min so that there is enough time for the EVs to get incorporated. More medium was added to the chamber and the LMSs were cultured for 24h.

**A**

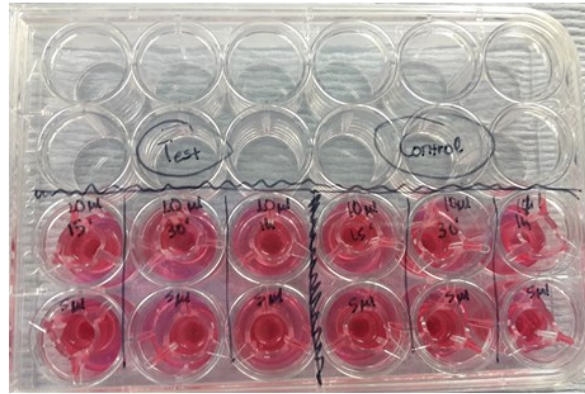
## EV isolation from Cardiomyocyte Progenitor Cells



Isolation performed at  
UMC Utrecht, Netherlands

**B**

## Transwell

**C**

## Liquid interface

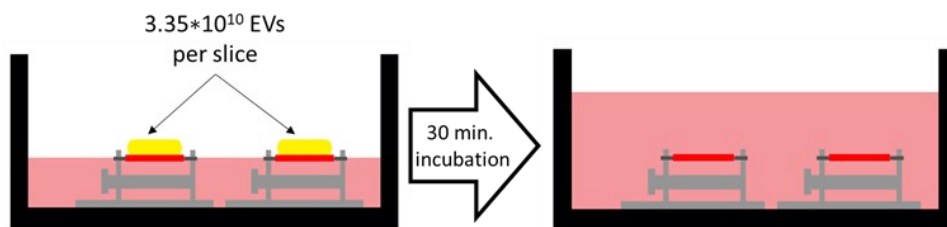


Figure 6.1-EV delivery on LMSs. A) EVs were isolated from human cardiac progenitor cells and stained with PKH to allow EV tracking. B) The transwell method was used to determine the concentration and volume of the EV solution that allows successful EV attachment on the LMSs. LMS disks were cut with a tissue puncher and placed on top of small transwells. The transwell were placed in 24 well plates and filled with culture media. C) Liquid interface method.  $3.35 \times 10^{10}$  in  $10 \mu\text{l}$  of culture medium was placed on top of LMSs that were mounted on stretchers and incubated in culture chambers.

#### **6.2.4 Confocal analysis**

Treated LMSs with prestained EVs were fixed with 4% PFA in PBS for 15min and visualised using a confocal microscope as described in section 2.12. The acquired images were analysed using Fiji software. The images were thresholded to remove any background and compared to control LMSs that remained untreated (no EV addition). The area of exosome positive signal was quantified as a percentage of total LMS area.

#### **6.2.5 Force measurements**

To assess LMS functionality, a force transducer was used. The LMSs were mounted and assessed as described in section 2.8. Control and cryoinjured LMSs were assessed at maximum isometric and intermediate stretch of 15%. The force amplitude, passive force and kinetics were analysed using Clampfit. A detailed description of the analysis can be found in section 2.8.2.

#### **6.2.6 RT-qPCR-molecular analysis**

LMSs were snap frozen in liquid nitrogen and stored at -80°C until use. Stainless steel beads (Qiagen, The Netherlands) and 500 µl TRIzol Reagent (Ambion, USA) were used to lyse the tissue and isolate the RNA. The frozen LMSs were added into the pre-cooled tubes containing TRIzol (one slice per tube) and were placed into a TissueLyser (Qiagen, The Netherlands) at 4°C. The samples were lysed by high-speed shaking for 1.5min at 40Hz followed by 2min resting on ice. This process was repeated 3 times (total of 4.5 min lysing). 100µl chloroform (Sigma, Germany) was added and the tubes were vortexed for 15s. The samples were left for 5min on ice and then centrifuged at 12000rpm at 4°C for 15min. Next, the top layer of the supernatant (aqueous phase) was taken, 350 µl pre-cooled 70% EtOH was added and the mixture was shaken thoroughly. Subsequently, RNA was isolated using the RNeasy Mini Kit protocol (Qiagen, The Netherlands). RNA was diluted in 35 µl of RNAase free water and stored

at -80°C. Finally, RNA concentration was measured using Nanodrop (Thermo Scientific, USA) and 260/280 measurements were evaluated for RNA purity.

For the cDNA synthesis an iScript cDNA Synthesis Kit (Biorad, USA) was used. 500ng of RNA was used and mixed with the reaction mix, reverse transcriptase and water as suggested by the company were added accordingly. The samples were incubated in thermocycler using the suggested protocol. Finally, RT-qPCR was performed using the iTaq Universal SYBR Green Supermix (Biorad, USA). Per well, 10 µl reaction mix was used consisting of 5 µl SYBR Green Supermix, 300 µM FW primer, 300 µM RV primer and 12,5 ng cDNA. Primer list can be found in Table 5.1.

## **6.3 Results**

### **6.3.1 Exosomes**

#### **6.3.1.1 Optimisation of the delivery method**

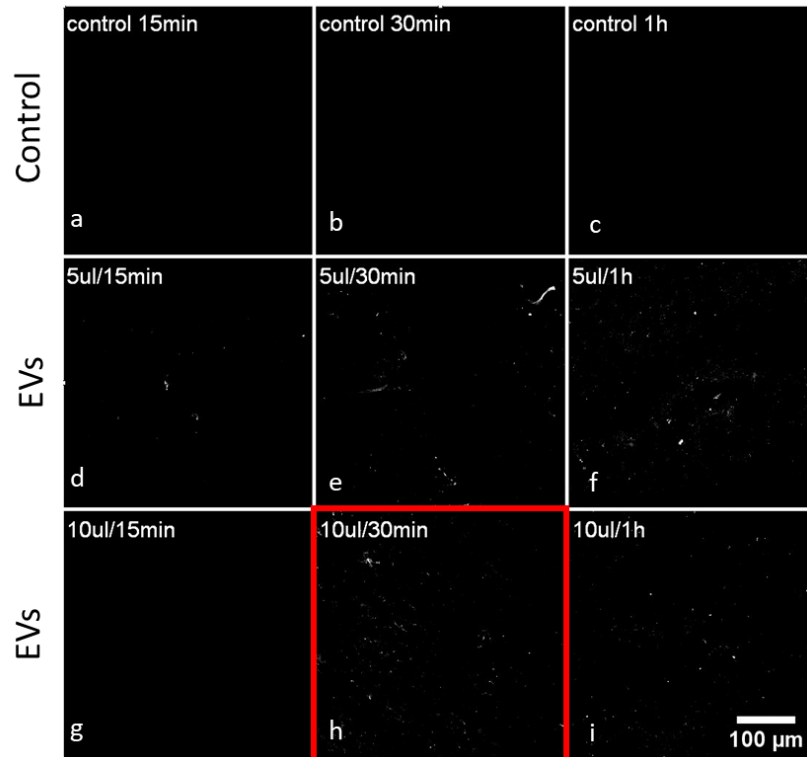
EV delivery varies significantly between studies and therefore optimisation of the concentration and the application method was necessary on LMSs (Gartz and Strande, 2018). The tissue was placed either on transwells or slice cultures and treated with different exosome concentrations. Evaluation of exosome incorporation to the LMSs was done by imaging of the pre-stained exosomes using a confocal microscope.

#### **6.3.1.2 EV concentration**

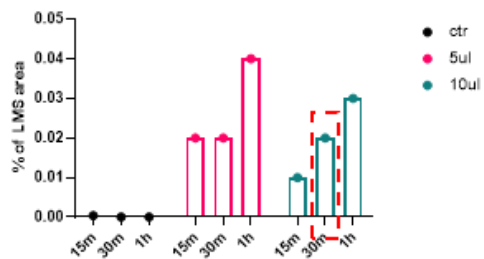
To make sure that the EVs successfully incorporated in the LMSs two different application methods and EV concentrations were used. The LMSs were treated with low ( $1.68 \times 10^{10}$  particles in  $5 \mu\text{l}$ ) and high ( $3.35 \times 10^{10}$  particles in  $10 \mu\text{l}$ ) concentration of EVs for either 15min, 30min or 1h. To detect the EVs on the LMSs, we used pre-stained exosomes prepared in the Netherlands from Professor Sluijter's lab. The EVs were stained with PKH, a non-toxic traceable membrane dye. As seen in Fig 6.2A there were traceable levels of EV even after the first 15min application; however, the levels of EVs increased after 30min and 1h. Therefore, to minimise the incubation time and preserve tissue viability, 30min of incubation time was chosen. The volume and concentration of EVs did not show significant differences and so the maximum concentration was chosen,  $10 \mu\text{l}$ . These conditions were, further, tested on LMSs incubated in the liquid interface. Fig 6.2B shows that the EVs could successfully attach on the LMSs, when cultured in chambers. Control samples showed absence of the PKH signal. These data demonstrate EVs attachment on the cardiac tissue which entails the possibility of cargo release to the LMSs.



## A Transwells



Exosome attachment on LMS



## B Liquid interface

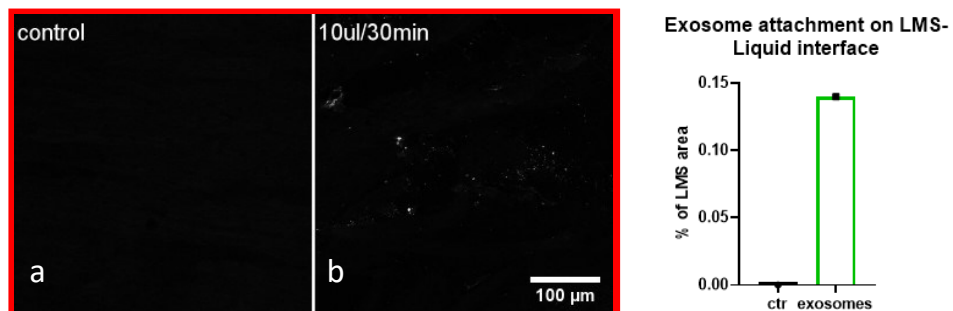


Figure 6.2-Optimisation of EVs on LMSs. A) EVs treatment on LMSs placed on transwells and incubated for 15, 30 and 60min, using either high (10μl) or low (5μl) concentration of EVs. B) High EV concentration (10μl) and 30min incubation was selected for treating the LMSs with the liquid interface method. N/n=1/1. N/n=biological replicates (animals)/technical replicates (LMSs).

### **6.3.1.3 LMS Contractility – EVs application**

The effect of EVs on healthy and cryoinjured LMSs was tested after 24h of incubation. Healthy or cryoinjured LMSs showed no differences in contraction amplitude or kinetics after EV treatment when tested under moderate stretch (15%), Fig 6.3-6.4. Maximum isometric stretch was used to evaluate LMS viability and maximum tissue performance. Similarly, to the moderate stretch, no significant differences were detected in active contraction between EV treated and untreated conditions, Fig 6.5.

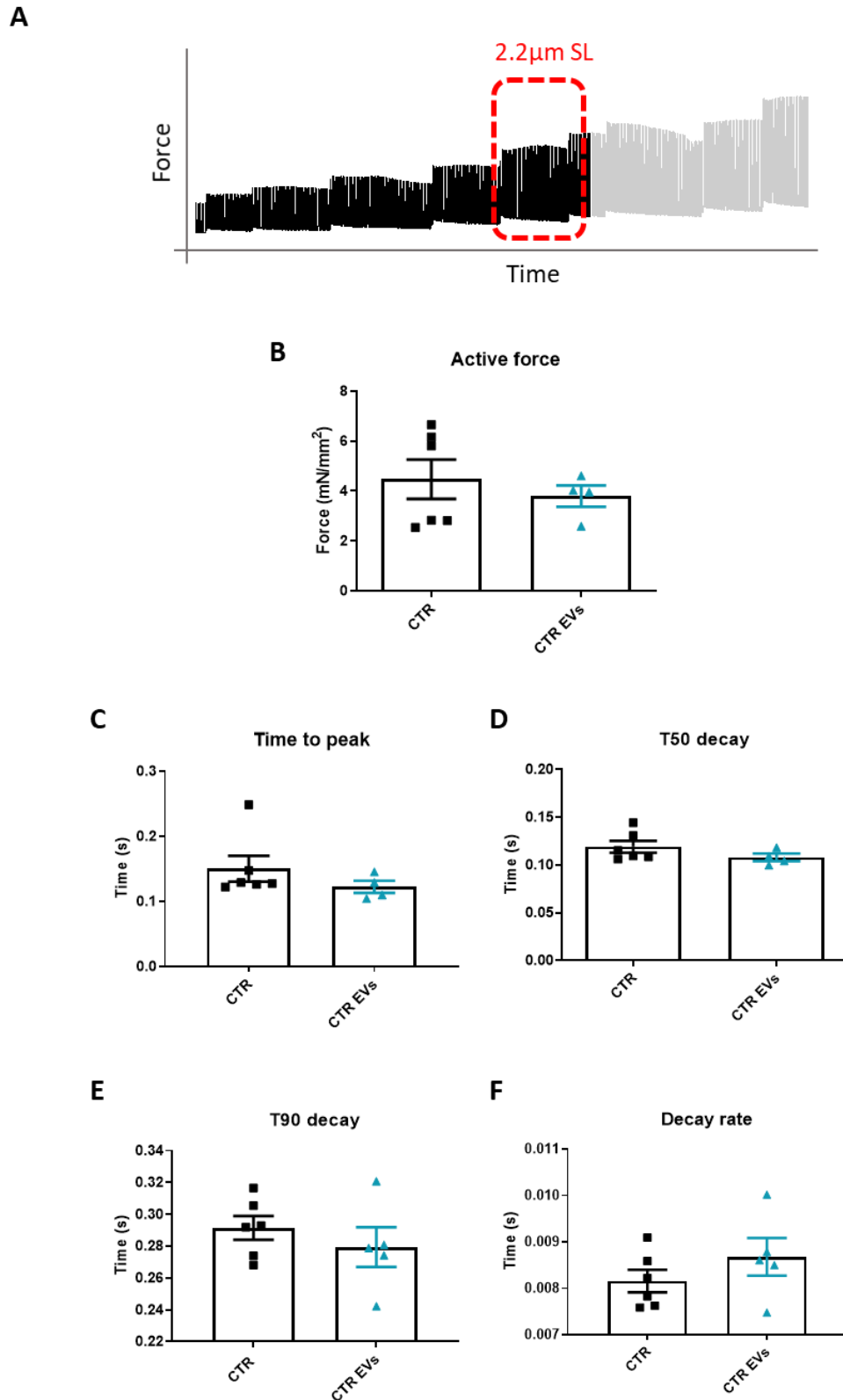


Figure 6.3-Contractility analysis of healthy LMSs treated with EVs for 24h. A) Schematic representation of the contractility traces. Control and treated healthy LMSs were evaluated at 15% LMS stretch, corresponding to 2.2µm in SL. B-F) Contraction active force and kinetics were assessed upon EVs application. N/n=3/4-6. Unpaired t-Test was used between CTR and CTR EVs, no significant differences were observed. N/n=biological replicates (animals)/technical replicates (LMSs).

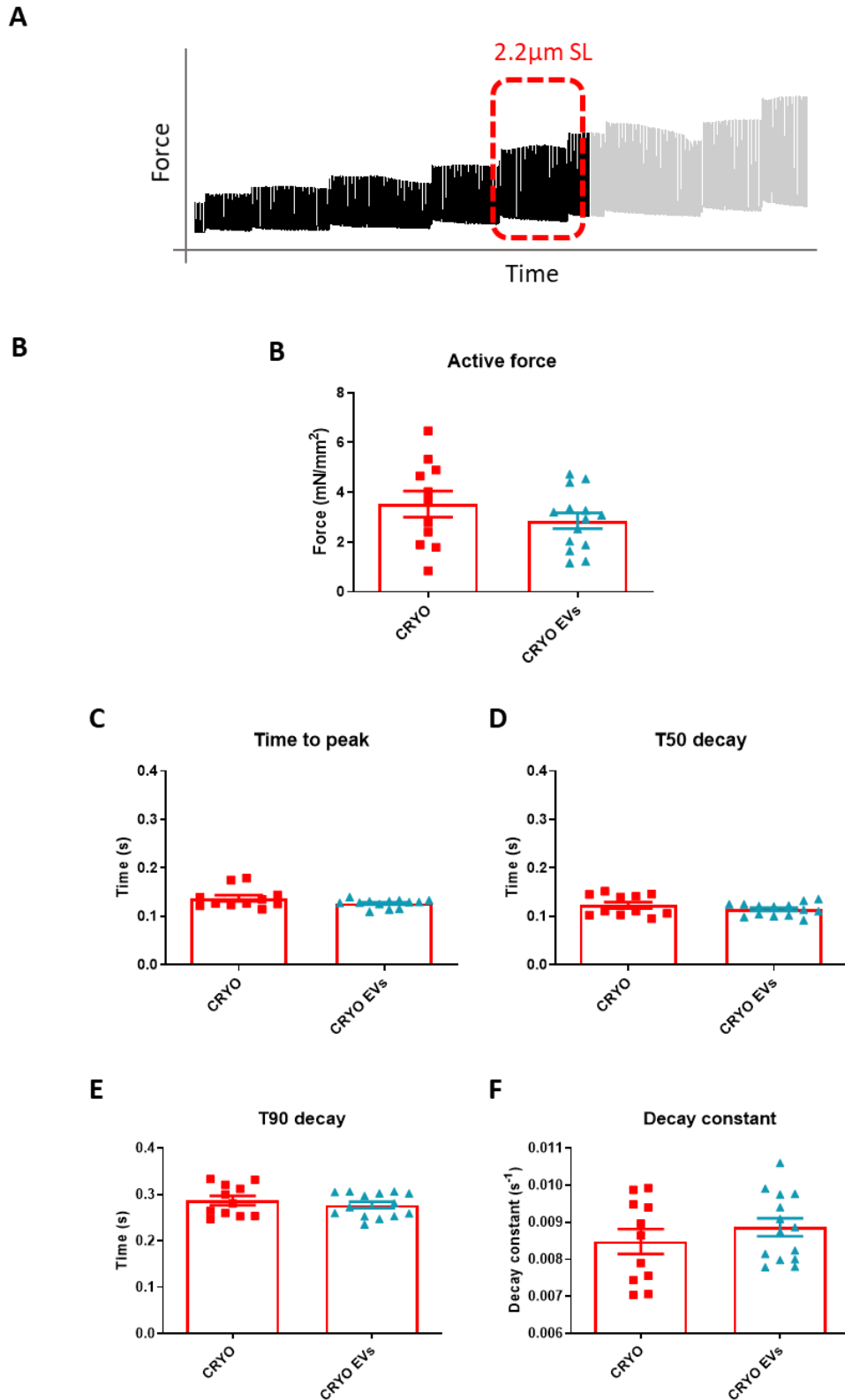


Figure 6.4- Contractility analysis of the cryoinjured LMSs treated with EVs for 24h. A) Schematic representation of the contractility traces. Control and treated healthy LMSs were evaluated at 15% LMS stretch, corresponding to 2.2 $\mu$ m in SL. B-F) Contraction active force and kinetics were assessed upon EVs application.  $N/n=9/11-14$ . Unpaired *t*-Test was used between CRYO and CRYO EVs, no significant differences were observed.  $N/n$ =biological replicates (animals)/technical replicates (LMSs).

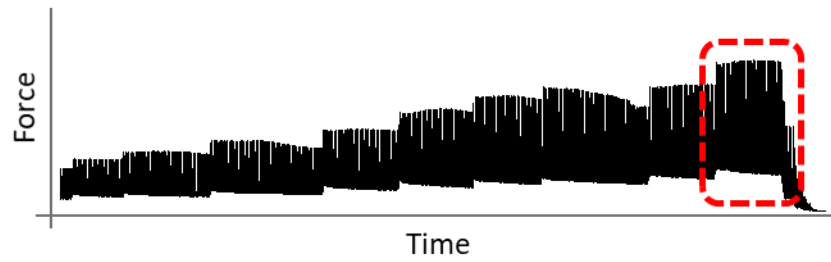
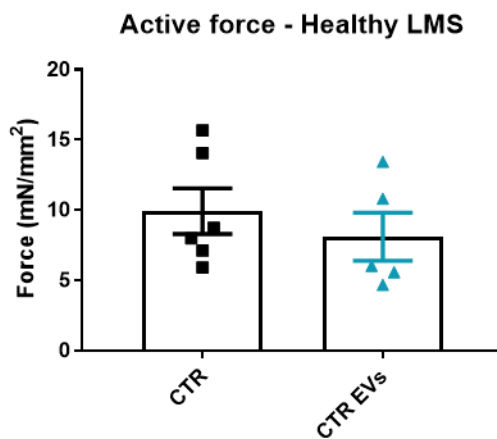
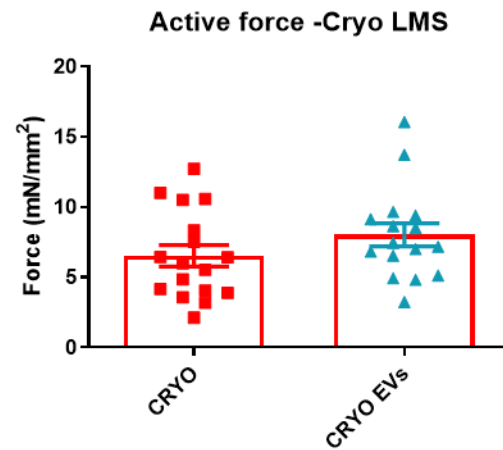
**A****B****C**

Figure 6.5- Contractility analysis at maximum isometric stretch of the healthy and cryoinjured LMSs treated with EVs for 24h. A) Schematic representation of the contractility traces. Control and treated cryoinjured LMSs were evaluated at maximum isometric force (max. stretch). B-C) Max. active force between control, healthy and cryoinjured LMSs.  $N/n=3/5-6$ . Unpaired *t*-Test was used to test the groups, but no significant differences were observed.  $N/n$ =biological replicates (animals)/technical replicates (LMSs).

#### **6.3.1.4 Gene transcription analysis**

EVs treatment has previously showed to affect gene regulation and promote tissue regeneration. In order to assess the early effects of the EV treatment in cryoinjured samples, RT-qPCR was performed. The genes selected in our studies included Ki-67, Collagen 1,  $\alpha$ -Smooth Muscle Actin ( $\alpha$ -SMA) and SERCA2. Ki-67 with cell proliferation, Collagen 1 and  $\alpha$ -SMA with fibrosis and SERCA with cell electrophysiology. Surprisingly, none of the genes showed changes upon EV treatment as shown in Fig 6.6, after 24h in culture. Fig 6.6A shows mRNA expression levels, whereas in Fig 6.6B data have been normalised to their respective control (untreated).

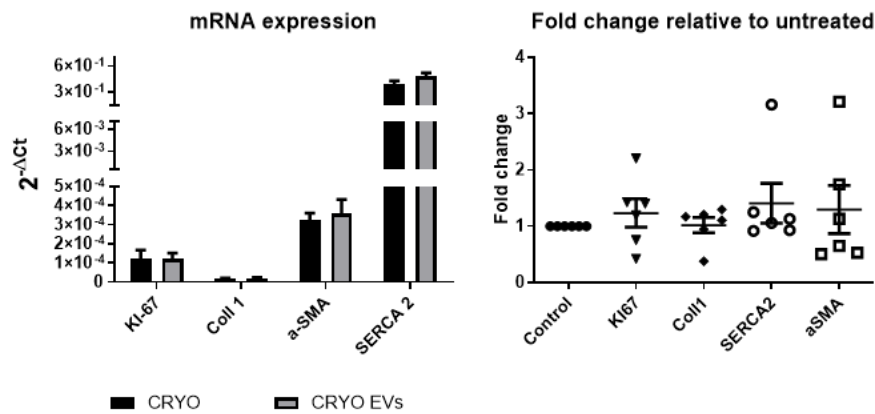


Figure 6.6- RT-qPCR data for Ki-67, Collagen 1,  $\alpha$ - Smooth Muscle Actin (A-SMA), and SERCA2. Genes were normalised to housekeeping gene GAPDH.  $\Delta\Delta C_t$  was calculated by comparing EV treated to untreated cryoinjured LMSs. N/n=6/6, 2-way ANOVA was used for statistical analysis, no significance was observed. N/n=biological replicates (animals)/technical replicates (LMSs).

Table 6.1-Primer sequence used for mRNA expression after EV administration.

Gene	Primer	Sequence (5' to 3')
ratGAPDH	Forward	AGTTCAACGGCACAGTCAAG
	Reverse	TACTCAGCACCAGCATCACC
ratColl1	Forward	CCCAGCCGCAAAGAGTCTAC
	Reverse	CAGGTTTCCACGTCTCACCA
rat $\alpha$ -SMA	Forward	ACCATCGGGAATGAACGCTT
	Reverse	CTGTCAGCAATGCCTGGGTA
ratSERCA2	Forward	TCATGGACGAGACGCTCAAG
	Reverse	TCCCCAAGCTCAGTCATGC
ratKi-67	Forward	AGTTCCGCCAATCCA ACTCA
	Reverse	CTCGGGAATTCTGTTGGCCT

## **6.4 Discussion**

This chapter shows that EV treatment does not induce significant changes in LMS contraction or gene regulation and therefore further experiments need to be done to clarify their role in cardioprotection.

### **6.4.1 Exosomes**

Regenerative medicine offers a wide range of different strategies targeting to repopulate the diseased tissue, including stimulation of the endogenous regenerative capacity of the cells, differentiation of residual cells towards cardiomyocyte or exogenous transplantation of cells on the area of injury (Tzahor and Poss, n.d.). Many attempts to regenerate the tissue with exogenous cell delivery in infarcted hearts showed minimal cell retention in both short- and long-term studies (Hou et al., 2005; Müller-Ehmsen et al., 2002). However, evidence of functional improvement were observed in many cell therapy cases (Hou et al., 2005; Tachibana et al., 2017). Therefore, it is believed that there is an alternative mechanism of action in cell therapy that is mediated indirectly from the cell's secretome. One of the recently appreciated components of the secretome can be seen in the field of EVs.

#### **6.4.1.1 Delivery method – EV concentration**

Delivery of the EVs into the heart has been frequently done by injections on the border zone of infarcted hearts. This method often results in diffusion of the EVs around the area of injury, where EVs either quickly attach on the tissue or are washed away to the heart's circulation because of the cardiac contraction. Poor retention of the EVs, has been overcome by directly delivering cell constructs of pluripotent cells that are able to continuously secrete EVs on the heart (Mancuso et al., 2020). This practice, however, does not ensure accurate control over the EV concentration and type of secreted EVs since this cannot be measured once the cells are



transplanted. For these reasons most of the studies are performed *in vitro* and more specifically on cell cultures. A similar approach was used in our experiments as well, where EVs were delivered on top of the LMSs and incorporation was monitored using prelabelled EVs and microscopy. EVs successfully attached on the LMSs after 30min of incubation. Other studies have shown that EV incorporation occurs within the first hour of incubation, with attachment peaking at 3h and then plateaus (Vrijssen et al., 2016b). In our model incubation of 30min and 1h were long enough to observe EV attachment; however, 30min incubation was chosen since unpublished data in our lab shows that longer LMS incubation in the in absence of media circulation and electrical stimulation impairs tissue functionality.

#### **6.4.1.2 Contractility upon EV treatment**

The effect of CPC derived exosomes has been evaluated in many studies, where it shows that exosomes manage to increase cardiac ejection fraction, lower scar formation, reduce apoptosis and increase vascularisation on acute ischemic rat models (Barile et al., 2014a; Bian et al., 2014). Experiments repeated on rats with exosomes derived from other cell types, such as fibroblast, showed no significant improvements in cardiac function, which indicates that the EV source play an important role in cardioprotection (Barile et al., 2014b). MSC derived exosomes could also induce functional improvement upon *in vivo* administration (Bian et al., 2014). Despite the fact that different studies used different EV isolation, concentration and administration method, most of them found similar results pointing towards improvement of contraction and induction of endothelial proliferation (Gartz and Strande, 2018). In our studies the effect of EVs on LMSs was evaluated by measuring force generation on the force transducer to evaluate cardiac contractility. Treated LMSs showed no functional changes after 24h in culture in either baseline or cryoinjured conditions. One of the possible explanations for this result could be that the incubation time of the EVs or culture time of the LMSs were not long enough for functional changes to occur. Therefore, longer application and incubation time

should be tested. Even though the amount of EVs,  $3.35 \times 10^{10}$ , used in the studies is high (Bian et al., 2014; Yi et al., 2020), the incorporation might have been reduced due to limited time of incubation. Other studies used longer EV incubation times on cells ranging from hours to days (Barile et al., 2014c; Maring et al., 2019; Mentkowski and Lang, 2019). Encapsulation of the EVs in ECM gels has also been used showing promising results which can improve EV retention (Liu et al., 2018). Perhaps a similar approach can be used with the LMSs as well to improve and control the EV administration on LMSs.

#### **6.4.1.3 Molecular response of the LMSs**

It has been shown that exosome derived either from MSCs or CPCs can induce their cardioprotective effect through activation of Akt and GSK3 or induce proliferation by upregulating markers such as Ki-67 (Arslan et al., 2013; Li et al., 2012). To test whether cardioprotection and cell proliferation occurred upon EV application RT-qPCR was performed. Ki-67 expression did not show significant changes upon EV treatment. To measure the effect of cryoinjury on scar formation, expression of collagen I and  $\alpha$ -SMA were measured, but again, no changes were observed in either of these markers upon EV treatment of cryoinjured LMSs. Total protein analysis was also reported to be unaffected in previously published studies (Vrijssen et al., 2016b). Further protein analysis of phosphorylated Akt was shown to be increased and therefore further analysis of these proteins need to be done in cryoinjured LMSs treated with EVs. Unfortunately, in our experimental design the limited EV supply did not allow further measurements of protein analysis.

The evaluation of scar formation and collagen deposition was also analysed when characterising the cryoinjury model, where no increase of collagen was observed after 24h of cryoinjury. Therefore, it is not surprising that exosomes had no effect on the collagen I and  $\alpha$ -SMA expression. In other studies, scar formation is being reduced upon exosome delivery on

the area of injury; however, in these studies longer incubation times were used (Dougherty et al., 2020; Gallet et al., 2017)

These findings suggest that in our conditions the EVs had no effect on LMSs; however, it cannot be excluded that in other conditions with longer EV incubation and LMS culture time would have a protective effect.

## 6.5 Limitations

Application of exosomes on healthy and cryoinjured LMSs showed limited cardioprotective effect. Therefore, further investigation focusing on the dose response, application method and incubation time that are necessary for the exosomes to exert a beneficial outcome on injured LMSs is necessary. The effect of exosomes has been shown to greatly affect apoptosis and therefore protein analysis of key antiapoptotic proteins (Bcl-2, ERK1/2, Akt) would better characterise the effect of exosomes on cryoinjured LMSs.

Additionally, more studies need to be done on the dose and incubation time of the EVs as well as their therapeutic cargos. The EVs in this study derived from healthy cardiac progenitor cells, from one donor; however, it is well known that there is significant heterogeneities between donors and thus further validation of EVs from multiple donors is necessary.

Additionally, in this study, increase of the n numbers is needed especially for the exosome application and transmural analysis. Due to time restrictions and/or availability of exosomes, experiments had limited samples that were utilised only for key experiments. Therefore, further investigation aims to better understand the mechanism of action of both exosome and AIP treatment.

## **6.6 Conclusions**

EV application on cryoinjured LMSs was successfully applied, with rapid EV internalisation was achieved in the first 30min of incubation. No significant improvements in tissue function were observed in cardiac function in terms of contractility and gene expression, therefore, further investigation needs to be done to elucidate the role of EVs in cardioprotection. In this direction the effect of EVs in other cell types such as endothelial cells should be investigated on LMSs, since previous studies have already established their regenerative role in vascularisation.

# **Chapter 7**

## **General Discussion**

## 7.1 Overview

Even though the idea of using LMSs was introduced years ago, it only gained popularity in the last decade, when new developments in the culturing system ensured preserved function after prolonged culture. Our group, along with others, significantly contributed to the development of a robust culturing method, which was further refined in the present thesis. This was a necessary step to enhance reproducibility and fully characterise the model. For this scope, a number of different slicing and culturing parameters were tested. The data suggest that tissue thickness plays a significant role in LMS stability during culture, with LMSs thinner than 300 $\mu\text{m}$ , showing arrhythmias after 24h of culture. 300 $\mu\text{m}$  LMSs were successfully cultured with preserved contractility and stability without the presence of spontaneous contractions. Tissue oxygenation and media oxygenation were also evaluated, with the LMSs having physiological levels of HIF1- $\alpha$ , indicating that there was no ischemia in the inner layers of the LMSs. Additional testing of the O<sub>2</sub> levels in the media, showed that LMSs were cultured in hyperoxic conditions when direct media oxygenation was applied, a technique that is often used in *ex vivo* tissue cardiac preparations. Significant decline of [O<sub>2</sub>] was observed when oxygenation was moved to the surface of the media, to levels close to those seen *in vivo*. The heart is a highly metabolic organ and therefore tissue energetics were also evaluated. The data showed that after the first hours of culture there was a rapid reduction in FAO, but sustained glycolysis. External addition of FAs was not solely capable to increase FAO and therefore more work should be done to bring FAO in physiological levels. Finally, regulation of mechanical stretch confirmed that physiological stretch of 15% (corresponding to 2.2 $\mu\text{m}$  SL) better preserved myocardial contraction in culture compared to more unloaded or overladed conditions. Acute stretch was able to increase  $m\Delta\Psi$  in a stretch related manner; however, this pattern was abolished in culture, where  $m\Delta\Psi$  was increased in all conditions regardless of the stretching condition. Stretching of the LMSs was applied with the help of 3D printed tissue

holders that stabilised attachment and eased manipulation, which allowed the LMSs to be stretched without detachments.

Collectively, these data show that cultured LMSs is a stable, functional, and reproducible *in vitro* tissue model with adequate oxygenation, mechanical stimulation, and functional acute metabolic responses.

Next, in order to establish an *in vitro* disease tissue model, tissue damage was induced by cryoinjury application on healthy LMSs and both the acute and chronic responses were measured. Cryoinjury application showed a very well-defined necrotic area, surrounded by a mixture of healthy and compromised cells, which was defined as the BZ. Acute measurements of contractility upon injury showed that increase in cell death significantly increased the passive force and relaxation time, without, surprisingly, affecting the contraction amplitude. The preservation in contraction suggested that there must be a compensatory mechanism derived from the remaining viable cells that maintained contractility. This observation made us investigate the hearts' contractile machinery, the sarcomeres, which indeed showed an increase in SL on BZ. The BZ has been identified as a potent contributor of arrhythmias in ischemic patients and further analysis showed that this area had higher density of cells with spontaneous  $\text{Ca}^{2+}$  waves, with high automaticity, wave speed and propagation. These changes were also observed on whole tissue level with the development of spontaneous contractions. Cellular irregularities were particularly apparent in endocardial LMSs, showing that the endocardium is more vulnerable upon tissue damage. In this process a known activator of arrhythmias, CamKII, was involved in the induction of spontaneous  $\text{Ca}^{2+}$  activity. Targeted inhibition of CamKII in endocardial LMSs significantly reduced spontaneous events, while the effect of the inhibitor on epicardium had little effect. CamKII had no effect on tissue contractility of either endocardial or epicardial LMSs, suggesting that there must be additional parameters that translate  $\text{Ca}^{2+}$  waves into whole tissue spontaneous contractions.



One of the most studied heart treatments of cardiac injury is tissue replacement by using regenerative mechanisms. Since tissue replacement is still hampered by the lack of cell retention, the role of other cell components such as EVs has been emphasised for their beneficial action upon cell transplantation. In this study application of EVs derived from cardiac progenitor cells did not show any significant improvements on tissue contractility or gene expression, when applied either in healthy or diseased tissue and therefore further studies need to be done to clarify their protective role.

## 7.2 Strengths & Limitations

The ultimate goal of translational research is to gain greater insights into the mechanisms of human physiology or disease progression and eventually test therapeutic interventions with the potential to reach the clinics. LMSs from adult hearts are able to provide a great multicellular preparation with preserved cell composition, heterocellularity, electrophysiological and mechanical properties similar to the *in vivo* conditions. They greatly benefit from being mechanically produced without the use of collagenase digestion, which removes the ECM and often damages the cell membrane. This model is versatile and can be applied in many animal species such as mice, rats, rabbits, guinea (Wang et al., 2014) pigs, dogs and most importantly humans (Perbellini et al., 2017; Watson et al., 2019), with no or little modification of the main protocol, which makes it applicable to many types of studies.

Typically, research on human cells/tissues is only limited to acute experiments (e.g. tissue wedges) or require long culturing methods (e.g. iPSC-CMs, with uncertain levels of maturity). Our lab and others have shown that long term culture with preserved function is now possible by adopting methods of electromechanical stimulation, media supplementation and oxygenation (Fischer et al., 2019; Watson et al., 2019). Under prolonged culture time fundamental or translational studies directly on human tissue are now feasible. This could potentially bridge the gap between preclinical and clinical testing, accelerate drug discovery and save significant amount of time and financial investments, which can be utilised in other ways.

Using human tissue from diseased patients is, also, an excellent way to reduce animal usage, which is a great burden in the pharmaceutical industry. Slicing of human tissue, also, results in a large number of LMS samples and therefore increases the throughput of the method, which is rather limited with smaller mammals, such as rats.

Even though LMSs is an exciting and useful model for translational and fundamental research it also comes with some limitations. Even though human LMSs culture has been reported to last for up to 4 months, in our hands humans LMSs cannot be cultured for more than 3-5 days without significant reduction in contractility. Short cultures are often limiting, especially for experiments that require longer incubation time such as drug testing and tissue transfection. Additionally, in this study LMSs were produced from rat hearts. Even though rats have differences in heart physiology with humans, they were readily available and provided with a high sample number. Unfortunately, human tissue requires heavy regulation and is often difficult to obtain. In this study, human tissue samples were rarely available and therefore, their use was restricted.

Besides the benefits of the cryoinjury as an experimental disease model, it is important to remember that tissue damage is induced by an artificial way. *In vivo* tissue damage usually occurs in response to ischemia/reperfusion and is followed by many other deleterious factors such as lack of O<sub>2</sub>, nutrients, accumulation of metabolites and ionic changes, that all affect disease progression in different ways. That means cryoinjury cannot fully mimic the MI injury that occurs *in vivo*. Despite this being a limitation, it can also work as an advantage since this is a way to isolate cell death and mechanical changes from other variables and study their effect in isolation. Cryoinjury can also provide a well-defined damaged area, which is usually difficult to achieve in *in vivo* models, where infarct size can depend on many factors such as animal variability, peripheral circulation, experience of the user and time of artery occlusion (Lindsey et al., 2018c; Vandeplassche et al., 1991; Yoran et al., 1982).

Another important parameter that was not considered in the present study is the use of multiple testing during statistical analysis. This extra step can adjust the statistical confidence of our measurements and make sure that significant differences did not occurred by chance. Therefore, future analysis should include this measurement.

Finally, tissue LMSs are produced from different transmural areas of the ventricle and therefore functional and structural characterisation of endocardial, midmyocardial and epicardial is feasible. Indeed, it has been shown that cells from different transmural areas had differences in their SL and their response to arrhythmia development and treatment. Others have also reported similar results, with the endocardial cells exhibiting longer AP (increased repolarisation time) and longer electromechanical delay (time between electrical and mechanical stimulation of the cells) (Cordeiro et al., 2004; Fedida et al., 1991; Vaverka et al., 2018)

### 7.3 Implications

This work adds to the growing understanding of prolonged tissue culturing using adult hearts. This is a big achievement, since for a long time, primary isolated CMs were considered as the golden standard for culturing human heart cells *in vitro*. In this study it was shown that even though LMSs were functionally stable after 24h in culture, there was a significant decline in FAO, with sustained glycolysis. Reduction of FAO in *in vitro* cultures of primary isolated CMS has previously been reported, where cultured CMs showed 2 fold reduction in FAO after 48h in culture (Rech et al., 2018).  $[O_2]$  is usually a strong contributor in FA uptake and improves FAO. In this study,  $[O_2]$  was adequate both intracellularly and extracellularly. Therefore, there must be another missing element that inhibits FAO in cultured LMSs.

Another important observation was that acute tissue stretch was correlated with acute changes in  $m\Delta\Psi$ . Recent studies showed using microscopic approaches or computational modelling that mitochondrial mechanical deformation occurs in response to cell stretch or contraction, suggesting that they may also play a significant role in mechanotransduction and regulation of ATP production (Kamoun et al., 2018; Rech et al., 2018). To our knowledge, changes in  $m\Delta\Psi$  upon cardiac tissue stretch have not been shown before. However, prolonged culture of LMSs abolished the stretch related differences, showing mitochondria changes upon culture.

In our studies the reduction in FAO and increase in  $m\Delta\Psi$  occurred at the same time and it would be interesting to further investigate if these responses are somehow linked.

In this thesis characterisation of the cryoinjured LMSs was performed. This localised necrosis showed a similar phenotype with that of the *in vivo* cryoinjury and cell death seen upon cardiac infarction in mammals (Ewout J. Van Den Bos et al., 2005). This provides a promising and cost-effective model that can be used to study local tissue responses or tissue regeneration. In previous studies, localised injury was also used in combination with cardiac muscle strips,

where half of the tissue was exposed to hypoxic conditions, by using custom made chambers (Alexandre et al., 2013). A closer model to ours can, also, be seen in cardiac organoids which were subjected to cryoinjury in order to study the regenerative potential of pluripotent cells (Holly K. Voges et al., 2017).

Finally, cryoinjury also provided a useful model for studying arrhythmias. In this model it was found that activation of CamKII was implicated in the development of arrhythmias. CamKII activation can be triggered by several upstream stimuli such as ROS, adrenergic stimulation and  $[Ca^{2+}]$ , which are of great importance since they are all implicated in pathological heart conditions and therefore their study on cryoinjured LMSs can be performed.

## **7.4 Future work**

### **7.4.1 LMS metabolic stability**

LMS metabolic switch from FAO to glycolysis is a pattern often seen in pathological conditions such as in heart failure and hypertrophy (Tran and Wang, 2019). Thus, it is important to better adjust the environmental conditions to reverse this phenotype. There are many reports supporting that FA uptake is being regulated by passive diffusion; however, there is increased evidence that it is also mediated through membrane transporters such as CD36, FATP1-6 and FABPpm (Glatz and Luiken, 2018). CD36 is a well-known FA transporter that is regulated by the nuclear peroxisome proliferator activated receptor (PPAR). PPARs are high expressed in oxidative tissues like the heart and can be activated by fatty acid metabolites such as: acyl-CoA esters, oxidized fatty acids or eicosanoids (Glatz and Luiken, 2018; Nakamura et al., 2004). Addition of these agonists to the media might improve FAO and enhance cardiac metabolism. Additionally, reducing media insulin could also favour FAO, since insulin downregulates the PPARs (Hamel et al., 2001). Finally, in this study LMSs were mainly cultured in the presence of palmitic acid; however, other types of FA such as oleic acid or omega-3 fatty acids, could be preferred for FA uptake. These lipids have shown to decrease cell apoptosis in the heart, reduce inflammation and hypertension. Omega-3 fatty acids, have the ability to get integrated in the plasma membrane of the cells and increase its fluidity and thus affect the activity of various plasma membrane proteins (Chang and Deckelbaum, 2013; W. S. Harris, 2013; Rizos et al., 2012).

#### **7.4.1.1 Reactive oxygen species**

Another area that has not been widely explored is the levels of ROS in LMSs. ROS can significantly affect tissue contraction and metabolism, and induce arrhythmias (Sovari, 2016). ROS can accumulate in response to increased O<sub>2</sub>, FAO, cardiac overload, high mitochondrial

Ca<sup>2+</sup> levels and reduction in antioxidants (Jeong et al., 2012). Evaluation of the ROS production can be investigated by commercially available staining or biochemical assays. ROS control can be regulated by supplementing the media with antioxidants or by intervening with the factors that induce ROS production.

#### **7.4.2 Increase of LMS culture time**

In comparison with other cardiac models, LMSs can only be cultured for a few days. That can often be restrictive when longer tissue cultures are required. To improve this, it is necessary to use more sophisticated culture systems, such as bioreactors. Bioreactors have the big advantage of providing accurate regulation of the culture conditions, such as temperature, oxygenation, mechanical load and, most importantly, constant monitoring of tissue contraction. Monitoring cardiac function over time is of immense importance, because it provides live information of LMS contraction without any human intervention, tissue manipulation or termination of culture to externally measure tissue contraction. This is important for minimizing variability and eliminating confounding factors derived from tissue manipulation.

Bioreactors are very useful, but they are also very expensive with very low throughput. Usually bioreactors for muscle tissue have the capacity for one sample, which significantly reduces the number of technical replicates and different conditions that can be used. On the other hand, bigger culture chambers, as the ones used in this study, can accommodate 4 LMSs per chamber; however, they require big media volume and a large sample size. Therefore, it is necessary to design chambers that can combine the benefits from both the bioreactor and the bigger chambers. The ideal system would include multiple smaller chambers for single LMS samples with constant monitoring of contractility, temperature, and oxygenation.

With regards to the cryoinjury model, it was shown that the increase of injury affected the mechanical properties of LMSs, particularly at the BZ where the SL was increased. This



observation was lost upon culture, suggesting that there was an addition of sarcomeres in series. To test this hypothesis, mRNA and protein quantification of key sarcomeric proteins could be further measured. The addition of sarcomeres has also been seen in pathological conditions under volume overload induced hypertrophy (Mihl et al., 2008), and therefore their study is relevant for understanding disease progression.

Tissue remodelling upon cell damage also resulted in arrhythmias related to CamKII activation. To strengthen the findings of CamKII inhibition with AIP, it is also important to measure direct CamKII activation, which is regulated by phosphorylation. Measurements of CamKII phosphorylation, both in the whole LMSs, and locally near the BZ, would better validate my hypothesis.

## 7.5 Conclusion

In this thesis it was shown that LMS culture can be further refined with emphasis on  $[O_2]$  and tissue metabolism. Utilisation of this model can be further exploited by designing and characterising *in vitro* disease models, such as the one described here by on cryoinjured LMSs. This model accurately controls the location and injury size with significant improvements in reproducibility over other *in vivo* methods. Local damage showed to change sarcomere morphology, induce spontaneous contractions and enhance  $Ca^{2+}$  waves in the BZ, partially attributed to CamKII activity. These findings show that both local and global responses can be analysed at either micro- or macroscopic level, with emphasis on electrophysiological and regenerative studies. Future experiments would further define the role of CamKII in protein level and better clarify the cardiac mechanical adaptation to local cell injury *in vitro*.

# Chapter 8

## References

- Abdelmagid, S.A., Clarke, S.E., Nielsen, D.E., Badawi, A., El-Sohemy, A., Mutch, D.M., Ma, D.W.L., 2015. Comprehensive profiling of plasma fatty acid concentrations in young healthy Canadian adults. *PLoS One* 10, e0116195.  
<https://doi.org/10.1371/journal.pone.0116195>
- Abe, H., Semba, H., Takeda, N., 2017. The roles of hypoxia signaling in the pathogenesis of cardiovascular diseases. *J. Atheroscler. Thromb.* <https://doi.org/10.5551/jat.RV17009>
- Abiria, S.A., Colbran, R.J., 2010. CaMKII associates with CaV1.2 L-type calcium channels via selected  $\beta$  subunits to enhance regulatory phosphorylation. *J. Neurochem.* 112, 150–161. <https://doi.org/10.1111/j.1471-4159.2009.06436.x>
- Aerni-Flessner, L., Abi-Jaoude, M., Koenig, A., Payne, M., Hruz, P.W., 2012. GLUT4, GLUT1, and GLUT8 are the dominant GLUT transcripts expressed in the murine left ventricle. *Cardiovasc. Diabetol.* 11. <https://doi.org/10.1186/1475-2840-11-63>
- Agarwal, U., George, A., Bhutani, S., Ghosh-Choudhary, S., Maxwell, J.T., Brown, M.E., Mehta, Y., Platt, M.O., Liang, Y., Sahoo, S., Davis, M.E., 2017. Experimental, systems, and computational approaches to understanding the MicroRNA-mediated reparative potential of cardiac progenitor cell-derived exosomes from pediatric patients. *Circ. Res.* 120, 701–712. <https://doi.org/10.1161/CIRCRESAHA.116.309935>
- Akhtar Khan, N., David Evans, R., Banni, S., Carta, G., Murru, E., Manca, C., 2017. Palmitic Acid: Physiological Role, Metabolism and Nutritional Implications 8.  
<https://doi.org/10.3389/fphys.2017.00902>

- Al-Ani, A., Toms, D., Kondro, D., Thundathil, J., Yu, Y., Ungrin, M., 2018. Oxygenation in cell culture: Critical parameters for reproducibility are routinely not reported. *PLoS One* 13. <https://doi.org/10.1371/journal.pone.0204269>
- Alexandre, J., Schiariti, M., Rouet, R., Puddu, P.E., 2013. Rabbit ventricular myocardium undergoing simulated ischemia and reperfusion in a double compartment tissue bath: a model to investigate both antiarrhythmic and arrhythmogenic likelihood. *Int. J. Physiol. Pathophysiol. Pharmacol.* 5, 52–60.
- Allen, D.G., Eisner, D.A., Orchard, C.H., 1984. Characterization of oscillations of intracellular calcium concentration in ferret ventricular muscle. *J. Physiol.* 352, 113–128. <https://doi.org/10.1113/jphysiol.1984.sp015281>
- Allen, D.G., Kentish, J.C., 1985. The cellular basis of the length-tension relation in cardiac muscle. *J. Mol. Cell. Cardiol.* [https://doi.org/10.1016/S0022-2828\(85\)80097-3](https://doi.org/10.1016/S0022-2828(85)80097-3)
- Amano, Y., Nishiguchi, A., Matsusaki, M., Iseoka, H., Miyagawa, S., Sawa, Y., Seo, M., Yamaguchi, T., Akashi, M., 2016. Development of vascularized iPSC derived 3D-cardiomyocyte tissues by filtration Layer-by-Layer technique and their application for pharmaceutical assays. *Acta Biomater.* 33, 110–121. <https://doi.org/10.1016/j.actbio.2016.01.033>
- Anderson, B.R., Granzier, H.L., 2012. Titin-based tension in the cardiac sarcomere: Molecular origin and physiological adaptations. *Prog. Biophys. Mol. Biol.* <https://doi.org/10.1016/j.pbiomolbio.2012.08.003>
- Anderson, M.E., Braun, A.P., Schulman, H., Premack, B.A., 1992. Multifunctional Ca<sup>2+</sup>/Calmodulin-Dependent Protein Kinase Mediates Ca<sup>2+</sup>-Induced Enhancement of the L-type Ca<sup>2+</sup> Current in Rabbit Ventricular Myocytes.

- Antzelevitch, C., Burashnikov, A., 2011. Overview of Basic Mechanisms of Cardiac Arrhythmia. *Card. Electrophysiol. Clin.* <https://doi.org/10.1016/j.ccep.2010.10.012>
- Arenja, N., Mueller, C., Ehl, N.F., Brinkert, M., Roost, K., Reichlin, T., Sou, S.M., Hochgruber, T., Osswald, S., Zellweger, M.J., 2013. Prevalence, extent, and independent predictors of silent myocardial infarction. *Am. J. Med.* 126, 515–522. <https://doi.org/10.1016/j.amjmed.2012.11.028>
- Arslan, F., Lai, R.C., Smeets, M.B., Akeroyd, L., Choo, A., Aguor, E.N.E., Timmers, L., van Rijen, H. V., Doevendans, P.A., Pasterkamp, G., Lim, S.K., de Kleijn, D.P., 2013. Mesenchymal stem cell-derived exosomes increase ATP levels, decrease oxidative stress and activate PI3K/Akt pathway to enhance myocardial viability and prevent adverse remodeling after myocardial ischemia/reperfusion injury. *Stem Cell Res.* 10, 301–312. <https://doi.org/10.1016/j.scr.2013.01.002>
- Baicu, S.C., Taylor, M.J., 2002. Acid-base buffering in organ preservation solutions as a function of temperature: New parameters for comparing buffer capacity and efficiency. *Cryobiology* 45, 33–48. [https://doi.org/10.1016/S0011-2240\(02\)00104-9](https://doi.org/10.1016/S0011-2240(02)00104-9)
- Bajaj, P., Tang, X., Saif, T.A., Bashir, R., 2010. Stiffness of the substrate influences the phenotype of embryonic chicken cardiac myocytes. *J. Biomed. Mater. Res. - Part A* 95, 1261–1269. <https://doi.org/10.1002/jbm.a.32951>
- Bányász, T., Fulop, L., Magyar, J., Szentandrassy, N., Varro, A., Nanasi, P., 2003. Endocardial versus epicardial differences in L-type calcium current in canine ventricular myocytes studied by action potential voltage clamp. *Cardiovasc. Res.* 58, 66–75. [https://doi.org/10.1016/S0008-6363\(02\)00853-2](https://doi.org/10.1016/S0008-6363(02)00853-2)
- Barile, L., Lionetti, V., Cervio, E., Matteucci, M., Gherghiceanu, M., Popescu, L.M., Torre, T., Siclari, F., Moccetti, T., Vassalli, G., 2014a. Extracellular vesicles from human

cardiac progenitor cells inhibit cardiomyocyte apoptosis and improve cardiac function aftermyocardial infarction. *Cardiovasc. Res.* 103, 530–541.

<https://doi.org/10.1093/cvr/cvu167>

Barile, L., Lionetti, V., Cervio, E., Matteucci, M., Gherghiceanu, M., Popescu, L.M., Torre, T., Siclari, F., Moccetti, T., Vassalli, G., 2014b. Extracellular vesicles from human cardiac progenitor cells inhibit cardiomyocyte apoptosis and improve cardiac function aftermyocardial infarction. *Cardiovasc. Res.* 103, 530–541.

<https://doi.org/10.1093/cvr/cvu167>

Barile, L., Lionetti, V., Cervio, E., Matteucci, M., Gherghiceanu, M., Popescu, L.M., Torre, T., Siclari, F., Moccetti, T., Vassalli, G., 2014c. Extracellular vesicles from human cardiac progenitor cells inhibit cardiomyocyte apoptosis and improve cardiac function aftermyocardial infarction. *Cardiovasc. Res.* 103, 530–541.

<https://doi.org/10.1093/cvr/cvu167>

Barr, R.L., Lopaschuk, G.D., 2000. Methodology for measuring in vitro/ex vivo cardiac energy metabolism. *J. Pharmacol. Toxicol. Methods* 43, 141–152.

[https://doi.org/10.1016/S1056-8719\(00\)00096-4](https://doi.org/10.1016/S1056-8719(00)00096-4)

Barreto-Chang, O.L., Dolmetsch, R.E., 2009. Calcium imaging of cortical neurons using Fura-2 AM. *J. Vis. Exp.* 23. <https://doi.org/10.3791/1067>

Barretti, D.L.M., Melo, S.F.S., Oliveira, E.M., Barauna, V.G., 2017. Resistance training attenuates salt overload-induced cardiac remodeling and diastolic dysfunction in normotensive rats. *Brazilian J. Med. Biol. Res.* 50. <https://doi.org/10.1590/1414-431x20176146>

Barry, W.H., 2004. *Heart Physiology From Cell to Circulation*, 4th ed. Circulation 110.

<https://doi.org/10.1161/01.cir.0000143724.99618.62>

- Basso, C., Fox, P.R., Meurs, K.M., Towbin, J.A., Spier, A.W., Calabrese, F., Maron, B.J., Thiene, G., 2004. Arrhythmogenic Right Ventricular Cardiomyopathy Causing Sudden Cardiac Death in Boxer Dogs: A New Animal Model of Human Disease. *Circulation* 109, 1180–1185. <https://doi.org/10.1161/01.CIR.0000118494.07530.65>
- Bauer, M., Meyer, M., Grimm, L., Meitinger, T., Zimmer, J., Gasser, T., Ueffing, M., Widmer, H.R., 2000. Nonviral Glial Cell-Derived Neurotrophic Factor Gene Transfer Enhances Survival of Cultured Dopaminergic Neurons and Improves Their Function after Transplantation in a Rat Model of Parkinson's Disease. *Hum. Gene Ther.* 11, 1529–1541.
- Bedada, F.B., Wheelwright, M., Metzger, J.M., 2016. Maturation status of sarcomere structure and function in human iPSC-derived cardiac myocytes. *Biochim. Biophys. Acta - Mol. Cell Res.* <https://doi.org/10.1016/j.bbamcr.2015.11.005>
- Beer, M., Seyfarth, T., Sandstede, J., Landschütz, W., Lipke, C., Köstler, H., Von Kienlin, M., Harre, K., Hahn, D., Neubauer, S., 2002. Absolute concentrations of high-energy phosphate metabolites in normal, hypertrophied, and failing human myocardium measured noninvasively with <sup>31</sup>P-SLOOP magnetic resonance spectroscopy. *J. Am. Coll. Cardiol.* 40, 1267–1274. [https://doi.org/10.1016/S0735-1097\(02\)02160-5](https://doi.org/10.1016/S0735-1097(02)02160-5)
- Beez, C.M., Haag, M., Klein, O., Van Linthout, S., Sittinger, M., Seifert, M., 2019. Extracellular vesicles from regenerative human cardiac cells act as potent immune modulators by priming monocytes. *J. Nanobiotechnology* 17, 72. <https://doi.org/10.1186/s12951-019-0504-0>
- Bell, R.M., Mocanu, M.M., Yellon, D.M., 2011. Retrograde heart perfusion: the Langendorff technique of isolated heart perfusion. *J. Mol. Cell. Cardiol.* 50, 940–50. <https://doi.org/10.1016/j.yjmcc.2011.02.018>

- Benam, K.H., Dauth, S., Hassell, B., Herland, A., Jain, A., Jang, K.-J., Karalis, K., Kim, H.J., Macqueen, L., Mahmoodian, R., Musah, S., Torisawa, Y.-S., Van Der Meer, A.D., Villenave, R., Yadid, M., Parker, K.K., Ingber, D.E., 2015. Keywords disease model, tissue engineering, 3D culture, organ-on-a-chip, microfluidic, in vitro tool. *Annu. Rev. Pathol. Mech. Dis* 10, 195–262. <https://doi.org/10.1146/annurev-pathol-012414-040418>
- Berk, B.C., Fujiwara, K., Lehoux, S., 2007. ECM remodeling in hypertensive heart disease. *J. Clin. Invest.* <https://doi.org/10.1172/JCI31044>
- Beyersdorf, F., Buckberg, G.D., Acar, C., Okamoto, F., Sjostrand, F., Young, H., Bugyi, H.I., Allen, B.S., 1989. Cardiogenic shock after acute coronary occlusion. Pathogenesis, early diagnosis, and treatment. *Thorac. Cardiovasc. Surg.* 37, 28–36. <https://doi.org/10.1055/s-2007-1013901>
- Bhana, B., Iyer, R.K., Chen, W.L.K., Zhao, R., Sider, K.L., Likhitpanichkul, M., Simmons, C.A., Radisic, M., 2010. Influence of substrate stiffness on the phenotype of heart cells. *Biotechnol. Bioeng.* 105, 1148–1160. <https://doi.org/10.1002/bit.22647>
- Bian, S., Zhang, L., Duan, L., Wang, X., Min, Y., Yu, H., 2014. Extracellular vesicles derived from human bone marrow mesenchymal stem cells promote angiogenesis in a rat myocardial infarction model. *J. Mol. Med.* 92, 387–397. <https://doi.org/10.1007/s00109-013-1110-5>
- Bigaeva, E., Gore, E., Simon, E., Zwick, M., Oldenburger, A., de Jong, K.P., Hofker, H.S., Schlepütz, M., Nicklin, P., Boersema, M., Rippmann, J.F., Olinga, P., 2019. Transcriptomic characterization of culture-associated changes in murine and human precision-cut tissue slices. *Arch. Toxicol.* 93, 3549–3583. <https://doi.org/10.1007/s00204-019-02611-6>
- Biochemistr, and, Pillekamp, F., Halbach, M., Reppel, M., Rubenchyk, O., Pfannkuche, K.,



- Xi, J.-Y., Bloch, W., Sreeram, N., Brockmeier, K., Hescheler, J., 2007. Neonatal Murine Heart Slices. A Robust Model to Study Ventricular Isometric Contractions. Orig. Pap. Cell Physiol Biochem 20, 837–846.
- Bird, S., Doevendans, P.A., van Rooijen, M.A., Brutel de la Riviere, A., Hassink, R.J., Passier, R., Mummery, C.L., 2003. The human adult cardiomyocyte phenotype. Cardiovasc. Res. 58, 423–434. [https://doi.org/10.1016/S0008-6363\(03\)00253-0](https://doi.org/10.1016/S0008-6363(03)00253-0)
- Bise, T., Sallin, P., Pfefferli, C., Jaźwińska, A., 2020. Multiple cryoinjuries modulate the efficiency of zebrafish heart regeneration. Sci. Rep. 10, 1–15. <https://doi.org/10.1038/s41598-020-68200-1>
- Bittl, J.A., Ingwall, J.S., n.d. BRIEF COMMUNICATIONS The Energetics of Myocardial Stretch Creatine Kinase Flux and Oxygen Consumption in the Noncontracting Rat Heart.
- Black, L.D., Meyers, J.D., Weinbaum, J.S., Shvelidze, Y.A., Tranquillo, R.T., 2009. Cell-Induced Alignment Augments Twitch Force in Fibrin Gel-Based Engineered Myocardium via Gap Junction Modification. Tissue Eng. - Part A 15, 3099–3108. <https://doi.org/10.1089/ten.tea.2008.0502>
- Bnrnashev, N.A., Edwards, F.A., Verkhatsky, A.N., 1990. Patch-clamp recordings on rat cardiac muscle slices. Pflfigers Arch 417, 123–125.
- Böing, A.N., van der Pol, E., Grootemaat, A.E., Coumans, F.A.W., Sturk, A., Nieuwland, R., 2014. Single-step isolation of extracellular vesicles by size-exclusion chromatography. J. Extracell. Vesicles 3. <https://doi.org/10.3402/jev.v3.23430>
- Borile, G., De Mauro, C., Urbani, A., Alfieri, D., Pavone, F.S., Mongillo, M., 2014. Multispot multiphoton Ca<sup>2+</sup> imaging in acute myocardial slices.

<https://doi.org/10.1117/1>

Bosch-Marce, M., Okuyama, H., Wesley, J.B., Sarkar, K., Kimura, H., Liu, Y. V., Zhang, H., Strazza, M., Rey, S., Savino, L., Zhou, Y.F., McDonald, K.R., Na, Y., Vandiver, S., Rabi, A., Shaked, Y., Kerbel, R., LaVallee, T., Semenza, G.L., 2007. Effects of aging and hypoxia-inducible factor-1 activity on angiogenic cell mobilization and recovery of perfusion after limb ischemia. *Circ. Res.* 101, 1310–1318.

<https://doi.org/10.1161/CIRCRESAHA.107.153346>

Bøtker, H.E., Hausenloy, D., Andreadou, I., Antonucci, S., Boengler, K., Davidson, S.M., Deshwal, S., Devaux, Y., Di Lisa, F., Di Sante, M., Efentakis, P., Femminò, S., García-Dorado, D., Gircz, Z., Ibanez, B., Iliodromitis, E., Kaludercic, N., Kleinbongard, P., Neuhäuser, M., Ovize, M., Pagliaro, P., Rahbek-Schmidt, M., Ruiz-Meana, M., Schlüter, K.D., Schulz, R., Skyschally, A., Wilder, C., Yellon, D.M., Ferdinandy, P., Heusch, G., 2018. Practical guidelines for rigor and reproducibility in preclinical and clinical studies on cardioprotection. *Basic Res. Cardiol.* <https://doi.org/10.1007/s00395-018-0696-8>

Bovendeerd, P.H.M., Arts, T., Huyghe, J.M., van Campen, D.H., Reneman, R.S., 1992.

Dependence of local left ventricular wall mechanics on myocardial fiber orientation: A model study. *J. Biomech.* 25, 1129–1140. [https://doi.org/10.1016/0021-9290\(92\)90069-D](https://doi.org/10.1016/0021-9290(92)90069-D)

Boyden, P.A., Dun, W., Stuyvers, B.D., 2015. What is a Ca<sup>2+</sup> wave? Is it like an electrical wave? *Arrhythmia Electrophysiol. Rev.* 4, 35–39.

<https://doi.org/10.15420/aer.2015.4.1.35>

Boyet, M.R., Honjo, H., Kodama, I., 2000. The sinoatrial node, a heterogeneous pacemaker structure. *Cardiovasc. Res.* [https://doi.org/10.1016/S0008-6363\(00\)00135-8](https://doi.org/10.1016/S0008-6363(00)00135-8)

Brandenburger, M., Wenzel, J., Bogdan, R., Richardt, D., Nguemo, F., Reppel, M.,

Hescheler, J., Terlau, H., Dendorfer, A., 2012a. Organotypic slice culture from human adult ventricular myocardium. *Cardiovasc. Res.* 93, 50–59.

<https://doi.org/10.1093/cvr/cvr259>

Brandenburger, M., Wenzel, J., Bogdan, R., Richardt, D., Nguemo, F., Reppel, M.,

Hescheler, J., Terlau, H., Dendorfer, A., 2012b. Organotypic slice culture from human adult ventricular myocardium. *Cardiovasc. Res.* 93, 50–59.

<https://doi.org/10.1093/cvr/cvr259>

Brandenburger, M., Wenzel, J., Bogdan, R., Richardt, D., Nguemo, F., Reppel, M.,

Hescheler, J., Terlau, H., Dendorfer, A., 2012c. Organotypic slice culture from human adult ventricular myocardium. *Cardiovasc. Res.* 93, 50–59.

<https://doi.org/10.1093/cvr/cvr259>

Brandenburger, M., Wenzel, J., Bogdan, R., Richardt, D., Nguemo, F., Reppel, M.,

Hescheler, J., Terlau, H., Dendorfer, A., 2012d. Organotypic slice culture from human adult ventricular myocardium. *Cardiovasc. Res.* 93, 50–9.

<https://doi.org/10.1093/cvr/cvr259>

Braun, A.P., Schulman, H., 1995. The Multifunctional Calcium/Calmodulin-Dependent Protein Kinase: From Form to Function. *Annu. Rev. Physiol.* 57, 417–445.

<https://doi.org/10.1146/annurev.ph.57.030195.002221>

Brueckl, C., Kaestle, S., Kerem, A., Habazettl, H., Krombach, F., Kuppe, H., Kuebler, W.M.,

2006. Hyperoxia-induced reactive oxygen species formation in pulmonary capillary endothelial cells in situ. *Am. J. Respir. Cell Mol. Biol.* 34, 453–463.

<https://doi.org/10.1165/rcmb.2005-0223OC>

Brugniaux, J.V., Coombs, G.B., Barak, O.F., Dujic, Z., Sekhon, M.S., Ainslie, P.N., 2018.

Highs and lows of hyperoxia: Physiological, performance, and clinical aspects. *Am. J.*

Physiol. - Regul. Integr. Comp. Physiol. <https://doi.org/10.1152/ajpregu.00165.2017>

Bub, G., Camelliti, P., Bollensdorff, C., Stuckey, D.J., Picton, G., Burton, R.A.B., Clarke, K., Kohl, P., 2010. Measurement and analysis of sarcomere length in rat cardiomyocytes in situ and in vitro. *Am. J. Physiol. - Hear. Circ. Physiol.* 298, H1616–H1625.  
<https://doi.org/10.1152/ajpheart.00481.2009>

Buckberg, G., Hoffman, J.I.E., 2014. Right ventricular architecture responsible for mechanical performance: Unifying role of ventricular septum. *J. Thorac. Cardiovasc. Surg.* 148, 3166-3171.e4. <https://doi.org/10.1016/j.jtcvs.2014.05.044>

Burdette, W.J., Wilhelmi, A.E., 1946. Respiration of Heart Muscle Slices from Rats in the Terminal Stage of Hemorrhagic Shock. *Exp. Biol. Med.* 61, 411–413.  
<https://doi.org/10.3181/00379727-61-15336>

Burkhoff, D., Weiss, R.G., Schulman, S.P., Kalil-Filho, R., Wannenburg, T., Gerstenblith, G., 1991. Influence of metabolic substrate on rat heart function and metabolism at different coronary flows. *Am. J. Physiol. - Hear. Circ. Physiol.* 261.  
<https://doi.org/10.1152/ajpheart.1991.261.3.h741>

Burns, R.J., Gibbons, R.J., Yi, Q., Roberts, R.S., Miller, T.D., Schaer, G.L., Anderson, J.L., Yusuf, S., 2002. The relationships of left ventricular ejection fraction, end-systolic volume index and infarct size to six-month mortality after hospital discharge following myocardial infarction treated by thrombolysis. *J. Am. Coll. Cardiol.* 39, 30–36.  
[https://doi.org/10.1016/S0735-1097\(01\)01711-9](https://doi.org/10.1016/S0735-1097(01)01711-9)

Burrows, M.T., 1912. Rhythmical Activity of Isolated Heart Muscle Cells in Vitro, Source: Science.

Burstein, B., Comtois, P., Michael, G., Nishida, K., Villeneuve, L., Yeh, Y.H., Nattel, S.,

2009. Changes in connexin expression and the atrial fibrillation substrate in congestive heart failure. *Circ. Res.* 105, 1213–1222.  
<https://doi.org/10.1161/CIRCRESAHA.108.183400>
- Bussek, A., Schmidt, M., Bauriedl, J., Ravens, U., Wettwer, E., Lohmann, H., 2012. Cardiac tissue slices with prolonged survival for in vitro drug safety screening. *J. Pharmacol. Toxicol. Methods* 66, 145–51. <https://doi.org/10.1016/j.vascn.2011.12.002>
- Bussek, A., Wettwer, E., Christ, T., Lohmann, H., Camelliti, P., Ravens, U., 2009. Tissue slices from adult mammalian hearts as a model for pharmacological drug testing. *Cell. Physiol. Biochem.* 24, 527–536. <https://doi.org/10.1159/000257528>
- Calligaris, S.D., Lecanda, M., Solis, F., Ezquer, M., Gutiérrez, J., Brandan, E., Leiva, A., Sobrevia, L., Conget, P., 2013. Mice Long-Term High-Fat Diet Feeding Recapitulates Human Cardiovascular Alterations: An Animal Model to Study the Early Phases of Diabetic Cardiomyopathy. *PLoS One* 8. <https://doi.org/10.1371/journal.pone.0060931>
- Calvo, D., Atienza, F., Jalife, J., Martínez-Alzamora, N., Bravo, L., Almendral, J., González-Torrecilla, E., Arenal, N., Bermejo, J., Fernández-Avilé, F., Berenfeld, O., 2012. High-rate pacing-induced atrial fibrillation effectively reveals properties of spontaneously occurring paroxysmal atrial fibrillation in humans. *Eur. Soc. Cardiol.* 1560–1566.  
<https://doi.org/10.1093/europace/eus180>
- Camelliti, P., Al-Saud, S.A., Smolenski, R.T., Al-Ayoubi, S., Bussek, A., Wettwer, E., Banner, N.R., Bowles, C.T., Yacoub, M.H., Terracciano, C.M., 2011a. Adult human heart slices are a multicellular system suitable for electrophysiological and pharmacological studies. *J. Mol. Cell. Cardiol.* 51, 390–398.  
<https://doi.org/10.1016/j.yjmcc.2011.06.018>
- Camelliti, P., Al-Saud, S.A., Smolenski, R.T., Al-Ayoubi, S., Bussek, A., Wettwer, E.,

Banner, N.R., Bowles, C.T., Yacoub, M.H., Terracciano, C.M., 2011b. Adult human heart slices are a multicellular system suitable for electrophysiological and pharmacological studies. *J. Mol. Cell. Cardiol.* 51, 390–398.  
<https://doi.org/10.1016/J.YJMCC.2011.06.018>

Camelliti, P., Al-Saud, S.A., Smolenski, R.T., Al-Ayoubi, S., Bussek, A., Wettwer, E., Banner, N.R., Bowles, C.T., Yacoub, M.H., Terracciano, C.M., 2011c. Adult human heart slices are a multicellular system suitable for electrophysiological and pharmacological studies. *J. Mol. Cell. Cardiol.* 51, 390–8.  
<https://doi.org/10.1016/j.yjmcc.2011.06.018>

Camelliti, P., Al-Saud, S.A., Smolenski, R.T., Al-Ayoubi, S., Bussek, A., Wettwer, E., Banner, N.R., Bowles, C.T., Yacoub, M.H., Terracciano, C.M., 2011d. Adult human heart slices are a multicellular system suitable for electrophysiological and pharmacological studies. *J. Mol. Cell. Cardiol.* 51, 390–398.  
<https://doi.org/10.1016/J.YJMCC.2011.06.018>

Cao, J., Dai, D.L., Yao, L., Yu, H.H., Ning, B., Zhang, Q., Chen, J., Cheng, W.H., Shen, W., Yang, Z.X., 2012. Saturated fatty acid induction of endoplasmic reticulum stress and apoptosis in human liver cells via the PERK/ATF4/CHOP signaling pathway. *Mol. Cell. Biochem.* 364, 115–129. <https://doi.org/10.1007/s11010-011-1211-9>

Cao, N., Liu, Z., Chen, Z., Wang, J., Chen, T., Zhao, X., Ma, Y., Qin, L., Kang, J., Wei, B., Wang, L., Jin, Y., Yang, H.T., 2012. Ascorbic acid enhances the cardiac differentiation of induced pluripotent stem cells through promoting the proliferation of cardiac progenitor cells. *Cell Res.* 22, 219–236. <https://doi.org/10.1038/cr.2011.195>

Capogrossi, M.C., Houser, S.R., Bahinski, A., Lakatta, E.G., 1987. Synchronous Occurrence of Spontaneous Localized Calcium Release From the Sarcoplasmic Reticulum Generates

Action Potentials in Rat Cardiac Ventricular Myocytes at Normal Resting Membrane Potential.

Carlsen, F., Knappeis, G.G., Buchthal, F., 1961. ULTRASTRUCTURE OF THE RESTING AND CONTRACTED STRIATED MUSCLE FIBER AT DIFFERENT DEGREES OF STRETCH. *J. Biophys. Biochem. Cytol.* 11, 95.

Carmeliet, P., Jain, R.K., 2000. Angiogenesis in cancer and other diseases. *Nature*.  
<https://doi.org/10.1038/35025220>

Carta, G., Murru, E., Banni, S., Manca, C., 2017. Palmitic acid: Physiological role, metabolism and nutritional implications. *Front. Physiol.*  
<https://doi.org/10.3389/fphys.2017.00902>

Carta, G., Murru, E., Lisai, S., Sirigu, A., Piras, A., Collu, M., Batetta, B., Gambelli, L., Banni, S., 2015. Dietary triacylglycerols with palmitic acid in the sn-2 position modulate levels of N-Acylethanolamides in rat tissues. *PLoS One* 10.  
<https://doi.org/10.1371/journal.pone.0120424>

Chablais, F., Veit, J., Rainer, G., Jawiska, A., 2011a. The zebrafish heart regenerates after cryoinjury-induced myocardial infarction. *BMC Dev. Biol.* 11, 21.  
<https://doi.org/10.1186/1471-213X-11-21>

Chablais, F., Veit, J., Rainer, G., Jawiska, A., 2011b. The zebrafish heart regenerates after cryoinjury-induced myocardial infarction. *BMC Dev. Biol.* 11, 21.  
<https://doi.org/10.1186/1471-213X-11-21>

Chalisova, N.I., Penniyainen, V.A., Nozdrachev, A.D., n.d. Regulatory effects of essential and nonessential amino acids on organotypic cultures of spleen and liver tissues. *Dokl. Biol. Sci. Proc. Acad. Sci. USSR, Biol. Sci. Sect.* 393, 488–91.

- Chang, C.L., Deckelbaum, R.J., 2013. Omega-3 fatty acids: Mechanisms underlying “protective effects” in atherosclerosis. *Curr. Opin. Lipidol.*  
<https://doi.org/10.1097/MOL.0b013e3283616364>
- Chen, L., Wang, Y., Pan, Y., Zhang, L., Shen, C., Qin, G., Ashraf, M., Weintraub, N., Ma, G., Tang, Y., 2013. Cardiac progenitor-derived exosomes protect ischemic myocardium from acute ischemia/reperfusion injury. *Biochem. Biophys. Res. Commun.* 431, 566–571. <https://doi.org/10.1016/j.bbrc.2013.01.015>
- Chen, T., Vunjak-Novakovic, G., 2018. In Vitro Models of Ischemia-Reperfusion Injury. *Regen. Eng. Transl. Med.* <https://doi.org/10.1007/s40883-018-0056-0>
- Chen, X., Cordes, J.S., Bradley, J.A., Sun, Z., Zhou, J., 2006. Use of arterially perfused rabbit ventricular wedge in predicting arrhythmogenic potentials of drugs. *J. Pharmacol. Toxicol. Methods* 54, 261–272. <https://doi.org/10.1016/j.vascn.2006.02.005>
- Chen, X., Yin, X.M., 2011. Coordination of autophagy and the proteasome in resolving endoplasmic reticulum stress. *Vet. Pathol.* 48, 245–253.  
<https://doi.org/10.1177/0300985810385154>
- Chitwood, W.R., Sink, J.D., Hill, R.C., Wechsler, A.S., Sabiston, D.C., 1979. The effects of hypothermia on myocardial oxygen consumption and transmural coronary blood flow in the potassium-arrested heart. *Ann. Surg.* 190, 106–116.  
<https://doi.org/10.1097/00000658-197907000-00022>
- Chowdhury, R.A., Tzortzis, K.N., Dupont, E., Selvadurai, S., Perbellini, F., Cantwell, C.D., Ng, F.S., Simon, A.R., Terracciano, C.M., Peters, N.S., 2018. Concurrent micro-to macro-cardiac electrophysiology in myocyte cultures and human heart slices. *Sci. Rep.* 8. <https://doi.org/10.1038/s41598-018-25170-9>



- Chudin, E., Goldhaber, J., Garfinkel, A., Weiss, J., Kogan, B., 1999. Intracellular Ca<sup>2+</sup> dynamics and the stability of ventricular tachycardia. *Biophys. J.* 77, 2930–2941.  
[https://doi.org/10.1016/S0006-3495\(99\)77126-2](https://doi.org/10.1016/S0006-3495(99)77126-2)
- Colombo, M., Raposo, G., Théry, C., 2014. Biogenesis, secretion, and intercellular interactions of exosomes and other extracellular vesicles. *Annu. Rev. Cell Dev. Biol.*  
<https://doi.org/10.1146/annurev-cellbio-101512-122326>
- Cordeiro, J.M., Greene, L., Heilmann, C., Antzelevitch, D., Antzelevitch, C., 2004. Transmural heterogeneity of calcium activity and mechanical function in the canine left ventricle. *Am. J. Physiol. - Hear. Circ. Physiol.* 286, 1471–1479.  
<https://doi.org/10.1152/ajpheart.00748.2003>
- Costa, A.R., Panda, N.C., Yong, S., Mayorga, M.E., Pawlowski, G.P., Fan, K., Penn, M.S., Laurita, K.R., 2012. Optical mapping of cryoinjured rat myocardium grafted with mesenchymal stem cells. *Am. J. Physiol. - Hear. Circ. Physiol.* 302, H270.  
<https://doi.org/10.1152/ajpheart.00019.2011>
- Couchonnal, L.F., Anderson, M.E., 2008. The Role of Calmodulin Kinase II in Myocardial Physiology and Disease. *Physiology* 23, 151–159.  
<https://doi.org/10.1152/physiol.00043.2007>
- Crain, S.M., 1966. Development of “Organotypic” Bioelectric Activities in Central Nervous Tissues During Maturation in Culture. *Int. Rev. Neurobiol.* 9, 1–43.  
[https://doi.org/10.1016/S0074-7742\(08\)60135-X](https://doi.org/10.1016/S0074-7742(08)60135-X)
- Cross, H.R., West, R.L., Dutson, T.R., 1981. Comparison of methods for measuring sarcomere length in beef semitendinosus muscle. *Meat Sci.* 5, 261–266.  
[https://doi.org/10.1016/0309-1740\(81\)90016-4](https://doi.org/10.1016/0309-1740(81)90016-4)

- Crossman, D.C., 2004. The pathophysiology of myocardial ischaemia. *Heart*.  
<https://doi.org/10.1136/hrt.2003.029017>
- Dale Abel, E., 2004. Glucose transport in the heart. *Front. Biosci.*  
<https://doi.org/10.2741/1216>
- Daniels, L.J., Wallace, R.S., Nicholson, O.M., Wilson, G.A., McDonald, F.J., Jones, P.P., Baldi, J.C., Lamberts, R.R., Erickson, J.R., 2018. Inhibition of calcium/calmodulin-dependent kinase II restores contraction and relaxation in isolated cardiac muscle from type 2 diabetic rats. *Cardiovasc. Diabetol.* 17, 89. <https://doi.org/10.1186/s12933-018-0732-x>
- Danowski, B.A., Imanaka-Yoshida, K., Sanger, J.M., Sanger, J.W., 1992. Costameres are sites of force transmission to the substratum in adult rat cardiomyocytes. *J. Cell Biol.* 118, 1411–1419. <https://doi.org/10.1083/jcb.118.6.1411>
- Davidson, M.M., Nesti, C., Palenzuela, L., Walker, W.F., Hernandez, E., Protas, L., Hirano, M., Isaac, N.D., 2005. Novel cell lines derived from adult human ventricular cardiomyocytes. *J. Mol. Cell. Cardiol.* 39, 133–147.  
<https://doi.org/10.1016/j.yjmcc.2005.03.003>
- De Bakker, J.M.T., Van Capelle, F.J.L., Janse, M.J., Wilde, A.A.M., Coronel, R., Becker, A.E., Dingemans, K.P., Van Hemel, N.M., Hauer, R.N.W., 1988. Reentry as a cause of ventricular tachycardia in patients with chronic ischemic heart disease: Electrophysiology and anatomic correlation. *Circulation* 77, 589–606.  
<https://doi.org/10.1161/01.CIR.77.3.589>
- de Lange, W.J., Grimes, A.C., Hegge, L.F., Ralphe, C.J., 2013. Ablation of cardiac myosin-binding protein-C accelerates contractile kinetics in engineered cardiac tissue. *J. Gen. Physiol.* 141, 73–84. <https://doi.org/10.1085/jgp.201210837>

- De Tombe, P.P., Little, W.C., 1994. Inotropic effects of ejection are myocardial properties. *Am. J. Physiol. - Hear. Circ. Physiol.* 266.  
<https://doi.org/10.1152/ajpheart.1994.266.3.h1202>
- Deatheragea, B.L., Cooksona, B.T., 2012. Membrane vesicle release in bacteria, eukaryotes, and archaea: A conserved yet underappreciated aspect of microbial life. *Infect. Immun.*  
<https://doi.org/10.1128/IAI.06014-11>
- Denis, A., Sacher, F., Derval, N., Lim, H.S., Cochet, H., Shah, A.J., Daly, M., Pillois, X., Ramoul, K., Komatsu, Y., Zemmoura, A., Amraoui, S., Ritter, P., Ploux, S., Bordachar, P., Hocini, M., Jaïs, P., Haïssaguerre, M., 2014. Diagnostic Value of Isoproterenol Testing in Arrhythmogenic Right Ventricular Cardiomyopathy. *Circ. Arrhythmia Electrophysiol.* 7, 590–597. <https://doi.org/10.1161/CIRCEP.113.001224>
- Denning, C., Borgdorff, V., Crutchley, J., Firth, K.S.A., George, V., Kalra, S., Kondrashov, A., Hoang, M.D., Mosqueira, D., Patel, A., Prodanov, L., Rajamohan, D., Skarnes, W.C., Smith, J.G.W., Young, L.E., 2016. Cardiomyocytes from human pluripotent stem cells: From laboratory curiosity to industrial biomedical platform. *Biochim. Biophys. Acta - Mol. Cell Res.* 1863, 1728–1748. <https://doi.org/10.1016/j.bbamcr.2015.10.014>
- Desantiago, J., Ai, X., Islam, M., Acuna, G., Ziolo, M.T., Bers, D.M., Pogwizd, S.M., 2008. Arrhythmogenic effects of  $\beta_2$ -adrenergic stimulation in the failing heart are attributable to enhanced sarcoplasmic reticulum Ca load. *Circ. Res.* 102, 1389–1397.  
<https://doi.org/10.1161/CIRCRESAHA.107.169011>
- Di Diego, J.M., Sicouri, S., Myles, R.C., Burton, F.L., Smith, G.L., Antzelevitch, C., 2013. Optical and electrical recordings from isolated coronary-perfused ventricular wedge preparations. *J. Mol. Cell. Cardiol.* 54, 53–64.  
<https://doi.org/10.1016/j.yjmcc.2012.10.017>

- Diakos, N.A., Selzman, C.H., Sachse, F.B., Stehlik, J., Kfoury, A.G., Wever-Pinzon, O., Catino, A., Alharethi, R., Reid, B.B., Miller, D. V., Salama, M., Zaitsev, A. V., Shibayama, J., Li, H., Fang, J.C., Li, D.Y., Drakos, S.G., 2014. Myocardial atrophy and chronic mechanical unloading of the failing human heart: Implications for cardiac assist device-induced myocardial recovery. *J. Am. Coll. Cardiol.* 64, 1602–1612.  
<https://doi.org/10.1016/j.jacc.2014.05.073>
- Dickhout, J.G., Carlisle, R.E., Austin, R.C., 2011. Interrelationship between cardiac hypertrophy, heart failure, and chronic kidney disease: Endoplasmic reticulum stress as a mediator of pathogenesis. *Circ. Res.*  
<https://doi.org/10.1161/CIRCRESAHA.110.226803>
- Disertori, M., Masè, M., Ravelli, F., 2017. Myocardial fibrosis predicts ventricular tachyarrhythmias. *Trends Cardiovasc. Med.* <https://doi.org/10.1016/j.tcm.2017.01.011>
- Doenst, T., Nguyen, T.D., Abel, E.D., 2013. Cardiac metabolism in heart failure: implications beyond ATP production. *Circ. Res.* 113, 709–24.  
<https://doi.org/10.1161/CIRCRESAHA.113.300376>
- Dos Remedios, C.G., Chhabra, D., Kekic, M., Dedova, I. V., Tsubakihara, M., Berry, D.A., Nosworthy, N.J., 2003. Actin binding proteins: Regulation of cytoskeletal microfilaments. *Physiol. Rev.* <https://doi.org/10.1152/physrev.00026.2002>
- Dougherty, J.A., Patel, N., Kumar, N., Rao, S.G., Angelos, M.G., Singh, H., Cai, C., Khan, M., 2020. Human Cardiac Progenitor Cells Enhance Exosome Release and Promote Angiogenesis Under Physoxia. *Front. Cell Dev. Biol.* 8, 130.  
<https://doi.org/10.3389/fcell.2020.00130>
- Drake, K.J., Sidorov, V.Y., McGuinness, O.P., Wasserman, D.H., Wikswo, J.P., 2012. Amino acids as metabolic substrates during cardiac ischemia. *Exp. Biol. Med.*

(Maywood). 237, 1369–78. <https://doi.org/10.1258/ebm.2012.012025>

Duran, J.M., Taghavi, S., Berretta, R.M., Makarewich, C.A., Sharp, T., Starosta, T., Udeshi, F., George, J.C., Kubo, H., Houser, S.R., 2012. A Characterization and Targeting of the Infarct Border Zone in a Swine Model of Myocardial Infarction. *Clin. Transl. Sci.* 5, 416–421. <https://doi.org/10.1111/j.1752-8062.2012.00432.x>

Ericsson, A.C., Crim, M.J., Franklin, C.L., 2013. A brief history of animal modeling. *Mo. Med.* 110, 201–205.

Eschenhagen, T., Fink, C., Remmers, U., Scholz, H., Wattachow, J., Weil, J., Zimmermann, W., Dohmen, H.H., Schäfer, H., Bishopric, N., Wakatsuki, T., Elson, E.L., 1997. Three-dimensional reconstitution of embryonic cardiomyocytes in a collagen matrix: a new heart muscle model system. *FASEB J.* 11, 683–694.  
<https://doi.org/10.1096/fasebj.11.8.9240969>

Fedida, David, Gilest, W.R., Fedida, D, Giles, W.R., 1991. REGIONAL VARIATIONS IN ACTION POTENTIALS AND TRANSIENT OUTWARD CURRENT IN MYOCYTES ISOLATED FROM RABBIT LEFT VENTRICLE, *Journal of Physiology*.

Feinberg, A.W., Ripplinger, C.M., Van Der Meer, P., Sheehy, S.P., Domian, I., Chien, K.R., Parker, K.K., 2013. Functional differences in engineered myocardium from embryonic stem cell-derived versus neonatal cardiomyocytes. *Stem Cell Reports* 1, 387–396.  
<https://doi.org/10.1016/j.stemcr.2013.10.004>

Feng, Y., Cheng, J., Wei, B., Wang, Y., 2017. CaMKII inhibition reduces isoproterenol-induced ischemia and arrhythmias in hypertrophic mice, *Oncotarget*.

Feyen, D.A.M., Mckeithan, W.L., Bruyneel, A.A.N., Eschenhagen, T., Metallo, C.M.,

- Correspondence, M.M., Spiering, S., Hö, L., Rbel Ulmer, B., Zhang, H., Briganti, F., Schweizer, M., Hegyi, B., Liao, Z., Pö, R.-P., Nen, L., Ginsburg, K.S., Lam, C.K., Serrano, R., Wahlquist, C., Kreymerman, A., Vu, M., Amatya, P.L., Behrens, C.S., Ranjbarvaziri, S., Maas, R.G.C., Greenhaw, M., Bernstein, D., Wu, J.C., Bers, D.M., Mercola, M., 2020. Metabolic Maturation Media Improve Physiological Function of Human iPSC-Derived Cardiomyocytes II Resource Metabolic Maturation Media Improve Physiological Function of Human iPSC-Derived Cardiomyocytes. *CellReports* 32, 107925. <https://doi.org/10.1016/j.celrep.2020.107925>
- Fischer, C., Milting, H., Fein, E., Reiser, E., Lu, K., Seidel, T., Schinner, C., Schwarzmayr, T., Schramm, R., Tomasi, R., Husse, B., Cao-Ehlker, X., Pohl, U., Dendorfer, A., 2019. Long-term functional and structural preservation of precision-cut human myocardium under continuous electromechanical stimulation in vitro. *Nat. Commun.* 10, 117. <https://doi.org/10.1038/s41467-018-08003-1>
- Fleischaker, R.J., Sinskey, A.J., 1981. Oxygen demand and supply in cell culture. *Eur. J. Appl. Microbiol. Biotechnol.* 12, 193–197. <https://doi.org/10.1007/BF00499486>
- Fontes, M.S.C., Van Veen, T.A.B., De Bakker, J.M.T., Van Rijen, H.V.M., 2012. Functional consequences of abnormal Cx43 expression in the heart. *Biochim. Biophys. Acta - Biomembr.* 1818, 2020–2029. <https://doi.org/10.1016/j.bbamem.2011.07.039>
- Frangogiannis, N.G., 2014. The immune system and the remodeling infarcted heart: Cell biological insights and therapeutic opportunities. *J. Cardiovasc. Pharmacol.* <https://doi.org/10.1097/FJC.0000000000000003>
- Frankenreiter, S., Bednarczyk, P., Kniess, A., Bork, N.I., Straubinger, J., Koprowski, P., Wrzosek, A., Mohr, E., Logan, A., Murphy, M.P., Gawaz, M., Krieg, T., Szewczyk, A., Nikolaev, V.O., Ruth, P., Lukowski, R., 2017. cGMP-Elevating Compounds and

Ischemic Conditioning Provide Cardioprotection Against Ischemia and Reperfusion Injury via Cardiomyocyte-Specific BK Channels. *Circulation* 136, 2337–2355.

<https://doi.org/10.1161/CIRCULATIONAHA.117.028723>

Franz, M.R., Bode, F., 2003. Mechano-electrical feedback underlying arrhythmias: The atrial fibrillation case. *Prog. Biophys. Mol. Biol.* 82, 163–174. [https://doi.org/10.1016/S0079-6107\(03\)00013-0](https://doi.org/10.1016/S0079-6107(03)00013-0)

Fried, S.I., Lasker, A.C.W., Desai, N.J., Eddington, D.K., Rizzo, J.F., 2009. Axonal sodium-channel bands shape the response to electric stimulation in retinal ganglion cells. *J. Neurophysiol.* 101, 1972–1987. <https://doi.org/10.1152/jn.91081.2008>

Fritzen, A.M., Lundsgaard, A.M., Kiens, B., 2020. Tuning fatty acid oxidation in skeletal muscle with dietary fat and exercise. *Nat. Rev. Endocrinol.* 16, 683–696. <https://doi.org/10.1038/s41574-020-0405-1>

Fromm, H.J., 1975. *The Effect of Temperature and pH on Enzyme Activity*. Springer Berlin Heidelberg, pp. 201–235. [https://doi.org/10.1007/978-3-642-80966-8\\_8](https://doi.org/10.1007/978-3-642-80966-8_8)

Fuchs, F., Smith, S.H., 2001. Calcium, Cross-Bridges, and the Frank-Starling Relationship. *Physiology* 16, 5–10. <https://doi.org/10.1152/physiologyonline.2001.16.1.5>

Fukai, T., Ushio-Fukai, M., 2011. Superoxide dismutases: Role in redox signaling, vascular function, and diseases. *Antioxidants Redox Signal.* <https://doi.org/10.1089/ars.2011.3999>

Galbiati, F., Engelman, J.A., Volonte, D., Zhang, X.L., Minetti, C., Li, M., Hou, H., Kneitz, B., Edelmann, W., Lisanti, M.P., 2001. Caveolin-3 Null Mice Show a Loss of Caveolae, Changes in the Microdomain Distribution of the Dystrophin-Glycoprotein Complex, and T-tubule Abnormalities. *J. Biol. Chem.* 276, 21425–21433.

<https://doi.org/10.1074/jbc.M100828200>

Gallet, R., Dawkins, J., Valle, J., Simsolo, E., De Couto, G., Middleton, R., Tseliou, E., Luthringer, D., Kreke, M., Smith, R.R., Marbán, L., Ghaleh, B., Marbán, E., 2017. Exosomes secreted by cardiosphere-derived cells reduce scarring, attenuate adverse remodelling, and improve function in acute and chronic porcine myocardial infarction. *Eur. Heart J.* 38, 201–211. <https://doi.org/10.1093/eurheartj/ehw240>

Garcia-Dorado, D., Ruiz-Meana, M., 2000. Propagation of cell death during myocardial reperfusion. *News Physiol. Sci.* 15, 326–330. <https://doi.org/10.1152/physiologyonline.2000.15.6.326>

Garcia-Dorado, D., Ruiz-Meana, M., Insete, J., Rodriguez-Sinovas, A., Piper, H.M., n.d. Calcium-mediated cell death during myocardial reperfusion. <https://doi.org/10.1093/cvr/cvs116>

Garoffolo, G., Pesce, M., 2019. Mechanotransduction in the Cardiovascular System: From Developmental Origins to Homeostasis and Pathology. *Cells.* <https://doi.org/10.3390/cells8121607>

Gartz, M., Strande, J.L., 2018. Examining the Paracrine Effects of Exosomes in Cardiovascular Disease and Repair. <https://doi.org/10.1161/JAHA.117.007954>

Gélinas, R., Mailleux, F., Dontaine, J., Bultot, L., Demeulder, B., Ginion, A., Daskalopoulos, E.P., Esfahani, H., Dubois-Deruy, E., Lauzier, B., Gauthier, C., Olson, A.K., Bouchard, B., Des Rosiers, C., Viollet, B., Sakamoto, K., Balligand, J.L., Vanoverschelde, J.L., Beauloye, C., Horman, S., Bertrand, L., 2018. AMPK activation counteracts cardiac hypertrophy by reducing O-GlcNAcylation. *Nat. Commun.* 9. <https://doi.org/10.1038/s41467-017-02795-4>



- Gertz, E.W., Wisneski, J.A., Stanley, W.C., Neese, R.A., 1988. Myocardial substrate utilization during exercise in humans. Dual carbon-labeled carbohydrate isotope experiments. *J. Clin. Invest.* 82, 2017–2025. <https://doi.org/10.1172/JCI113822>
- Gherardi, G., Nogara, L., Ciciliot, S., Fadini, G.P., Blaauw, B., Braghetta, P., Bonaldo, P., De Stefani, D., Rizzuto, R., Mammucari, C., 2019. Loss of mitochondrial calcium uniporter rewires skeletal muscle metabolism and substrate preference. *Cell Death Differ.* 26, 362–381. <https://doi.org/10.1038/s41418-018-0191-7>
- Gherghiceanu, M., Barad, L., Novak, A., Reiter, I., Itskovitz-Eldor, J., Binah, O., Popescu, L.M., 2011. Cardiomyocytes derived from human embryonic and induced pluripotent stem cells: Comparative ultrastructure. *J. Cell. Mol. Med.* 15, 2539–2551. <https://doi.org/10.1111/j.1582-4934.2011.01417.x>
- Ghigo, A., Franco, I., Morello, F., Hirsch, E., 2014. Myocyte signalling in leucocyte recruitment to the heart. *Cardiovasc. Res.* <https://doi.org/10.1093/cvr/cvu030>
- Gibb, A.A., Hill, B.G., 2018. Metabolic coordination of physiological and pathological cardiac remodeling. *Circ. Res.* <https://doi.org/10.1161/CIRCRESAHA.118.312017>
- Giordano, F.J., 2005. Oxygen, oxidative stress, hypoxia, and heart failure. *J. Clin. Invest.* <https://doi.org/10.1172/JCI200524408>
- Giorgi, C., Marchi, S., Pinton, P., 2018. The machineries, regulation and cellular functions of mitochondrial calcium. *Nat. Rev. Mol. Cell Biol.* <https://doi.org/10.1038/s41580-018-0052-8>
- Glancy, B., Hartnell, L.M., Malide, D., Yu, Z.-X., Combs, C.A., Connelly, P.S., Subramaniam, S., Balaban, R.S., 2015. Mitochondrial reticulum for cellular energy distribution in muscle. *Nature* 523, 617–620. <https://doi.org/10.1038/nature14614>

- Glatz, J.F.C., Luiken, J.J.F.P., 2018. Dynamic role of the transmembrane glycoprotein CD36 (SR-B2) in cellular fatty acid uptake and utilization, *Journal of Lipid Research Thematic review series on Lipid Transfer Proteins*.
- González-Rosa, J.M., Martín, V., Peralta, M., Torres, M., Mercader, N., 2011a. Extensive scar formation and regression during heart regeneration after cryoinjury in zebrafish. *Development* 138, 1663–1674. <https://doi.org/10.1242/dev.060897>
- González-Rosa, J.M., Martín, V., Peralta, M., Torres, M., Mercader, N., 2011b. Extensive scar formation and regression during heart regeneration after cryoinjury in zebrafish. *Development* 138, 1663–74. <https://doi.org/10.1242/dev.060897>
- Gonzalez, F., Huangfu, D., 2015. Mechanisms underlying the formation of induced pluripotent stem cells. *Wiley Interdiscip. Rev. Dev. Biol.* 5. <https://doi.org/10.1002/wdev.206>
- Gordon, A.M., Huxley, A.F., Julian, F.J., 1966. The variation in isometric tension with sarcomere length in vertebrate muscle fibres. *J. Physiol.* 184, 170–192. <https://doi.org/10.1113/jphysiol.1966.sp007909>
- Gorenk, B., Lundqvist, B., Carina, T., Josep, B., John Camm, A., 2014. Cardiac arrhythmias in acute coronary syndromes. *EuroIntervention* 10, 1–21. [https://doi.org/10.4244/EIJY14M08\\_19](https://doi.org/10.4244/EIJY14M08_19)
- Gourdie, R.G., Severs, N.J., Green, C.R., Rothery, S., Germroth, P., Thompson, R.P., 1993. The spatial distribution and relative abundance of gap-junctional connexin40 and connexin43 correlate to functional properties of components of the cardiac atrioventricular conduction system. *J. Cell Sci.* 105, 985–991.
- Goversen, B., van der Heyden, M.A.G., van Veen, T.A.B., de Boer, T.P., 2018. The

immature electrophysiological phenotype of iPSC-CMs still hampers in vitro drug screening: Special focus on I K1. *Pharmacol. Ther.* 183, 127–136.

<https://doi.org/10.1016/j.pharmthera.2017.10.001>

Grossman, W., Paulus, W.J., 2013. Myocardial stress and hypertrophy: A complex interface between biophysics and cardiac remodeling. *J. Clin. Invest.* 123, 3701–3703.

<https://doi.org/10.1172/JCI69830>

Guccione, J.M., McCULLOCH, A.D., Hunter, W.C., McCulloch, A.D., 1997. Anterior and posterior left ventricular sarcomere lengths behave similarly during ejection.

Güven, C., 2018. The effect of Diazoxide on norepinephrine-induced cardiac hypertrophy, in vitro. *Cell. Mol. Biol.* 64, 50–54. <https://doi.org/10.14715/cmb/2018.64.10.8>

Habeler, W., Peschanski, M., Monville, C., 2009a. Organotypic heart slices for cell transplantation and physiological studies. *Organogenesis* 5, 62–66.

Habeler, W., Pouillot, S., Plancheron, A., Pucéat, M., Peschanski, M., Monville, C., 2009b. An in vitro beating heart model for long-term assessment of experimental therapeutics.

*Cardiovasc. Res.* 81, 253–259. <https://doi.org/10.1093/cvr/cvn299>

Halbach, M., Pillekamp, F., Brockmeier, K., Hescheler, J., Müller-Ehmsen, J., Reppel, M., 2006. Ventricular Slices of Adult Mouse Hearts - a new Multicellular In Vitro Model for Electrophysiological Studies. *Cell. Physiol. Biochem.* 18, 1–8.

<https://doi.org/10.1159/000095132>

Halbach, M.D., Egert, U., Hescheler, J., Banach, K., 2003. Estimation of Action Potential Changes from Field Potential Recordings in Multicellular Mouse Cardiac Myocyte Cultures, Original Paper *Cell Physiol Biochem.*

Hallböck, M., Isaksson, O., Noresson, E., 1975. Consequences of Myocardial Structural

Adaptation on Left Ventricular Compliance and the Frank-Starling Relationship in Spontaneously Hypertensive Rats. *Acta Physiol. Scand.* 94, 259–270.

<https://doi.org/10.1111/j.1748-1716.1975.tb05885.x>

Hamdani, N., Kooij, V., Van Dijk, S., Merkus, D., Paulus, W.J., Dos Remedios, C., Duncker, D.J., Stienen, G.J.M., Van Der Velden, J., n.d. Sarcomeric dysfunction in heart failure.

<https://doi.org/10.1093/cvr/cvm079>

Hamel, F.G., Bennett, R.G., Upward, J.L., Duckworth, W.C., 2001. Insulin Inhibits Peroxisomal Fatty Acid Oxidation in Isolated Rat Hepatocytes <sup>1</sup>. *Endocrinology* 142, 2702–2706. <https://doi.org/10.1210/endo.142.6.8178>

Hamlin, R.L., Altschuld, R.A., 2011. Extrapolation from mouse to man. *Circ. Cardiovasc. Imaging.* <https://doi.org/10.1161/CIRCIMAGING.110.961979>

Hammerstedt, R.H., 1973. The use of dowex-1-borate to separate 3HOH from 2-3H-glucose. *Anal. Biochem.* 56, 292–293. [https://doi.org/10.1016/0003-2697\(73\)90192-9](https://doi.org/10.1016/0003-2697(73)90192-9)

Han, C.H., Guan, Z.B., Zhang, P.X., Fang, H.L., Li, L., Zhang, H.M., Zhou, F.J., Mao, Y.F., Liu, W.W., 2018. Oxidative stress induced necroptosis activation is involved in the pathogenesis of hyperoxic acute lung injury. *Biochem. Biophys. Res. Commun.* 495, 2178–2183. <https://doi.org/10.1016/j.bbrc.2017.12.100>

Harding, S.E., Vescovo, G., Kirby, M., Jones, S.M., Gurden, J., Poole-Wilson, P.A., 1988. Contractile responses of isolated adult rat and rabbit cardiac myocytes to isoproterenol and calcium. *J. Mol. Cell. Cardiol.* 20, 635–647. [https://doi.org/10.1016/S0022-2828\(88\)80121-4](https://doi.org/10.1016/S0022-2828(88)80121-4)

Harris, R.A., 2013. Glycolysis Overview, in: *Encyclopedia of Biological Chemistry: Second Edition.* Elsevier Inc., pp. 443–447. <https://doi.org/10.1016/B978-0-12-378630-2.00044->

- Harris, W.S., 2013. Are n-3 fatty acids still cardioprotective? *Curr. Opin. Clin. Nutr. Metab. Care.* <https://doi.org/10.1097/MCO.0b013e32835bf380>
- Hassan, M., Sheikh Ibrahim, H., Ellahham, S., 2019. Frailty in Myocardial Infarction Patients: A Paradigm Shift. <https://doi.org/10.35248/2329-6607.19.8.254>
- Hawley, J.A., Burke, L.M., Angus, D.J., Fallon, K.E., Martin, D.T., Febbraio, M.A., 2000. Effect of altering substrate availability on metabolism and performance during intense exercise. *Br. J. Nutr.* 84, 829–838. <https://doi.org/10.1017/S0007114500002440>
- He, S., Wen, Q., OShea, C., Muu-Min, R., Kou, K., Grassam-Rowe, A., Liu, Y., Tan, X., Ou, X., Camelliti, P., Pavlovic, D., Lei, M., 2019. A protocol for transverse cardiac slicing and optical mapping in murine heart. *Front. Physiol.* 10, 755. <https://doi.org/10.3389/fphys.2019.00755>
- Helmerhorst, H.J.F., Roos-Blom, M.J., Van Westerloo, D.J., De Jonge, E., 2015. Association between arterial hyperoxia and outcome in subsets of critical illness: A systematic review, meta-analysis, and meta-regression of cohort studies. *Crit. Care Med.* 43, 1508–1519. <https://doi.org/10.1097/CCM.0000000000000998>
- Henning, S.L., Wambolt, R.B., Schönekeess, B.O., Lopaschuk, G.D., Allard, M.F., 1996. Contribution of Glycogen to Aerobic Myocardial Glucose Utilization. *Circulation* 93, 1549–1555. <https://doi.org/10.1161/01.CIR.93.8.1549>
- Hesketh, G.G., Shah, M.H., Halperin, V.L., Cooke, C.A., Akar, F.G., Yen, T.E., Kass, D.A., MacHamer, C.E., Van Eyk, J.E., Tomaselli, G.F., 2010. Ultrastructure and regulation of lateralized connexin43 in the failing heart. *Circ. Res.* 106, 1153–1163. <https://doi.org/10.1161/CIRCRESAHA.108.182147>

- Hibberd, M.G., Jewell, B.R., 1982. Calcium- and length-dependent force production in rat ventricular muscle. *J. Physiol.* 329, 527–540.  
<https://doi.org/10.1113/jphysiol.1982.sp014317>
- Hinderer, S., Schenke-Layland, K., 2019. Cardiac fibrosis – A short review of causes and therapeutic strategies. *Adv. Drug Deliv. Rev.* <https://doi.org/10.1016/j.addr.2019.05.011>
- Hinz, B., Pittet, P., Smith-Clerc, J., Chaponnier, C., Meister, J.J., 2004. Myofibroblast development is characterized by specific cell-cell adherens junctions. *Mol. Biol. Cell* 15, 4310–4320. <https://doi.org/10.1091/mbc.E04-05-0386>
- Hoes, M.F., Bomer, N., van der Meer, P., 2019. Concise Review: The Current State of Human In Vitro Cardiac Disease Modeling: A Focus on Gene Editing and Tissue Engineering. *Stem Cells Transl. Med.* 8, 66–74. <https://doi.org/10.1002/sctm.18-0052>
- Hoffman, B.F., Penefsky, Z.J., 1962. Effects of stretch on mechanical and electrical properties of cardiac muscle<sup>1</sup>’2 Effects on mechanical and electrical properties of cardiac muscle.
- Hofmann, P.A., Fuchs, F., 1988. Bound calcium and force development in skinned cardiac muscle bundles: Effect of sarcomere length. *J. Mol. Cell. Cardiol.* 20, 667–677.  
[https://doi.org/10.1016/S0022-2828\(88\)80012-9](https://doi.org/10.1016/S0022-2828(88)80012-9)
- Hong, K.U., Guo, Y., Li, Q.H., Cao, P., Al-Maqtari, T., Vajravelu, B.N., Du, J., Book, M.J., Zhu, X., Nong, Y., Bhatnagar, A., Bolli, R., 2014. c-kit<sup>+</sup> cardiac stem cells alleviate post-myocardial infarction left ventricular dysfunction despite poor engraftment and negligible retention in the recipient heart. *PLoS One* 9.  
<https://doi.org/10.1371/journal.pone.0096725>
- Hong, S.G., Kim, M.K., Jang, G., Oh, H.J., Park, J.E., Kang, J.T., Koo, O.J., Kim, T., Kwon,

- M.S., Koo, B.C., Ra, J.C., Kim, D.Y., Ko, C.M., Lee, B.C., 2009. Generation of red fluorescent protein transgenic dogs. *Genesis* 47, 314–322.  
<https://doi.org/10.1002/dvg.20504>
- Hopkins, E., Sharma, S., 2018. *Physiology , Acid Base Balance*.
- Hou, D., Youssef, E.A.S., Brinton, T.J., Zhang, P., Rogers, P., Price, E.T., Yeung, A.C., Johnstone, B.H., Yock, P.G., March, K.L., 2005. Radiolabeled cell distribution after intramyocardial, intracoronary, and interstitial retrograde coronary venous delivery: Implications for current clinical trials. *Circulation* 112.  
<https://doi.org/10.1161/CIRCULATIONAHA.104.526749>
- Huang, N.F., Serpooshan, V., Morris, V.B., Sayed, N., Pardon, G., Abilez, O.J., Nakayama, K.H., Pruitt, B.L., Wu, S.M., Yoon, Y. sup, Zhang, J., Wu, J.C., 2018. Big bottlenecks in cardiovascular tissue engineering. *Commun. Biol.* 1, 8–11.  
<https://doi.org/10.1038/s42003-018-0202-8>
- Ingwall, J.S., 2008. Energy metabolism in heart failure and remodelling. *Cardiovasc. Res.* 81, 412–419. <https://doi.org/10.1093/cvr/cvn301>
- Ingwall, J.S., 2002. ATP and the Heart: An Overview. pp. 3–6. [https://doi.org/10.1007/978-1-4615-1093-2\\_1](https://doi.org/10.1007/978-1-4615-1093-2_1)
- Ishida, A., Kameshita, I., Okuno, S., Kitani, T., Fujisawa, H., 1995. A novel highly specific and potent inhibitor of calmodulin-dependent protein kinase II. *Biochem. Biophys. Res. Commun.* 212, 806–812. <https://doi.org/10.1006/bbrc.1995.2040>
- Jain, A., Hasan, J., Desingu, P.A., Sundaresan, N.R., Chatterjee, K., 2018. Engineering an in vitro organotypic model for studying cardiac hypertrophy. *Colloids Surfaces B Biointerfaces* 165, 355–362. <https://doi.org/10.1016/j.colsurfb.2018.02.036>

- Janse, M.J., Cinca, J., Morena, H., Fiolet, J.W., Kléber, A.G., de Vries, G.P., Becker, A.E., Durrer, D., 1979. The “border zone” in myocardial ischemia. An electrophysiological, metabolic, and histochemical correlation in the pig heart. *Circ. Res.* 44, 576–588.  
<https://doi.org/10.1161/01.RES.44.4.576>
- Jeong, E.M., Liu, M., Sturdy, M., Gao, G., Varghese, S.T., Sovari, A.A., Dudley, S.C., 2012. Metabolic stress, reactive oxygen species, and arrhythmia. *J. Mol. Cell. Cardiol.*  
<https://doi.org/10.1016/j.yjmcc.2011.09.018>
- Jiang, Y., Park, P., Hong, S.M., Ban, K., 2018. Maturation of cardiomyocytes derived from human pluripotent stem cells: Current strategies and limitations. *Mol. Cells.*  
<https://doi.org/10.14348/molcells.2018.0143>
- Joris, P.J., Mensink, R.P., 2016. Role of cis-Monounsaturated Fatty Acids in the Prevention of Coronary Heart Disease. *Curr. Atheroscler. Rep.* <https://doi.org/10.1007/s11883-016-0597-y>
- Joshi, D.C., Bakowska, J.C., 2011. Determination of mitochondrial membrane potential and reactive oxygen species in live rat cortical neurons. *J. Vis. Exp.* 2704.  
<https://doi.org/10.3791/2704>
- Kahan, T., Bergfeldt, L., 2005. Left ventricular hypertrophy in hypertension: Its arrhythmogenic potential. *Heart* 91, 250–256. <https://doi.org/10.1136/hrt.2004.042473>
- Kalifa, J., Maixent, J.M., Chalvidan, T., Dalmaso, C., Colin, D., Cozma, D., Laurent, P., Deharo, J.C., Djiane, P., Cozzone, P., Bernard, M., 2008. Energetic metabolism during acute stretch-related atrial fibrillation. *Mol. Cell. Biochem.* 317, 69–75.  
<https://doi.org/10.1007/s11010-008-9832-3>
- Kalluri, R., LeBleu, V.S., 2020. The biology, function, and biomedical applications of



exosomes. *Science* (80-. ). <https://doi.org/10.1126/science.aau6977>

- Kalogeris, T., Baines, C.P., Krenz, M., Korthuis, R.J., n.d. *Cell Biology of Ischemia/Reperfusion Injury*. <https://doi.org/10.1016/B978-0-12-394309-5.00006-7>
- Kamoun, D., Behar, J., Leichner, J.M., Yaniv, Y., 2018. Bioenergetic Feedback between Heart Cell Contractile Machinery and Mitochondrial 3D Deformations. *Biophysj* 115, 1603–1613. <https://doi.org/10.1016/j.bpj.2018.08.039>
- Kaneko, M., R. Coppen, S., Fukushima, S., Yacoub, M.H., Suzuki, K., 2012a. Histological Validation of Heart Slices as a Model in Cardiac Research. *J Cell Sci Ther* 3. <https://doi.org/10.4172/2157-7013.1000126>
- Kaneko, M., R. Coppen, S., Fukushima, S., Yacoub, M.H., Suzuki, K., 2012b. Histological Validation of Heart Slices as a Model in Cardiac Research. *J. Cell Sci. Ther.* 03. <https://doi.org/10.4172/2157-7013.1000126>
- Kang, C., Qiao, Y., Li, G., Baechle, K., Camelliti, P., Rentschler, S., Efimov, I.R., 2016. Human Organotypic Cultured Cardiac Slices: New Platform For High Throughput Preclinical Human Trials. *Sci. Rep.* 6, 28798. <https://doi.org/10.1038/srep28798>
- Kanno, S., Saffitz, J.E., 2001. The role of myocardial gap junctions in electrical conduction and arrhythmogenesis. *Cardiovasc. Pathol.* [https://doi.org/10.1016/S1054-8807\(01\)00078-3](https://doi.org/10.1016/S1054-8807(01)00078-3)
- Kappler, B., Ledezma, C.A., Van Tuijl, S., Meijborg, V., Boukens, B.J., Ergin, B., Tan, P.J., Stijnen, M., Ince, C., Díaz-Zuccarini, V., De Mol, B.A.J.M., 2019. Investigating the physiology of normothermic ex vivo heart perfusion in an isolated slaughterhouse porcine model used for device testing and training. *BMC Cardiovasc. Disord.* 19. <https://doi.org/10.1186/s12872-019-1242-9>

- Katano, Y., Akera, T., Temma, K., Kennedy, R.H., 1984. ENHANCED OUABAIN SENSITIVITY OF THE HEART AND MYOCARDIAL SODIUM PUMP IN AGED RATS. *Eur. J. Pharmacol.* 105, 95–103.
- Katz, A.M., 2002. Ernest Henry Starling, his predecessors, and the “Law of the Heart”. *Circulation* 106, 2986–2992. <https://doi.org/10.1161/01.CIR.0000040594.96123.55>
- Kentish, J.C., Stienen, G.J., 1994. Differential effects of length on maximum force production and myofibrillar ATPase activity in rat skinned cardiac muscle. *J. Physiol.* 475, 175–184. <https://doi.org/10.1113/jphysiol.1994.sp020059>
- Khokhlova, A., Iribe, G., Katsnelson, L., Naruse, K., Solovyova, O., 2018. The effects of load on transmural differences in contraction of isolated mouse ventricular cardiomyocytes. *J. Mol. Cell. Cardiol.* 114, 276–287. <https://doi.org/10.1016/j.yjmcc.2017.12.001>
- Kicinska, A., Augustynek, B., Kulawiak, B., Jarmuszkiewicz, W., Szewczyk, A., Bednarczyk, P., 2016. A large-conductance calcium-regulated K<sup>+</sup> channel in human dermal fibroblast mitochondria. *Biochem. J.* 473, 4457–4471. <https://doi.org/10.1042/BCJ20160732>
- Kilic, A., Li, T., Nolan, T.D.C., Nash, J.R., Li, S., Prastein, D.J., Schwartzbauer, G., Moainie, S.L., Yankey, G.K., Defilippi, C., Wu, Z., Griffith, B.P., 2006. Strain-related regional alterations of calcium-handling proteins in myocardial remodeling. <https://doi.org/10.1016/j.jtcvs.2006.07.016>
- Kim, J.W., Tchernyshyov, I., Semenza, G.L., Dang, C. V., 2006. HIF-1-mediated expression of pyruvate dehydrogenase kinase: A metabolic switch required for cellular adaptation to hypoxia. *Cell Metab.* 3, 177–185. <https://doi.org/10.1016/j.cmet.2006.02.002>

- Kléber, A.G., 1990. Consequences of acute ischemia for the electrical and mechanical function of the ventricular myocardium. A brief review. *Experientia*.  
<https://doi.org/10.1007/BF01936928>
- Kléber, A.G., Rudy, Y., 2004. Basic Mechanisms of Cardiac Impulse Propagation and Associated Arrhythmias. *Physiol. Rev.* <https://doi.org/10.1152/physrev.00025.2003>
- Knöll, R., Hoshijima, M., Hoffman, H.M., Person, V., Lorenzen-Schmidt, I., Bang, M.L., Hayashi, T., Shiga, N., Yasukawa, H., Schaper, W., McKenna, W., Yokoyama, M., Schork, N.J., Omens, J.H., McCulloch, A.D., Kimura, A., Gregorio, C.C., Poller, W., Schaper, J., Schultheiss, H.P., Chien, K.R., 2002. The cardiac mechanical stretch sensor machinery involves a Z disc complex that is defective in a subset of human dilated cardiomyopathy. *Cell* 111, 943–955. [https://doi.org/10.1016/S0092-8674\(02\)01226-6](https://doi.org/10.1016/S0092-8674(02)01226-6)
- Kolwicz, S.C., Purohit, S., Tian, R., 2013. Cardiac metabolism and its interactions with contraction, growth, and survival of cardiomyocytes. *Circ. Res.*  
<https://doi.org/10.1161/CIRCRESAHA.113.302095>
- Komamura, K., Shannon, R.P., Ihara, T., Shen, Y.T., Mirsky, I., Bishop, S.P., Vatner, S.F., 1993. Exhaustion of Frank-Starling mechanism in conscious dogs with heart failure. *Am. J. Physiol. - Hear. Circ. Physiol.* 265.  
<https://doi.org/10.1152/ajpheart.1993.265.4.h1119>
- Korvald, C., Elvenes, O.P., Myrnes, T., 2000. Myocardial substrate metabolism influences left ventricular energetics in vivo. *Am. J. Physiol. - Hear. Circ. Physiol.* 278.  
<https://doi.org/10.1152/ajpheart.2000.278.4.h1345>
- Kraft, F., Andel, H., Gamper, J., Markstaller, K., Ullrich, R., Klein, K.U., 2018. Incidence of hyperoxia and related in-hospital mortality in critically ill patients: a retrospective data analysis. *Acta Anaesthesiol. Scand.* 62, 347–356. <https://doi.org/10.1111/aas.13047>

- Krenek, P., Kmecova, J., Kucerova, D., Bajuszova, Z., Musil, P., Gazova, A., Ochodnický, P., Klimas, J., Kyselovic, J., 2009. Isoproterenol-induced heart failure in the rat is associated with nitric oxide-dependent functional alterations of cardiac function. *Eur. J. Heart Fail.* 11, 140–146. <https://doi.org/10.1093/eurjhf/hfn026>
- Krogh, A., 1919. The supply of oxygen to the tissues and the regulation of the capillary circulation. *J. Physiol.* 52, 457–474. <https://doi.org/10.1113/jphysiol.1919.sp001844>
- Kubalova, Z., Terentyev, D., Viatchenko-Karpinski, S., Nishijima, Y., Györke, I., Terentyeva, R., Da Cunha, D.N.Q., Sridhar, A., Feldman, D.S., Hamlin, R.L., Carnes, C.A., Györke, S., 2005. Abnormal intrastore calcium signaling in chronic heart failure. *Proc. Natl. Acad. Sci. U. S. A.* 102, 14104–14109. <https://doi.org/10.1073/pnas.0504298102>
- Kumar, M., Kasala, E.R., Bodduluru, L.N., Dahiya, V., Sharma, D., Kumar, V., Lahkar, M., 2016. Animal models of myocardial infarction: Mainstay in clinical translation. *Regul. Toxicol. Pharmacol.* 76, 221–230. <https://doi.org/10.1016/j.yrtph.2016.03.005>
- Kung, G.L., Vaseghi, M., Gahm, J.K., Shevtsov, J., Garfinkel, A., Shivkumar, K., Ennis, D.B., 2018. Microstructural infarct border zone remodeling in the post-infarct swine heart measured by diffusion tensor MRI. *Front. Physiol.* 9, 826. <https://doi.org/10.3389/fphys.2018.00826>
- L Janssen, P.M., Lehnart, S.E., rgen Prestle, J., Hasenfuss, G., 1999. Preservation of Contractile Characteristics of Human Myocardium in Multi-day Cell Culture. *J Mol Cell Cardiol J. Mol. Cell. Cardiol.* 31, 1419–1427.
- Laher, I., Yang, H.-T., Cai, B., Yuan, Y., Du, W., Liu, J., Ma, W., Zhang, L., Du, Z., 2018. Stem Cell-Derived Exosome in Cardiovascular Diseases: Macro Roles of Micro Particles. *Front. Pharmacol.* | [www.frontiersin.org](http://www.frontiersin.org) 1, 547.

<https://doi.org/10.3389/fphar.2018.00547>

Lederer, W.J., Tsien, R.W., 1976. Transient inward current underlying arrhythmogenic effects of cardiotonic steroids in Purkinje fibres. *J. Physiol.* 263, 73–100.

<https://doi.org/10.1113/jphysiol.1976.sp011622>

Legrice, I.J., Smaill, B.H., Chai, L.Z., Edgar, S.G., Gavin, J.B., Hunter, P.J., n.d. Laminar structure of the heart: ventricular myocyte arrangement and connective tissue architecture in the dog.

Lehman, J.J., Kelly, D.P., 2002. Gene regulatory mechanisms governing energy metabolism during cardiac hypertrophic growth. *Heart Fail. Rev.*

<https://doi.org/10.1023/A:1015332726303>

Lelovas, P.P., Kostomitsopoulos, N.G., Xanthos, T.T., 2014. A comparative anatomic and physiologic overview of the porcine heart. *J. Am. Assoc. Lab. Anim. Sci.* 53, 432–438.

Leung, A.F., 1982. Laser diffraction of single intact cardiac muscle cells at rest. *J. Muscle Res. Cell Motil.* 3, 399–418. <https://doi.org/10.1007/BF00712091>

Leychenko, A., Konorev, E., Jijiwa, M., Matter, M.L., 2011. Stretch-Induced hypertrophy activates NFkB-Mediated VEGF secretion in adult cardiomyocytes. *PLoS One* 6.

<https://doi.org/10.1371/journal.pone.0029055>

Li, D., Wu, J., Bai, Y., Zhao, X., Liu, L., 2014. Isolation and culture of adult mouse cardiomyocytes for cell signaling and in vitro cardiac hypertrophy. *J. Vis. Exp.* 87,

51357. <https://doi.org/10.3791/51357>

Li, R.A., Keung, W., Cashman, T.J., Backeris, P.C., Johnson, B. V., Bardot, E.S., Wong, A.O.T., Chan, P.K.W., Chan, C.W.Y., Costa, K.D., 2018. Bioengineering an electro-mechanically functional miniature ventricular heart chamber from human pluripotent

stem cells. *Biomaterials* 163, 116–127.

<https://doi.org/10.1016/j.biomaterials.2018.02.024>

Li, R.K., Jia, Z.Q., Weisel, R.D., Merante, F., Mickle, D.A.G., 1999. Smooth muscle cell transplantation into myocardial scar tissue improves heart function. *J. Mol. Cell. Cardiol.* 31, 513–522. <https://doi.org/10.1006/jmcc.1998.0882>

Li, S., Pan, H., Tan, C., Sun, Y., Song, Y., Zhang, X., Yang, W., Wang, X., Li, D., Dai, Y., Ma, Q., Xu, C., Zhu, X., Kang, L., Fu, Y., Xu, X., Shu, J., Zhou, N., Han, F., Qin, D., Huang, W., Liu, Z., Yan, Q., 2018. Mitochondrial Dysfunctions Contribute to Hypertrophic Cardiomyopathy in Patient iPSC-Derived Cardiomyocytes with MT-RNR2 Mutation. *Stem Cell Reports* 10, 808–821. <https://doi.org/10.1016/j.stemcr.2018.01.013>

Li, X., Arslan, F., Ren, Y., Adav, S.S., Poh, K.K., Sorokin, V., Lee, C.N., De Kleijn, D., Lim, S.K., Sze, S.K., 2012. Metabolic adaptation to a disruption in oxygen supply during myocardial ischemia and reperfusion is underpinned by temporal and quantitative changes in the cardiac proteome. *J. Proteome Res.* 11, 2331–2346. <https://doi.org/10.1021/pr201025m>

Liao, R., Nascimben, L., Friedrich, J., Gwathmey, J.K., Ingwall, J.S., 1996. Decreased energy reserve in an animal model of dilated cardiomyopathy: Relationship to contractile performance. *Circ. Res.* 78, 893–902. <https://doi.org/10.1161/01.RES.78.5.893>

Lieber, R.L., Yeh, Y., Baskin, R.J., 1984. SARCOMERE LENGTH DETERMINATION USING LASER DIFFRACTION Effect of Beam and Fiber Diameter.

Lindsey, M.L., Bolli, R., Canty, J.M., Du, X.-J., Frangogiannis, N.G., Frantz, S., Gourdie, R.G., Holmes, J.W., Jones, S.P., Kloner, R.A., Lefer, D.J., Liao, R., Murphy, E., Ping, P., Przyklenk, K., Recchia, F.A., Schwartz Longacre, L., Ripplinger, C.M., Van Eyk,

J.E., Heusch, G., 2018a. Guidelines for experimental models of myocardial ischemia and infarction. *Am. J. Physiol. Circ. Physiol.* 314, H812–H838.

<https://doi.org/10.1152/ajpheart.00335.2017>

Lindsey, M.L., Bolli, R., Canty, J.M., Du, X.J., Frangogiannis, N.G., Frantz, S., Gourdie, R.G., Holmes, J.W., Jones, S.P., Kloner, R.A., Lefer, D.J., Liao, R., Murphy, E., Ping, P., Przyklenk, K., Recchia, F.A., Longacre, L.S., Ripplinger, C.M., Van Eyk, J.E., Heusch, G., 2018b. Guidelines for experimental models of myocardial ischemia and infarction. *Am. J. Physiol. - Hear. Circ. Physiol.*

<https://doi.org/10.1152/ajpheart.00335.2017>

Lindsey, M.L., Bolli, R., Canty, J.M., Du, X.J., Frangogiannis, N.G., Frantz, S., Gourdie, R.G., Holmes, J.W., Jones, S.P., Kloner, R.A., Lefer, D.J., Liao, R., Murphy, E., Ping, P., Przyklenk, K., Recchia, F.A., Longacre, L.S., Ripplinger, C.M., Van Eyk, J.E., Heusch, G., 2018c. Guidelines for experimental models of myocardial ischemia and infarction. *Am. J. Physiol. - Hear. Circ. Physiol.*

<https://doi.org/10.1152/ajpheart.00335.2017>

Lipp, P., Hiiser, J., Pott, L., Niggli, E., 1996. Spatially non-uniform CaO signals induced by the reduction of transverse tubules in citrate-loaded guinea-pig ventricular myocytes in culture, *Journal of Physiology*.

Litovsky, S.H., Antzelevitch, C., 1988. Transient outward current prominent in canine ventricular epicardium but not endocardium. *Circ. Res.* 62, 116–126.

<https://doi.org/10.1161/01.RES.62.1.116>

Liu, B., Lee, B.W., Nakanishi, K., Villasante, A., Williamson, R., Metz, J., Kim, J., Kanai, M., Bi, L., Brown, K., Di Paolo, G., Homma, S., Sims, P.A., Topkara, V.K., Vunjak-Novakovic, G., 2018. Cardiac recovery via extended cell-free delivery of extracellular

- vesicles secreted by cardiomyocytes derived from induced pluripotent stem cells. *Nat. Biomed. Eng.* 2, 293–303. <https://doi.org/10.1038/s41551-018-0229-7>
- Lo, C.W., 2000. Role of Gap Junctions in Cardiac Conduction and Development. *Circ. Res.* 87.
- Lo Cicero, A., Stahl, P.D., Raposo, G., 2015. Extracellular vesicles shuffling intercellular messages: For good or for bad. *Curr. Opin. Cell Biol.* <https://doi.org/10.1016/j.ceb.2015.04.013>
- Lodish, H., Berk, A., Zipursky, S.L., Matsudaira, P., Baltimore, D., Darnell, J., 2000. Oxidation of Glucose and Fatty Acids to CO<sub>2</sub>.
- Lohse, M.J., Engelhardt, S., Eschenhagen, T., 2003. What Is the Role of  $\beta$ -Adrenergic Signaling in Heart Failure? *Circ. Res.* <https://doi.org/10.1161/01.RES.0000102042.83024.CA>
- Lopaschuk, G.D., Barr, R.L., 1997. Measurements of fatty acid and carbohydrate metabolism in the isolated working rat heart. *Mol. Cell. Biochem. Cell Biochem* 172, 137–147.
- Lopaschuk, G.D., Belke, D.D., Gamble, J., Itoi, T., Schönekeess, B.O., 1994. Regulation of fatty acid oxidation in the mammalian heart in health and disease. *Biochim. Biophys. Acta* 1213, 263–76.
- Lopaschuk, G.D., Stanley, W.C., 1997. Glucose Metabolism in the Ischemic Heart. *Circulation* 95, 313–315. <https://doi.org/10.1161/01.CIR.95.2.313>
- Lou, Q., Janardhan, A., Efimov, I.R., 2012. Remodeling of Calcium Handling in Human Heart Failure. [https://doi.org/10.1007/978-94-007-2888-2\\_52](https://doi.org/10.1007/978-94-007-2888-2_52)
- Louch, W.E., Bito, V., Heinzl, F.R., Macianskiene, R., Vanhaecke, J., Flameng, W., Mubagwa, K., Sipido, K.R., 2004. Reduced synchrony of Ca<sup>2+</sup> release with loss of T-



- tubules - A comparison to Ca<sup>2+</sup> release in human failing cardiomyocytes. *Cardiovasc. Res.* 62, 63–73. <https://doi.org/10.1016/j.cardiores.2003.12.031>
- Louch, W.E., Sheehan, K.A., Wolska, B.M., 2011. Methods in cardiomyocyte isolation, culture, and gene transfer. *J. Mol. Cell. Cardiol.* <https://doi.org/10.1016/j.yjmcc.2011.06.012>
- Lutgens, E., Daemen, J.A.P., De Muinck, E.D., Debets, J., Leenders, P., Smits, J.F.M., 1999. Chronic myocardial infarction in the mouse: cardiac structural and functional changes. *Cardiovascular Research.*
- Machiraju, P., Greenway, S.C., 2019. Current methods for the maturation of induced pluripotent stem cell-derived cardiomyocytes. *World J. Stem Cells.* <https://doi.org/10.4252/wjsc.v11.i1.33>
- Macqueen, L.A., Sheehy, S.P., Chantre, C.O., Zimmerman, J.F., Pasqualini, F.S., Liu, X., Goss, J.A., Campbell, P.H., Gonzalez, G.M., Park, S.J., Capulli, A.K., Ferrier, J.P., Fettah Kosar, T., Mahadevan, L., Pu, W.T., Parker, K.K., 2018. A tissue-engineered scale model of the heart ventricle. *Nat. Biomed. Eng.* 2, 930–941. <https://doi.org/10.1038/s41551-018-0271-5>
- Maier, L.S., Bers, D.M., 2002. Calcium, calmodulin, and calcium-calmodulin kinase II: Heartbeat to heartbeat and beyond. *J. Mol. Cell. Cardiol.* <https://doi.org/10.1006/jmcc.2002.2038>
- Majid, Q.A., Fricker, A.T.R., Gregory, D.A., Davidenko, N., Hernandez Cruz, O., Jabbour, R.J., Owen, T.J., Basnett, P., Lukasiewicz, B., Stevens, M., Best, S., Cameron, R., Sinha, S., Harding, S.E., Roy, I., 2020. Natural Biomaterials for Cardiac Tissue Engineering: A Highly Biocompatible Solution. *Front. Cardiovasc. Med.* 7, 554597. <https://doi.org/10.3389/fcvm.2020.554597>

- Malatesha, G., Singh, N.K., Bharija, A., Rehani, B., Goel, A., 2007. Comparison of arterial and venous pH, bicarbonate, PCO<sub>2</sub> and PO<sub>2</sub> in initial emergency department assessment. *Emerg. Med. J.* 24, 569–571. <https://doi.org/10.1136/emj.2007.046979>
- Mancuso, A., Barone, A., Cristiano, M.C., Cianflone, E., Fresta, M., Paolino, D., 2020. Cardiac stem cell-loaded delivery systems: A new challenge for myocardial tissue regeneration. *Int. J. Mol. Sci.* 21, 1–21. <https://doi.org/10.3390/ijms21207701>
- Mannhardt, I., Breckwoldt, K., Letuffe-Brenière, D., Schaaf, S., Schulz, H., Neuber, C., Benzin, A., Werner, T., Eder, A., Schulze, T., Klampe, B., Christ, T., Hirt, M.N., Huebner, N., Moretti, A., Eschenhagen, T., Hansen, A., 2016. Human Engineered Heart Tissue: Analysis of Contractile Force. *Stem Cell Reports* 7, 29–42. <https://doi.org/10.1016/j.stemcr.2016.04.011>
- Marban, E., Kitakaze, M., Kusuoka, H., Porterfield, J.K., Yue, D.T., Chacko, V.P., 1987. Intracellular free calcium concentration measured with <sup>19</sup>F NMR spectroscopy in intact ferret hearts. *Proc. Natl. Acad. Sci. U. S. A.* 84, 6005–6009. <https://doi.org/10.1073/pnas.84.16.6005>
- Marban, E., Robinson, S.W., Wier, W.G., 1986. Mechanisms of arrhythmogenic delayed and early afterdepolarizations in ferret ventricular muscle. *J. Clin. Invest.* 78, 1185–1192. <https://doi.org/10.1172/JCI112701>
- Marín-Juez, R., Marass, M., Gauvrit, S., Rossi, A., Lai, S.L., Materna, S.C., Black, B.L., Stainier, D.Y.R., 2016. Fast revascularization of the injured area is essential to support zebrafish heart regeneration. *Proc. Natl. Acad. Sci. U. S. A.* 113, 11237–11242. <https://doi.org/10.1073/pnas.1605431113>
- Maring, J.A., Lodder, K., Mol, E., Verhage, V., Wiesmeijer, K.C., Dingenouts, C.K.E., Moerkamp, A.T., Deddens, J.C., Vader, P., Smits, A.M., Sluijter, J.P.G., Goumans,

- M.J., 2019. Cardiac Progenitor Cell–Derived Extracellular Vesicles Reduce Infarct Size and Associate with Increased Cardiovascular Cell Proliferation. *J. Cardiovasc. Transl. Res.* 12, 5–17. <https://doi.org/10.1007/s12265-018-9842-9>
- Maroli, G., Braun, T., 2020. The long and winding road of cardiomyocyte maturation. *Cardiovasc. Res.* 12, 1–15. <https://doi.org/10.1093/cvr/cvaa159>
- Martin, Y., Vermette, P., 2005. Bioreactors for tissue mass culture: Design, characterization, and recent advances. *Biomaterials* 26, 7481–7503. <https://doi.org/10.1016/j.biomaterials.2005.05.057>
- Masuda, S., Shimizu, T., 2016. Three-dimensional cardiac tissue fabrication based on cell sheet technology. *Adv. Drug Deliv. Rev.* <https://doi.org/10.1016/j.addr.2015.05.002>
- McClelland, G.B., Brooks, G.A., 2002. Changes in MCT 1, MCT 4, and LDH expression are tissue specific in rats after long-term hypobaric hypoxia. *J. Appl. Physiol.* 92, 1573–1584. <https://doi.org/10.1152/jappphysiol.01069.2001>
- McLimans, W.F., Crouse, E.J., Tunnah, K. V., Moore, G.E., 1968. Kinetics of gas diffusion in mammalian cell culture systems. I. Experimental. *Biotechnol. Bioeng.* 10, 725–740. <https://doi.org/10.1002/bit.260100603>
- McMurtrey, R.J., 2016. Analytic models of oxygen and nutrient diffusion, metabolism dynamics, and architecture optimization in three-dimensional tissue constructs with applications and insights in cerebral organoids. *Tissue Eng. - Part C Methods* 22, 221–249. <https://doi.org/10.1089/ten.tec.2015.0375>
- Medvedev, S.P., Shevchenko, A.I., Zakian, S.M., 2010. Induced Pluripotent Stem Cells: Problems and Advantages when Applying them in Regenerative Medicine. *Acta Naturae* 2, 18–27. <https://doi.org/10.32607/20758251-2010-2-2-18-27>

- Mehta, J.L., Li, D.Y., 1999. Inflammation in ischemic heart disease: Response to tissue injury or a pathogenetic villain? *Cardiovasc. Res.* [https://doi.org/10.1016/S0008-6363\(99\)00132-7](https://doi.org/10.1016/S0008-6363(99)00132-7)
- Meiry, GIDEON, REISNER, Y., FELD, Y., GOLDBERG, S., ROSEN, M., ZIV, N., BINAH, O., 2001. Evolution of Action Potential Propagation and Repolarization in Cultured Neonatal Rat Ventricular Myocytes. *J. Cardiovasc. Electrophysiol.* 12, 1269–1277. <https://doi.org/10.1046/j.1540-8167.2001.01269.x>
- Melillo, G., Musso, T., Sica, A., Taylor, L.S., Cox, G.W., Varesio, L., 1995. A hypoxia-responsive element mediates a novel pathway of activation of the inducible nitric oxide synthase promoter. *J. Exp. Med.* 182, 1683–1693. <https://doi.org/10.1084/jem.182.6.1683>
- Mentkowski, K.I., Lang, J.K., 2019. Exosomes Engineered to Express a Cardiomyocyte Binding Peptide Demonstrate Improved Cardiac Retention in Vivo. *Sci. Rep.* 9, 1–13. <https://doi.org/10.1038/s41598-019-46407-1>
- Meyer, T., Stuerz, K., Guenther, E., Edamura, M., Kraushaar, U., 2010. Cardiac slices as a predictive tool for arrhythmogenic potential of drugs and chemicals. *Expert Opin. Drug Metab. Toxicol.* 6, 1461–1475. <https://doi.org/10.1517/17425255.2010.526601>
- Mihl, C., Dassen, W.R.M., Kuipers, H., 2008. Cardiac remodelling: Concentric versus eccentric hypertrophy in strength and endurance athletes. *Netherlands Hear. J.* <https://doi.org/10.1007/BF03086131>
- Milani-Nejad, N., Xu, Y., Davis, J.P., Campbell, K.S., Janssen, P.M.L., 2013. Effect of muscle length on cross-bridge kinetics in intact cardiac trabeculae at body temperature. *J. Gen. Physiol* 141, 133–139. <https://doi.org/10.1085/jgp.201210894>

- Miller, T.D., Christian, T.F., Hopfenspirger, M.R., Hodge, D.O., Gersh, B.J., Gibbons, R.J., 1995. Infarct Size After Acute Myocardial Infarction Measured by Quantitative Tomographic  $^{99m}\text{Tc}$  Sestamibi Imaging Predicts Subsequent Mortality. *Circulation* 92, 334–341. <https://doi.org/10.1161/01.CIR.92.3.334>
- Mitcheson, J.S., Hancox, J.C., Levi, A.J., 1998. Cultured adult cardiac myocytes: future applications, culture methods, morphological and electrophysiological properties. *Cardiovasc. Res.* 39, 280–300.
- Mitcheson, J.S., Hancox, J.C., Levi, A.J., 1996. Action potentials, ion channel currents and transverse tubule density in adult rabbit ventricular myocytes maintained for 6 days in cell culture. *Pflugers Arch.* 431, 814–27.
- Mitry, M.A., Edwards, J.G., 2016. Doxorubicin induced heart failure: Phenotype and molecular mechanisms. *IJC Hear. Vasc.* <https://doi.org/10.1016/j.ijcha.2015.11.004>
- Miura, M., Boyden, P.A., Ter Keurs, H.E.D.J., 1999.  $\text{Ca}^{2+}$  Waves During Triggered Propagated Contractions in Intact Trabeculae Determinants of the Velocity of Propagation From the Department of Medicine (M.
- Mizutani, M., Wu, J.C., Nusse, R., 2016. Fibrosis of the Neonatal Mouse Heart After Cryoinjury Is Accompanied by Wnt Signaling Activation and Epicardial-to-Mesenchymal Transition. <https://doi.org/10.1161/JAHA.115.002457>
- Mol, E.A., Goumans, M.J., Doevendans, P.A., Sluijter, J.P.G., Vader, P., 2017. Higher functionality of extracellular vesicles isolated using size-exclusion chromatography compared to ultracentrifugation. *Nanomedicine Nanotechnology, Biol. Med.* 13, 2061–2065. <https://doi.org/10.1016/j.nano.2017.03.011>
- Morgan, K.Y., Black, L.D., 2014. Mimicking isovolumic contraction with combined

electromechanical stimulation improves the development of engineered cardiac constructs. *Tissue Eng. - Part A* 20, 1654–1667.

<https://doi.org/10.1089/ten.tea.2013.0355>

Morin, J.-P., Fouquet, F., Monteil, C., Le Prieur, E., Vaz, E., Dionnet, F., 1999. Development of a new in vitro system for continuous in vitro exposure of lung tissue to complex atmospheres: Application to diesel exhaust toxicology. *Cell Biol. Toxicol.* 15, 143–152.

<https://doi.org/10.1023/A:1007625302215>

Morin, J.-P., Fouquet, F., Monteil, C., Le Prieur, E., Vaz, E., Dionnet, F., n.d. Development of a new in vitro system for continuous in vitro exposure of lung tissue to complex atmospheres: Application to diesel exhaust toxicology.

Morin, J.-P., Rumigny, J.F., Bion, A., Dionnet, F., 2002. Isoflavones protect against diesel engine exhaust injury in organotypic culture of lung tissue. *Environ. Toxicol. Pharmacol.* 12, 213–220. [https://doi.org/10.1016/S1382-6689\(02\)00066-2](https://doi.org/10.1016/S1382-6689(02)00066-2)

[https://doi.org/10.1016/S1382-6689\(02\)00066-2](https://doi.org/10.1016/S1382-6689(02)00066-2)

Morris, T.A., Naik, J., Fibben, K.S., Kong, X., Kiyono, T., Yokomori, K., Grosberg, A., 2020. Striated myocyte structural integrity: Automated analysis of sarcomeric z-discs.

*PLoS Comput. Biol.* 16, 1–21. <https://doi.org/10.1371/journal.pcbi.1007676>

Müller-Ehmsen, J., Whittaker, P., Kloner, R.A., Dow, J.S., Sakoda, T., Long, T.I., Laird, P.W., Kedes, L., 2002. Survival and development of neonatal rat cardiomyocytes transplanted into adult myocardium. *J. Mol. Cell. Cardiol.* 34, 107–116.

<https://doi.org/10.1006/jmcc.2001.1491>

Mullur, R., Liu, Y.Y., Brent, G.A., 2014. Thyroid hormone regulation of metabolism.

*Physiol. Rev.* 94, 355–382. <https://doi.org/10.1152/physrev.00030.2013>

Mustroph, J., Wagemann, O., Lebek, S., Tarnowski, D., Ackermann, J., Drzymalski, M.,

- Pabel, S., Schmid, C., Wagner, S., Sossalla, S., Maier, L.S., Neef, S., 2018. SR Ca<sup>2+</sup> - leak and disordered excitation-contraction coupling as the basis for arrhythmogenic and negative inotropic effects of acute ethanol exposure. *J. Mol. Cell. Cardiol.* 116, 81–90. <https://doi.org/10.1016/j.yjmcc.2018.02.002>
- Myerburg, R.J., Gelband, H., Nilsson, K., Sung, R.J., Thurer, R.J., Morales, A.R., Bassett, A.L., 1977. Long term electrophysiological abnormalities resulting from experimental myocardial infarction in cats. *Circ. Res.* 41, 73–84. <https://doi.org/10.1161/01.RES.41.1.73>
- Nakamura, M.T., Cheon, Y., Li, Y., Nara, T.Y., 2004. Mechanisms of regulation of gene expression by fatty acids, in: *Lipids*. *Lipids*, pp. 1077–1083. <https://doi.org/10.1007/s11745-004-1333-0>
- Nakanishi, C., Yamagishi, M., Yamahara, K., Hagino, I., Mori, H., Sawa, Y., Yagihara, T., Kitamura, S., Nagaya, N., 2008. Activation of cardiac progenitor cells through paracrine effects of mesenchymal stem cells. *Biochem. Biophys. Res. Commun.* 374, 11–16. <https://doi.org/10.1016/j.bbrc.2008.06.074>
- Nelson, L.J., Treskes, P., Howie, A.F., Walker, S.W., Hayes, P.C., Plevris, J.N., 2013. Profiling the Impact of Medium Formulation on Morphology and Functionality of Primary Hepatocytes in vitro. *Sci. Rep.* 3. <https://doi.org/10.1038/srep02735>
- Neri, B., Cini-Neri, G., D'Alterio, M., 1984. Effect of anthracyclines and mitoxantrone on oxygen uptake and ATP intracellular concentration in rat heart slices. *Biochem. Biophys. Res. Commun.* 125, 954–960. [https://doi.org/10.1016/0006-291X\(84\)91376-7](https://doi.org/10.1016/0006-291X(84)91376-7)
- Neubauer, S., 2007. The Failing Heart — An Engine Out of Fuel. *N. Engl. J. Med.* 356, 1140–1151. <https://doi.org/10.1056/nejmra063052>

- Nguyen, A.H., Marsh, P., Schmiess-Heine, L., Burke, P.J., Lee, A., Lee, J., Cao, H., 2019. Cardiac tissue engineering: State-of-the-art methods and outlook. *J. Biol. Eng.* <https://doi.org/10.1186/s13036-019-0185-0>
- Oh, G.C., Cho, H.-J., 2020. Blood pressure and heart failure. *Clin. Hypertens.* 26, 1. <https://doi.org/10.1186/s40885-019-0132-x>
- Olinga, P., Meijer, D.K.F., Slooff, M.J.H., Groothuis, G.M.M., n.d. Liver Slices in In Vitro Pharmacotoxicology with Special Reference to the Use of Human Liver Tissue 12, 77–100.
- Olson, H., Betton, G., Robinson, D., Thomas, K., Monroe, A., Kolaja, G., Lilly, P., Sanders, J., Sipes, G., Bracken, W., Dorato, M., Van Deun, K., Smith, P., Berger, B., Heller, A., 2000. Concordance of the toxicity of pharmaceuticals in humans and in animals. *Regul. Toxicol. Pharmacol.* 32, 56–67. <https://doi.org/10.1006/rtph.2000.1399>
- Ong, S.B., Hernández-Reséndiz, S., Crespo-Avilan, G.E., Mukhametshina, R.T., Kwek, X.Y., Cabrera-Fuentes, H.A., Hausenloy, D.J., 2018. Inflammation following acute myocardial infarction: Multiple players, dynamic roles, and novel therapeutic opportunities. *Pharmacol. Ther.* <https://doi.org/10.1016/j.pharmthera.2018.01.001>
- Orban, P.C., Chui, D., Marth, J.D., 1992. Tissue- and site-specific DNA recombination in transgenic mice. *Proc. Natl. Acad. Sci. U. S. A.* 89, 6861–6865. <https://doi.org/10.1073/pnas.89.15.6861>
- Orn, S., Dickstein, K., 2002. How do heart failure patients die? *Eur. Hear. J. Suppl.* 4, D59–D65. <https://doi.org/10.1093/oxfordjournals.ehjsupp.a000770>
- Ott, H.C., Matthiesen, T.S., Goh, S.K., Black, L.D., Kren, S.M., Netoff, T.I., Taylor, D.A., 2008. Perfusion-decellularized matrix: Using nature’s platform to engineer a bioartificial



- heart. *Nat. Med.* 14, 213–221. <https://doi.org/10.1038/nm1684>
- Pagliarosi, O., Picchio, V., Chimenti, I., Messina, E., Gaetani, R., 2020. Building an Artificial Cardiac Microenvironment: A Focus on the Extracellular Matrix. *Front. Cell Dev. Biol.* <https://doi.org/10.3389/fcell.2020.559032>
- Pan, C., Kumar, C., Bohl, S., Klingmueller, U., Mann, M., 2009. Comparative proteomic phenotyping of cell lines and primary cells to assess preservation of cell type-specific functions. *Mol. Cell. Proteomics* 8, 443–450. <https://doi.org/10.1074/mcp.M800258-MCP200>
- Pannu, S.R., 2016. Too Much Oxygen: Hyperoxia and Oxygen Management in Mechanically Ventilated Patients. *Semin. Respir. Crit. Care Med.* 37, 16–22. <https://doi.org/10.1055/s-0035-1570359>
- Paredes, R.M., Etzler, J.C., Watts, L.T., Zheng, W., Lechleiter, J.D., 2008. Chemical calcium indicators. *Methods* 46, 143–151. <https://doi.org/10.1016/j.ymeth.2008.09.025>
- Park, E.J., Lee, A.Y., Park, S., Kim, J.H., Cho, M.H., 2014. Multiple pathways are involved in palmitic acid-induced toxicity. *Food Chem. Toxicol.* 67, 26–34. <https://doi.org/10.1016/j.fct.2014.01.027>
- Parrish, A.R., Gandolfi, A.J., Brendel, K., 1995. PRECISION-CUT TISSUE SLICES: APPLICATIONS IN PHARMACOLOGY AND TOXICOLOGY. *Liver* 57, 1887–1901.
- Pascual, F., Coleman, R.A., 2016. Fuel availability and fate in cardiac metabolism: A tale of two substrates. *Biochim. Biophys. Acta - Mol. Cell Biol. Lipids.* <https://doi.org/10.1016/j.bbalip.2016.03.014>
- Pasqualin, C., Gannier, F., Yu, A., Malécot, C.O., Bredeloux, P., Maupoil, V., 2016. SarcOptiM for ImageJ: High-frequency online sarcomere length computing on

stimulated cardiomyocytes. *Am. J. Physiol. - Cell Physiol.* 311, C277–C283.

<https://doi.org/10.1152/ajpcell.00094.2016>

Pasqualini, F.S., Nesmith, A.P., Horton, R.E., Sheehy, S.P., Parker, K.K., 2016.

Mechanotransduction and Metabolism in Cardiomyocyte Microdomains.

<https://doi.org/10.1155/2016/4081638>

Passier, R., Zeng, H., Frey, N., Naya, F.J., Nicol, R.L., McKinsey, T.A., Overbeek, P.,

Richardson, J.A., Grant, S.R., Olson, E.N., 2000. CaM kinase signaling induces cardiac hypertrophy and activates the MEF2 transcription factor in vivo. *J. Clin. Invest.* 105,

1395–1406. <https://doi.org/10.1172/JCI8551>

Paucek, P., Mironova, G., Mahdi, F., Beavis, A.D., Woldegiorgis, G., Garlid, K.D., 1992.

Reconstitution and partial purification of the glibenclamide-sensitive, ATP-dependent K<sup>+</sup> channel from rat liver and beef heart mitochondria. *J. Biol. Chem.* 267, 26062–26069.

Pellicena, P., Schulman, H., 2014. CaMKII inhibitors: From research tools to therapeutic

agents. *Front. Pharmacol.* <https://doi.org/10.3389/fphar.2014.00021>

Peng, Y.W., Mohammed, A., Deatrck, K.B., Major, T., Cheng, D., Charpie, I., Charpie, J.R.,

2019. Differential Effects of Normoxic and Hyperoxic Reperfusion on Global Myocardial Ischemia-Reperfusion Injury. *Semin. Thorac. Cardiovasc. Surg.* 31, 188–

198. <https://doi.org/10.1053/j.semtcvs.2018.09.018>

Perbellini, F., Watson, S.A., Scigliano, M., Alayoubi, S., Tkach, S., Bardi, I., Quaipe, N.,

Kane, C., Dufton, N.P., Simon, A., Sikkell, M.B., Faggian, G., Randi, A.M., Gorelik, J., Harding, S.E., Terracciano, C.M., 2017. Investigation of cardiac fibroblasts using

myocardial slices. *Cardiovasc. Res.* 114, 77–89. <https://doi.org/10.1093/cvr/cvx152>

- Perdomo, L., Beneit, N., Otero, Y.F., Escribano, Ó., Díaz-Castroverde, S., Gómez-Hernández, A., Benito, M., 2015. Protective role of oleic acid against cardiovascular insulin resistance and in the early and late cellular atherosclerotic process. *Cardiovasc. Diabetol.* 14, 75. <https://doi.org/10.1186/s12933-015-0237-9>
- Pernot, M., Lee, W.N., Bel, A., Mateo, P., Couade, M., Tanter, M., Crozatier, B., Messas, E., 2016. Shear Wave Imaging of Passive Diastolic Myocardial Stiffness: Stunned Versus Infarcted Myocardium. *JACC Cardiovasc. Imaging* 9, 1023–1030. <https://doi.org/10.1016/j.jcmg.2016.01.022>
- Perrelli, M.-G., Pagliaro, P., Penna, C., 2011. Ischemia/reperfusion injury and cardioprotective mechanisms: Role of mitochondria and reactive oxygen species. *World J. Cardiol.* 3, 186–200. <https://doi.org/10.4330/wjc.v3.i6.186>
- Perry, S.W., Norman, J.P., Barbieri, J., Brown, E.B., Gelbard, H.A., 2011. Mitochondrial membrane potential probes and the proton gradient: a practical usage guide. *Biotechniques* 50, 98–115. <https://doi.org/10.2144/000113610>
- Pertsov, A.M., Davidenko, J.M., Salomonsz, R., Baxter, W.T., Jalife, J., 1992. Spiral Waves of Excitation Underlie Reentrant Activity in Isolated Cardiac Muscle.
- Pesl, M., Pribyl, J., Caluori, G., Cmiel, V., Acimovic, I., Jelinkova, S., Dvorak, P., Starek, Z., Skladal, P., Rotrekl, V., 2017. Phenotypic assays for analyses of pluripotent stem cell–derived cardiomyocytes. *J. Mol. Recognit.* 30. <https://doi.org/10.1002/jmr.2602>
- Peters, N.S., Green, C.R., Poole-Wilson, P.A., Severs, N.J., 1993. Reduced content of connexin43 gap junctions in ventricular myocardium from hypertrophied and ischemic human hearts. *Circulation* 88, 864–875. <https://doi.org/10.1161/01.CIR.88.3.864>
- Peuch, C.J.L., Haiech, J., Demaille, J.G., 1979. Concerted Regulation of Cardiac

- Sarcoplasmic Reticulum Calcium Transport by Cyclic Adenosine Monophosphate Dependent and Calcium-Calmodulin-Dependent Phosphorylations. *Biochemistry* 18, 5150–5157. <https://doi.org/10.1021/bi00590a019>
- Picard, S., Rouet, R., Ducouret, P., Puddu, P.E., Flais, F., Criniti, A., Monti, F., Gérard, J.L., 1999. K(ATP) channels and “border zone” arrhythmias: Role of the repolarization dispersion between normal and ischaemic ventricular regions. *Br. J. Pharmacol.* 127, 1687–1695. <https://doi.org/10.1038/sj.bjp.0702704>
- Pillekamp, F., Reppel, M., Brockmeier, K., Hescheler, J., n.d. Impulse propagation in late-stage embryonic and neonatal murine ventricular slices.  
<https://doi.org/10.1016/j.jelectrocard.2006.02.008>
- Piper, H.M., García-Dorado, D., Ovize, M., 1998. A fresh look at reperfusion injury. *Cardiovasc. Res.* 38, 291–300. [https://doi.org/10.1016/S0008-6363\(98\)00033-9](https://doi.org/10.1016/S0008-6363(98)00033-9)
- Pitoulis, Fotios G., Hasan, W., Papadaki, M., Clavere, N.G., Perbellini, F., Harding, S.E., Kirk, J.A., Boateng, S.Y., de Tombe, P.P., Terracciano, C.M., 2020. Intact myocardial preparations reveal intrinsic transmural heterogeneity in cardiac mechanics. *J. Mol. Cell. Cardiol.* 141, 11–16. <https://doi.org/10.1016/j.yjmcc.2020.03.007>
- Pitoulis, Fotios G, Watson, S.A., Perbellini, F., Terracciano, C.M., 2020. Myocardial slices come to age: an intermediate complexity in vitro cardiac model for translational research. <https://doi.org/10.1093/cvr/cvz341>
- Place, T.L., Domann, F.E., Case, A.J., 2017. Limitations of oxygen delivery to cells in culture: An underappreciated problem in basic and translational research. *Free Radic. Biol. Med.* <https://doi.org/10.1016/j.freeradbiomed.2017.10.003>
- Pogwizd, S.M., Bers, D.M., 2004. Cellular basis of triggered arrhythmias in heart failure.


Trends Cardiovasc. Med. <https://doi.org/10.1016/j.tcm.2003.12.002>

Pogwizd, S.M., Schlotthauer, K., Li, L., Yuan, W., Bers, D.M., 2001a. Arrhythmogenesis and Contractile Dysfunction in Heart Failure. *Circ. Res.* 88, 1159–1167.

<https://doi.org/10.1161/hh1101.091193>

Pogwizd, S.M., Schlotthauer, K., Li, L., Yuan, W., Bers, D.M., 2001b. Arrhythmogenesis and contractile dysfunction in heart failure: Roles of sodium-calcium exchange, inward rectifier potassium current, and residual  $\beta$ -adrenergic responsiveness. *Circ. Res.* 88, 1159–1167. <https://doi.org/10.1161/hh1101.091193>

Poulter, N., 1999. Coronary heart disease is a multifactorial disease. *Am. J. Hypertens.* 12, 92S-95S. [https://doi.org/10.1016/s0895-7061\(99\)00163-6](https://doi.org/10.1016/s0895-7061(99)00163-6)

Qaid, M.M., Abdelrahman, M.M., 2016. Role of insulin and other related hormones in energy metabolism  A review. *Cogent Food Agric.* 2.

<https://doi.org/10.1080/23311932.2016.1267691>

Qin, S., Chen, M., Ji, H., Liu, G.Y., Mei, H., Li, K., Chen, T., 2018. MiR-21-5p regulates type II alveolar epithelial cell apoptosis in hyperoxic acute lung injury. *Mol. Med. Rep.* 17, 5796–5804. <https://doi.org/10.3892/mmr.2018.8560>

Quinn, T.A., Kohl, P., 2016. Rabbit models of cardiac mechano-electric and mechano-mechanical coupling. *Prog. Biophys. Mol. Biol.*

<https://doi.org/10.1016/j.pbiomolbio.2016.05.003>

Radisic, M., Park, H., Shing, H., Consi, T., Schoen, F.J., Langer, R., Freed, L.E., Vunjak-Novakovic, G., 2004. Functional assembly of engineered myocardium by electrical stimulation of cardiac myocytes cultured on scaffolds. *Proc. Natl. Acad. Sci. U. S. A.*

101, 18129–18134. <https://doi.org/10.1073/pnas.0407817101>

- Raturi, A., Simmen, T., 2013. Where the endoplasmic reticulum and the mitochondrion tie the knot: The mitochondria-associated membrane (MAM). *Biochim. Biophys. Acta - Mol. Cell Res.* <https://doi.org/10.1016/j.bbamcr.2012.04.013>
- Razeghi, P., Young, M.E., Alcorn, J.L., Moravec, C.S., Frazier, O.H., Taegtmeier, H., 2001. Metabolic Gene Expression in Fetal and Failing Human Heart. *Circulation* 104, 2923–2931. <https://doi.org/10.1161/hc4901.100526>
- Rech, M., Luiken, J.J.F.P., Glatz, J.F.C., Bilsen, M. Van, Schroen, B., Nabben, M., 2018. Assessing fatty acid oxidation flux in rodent cardiomyocyte models. *Sci. Rep.* 1–6. <https://doi.org/10.1038/s41598-018-19478-9>
- Rizos, E.C., Ntzani, E.E., Bika, E., Kostapanos, M.S., Elisaf, M.S., 2012. Association between omega-3 fatty acid supplementation and risk of major cardiovascular disease events: A systematic review and meta-analysis. *JAMA - J. Am. Med. Assoc.* <https://doi.org/10.1001/2012.jama.11374>
- Robinson, D.G., Ding, Y., Jiang, L., 2016. Unconventional protein secretion in plants: a critical assessment. *Protoplasma.* <https://doi.org/10.1007/s00709-015-0887-1>
- Roche, S.M., Gumucio, J.P., Brooks, S. V., Mendias, C.L., Claflin, D.R., 2015. Measurement of Maximum Isometric Force Generated by Permeabilized Skeletal Muscle Fibers. *J. Vis. Exp.* e52695–e52695. <https://doi.org/10.3791/52695>
- Rodrigo, R., Libuy, M., Feliú, F., Hasson, D., 2013. Molecular basis of cardioprotective effect of antioxidant vitamins in myocardial infarction. *Biomed Res. Int.* 2013, 437613. <https://doi.org/10.1155/2013/437613>
- Roell, W., Klein, A.M., Breitbach, M., Becker, T.S., Parikh, A., Lee, J., Zimmermann, K., Reining, S., Gabris, B., Ottersbach, A., Doran, R., Engelbrecht, B., Schiffer, M.,

- Kimura, K., Freitag, P., Carls, E., Geisen, C., Duerr, G.D., Sasse, P., Welz, A., Pfeifer, A., Salama, G., Kotlikoff, M., Fleischmann, B.K., 2018. Overexpression of Cx43 in cells of the myocardial scar: Correction of post-infarct arrhythmias through heterotypic cell-cell coupling OPEN. <https://doi.org/10.1038/s41598-018-25147-8>
- Ronaldson-Bouchard, K., Ma, S.P., Yeager, K., Chen, T., Song, L.J., Sirabella, D., Morikawa, K., Teles, D., Yazawa, M., Vunjak-Novakovic, G., 2018. Advanced maturation of human cardiac tissue grown from pluripotent stem cells. *Nature* 556, 239–243. <https://doi.org/10.1038/s41586-018-0016-3>
- Ruan, J.L., Tulloch, N.L., Razumova, M. V., Saiget, M., Muskheli, V., Pabon, L., Reinecke, H., Regnier, M., Murry, C.E., 2016. Mechanical Stress Conditioning and Electrical Stimulation Promote Contractility and Force Maturation of Induced Pluripotent Stem Cell-Derived Human Cardiac Tissue. *Circulation* 134, 1557–1567. <https://doi.org/10.1161/CIRCULATIONAHA.114.014998>
- Ruegg, C.E., 1994. Preparation of precision-cut renal slices and renal proximal tubular fragments for evaluating segment-specific nephrotoxicity. *J. Pharmacol. Toxicol. Methods* 31, 125–133. [https://doi.org/10.1016/1056-8719\(94\)90074-4](https://doi.org/10.1016/1056-8719(94)90074-4)
- Ruiz-Meana, M., Garcia-Dorado, D., Hofstaetter, B., Piper, H.M., Soler-Soler, J., 1999. Propagation of Cardiomyocyte Hypercontracture by Passage of Na Through Gap Junctions.
- Rutter, G.A., Pinton, P., 2014. Mitochondria-associated endoplasmic reticulum membranes in insulin signaling. *Diabetes* 63, 3163–3165. <https://doi.org/10.2337/db14-0812>
- Rysä, J., Tokola, H., Ruskoaho, H., 2018. Mechanical stretch induced transcriptomic profiles in cardiac myocytes. *Sci. Rep.* 8, 1–14. <https://doi.org/10.1038/s41598-018-23042-w>

- Saez, J.C., Connor, J.A., Spray, D.C., Bennett, M.V.L., 1989. Hepatocyte gap junctions are permeable to the second messenger, inositol 1,4,5-trisphosphate, and to calcium ions. *Proc. Natl. Acad. Sci. U. S. A.* 86, 2708–2712. <https://doi.org/10.1073/pnas.86.8.2708>
- Sag, C.M., Köhler, A.C., Anderson, M.E., Backs, J., Maier, L.S., 2011. CaMKII-dependent SR Ca leak contributes to doxorubicin-induced impaired Ca handling in isolated cardiac myocytes. *J. Mol. Cell. Cardiol.* 51, 749–759. <https://doi.org/10.1016/j.yjmcc.2011.07.016>
- Sakai, T., Li, R.K., Weisel, R.D., Mickle, D.A.G., Kim, E.J., Tomita, S., Jia, Z.Q., Yau, T.M., 1999. Autologous heart cell transplantation improves cardiac function after myocardial injury. *Ann. Thorac. Surg.* 68, 2074–2080. [https://doi.org/10.1016/S0003-4975\(99\)01148-0](https://doi.org/10.1016/S0003-4975(99)01148-0)
- Sanada, S., Komuro, I., Kitakaze, M., 2011. Pathophysiology of myocardial reperfusion injury: Preconditioning, postconditioning, and translational aspects of protective measures. *Am. J. Physiol. - Hear. Circ. Physiol.* <https://doi.org/10.1152/ajpheart.00553.2011>
- Sandow, A., 1936. Diffraction patterns of the frog sartorius and sarcomere behavior during contraction. *J. Cell. Comp. Physiol.* 9, 55–75. <https://doi.org/10.1002/jcp.1030090106>
- Santoni, S.M., Winston, T., Hoang, P., Ma, Z., 2018. Microsystems for electromechanical stimulations to engineered cardiac tissues. *Microphysiological Syst.* 2, 11–11. <https://doi.org/10.21037/mps.2018.11.01>
- Sato, T., Paquet-Fifield, S., Harris, N.C., Roufail, S., Turner, D.J., Yuan, Y., Zhang, Y.F., Fox, S.B., Hibbs, M.L., Wilkinson-Berka, J.L., Williams, R.A., Stacker, S.A., Sly, P.D., Achen, M.G., 2016. VEGF-D promotes pulmonary oedema in hyperoxic acute lung injury. *J. Pathol.* 239, 152–161. <https://doi.org/10.1002/path.4708>



- Savoji, H., Mohammadi, M.H., Rafatian, N., Toroghi, M.K., Wang, E.Y., Zhao, Y., Korolj, A., Ahadian, S., Radisic, M., 2019. Cardiovascular disease models: A game changing paradigm in drug discovery and screening. *Biomaterials* 198, 3–26.  
<https://doi.org/10.1016/j.biomaterials.2018.09.036>
- Schaaf, S., Shibamiya, A., Mewe, M., Eder, A., Stö Hr, A., 2011. Human Engineered Heart Tissue as a Versatile Tool in Basic Research and Preclinical Toxicology. *PLoS One* 6, 26397. <https://doi.org/10.1371/journal.pone.0026397>
- Schirone, L., Forte, M., Palmerio, S., Yee, D., Nocella, C., Angelini, F., Pagano, F., Schiavon, S., Bordin, A., Carrizzo, A., Vecchione, C., Valenti, V., Chimenti, I., Falco, E. De, Sciarretta, S., Frati, G., 2017. A Review of the Molecular Mechanisms Underlying the Development and Progression of Cardiac Remodeling. *Oxid. Med. Cell. Longev.* 2017. <https://doi.org/10.1155/2017/3920195>
- Schnabel, K., Wu, C.-C., Kurth, T., Weidinger, G., 2011. Regeneration of Cryoinjury Induced Necrotic Heart Lesions in Zebrafish Is Associated with Epicardial Activation and Cardiomyocyte Proliferation. *PLoS One* 6, e18503.  
<https://doi.org/10.1371/journal.pone.0018503>
- Schomig, A., 1990. Catecholamines in myocardial ischemia. Systemic and cardiac release, in: *Circulation*. pp. II13-22.
- Schorey, J.S., Cheng, Y., Singh, P.P., Smith, V.L., 2015. Exosomes and other extracellular vesicles in host–pathogen interactions. *EMBO Rep.* 16, 24–43.  
<https://doi.org/10.15252/embr.201439363>
- Schulz, R., Görge, P.M., Görbe, A., Ferdinandy, P., Lampe, P.D., Leybaert, L., Schulz, P.R., Institut, G., Direktor, J.-L., 2015. Connexin 43 is an emerging therapeutic target in ischemia/ reperfusion injury, cardioprotection and neuroprotection HHS Public Access.

- Pharmacol Ther 153, 90–106. <https://doi.org/10.1016/j.pharmthera.2015.06.005>
- Segal, O.R., Chow, A.W.C., Peters, N.S., Davies, D.W., 2010. Mechanisms that initiate ventricular tachycardia in the infarcted human heart. *Hear. Rhythm* 7, 57–64. <https://doi.org/10.1016/j.hrthm.2009.09.025>
- Semenza, G.L., 2014. Hypoxia-inducible factor 1 and cardiovascular disease. *Annu. Rev. Physiol.* 76, 39–56. <https://doi.org/10.1146/annurev-physiol-021113-170322>
- Semenza, G.L., Wang, G.L., 1992. A nuclear factor induced by hypoxia via de novo protein synthesis binds to the human erythropoietin gene enhancer at a site required for transcriptional activation. *Mol. Cell. Biol.* 12, 5447–5454. <https://doi.org/10.1128/mcb.12.12.5447>
- Sen, C.K., Khanna, S., Roy, S., 2006. Perceived hyperoxia: Oxygen-induced remodeling of the reoxygenated heart. *Cardiovasc. Res.* <https://doi.org/10.1016/j.cardiores.2006.01.003>
- Sengupta, P.P., Korinek, J., Belohlavek, M., Narula, J., Vannan, M.A., Jahangir, A., Khandheria, B.K., 2006. Left Ventricular Structure and Function. *Basic Science for Cardiac Imaging. J. Am. Coll. Cardiol.* <https://doi.org/10.1016/j.jacc.2006.08.030>
- Seo, K., Inagaki, M., Nishimura, S., Hidaka, I., Sugimachi, M., Hisada, T., Sugiura, S., 2009. Structural Heterogeneity in the Ventricular Wall Plays a Significant Role in the Initiation of Stretch-Induced Arrhythmias in Perfused Rabbit Right Ventricular Tissues and Whole Heart Preparations. <https://doi.org/10.1161/CIRCRESAHA.109.203828>
- Sepp, R., Severs, N.J., Gourdie, R.G., 1996. Altered patterns of cardiac intercellular junction distribution in hypertrophic cardiomyopathy. *Heart* 76, 412–417. <https://doi.org/10.1136/hrt.76.5.412>
- Sequeira, V., van der Velden, J., 2015. Historical perspective on heart function: the Frank–

Starling Law. *Biophys. Rev.* <https://doi.org/10.1007/s12551-015-0184-4>

Sergeant, G.P., Ohya, S., Reihill, J.A., Perrino, B.A., Amberg, G.C., Imaizumi, Y., Horowitz, B., Sanders, K.M., Sang, D.K., 2005. Regulation of Kv4.3 currents by Ca<sup>2+</sup>/calmodulin-dependent protein kinase II. *Am. J. Physiol. - Cell Physiol.* 288. <https://doi.org/10.1152/ajpcell.00293.2004>

Shakp, W.W., Simpson, D.G., Borg, T.K., Samarel, A.M., Terracio, L., 1997. Mechanical forces regulate focal adhesion and costamere assembly in cardiac myocytes. *Am. J. Physiol. - Hear. Circ. Physiol.* 273. <https://doi.org/10.1152/ajpheart.1997.273.2.h546>

Shiels, H.A., White, E., 2008. The Frank-Starling mechanism in vertebrate cardiac myocytes. *J. Exp. Biol.* <https://doi.org/10.1242/jeb.003145>

Shiferaw, Y., Aistrup, G.L., Wasserstrom, J.A., 2012. Intracellular Ca<sup>2+</sup> waves, afterdepolarizations, and triggered arrhythmias. <https://doi.org/10.1093/cvr/cvs155>

Shimizu, T., Yamato, M., Kikuchi, A., Okano, T., 2003. Cell sheet engineering for myocardial tissue reconstruction. *Biomaterials* 24, 2309–2316. [https://doi.org/10.1016/S0142-9612\(03\)00110-8](https://doi.org/10.1016/S0142-9612(03)00110-8)

Sigurdson, W., Ruknudin, A., Sachs, F., 1992. Calcium imaging of mechanically induced fluxes in tissue-cultured chick heart: Role of stretch-activated ion channels. *Am. J. Physiol. - Hear. Circ. Physiol.* 262. <https://doi.org/10.1152/ajpheart.1992.262.4.h1110>

Simmerman, H.K.B., Collins, J.H., Theiberts, J.L., Wegeners, A.D., Jonesst, L.R., n.d. Sequence Analysis of Phospholamban.

Simon, M.C., Keith, B., 2008. The role of oxygen availability in embryonic development and stem cell function. *Nat. Rev. Mol. Cell Biol.* <https://doi.org/10.1038/nrm2354>

Simpson, D.G., Sharp, W.W., Borg, T.K., Price, R.L., Terracio, L., Samarel, A.M., 1996.

- Mechanical regulation of cardiac myocyte protein turnover and myofibrillar structure. *Am. J. Physiol. - Cell Physiol.* 270. <https://doi.org/10.1152/ajpcell.1996.270.4.c1075>
- Slanzi, A., Iannoto, G., Rossi, B., Zenaro, E., Constantin, G., 2020. In vitro Models of Neurodegenerative Diseases. *Front. Cell Dev. Biol.* <https://doi.org/10.3389/fcell.2020.00328>
- Smith, R.R., Barile, L., Cho, H.C., Leppo, M.K., Hare, J.M., Messina, E., Giacomello, A., Abraham, M.R., Marbán, E., 2007. Regenerative potential of cardiosphere-derived cells expanded from percutaneous endomyocardial biopsy specimens. *Circulation* 115, 896–908. <https://doi.org/10.1161/CIRCULATIONAHA.106.655209>
- Sovari, A.A., 2016. Cellular and Molecular Mechanisms of Arrhythmia by Oxidative Stress. *Cardiol. Res. Pract.* <https://doi.org/10.1155/2016/9656078>
- Spannbauer, A., Traxler, D., Zlabinger, K., Gugerell, A., Winkler, J., Mester-Tonczar, J., Lukovic, D., Müller, C., Riesenhuber, M., Pavo, N., Gyöngyösi, M., 2019. Large Animal Models of Heart Failure With Reduced Ejection Fraction (HFrEF). *Front. Cardiovasc. Med.* <https://doi.org/10.3389/fcvm.2019.00117>
- St. Croix, C.M., Shand, S.H., Watkins, S.C., 2005. Confocal microscopy: comparisons, applications, and problems. *Biotechniques* 39, S2–S5. <https://doi.org/10.2144/000112089>
- Stankovicova, T., Szilard, M., De Scheerder, I., Sipido, K.R., 2000. M cells and transmural heterogeneity of action potential configuration in myocytes from the left ventricular wall of the pig heart. *Cardiovasc. Res.* 45, 952–960. [https://doi.org/10.1016/S0008-6363\(99\)00418-6](https://doi.org/10.1016/S0008-6363(99)00418-6)
- Stanley, W.C., Recchia, F.A., Lopaschuk, G.D., 2005. Myocardial Substrate Metabolism in

the Normal and Failing Heart. *Physiol. Rev.* 85.

Stavrou, B.M., Beck, C., Flores, N.A., 2001. Changes in extracellular pH and myocardial ischaemia alter the cardiac effects of diadenosine tetraphosphate and pentaphosphate. *Br. J. Pharmacol.* 134, 639–647. <https://doi.org/10.1038/sj.bjp.0704288>

Stone, G.W., Selker, H.P., Thiele, H., Patel, M.R., Udelson, J.E., Ohman, E.M., Maehara, A., Eitel, I., Granger, C.B., Jenkins, P.L., Nichols, M., Ben-Yehuda, O., 2016. Relationship between Infarct Size and Outcomes Following Primary PCI Patient-Level Analysis from 10 Randomized Trials. *J. Am. Coll. Cardiol.* 67, 1674–1683. <https://doi.org/10.1016/j.jacc.2016.01.069>

Stoppel, W.L., Kaplan, D.L., Black, L.D., 2016. Electrical and mechanical stimulation of cardiac cells and tissue constructs. *Adv. Drug Deliv. Rev.* <https://doi.org/10.1016/j.addr.2015.07.009>

Stoppini, L., Buchs, P.A., Muller, D., 1991. A simple method for organotypic cultures of nervous tissue. *J. Neurosci. Methods* 37, 173–82.

Støttrup, N.B., Løfgren, B., Dupont Birkler, R., Nielsen, J.M., Wang, L., Caldarone, C.A., Buus Kristiansen, S., Contractor, H., Johannsen, M., Bøtker, H.E., Nielsen, T.T., n.d. Inhibition of the malate-aspartate shuttle by pre-ischaemic aminooxyacetate loading of the heart induces cardioprotection. <https://doi.org/10.1093/cvr/cvq205>

Streeter, D.D., Spotnirz, H.M., Patel, D.P., Ross, J., Sonnenblick, E.H., n.d. Fiber Orientation in the Canine Left Ventricle during Diastole and Systole.

Sun, H., Chartier, D., Leblanc, N., Nattel, S., 2001. Intracellular calcium changes and tachycardia-induced contractile dysfunction in canine atrial myocytes, *Cardiovascular Research*.

- Szablewski, L., 2017. Glucose transporters in healthy heart and in cardiac disease. *Int. J. Cardiol.* <https://doi.org/10.1016/j.ijcard.2016.12.083>
- Tachibana, A., Santoso, M.R., Mahmoudi, M., Shukla, P., Wang, L., Bennett, M., Goldstone, A.B., Wang, M., Fukushi, M., Ebert, A.D., Woo, Y.J., Rulifson, E., Yang, P.C., 2017. Paracrine effects of the pluripotent stem cell-derived cardiac myocytes salvage the injured myocardium. *Circ. Res.* 121, e22–e36.  
<https://doi.org/10.1161/CIRCRESAHA.117.310803>
- Taegtmeyer, H., Harinstein, M.E., Gheorghide, M., 2008. More Than Bricks and Mortar: Comments on Protein and Amino Acid Metabolism in the Heart.  
<https://doi.org/10.1016/j.amjcard.2008.02.064>
- Takahashi, K., Yamanaka, S., 2006. Induction of Pluripotent Stem Cells from Mouse Embryonic and Adult Fibroblast Cultures by Defined Factors. *Cell* 126, 663–676.  
<https://doi.org/10.1016/j.cell.2006.07.024>
- Takaki, M., Kohzuki, H., Kawatani, Y., Yoshida, A., Ishidate, H., Suga, H., 1998. Sarcoplasmic Reticulum Ca<sup>2+</sup>Pump Blockade Decreases O<sub>2</sub>Use of Unloaded Contracting Rat Heart Slices: Thapsigargin and Cyclopiazonic Acid. *J. Mol. Cell. Cardiol.* 30, 649–659. <https://doi.org/10.1006/JMCC.1997.0630>
- Tarasova, N. V., Vishnyakova, P.A., Logashina, Y.A., Elchaninov, A. V., 2019. Mitochondrial calcium uniporter structure and function in different types of muscle tissues in health and disease. *Int. J. Mol. Sci.* 20. <https://doi.org/10.3390/ijms20194823>
- Teslaa, T., Teitell, M.A., 2014. Techniques to monitor glycolysis, in: *Methods in Enzymology*. Academic Press Inc., pp. 91–114. <https://doi.org/10.1016/B978-0-12-416618-9.00005-4>

- The Scientist's Guide to Cardiac Metabolism, 2016. , The Scientist's Guide to Cardiac Metabolism. Elsevier. <https://doi.org/10.1016/B978-0-12-802394-5.00008-X>
- Theroux, P., Ross, J., Franklin, D., Covell, J.W., Bloor, C.M., Sasayama, S., 1977. Regional myocardial function and dimensions early and late after myocardial infarction in the unanesthetized dog. *Circ. Res.* 40, 158–165. <https://doi.org/10.1161/01.RES.40.2.158>
- Thilo-Körner, D.G., Marre, U., Savion, N., Hehrlein, F.W., Bödeker, R.H., 1992. Hyperoxia (145 mmHg pO<sub>2</sub>) and tissue normoxia (20-40 mmHg pO<sub>2</sub>) modulate human vascular cell functions. *EXS* 61, 400–404. [https://doi.org/10.1007/978-3-0348-7001-6\\_65](https://doi.org/10.1007/978-3-0348-7001-6_65)
- Thomas, R.C., Singh, A., Cowley, P.M., Myagmar, B.-E., Montgomery, M.D., Swigart, P.M., De Marco, T., Baker, A.J., Simpson, P.C., 2016. A Myocardial Slice Culture Model Reveals Alpha-1A-Adrenergic Receptor Signaling in the Human Heart. *JACC Basic to Transl. Sci.* 1, 155–167. <https://doi.org/10.1016/J.JACBTS.2016.03.005>
- Tissue-engineered disease models, 2018. . *Nat. Biomed. Eng.* <https://doi.org/10.1038/s41551-018-0339-2>
- Tobian, L., 1991. Salt and hypertension lessons from animal models that relate to human hypertension. *Hypertension* 17. [https://doi.org/10.1161/01.hyp.17.1\\_suppl.i52](https://doi.org/10.1161/01.hyp.17.1_suppl.i52)
- Tomek, J., Hao, G., Tomková, M., Lewis, A., Carr, C., Paterson, D.J., Rodriguez, B., Bub, G., Herring, N., 2019.  $\beta$ -Adrenergic Receptor Stimulation and Alternans in the Border Zone of a Healed Infarct: An ex vivo Study and Computational Investigation of Arrhythmogenesis. *Front. Physiol.* 10, 350. <https://doi.org/10.3389/fphys.2019.00350>
- Tran, D.H., Wang, Z. V., 2019. Glucose Metabolism in Cardiac Hypertrophy and Heart Failure. *J. Am. Heart Assoc.* <https://doi.org/10.1161/JAHA.119.012673>
- Travers, J.G., Kamal, F.A., Robbins, J., Yutzey, K.E., Blaxall, B.C., 2016. Cardiac Fibrosis:

The Fibroblast Awakens. <https://doi.org/10.1161/CIRCRESAHA.115.306565>

Tsai, W.-H., 1995. Moment-preserving thresholding | Document image analysis.

Tsang, H.G., Rashdan, N.A., Whitelaw, C.B.A., Corcoran, B.M., Summers, K.M., MacRae, V.E., 2016. Large animal models of cardiovascular disease. *Cell Biochem. Funct.* 34, 113–132. <https://doi.org/10.1002/cbf.3173>

Tuder, R.M., Flook, B.E., Voelkel, N.F., 1995. Increased gene expression for VEGF and the VEGF receptors KDR/Flk and Flt in lungs exposed to acute or to chronic hypoxia: Modulation of gene expression by nitric oxide. *J. Clin. Invest.* 95, 1798–1807. <https://doi.org/10.1172/JCI117858>

Tulloch, N.L., Muskheli, V., Razumova, M. V., Korte, F.S., Regnier, M., Hauch, K.D., Pabon, L., Reinecke, H., Murry, C.E., 2011. Growth of engineered human myocardium with mechanical loading and vascular coculture. *Circ. Res.* 109, 47–59. <https://doi.org/10.1161/CIRCRESAHA.110.237206>

Tzahor, E., Poss, K.D., n.d. Cardiac regeneration strategies: Staying young at heart.

Udenwobele, D.I., Su, R.C., Good, S. V., Ball, T.B., Shrivastav, S.V., Shrivastav, A., 2017. Myristoylation: An important protein modification in the immune response. *Front. Immunol.* <https://doi.org/10.3389/fimmu.2017.00751>

Ungerer, M., Kessebohm, K., Kronsbein, K., Lohse, M.J., Richardt, G., 1996. Activation of  $\beta$ -Adrenergic Receptor Kinase During Myocardial Ischemia. *Circ. Res.* 79, 455–460. <https://doi.org/10.1161/01.RES.79.3.455>

Ursell, P.C., Gardner, P.I., Albala, A., Fenoglio, J.J., Wit, A.L., 1985. Structural and electrophysiological changes in the epicardial border zone of canine myocardial infarcts during infarct healing. *Circ. Res.* 56, 436–451. <https://doi.org/10.1161/01.RES.56.3.436>



- Van Den Akker, F., De Jager, S.C.A., Sluijter, J.P.G., 2013. Mesenchymal stem cell therapy for cardiac inflammation: Immunomodulatory properties and the influence of toll-like receptors. *Mediators Inflamm.* 2013. <https://doi.org/10.1155/2013/181020>
- Van Den Bos, Ewout J, Mees, B.M.E., De Waard, M.C., De Crom, R., Duncker, D.J., 2005a. Innovative Methodology A novel model of cryoinjury-induced myocardial infarction in the mouse: a comparison with coronary artery ligation. *Am J Physiol Hear. Circ Physiol* 289. <https://doi.org/10.1152/ajpheart.00111.2005.-Mouse>
- Van Den Bos, Ewout J, Mees, B.M.E., De Waard, M.C., De Crom, R., Duncker, D.J., 2005b. Innovative Methodology A novel model of cryoinjury-induced myocardial infarction in the mouse: a comparison with coronary artery ligation. *Am J Physiol Hear. Circ Physiol* 289. <https://doi.org/10.1152/ajpheart.00111.2005.-Mouse>
- Van Den Bos, Ewout J., Mees, B.M.E., De Waard, M.C., De Crom, R., Duncker, D.J., 2005. A novel model of cryoinjury-induced myocardial infarction in the mouse: A comparison with coronary artery ligation. *Am. J. Physiol. - Hear. Circ. Physiol.* 289. <https://doi.org/10.1152/ajpheart.00111.2005>
- Van Der Vusse, G.J., Van Bilsen, M., Glatz, J.F.C., 2000. Cardiac fatty acid uptake and transport in health and disease. *Cardiovasc. Res.* [https://doi.org/10.1016/S0008-6363\(99\)00263-1](https://doi.org/10.1016/S0008-6363(99)00263-1)
- van Niel, G., Raposo, G., 2018. Shedding light on the cell biology of extracellular vesicles. *Nat. Publ. Gr.* 19. <https://doi.org/10.1038/nrm.2017.125>
- Van Vliet, P., Roccio, M., Smits, A.M., Van Oorschot, A.A.M., Metz, C.H.G., Van Veen, T.A.B., Sluijter, J.P.G., Doevendans, P.A., Goumans, M.J., 2008. Progenitor cells isolated from the human heart: A potential cell source for regenerative therapy. *Netherlands Hear. J.* 16, 163–169. <https://doi.org/10.1007/BF03086138>

- Van Winkle, A.P., Gates, I.D., Kallos, M.S., 2012. Mass Transfer Limitations in Embryoid Bodies during Human Embryonic Stem Cell Differentiation. *Cells Tissues Organs* 196, 34–47. <https://doi.org/10.1159/000330691>
- Vandeplassche, G., Hermans, C., Haecke, J. Van, Wouters, L., Borgers, M., Flameng, W., 1991. Evaluation of factors influencing myocardial infarct size in unconscious dogs. *Cardiovasc. Res.* <https://doi.org/10.1093/cvr/25.10.844>
- Vaverka, J., Burša, J., Šumbera, J., Pásek, M., 2018. Effect of Transmural Differences in Excitation-Contraction Delay and Contraction Velocity on Left Ventricle Isovolumic Contraction: A Simulation Study. *Biomed Res. Int.* 2018. <https://doi.org/10.1155/2018/4798512>
- Veerman, C.C., Mengarelli, I., Lodder, E.M., Kosmidis, G., Bellin, M., Zhang, M., Dittmann, S., Guan, K., Wilde, A.A.M., Schulze-Bahr, E., Greber, B., Bezzina, C.R., Verkerk, A.O., 2017. Switch from fetal to adult SCN5A isoform in human induced pluripotent stem cell-derived cardiomyocytes unmasks the cellular phenotype of a conduction disease-causing mutation. *J. Am. Heart Assoc.* 6. <https://doi.org/10.1161/JAHA.116.005135>
- Vendelin, M., Béraud, N., Guerrero, K., Andrienko, T., Kuznetsov, A. V., Olivares, J., Kay, L., Saks, V.A., 2005. Mitochondrial regular arrangement in muscle cells: A “crystal-like” pattern. *Am. J. Physiol. - Cell Physiol.* 288, 757–767. <https://doi.org/10.1152/ajpcell.00281.2004>
- Vickers, A.E.M., Fisher, R.L., 2004. Organ slices for the evaluation of human drug toxicity. *Chem. Biol. Interact.* 150, 87–96. <https://doi.org/10.1016/j.cbi.2004.09.005>
- Vila-Petroff, M., Salas, M.A., Said, M., Valverde, C.A., Sapia, L., Portiansky, E., Hajjar, R.J., Kranias, E.G., Mundiña-Weilenmann, C., Mattiazzi, A., 2007. CaMKII inhibition

protects against necrosis and apoptosis in irreversible ischemia-reperfusion injury.

*Cardiovasc. Res.* 73, 689–698. <https://doi.org/10.1016/j.cardiores.2006.12.003>

Voges, Holly K., Mills, R.J., Elliott, D.A., Parton, R.G., Porrello, E.R., Hudson, J.E., 2017.

Development of a Human Cardiac Organoid Injury Model Reveals Innate Regenerative Potential. <https://doi.org/10.1242/dev.143966>

Voges, Holly K., Mills, R.J., Elliott, D.A., Parton, R.G., Porrello, E.R., Hudson, J.E., 2017.

Development of a human cardiac organoid injury model reveals innate regenerative potential. *Dev.* 144, 1118–1127. <https://doi.org/10.1242/dev.143966>

Von Lewinski, D., Stumme, B., Fialka, F., Luers, C., Pieske, B., 2004. Functional relevance

of the stretch-dependent slow force response in failing human myocardium. *Circ. Res.* 94, 1392–1398. <https://doi.org/10.1161/01.RES.0000129181.48395.ff>

Vrijisen, K.R., Maring, J.A., Chamuleau, S.A.J., Verhage, V., Mol, E.A., Deddens, J.C., Metz,

C.H.G., Lodder, K., van Eeuwijk, E.C.M., van Dommelen, S.M., Doevendans, P.A., Smits, A.M., Goumans, M.-J., Sluijter, J.P.G., 2016a. Exosomes from Cardiomyocyte Progenitor Cells and Mesenchymal Stem Cells Stimulate Angiogenesis Via EMMPRIN. *Adv. Healthc. Mater.* 5, 2555–2565. <https://doi.org/10.1002/adhm.201600308>

Vrijisen, K.R., Maring, J.A., Chamuleau, S.A.J., Verhage, V., Mol, E.A., Deddens, J.C., Metz,

C.H.G., Lodder, K., van Eeuwijk, E.C.M., van Dommelen, S.M., Doevendans, P.A., Smits, A.M., Goumans, M.J., Sluijter, J.P.G., 2016b. Exosomes from Cardiomyocyte Progenitor Cells and Mesenchymal Stem Cells Stimulate Angiogenesis Via EMMPRIN. *Adv. Healthc. Mater.* 5, 2555–2565. <https://doi.org/10.1002/adhm.201600308>

Wagner, S., Hacker, E., Grandi, E., Weber, S.L., Dybkova, N., Sossalla, S., Sowa, T., Fabritz,

L., Kirchhof, P., Bers, D.M., Maier, L.S., 2009. Ca/calmodulin kinase II differentially modulates potassium currents. *Circ. Arrhythmia Electrophysiol.* 2, 285–294.

<https://doi.org/10.1161/CIRCEP.108.842799>

Wagner, S., Ruff, H.M., Weber, S.L., Bellmann, S., Sowa, T., Schulte, T., Anderson, M.E., Grandi, E., Bers, D.M., Backs, J., Belardinelli, L., Maier, L.S., 2011. Reactive oxygen species-activated Ca/calmodulin kinase II $\delta$  is required for late INa augmentation leading to cellular Na and Ca overload. *Circ. Res.* 108, 555–565.

<https://doi.org/10.1161/CIRCRESAHA.110.221911>

Walborg, E.F., Lantz, R.S., 1968. Separation and quantitation of saccharides by ion-exchange chromatography utilizing boric acid/glycerol buffers. *Anal. Biochem.* 22, 123–133.

[https://doi.org/10.1016/0003-2697\(68\)90266-2](https://doi.org/10.1016/0003-2697(68)90266-2)

Walewska, A., Kulawiak, B., Szewczyk, A., Koprowski, P., 2018. Mechanosensitivity of mitochondrial large-conductance calcium-activated potassium channels. *Biochim. Biophys. Acta - Bioenerg.* 1859, 797–805. <https://doi.org/10.1016/j.bbabi.2018.05.006>

Wang, B.X., Kit-Anan, W., Terracciano, C.M.N., 2018. Many cells make life work—multicellularity in stem cell-based cardiac disease modelling. *Int. J. Mol. Sci.*

<https://doi.org/10.3390/ijms19113361>

Wang, K., Lee, P., Mirams, G.R., Sarathchandra, P., Borg, T.K., Gavaghan, D.J., Kohl, P., Bollensdorff, C., 2015. Cardiac tissue slices: preparation, handling, and successful optical mapping. *Am. J. Physiol. Circ. Physiol.* 308, H1112–H1125.

<https://doi.org/10.1152/ajpheart.00556.2014>

Wang, K., Lee, P., Mirams, G.R., Sarathchandra, P., Borg, T.K., Gavaghan, D.J., Kohl, P., Bollensdorff, X.C., n.d. Cardiac tissue slices: preparation, handling, and successful optical mapping.

Wang, K., Terrar, D., Gavaghan, D.J., Mu-U-Min, R., Kohl, P., Bollensdorff, C., 2014.

Living cardiac tissue slices: An organotypic pseudo two-dimensional model for cardiac biophysics research. *Prog. Biophys. Mol. Biol.* 115, 314–327.

<https://doi.org/10.1016/j.pbiomolbio.2014.08.006>

Wang, L.-K.H. and M.-J.J., 1995. Image Thresholding by minimizing the measures of fuzziness.

Ward, M.C., Gilad, Y., 2019. A generally conserved response to hypoxia in iPSC-derived cardiomyocytes from humans and chimpanzees. *Elife* 8.

<https://doi.org/10.7554/eLife.42374>

Watson, S.A., Duff, J., Bardi, I., Zabielska, M., Atanur, S.S., Jabbour, R.J., Simon, A., Tomas, A., Smolenski, R.T., Harding, S.E., Perbellini, F., Terracciano, C.M., 2019. Biomimetic electromechanical stimulation to maintain adult myocardial slices in vitro.

*Nat. Commun.* 10, 2168. <https://doi.org/10.1038/s41467-019-10175-3>

Watson, S.A., Scigliano, M., Bardi, I., Ascione, R., Terracciano, C.M., Perbellini, F., 2017. Preparation of viable adult ventricular myocardial slices from large and small mammals.

*Nat. Publ. Gr.* 12, 2623–2639. <https://doi.org/10.1038/nprot.2017.139>

Watts, E.R., Walmsley, S.R., 2019. Inflammation and Hypoxia: HIF and PHD Isoform Selectivity. *Trends Mol. Med.* <https://doi.org/10.1016/j.molmed.2018.10.006>

Weinreuter, M., Kreusser, M.M., Beckendorf, J., Schreiter, F.C., Leuschner, F., Lehmann, L.H., Hofmann, K.P., Rostosky, J.S., Diemert, N., Xu, C., Volz, H.C., Jungmann, A., Nickel, A., Sticht, C., Gretz, N., Maack, C., Schneider, M.D., Gröne, H., Müller, O.J., Katus, H.A., Backs, J., 2014. Ca<sup>2+</sup> M Kinase II mediates maladaptive post-infarct remodeling and pro-inflammatory chemoattractant signaling but not acute myocardial ischemia/reperfusion injury. *EMBO Mol. Med.* 6, 1231–1245.

<https://doi.org/10.15252/emmm.201403848>

- Weisfeldt, M.L., Armstrong, P., Scully, H.E., Sanders, C.A., Daggett, W.M., 1974. Incomplete relaxation between beats after myocardial hypoxia and ischemia. *J. Clin. Invest.* 53, 1626–1636. <https://doi.org/10.1172/JCI107713>
- Weiss, S.A., Lester, T.L., Kalter, S.S., Heberling, R.L., 1980. Chemically defined serum-free media for the cultivation of primary cells and their susceptibility to viruses. *In Vitro* 16, 616–628. <https://doi.org/10.1007/BF02618387>
- Wen, Q., Gandhi, K., Capel, R.A., Hao, G., O’Shea, C., Neagu, G., Pearcey, S., Pavlovic, D., Terrar, D.A., Wu, J., Faggian, G., Camelliti, P., Lei, M., 2018. Transverse cardiac slicing and optical imaging for analysis of transmural gradients in membrane potential and Ca<sup>2+</sup> transients in murine heart. *J. Physiol.* <https://doi.org/10.1113/JP276239>
- Wisneski, J.A., Gertz, E.W., Neese, R.A., Gruenke, L.D., Cymerman Craig, J., 1985. Dual carbon-labeled isotope experiments using D-[6-<sup>14</sup>C] glucose and L-[1,2,3-<sup>13</sup>C<sub>3</sub>] lactate: A new approach for investigating human myocardial metabolism during ischemia. *J. Am. Coll. Cardiol.* 5, 1138–1146. [https://doi.org/10.1016/S0735-1097\(85\)80016-4](https://doi.org/10.1016/S0735-1097(85)80016-4)
- Wong, D.T.L., Weightman, M.J., Baumert, M., Tayeb, H., Richardson, J.D., Puri, R., Bertaso, A.G., Roberts-Thomson, K.C., Sanders, P., Worthley, M.I., Worthley, S.G., 2012. Electro-mechanical characteristics of myocardial infarction border zones and ventricular arrhythmic risk: Novel insights from grid-tagged cardiac magnetic resonance imaging. *Eur. Radiol.* 22, 1651–1658. <https://doi.org/10.1007/s00330-012-2417-2>
- Wongsrikeao, P., Saenz, D., Rinkoski, T., Otoi, T., Poeschla, E., 2011. Antiviral restriction factor transgenesis in the domestic cat. *Nat. Methods* 8, 853–859. <https://doi.org/10.1038/nmeth.1703>
- Woodman, S.E., Park, D.S., Cohen, A.W., Cheung, M.W.C., Chandra, M., Shirani, J., Tang, B., Jelicks, L.A., Kitsis, R.N., Christ, G.J., Factor, S.M., Tanowitz, H.B., Lisanti, M.P.,

2002. Caveolin-3 knock-out mice develop a progressive cardiomyopathy and show hyperactivation of the p42/44 MAPK cascade. *J. Biol. Chem.* 277, 38988–38997.  
<https://doi.org/10.1074/jbc.M205511200>
- Xia, Y., Buja, L.M., McMillin, J.B., 1998. Activation of the cytochrome c gene by electrical stimulation in neonatal rat cardiac myocytes. *J. Biol. Chem.* 273, 12593–12598.  
<https://doi.org/10.1074/jbc.273.20.12593>
- Xiao, R.P., Cheng, H., Lederer, W.J., Suzuki, T., Lakatta, E.G., 1994. Dual regulation of Ca<sup>2+</sup>/calmodulin-dependent kinase II activity by membrane voltage and by calcium influx. *Proc. Natl. Acad. Sci. U. S. A.* 91, 9659–9663.  
<https://doi.org/10.1073/pnas.91.20.9659>
- Xu, A., Hawkins, C., Narayanang, N., 1993. Phosphorylation and Activation of the Ca<sup>2+</sup>-pumping ATPase of Cardiac Sarcoplasmic Reticulum by Ca<sup>2+</sup>/Calmodulin-dependent Protein Kinase\*, *THE JOURNAL OF BIOLOGICAL CHEMISTRY*.
- Yamashita, D., Kohzuki, H., Kitagawa, Y., Nakashima, T., Kikuta, A., Takaki, M., 2004a. O<sub>2</sub> consumption of mechanically unloaded contractions of mouse left ventricular myocardial slices. *Am. J. Physiol. Circ. Physiol.* 287, H54–H62.  
<https://doi.org/10.1152/ajpheart.01082.2003>
- Yamashita, D., Kohzuki, H., Kitagawa, Y., Nakashima, T., Kikuta, A., Takaki, M., 2004b. O<sub>2</sub> consumption of mechanically unloaded contractions of mouse left ventricular myocardial slices. *Am. J. Physiol. Heart Circ. Physiol.* 287, H54–62.  
<https://doi.org/10.1152/ajpheart.01082.2003>
- Yang, X., Pabon, L., Murry, C.E., 2014a. Engineering adolescence: Maturation of human pluripotent stem cell-derived cardiomyocytes. *Circ. Res.*  
<https://doi.org/10.1161/CIRCRESAHA.114.300558>

- Yang, X., Rodriguez, M., Pabon, L., Fischer, K.A., Reinecke, H., Regnier, M., Sniadecki, N.J., Ruohola-Baker, H., Murry, C.E., 2014b. Tri-iodo-L-thyronine promotes the maturation of human cardiomyocytes-derived from induced pluripotent stem cells. <https://doi.org/10.1016/j.yjmcc.2014.04.005>
- Yao, J.A., Hussain, W., Patel, P., Peters, N.S., Boyden, P.A., Wit, A.L., 2003. Remodeling of gap junctional channel function in epicardial border zone of healing canine infarcts. *Circ. Res.* 92, 437–443. <https://doi.org/10.1161/01.RES.0000059301.81035.06>
- Yasuhara, S., Takaki, M., Kikuta, A., Ito, H., Suga, H., 1996. Myocardial VO<sub>2</sub> of mechanically unloaded contraction of rat ventricular slices measured by a new approach. *Am. J. Physiol.* 270, H1063-70.
- Yatani, A., Brown, A.M., 1989. Rapid  $\beta$ -adrenergic modulation of cardiac calcium channel currents by a fast G protein pathway. *Science* (80-. ). 245, 71–74. <https://doi.org/10.1126/science.2544999>
- Yi, Y.W., Lee, J.H., Kim, S.Y., Pack, C.G., Ha, D.H., Park, S.R., Youn, J., Cho, B.S., 2020. Advances in analysis of biodistribution of exosomes by molecular imaging. *Int. J. Mol. Sci.* <https://doi.org/10.3390/ijms21020665>
- Yoran, C., Sonnenblick, E.H., Kirk, E.S., 1982. Contractile Reserve and Left Ventricular Function in Regional Myocardial Ischemia in the Dog.
- Youn, J.B., Han, J., Kim, N., Zhang, Y.-H., Kim, E., Leem, C.H., Kim, S.J., Earm, Y.E., 2005. Role of Stretch-activated Channels in the Heart: Action Potential and Ca<sup>2+</sup> Transients, Mechanosensitivity in Cells and Tissues. Academia.
- Youn, S.W., Li, Y., Kim, Y.M., Sudhakar, V., Abdelsaid, K., Kim, H.W., Liu, Y., Fulton, D.J.R., Ashraf, M., Tang, Y., Fukai, T., Ushio-Fukai, M., 2019. Modification of cardiac



progenitor cell-derived exosomes by miR-322 provides protection against myocardial infarction through nox2-dependent angiogenesis. *Antioxidants* 8.

<https://doi.org/10.3390/antiox8010018>

Young, M.E., Laws, F.A., Goodwin, G.W., Taegtmeier, H., 2001. Reactivation of Peroxisome Proliferator-activated Receptor  $\alpha$  Is Associated with Contractile Dysfunction in Hypertrophied Rat Heart. *J. Biol. Chem.* 276, 44390–44395.

<https://doi.org/10.1074/jbc.M103826200>

Yu, J.K., Sarathchandra, P., Chester, A., Yacoub, M., Brand, T., Butcher, J.T., 2018. Cardiac regeneration following cryoinjury in the adult zebrafish targets a maturation-specific biomechanical remodeling program. *Sci. Rep.* 8, 1–10. <https://doi.org/10.1038/s41598-018-33994-8>

Yuan, W., Bers, D.M., 1994. Ca-dependent facilitation of cardiac Ca current is due to Ca-calmodulin-dependent protein kinase. *Am. J. Physiol. - Hear. Circ. Physiol.* 267.

<https://doi.org/10.1152/ajpheart.1994.267.3.h982>

Zhang, S.J., Truskey, G.A., Kraus, W.E., 2007. Effect of cyclic stretch on  $\beta_{1D}$ -integrin expression and activation of FAK and RhoA. *Am. J. Physiol. Physiol.* 292, C2057–

C2069. <https://doi.org/10.1152/ajpcell.00493.2006>

Zhang, T., Brown, J.H., 2004. Role of Ca<sup>2+</sup>/calmodulin-dependent protein kinase II in cardiac hypertrophy and heart failure. <https://doi.org/10.1016/j.cardiores.2004.04.026>

Zhang, Y., Chen, X., Gueydan, C., Han, J., 2018. Plasma membrane changes during programmed cell deaths. *Cell Res.* 28, 9–21. <https://doi.org/10.1038/cr.2017.133>

Zhang, Y., Li, T.-S., Lee, S.-T., Wawrowsky, K.A., Cheng, K., Galang, G., Malliaras, K., Abraham, M.R., Wang, C., Marb?n, E., 2010a. Dedifferentiation and Proliferation of

Mammalian Cardiomyocytes. *PLoS One* 5, e12559.

<https://doi.org/10.1371/journal.pone.0012559>

Zhang, Y., Li, T.-S., Lee, S.-T., Wawrowsky, K.A., Cheng, K., Galang, G., Malliaras, K., Abraham, M.R., Wang, C., Marbán, E., 2010b. Dedifferentiation and Proliferation of Mammalian Cardiomyocytes. *PLoS One* 5, e12559.

<https://doi.org/10.1371/journal.pone.0012559>

Zhao, Z., Xie, Y., Wen, H., Xiao, D., Allen, C., Fefelova, N., Dun, W., Boyden, P.A., Qu, Z., Xie, L.H., 2012. Role of the transient outward potassium current in the genesis of early afterdepolarizations in cardiac cells. *Cardiovasc. Res.* 95, 308–316.

<https://doi.org/10.1093/cvr/cvs183>

Zhu, W., Shou, W., Payne, R.M., Caldwell, R., Field, L.J., 2008. A mouse model for juvenile doxorubicin-induced cardiac dysfunction. *Pediatr. Res.* 64, 488–494.

<https://doi.org/10.1203/PDR.0b013e318184d732>

Zhu, W.Z., Xie, Y., Moyes, K.W., Gold, J.D., Askari, B., Laflamme, M.A., 2010.

Neuregulin/ErbB signaling regulates cardiac subtype specification in differentiating human embryonic stem cells. *Circ. Res.* 107, 776–786.

<https://doi.org/10.1161/CIRCRESAHA.110.223917>

Zimmermann, W.H., Melnychenko, I., Wasmeier, G., Didié, M., Naito, H., Nixdorff, U., Hess, A., Budinsky, L., Brune, K., Michaelis, B., Dhein, S., Schwoerer, A., Ehmke, H., Eschenhagen, T., 2006. Engineered heart tissue grafts improve systolic and diastolic function in infarcted rat hearts. *Nat. Med.* 12, 452–458. <https://doi.org/10.1038/nm1394>

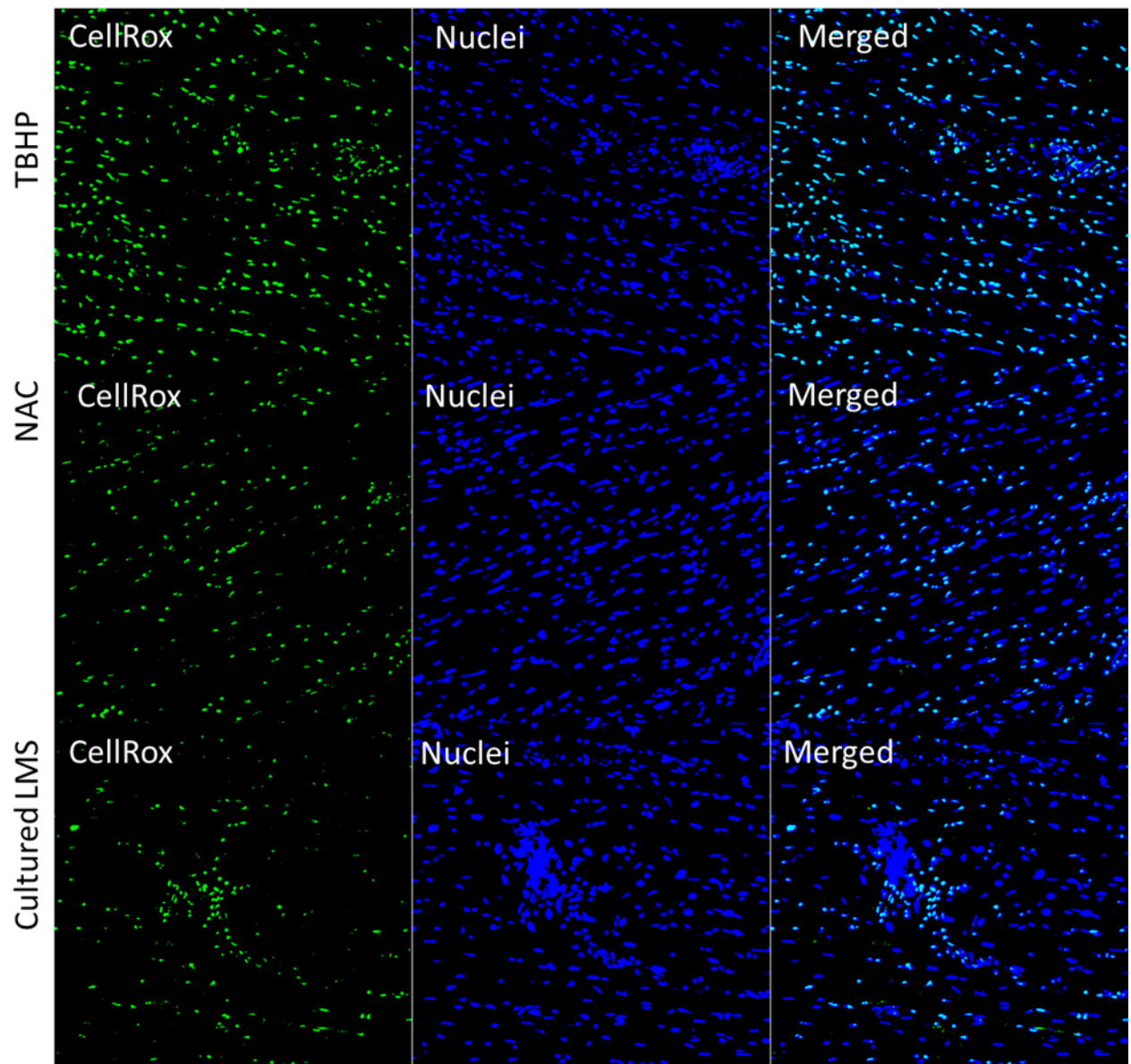
Zimmermann, W.H., Schneiderbanger, K., Schubert, P., Didié, M., Münzel, F., Heubach, J.F., Kostin, S., Neuberger, W.L., Eschenhagen, T., 2002. Tissue engineering of a differentiated cardiac muscle construct. *Circ. Res.* 90, 223–230.

<https://doi.org/10.1161/hh0202.103644>

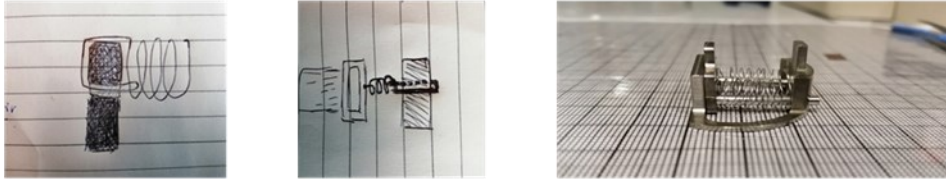
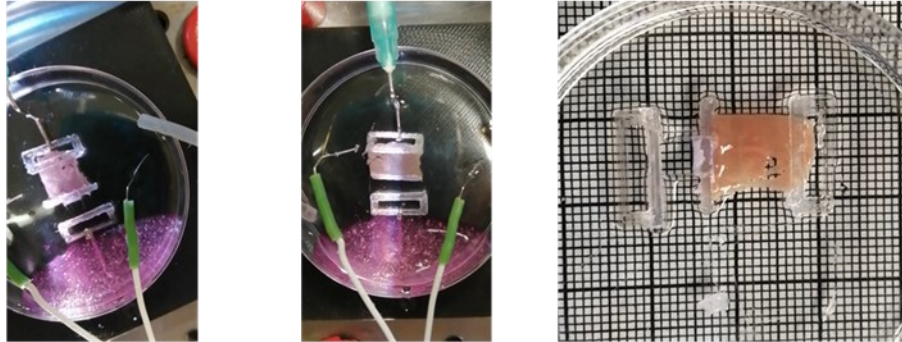
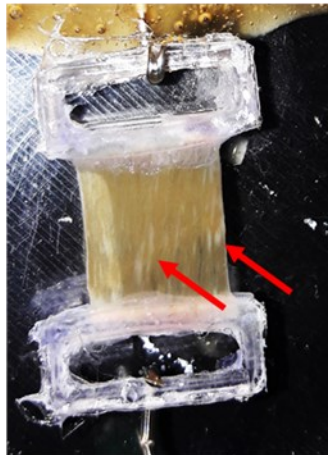
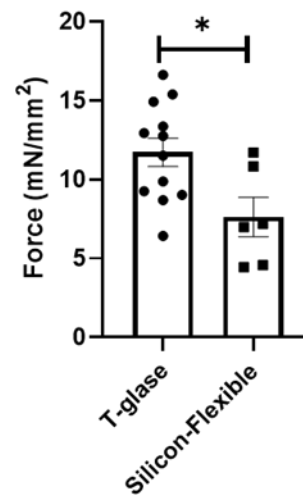
Zlabinger, K., Spannbauer, A., Traxler, D., Gugerell, A., Lukovic, D., Winkler, J., Mester-Tonczar, J., Podesser, B., Gyöngyösi, M., 2019. MiR-21, MiR-29a, GATA4, and MEF2c Expression Changes in Endothelin-1 and Angiotensin II Cardiac Hypertrophy Stimulated Isl-1+Sca-1+c-kit+ Porcine Cardiac Progenitor Cells In Vitro. *Cells* 8, 1–19.  
<https://doi.org/10.3390/cells8111416>

# Chapter 9

# Appendices

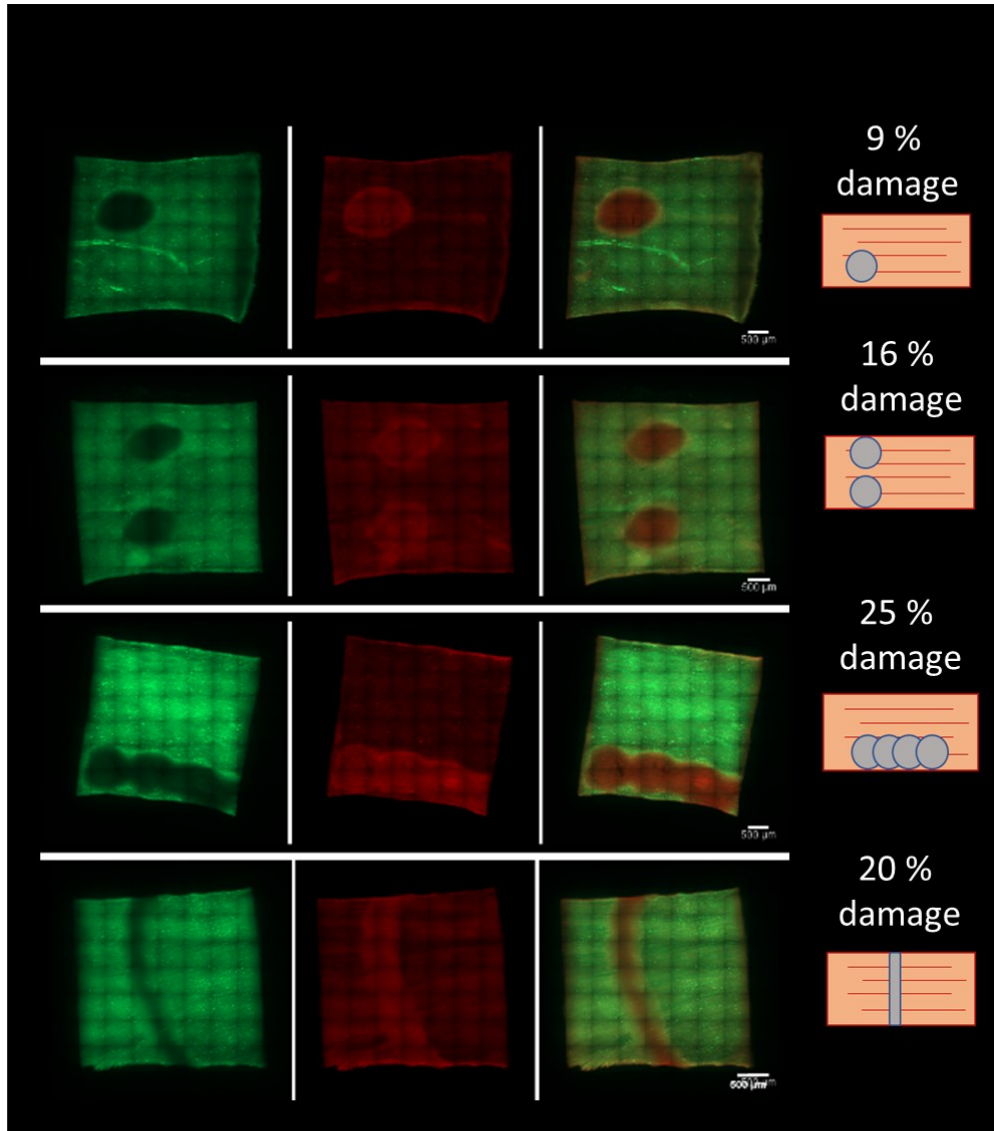


*Appendix 1-CellRox Staining for visualising ROS production in cells. Control cultured LMSs were treated with N-acetyl cysteine (NAC) to scavenge ROS, whereas tert-Butyl Hydroperoxide (tBHP) was used to induce ROS production. Co-localisation of the CelROX (green) staining with the nucleus (blue) shows increased ROS in the cells.*

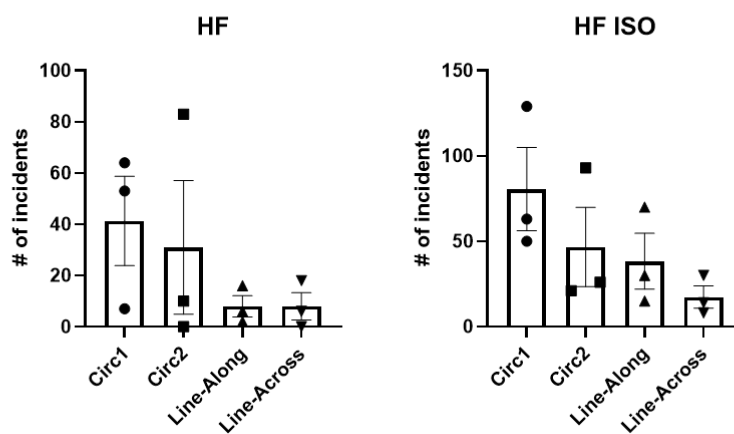
**A****B****C****Maximum active force**

Appendix 2- Designs that allow LMS shortening in culture. A) A spring was placed between the two movable posts to allow LMS shortening during contraction. B) Tissue holders were attached to a flexible PDMS stripe to allow tissue shortening in culture. C) Fully flexible tissue holders were tested in culture, showing signs of fibre death and reduction of active force. N/n=biological replicates (animals)/technical replicates (LMSs).

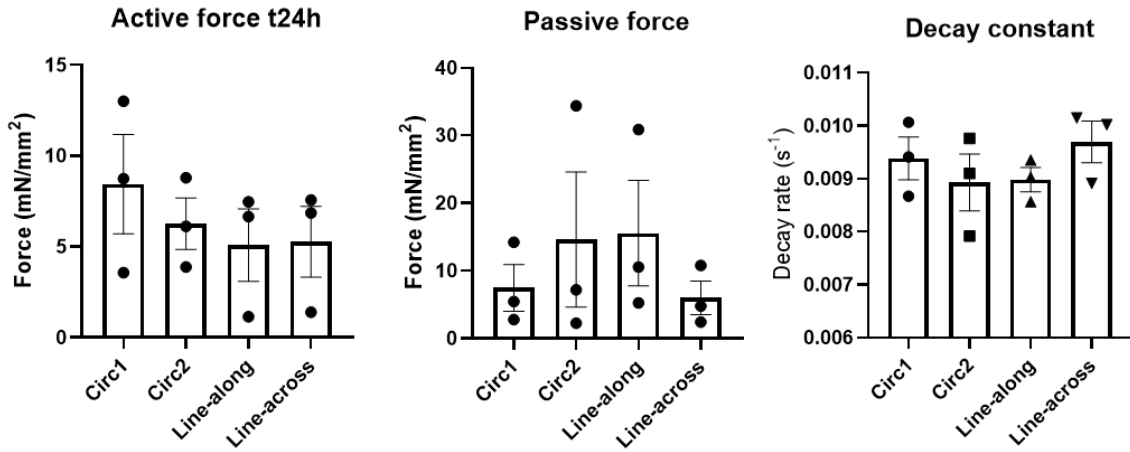
A



B



Appendix 3- Assessing the effect of location and shape of cryoinjury on cultured LMSs. A) Representative images of LIVE/DEAD staining (red-dead, green-viable). B) Arrhythmias incidence after 24h of culture with or without the presence of ISO. N/n-3/3. One-way ANOVA was used for statistical analysis. N/n=biological replicates (animals)/technical replicates (LMSs).



Appendix 4- Assessing the effect of location and shape of cryoinjury on cultured LMSs. Contraction was measured at 15% of stretch (2.2 $\mu$ m SL). N/n=3/3. One-way ANOVA was used for statistical analysis. N/n=biological replicates (animals)/technical replicates (LMSs).